Modulation of the Clp protease by agonist molecules as a tool to investigate the functional properties of the complex machinery

Dissertation

der Mathematisch-Naturwissenschaftlichen Fakultät

der Eberhard Karls Universität Tübingen

zur Erlangung des Grades eines

Doktors der Naturwissenschaften

(Dr. rer. nat.)

vorgelegt von

Imran Tarik Malik

aus Oberkirch

Tübingen

2019

Gedruckt mit Genehmigung der Mathematisch-Naturwissenschaftlichen Fakultät der Eberhard Karls Universität Tübingen.

Tag der mündlichen Qualifikation:	05.07.2019
Dekan:	Prof. Dr. Wolfgang Rosenstiel
1. Berichterstatter:	Prof. Dr. Heike Brötz-Oesterhelt
2. Berichterstatter:	Prof. Dr. Friedrich Götz

Table of contents

Summary

Protein digestion is a vital process of the bacterial cell. Proteolytic activity is not just required for the degradation of misfolded or miscoded proteins but for all kinds of cellular regulatory processes, e. g. during developmental programs, in response to environmental stimuli, during host infection or cell division. One important member of the group of bacterial proteases is the caseinolytic (Clp) protease. The Clp protease belongs to the AAA+ family of proteases and consists of two major components. The first component, the Clp-ATPase (e. g. ClpX or ClpC in *Staphylococcus aureus*), recognizes protein substrates targeted for degradation and is responsible for unfolding and translocation of substrates into the second component ClpP. Here, cleavage of the linearized polypeptide chain takes place. ClpP is a barrel-shaped tetradecameric complex. The catalytic sites are within the sequestered lumen of ClpP and inaccessible to cytosolic proteins. The Clp-ATPases actively feed linearized protein substrates through narrow entrance pores at the two poles of the ClpP barrel. This compartmentalized system allows for a regulated and safe degradation process.

In this study, the effects of various agonist molecules on the activity and conformational state of ClpP were analyzed. Most prominently, acyldepsipeptide antibiotics of the ADEP class (ADEPs) are dysregulators of the Clp protease and deprive ClpP of the regulation by Clp-ATPases. At the same time, they activate ClpP to degrade proteins in an uncontrolled fashion by increasing the diameter of the entrance pores. This unregulated protein degradation by ClpP is toxic for Gram-positive bacteria and leads to cellular death. However, in certain bacterial species the inhibition of the functional association of ClpP with Clp-ATPases by ADEPs can also be the mechanism of antibiotic action. In the case of mycobacteria, where a functional Clp system is essential for viability, inhibition rather than activation of the Clp system is responsible for cell death.

Moreover, mycobacterial ClpP presents a special case *in vitro*, as here, functional assembly of the ClpP complex and consequently degradation activity is predicated on the presence of N-terminally blocked dipeptide activators (Z-LL). To investigate this

unusual activation mechanism of mycobacterial ClpP, I devised an *in vitro* competition assay and identified the active site as the target of Z-LL.

With the help of β-lactone covalent active site inhibitors of ClpP, ADEPs were found to also be responsible for allosteric enhancement of catalysis. Furthermore, they convert ClpP into an overall more active state via conformational control. In this context, a crucial structural element of ClpP is the hydrophobic pocket (H-pocket) at the interaction interface between ClpP and the Clp-ATPase. ADEPs as well as Clp-ATPases bind to the hydrophobic pocket which serves as the master switch of ClpP conformational control. These findings were obtained with *S. aureus* ClpP. My goal was to reconcile the acquired data with ClpP from *B. subtilis* and I was able to confirm that ADEPs exert conformational control on *B. subtilis* ClpP analogously.

To further investigate the interplay between ClpP and its cognate Clp-ATPase ClpX, Microcin J25 mutant lasso peptides were generated to mimic the IGF-loops of ClpX which are responsible for binding to ClpP. In the course of this investigation, a potential additional docking site for ClpX on the surface of ClpP could be identified. This additional binding pocket is termed the C-pocket and my data suggest that it plays a role in the efficient communication between the two components of the Clp protease system.

Taken together, this study deepens our understanding of the Clp protease organization and the molecular operation mode. Furthermore, our discovery of the functional relevance of the C-pocket suggests a novel druggable target site for deregulating the activity of ClpP.

Zusammenfassung

Proteinverdau ist ein elementarer Vorgang in der bakteriellen Zelle. Proteolytische Aktivität kommt nicht nur beim Abbau fehlgefalteter oder falsch codierter Proteine zum Tragen, sondern wird auch für allerhand regulatorische Prozesse benötigt, z. B. während zellulärer Entwicklungsschritte, als Antwort auf Umwelteinflüsse, in der Infektion oder der Zellteilung. Ein wichtiger Vertreter bakterieller Proteasen ist die caseinolytische (Clp) Protease. Die Clp-Protease gehört der Familie der AAA+

Proteasen an und besteht aus zwei Hauptkomponenten. Die erste Komponente bildet die Clp-ATPase (z. B. ClpX oder ClpC in *Staphylococcus aureus*), welche Proteinsubstrate, die zum Abbau markiert wurden, erkennt, entfaltet und an die zweite Komponente ClpP weiterleitet. Hier findet die Spaltung der nun linearisierten Polypeptidkette statt. Die katalytischen Zentren ClpPs befinden sich Innern eines vom Zytoplasma abgeschiedenen Reaktionsraums, der für zytosolische Proteine unzugänglich ist. Die Clp-ATPasen führen das linearisierte Proteinsubstrat aktiv durch enge Eintrittsporen ein, die sich an den beiden Polen des fassförmigen ClpPs befinden. Dieses System gewährleistet den geregelten und sicheren Ablauf der Proteolyse.

In dieser Arbeit wurden die Einflüsse verschiedener agonistischer Moleküle auf die Aktivität und den Konformationszustand ClpPs untersucht. Allen voran die Acyldepsipeptid-Antibiotika der Klasse der ADEPs (kurz: ADEPs), die die Clp-Protease dysregulieren und ClpP von der Regulation durch Clp-ATPasen abkoppeln. Gleichzeitig aktivieren sie ClpP durch eine Vergrößerung des Durchmessers der Eintrittsporen, was zum unkontrollierten Abbau zytosolischer Proteine führt. Diese Überaktivierung ist toxisch für Gram-positive Bakterien und führt zum Zelltod. Je nach Spezies kann allerdings auch die Hemmung der Assoziierung von ClpP mit seiner Clp-ATPase der todbringende Effekt sein. Beispielsweise stellt in Mykobakterien, wo die Clp-Protease essentiell ist, die Hemmung der natürlichen Funktionen des Clp-Systems und nicht die Aktivierung den tödlichen Wirkmechanismus der ADEPs dar.

Darüber hinaus zeigt mykobakterielles ClpP ein außergewöhnliches *in vitro* Verhalten, da hier der Zusammenbau zu einem funktionellen ClpP-Komplex and folglich die Proteaseaktivität von der Zugabe N-terminal geschützter Dipeptide (Z-LL) abhängt. Um diesen ungewöhnlichen Aktivierungsmechanismus von mykobakteriellem ClpP näher zu untersuchen, habe ich ein *in vitro* Kompetitionsassay erdacht, mit dessen Hilfe es möglich war, das aktive Zentrum ClpPs als die Bindungsstelle für Z-LL zu identifizieren.

Mithilfe von β-Lactonen, die kovalent die aktiven Zentren ClpPs binden und damit inhibieren, konnte neben der Porenöffnung eine Wirkung der ADEPs als allosterische Aktivatoren der Katalyse nachgewiesen werden. Darüber hinaus üben sie Kontrolle über die Konformation aus, was ClpP in einen allgemein aktiveren Zustand überführt.

In diesem Kontext spielt die hydrophobe Bindetasche an der Schnittstelle der Kommunikation zwischen ClpP und Clp-ATPasen eine wichtige Rolle. Sie dient sowohl ADEPs als auch Clp-ATPasen als Ankerpunkt und bildet den Hauptschalter, der die ClpP-Konformation steuert. Diese Erkenntnisse wurden anhand von ClpP aus *S. aureus* gewonnen. Mein Ziel bestand darin, diese Daten mit ClpP aus *B. subtilis* in Einklang zu bringen und ich konnte bestätigen, dass ADEP in analoger Weise die Konformation von *B. subtilis* ClpP steuert.

Um das Zusammenspiel aus ClpP und der Clp-ATPase ClpX weiter zu untersuchen, wurden Mutanten des Lassopeptids Microcin J25 generiert, die als Imitate der ClpX IGF-Schlaufen, welche für den direkten Kontakt zu ClpP verantwortlich zeichnen, dienten. Im Zuge dieser Untersuchungen konnte eine weitere potentielle Bindestelle auf der ClpP-Oberfläche identifiziert werden. Diese zusätzliche Bindetasche wird als C-Tasche („C-pocket“) bezeichnet und meine gesammelten Daten deuten auf eine Rolle der C-Tasche in der effizienten Kommunikation zwischen den beiden Komponenten der Clp-Protease hin.

Abschließend betrachtet vertieft diese Arbeit das Verständnis der Organisation der Clp-Protease und die ihrer Arbeitsweise zugrundeliegenden molekularen Mechanismen. Desweiteren offenbart unsere Entdeckung der funktionellen Bedeutung der C-Tasche eine potentielle neue Zielstruktur für die Bindung von Wirkstoffen, die die ClpP-Aktivität deregulieren.

Introduction

Proteolytic enzymes are an integral part of cellular maintenance. They are not only responsible for maintaining proteostasis but also crucial players in the regulation of important cellular processes like stress responses, sporulation, competence development, cell division and also virulence in certain pathogenic bacteria (1–3). Bacterial proteases, like the Clp system, facilitate adaptation to rapidly changing environments that require immediate adjustment of the available repertoire of functional proteins within the cell as well as repair mechanisms in response to heat and other stresses. In general, they consist of AAA+ unfoldases ("ATPases associated with diverse cellular activities") of the Hsp100 chaperone family and a proteolytic core component. In protein quality control, unfoldases linearize misfolded proteins, thereby offering a chance to refold correctly. Alternatively, they thread unfolded proteins into the proteolytic core component for targeted degradation. In this work, the focus lies on the functional analysis of the Clp protease. The Clp protease is a member of the Clp family of proteases along with the HslUV (ClpYQ) protease. It consists of the proteolytic core ClpP that can pair up with a number of ATPases like ClpC and ClpX in *Bacillus subtilis* and *S. aureus* yielding the functional proteolytic complexes ClpCP and ClpXP in these organisms, ClpA and ClpX represent Clp-ATPases in *Escherichia coli* and ClpX and ClpC1 in *Mycobacterium tuberculosis*. While terminology is not definite in all publications, the term 'Clp protease' will refer to the system involving ClpP and its cognate Clp-ATPases in this thesis. This protease is conserved amongst almost all bacteria as well as some eukaryotic organelles and has gained increased recognition during the last fourteen years as a potential antibiotic drug target.

A Clp protease machinery comprises two major components, ClpP and a cognate Clp-ATPase. The Clp-ATPase recognizes protein substrates and routes them to the proteolytic core ClpP. The recognition of substrates by the Clp-ATPase is mediated by either specific degradation tags or molecular markers like phosphorylations (4–8). Additionally, adapter proteins like SspB or MecA can be involved. In the case of MecA, an adapter protein studied in most detail in *Bacillus subtilis*, the adapter is necessary for the activity of the Clp-ATPase ClpC by mediating oligomerization to a functional hexamer (9). Other adapters like SspB are supplemental as they increase the affinity

of the Clp-ATPase for their respective substrates (10). Once a substrate is bound to a Clp-ATPase like ClpX or ClpC, it is unfolded by ATP-driven mechanical force and then threaded into ClpP which represents the proteolytic component of the Clp protease.

ClpP is composed of 14 subunits which oligomerize to form a barrel of two stacked heptameric rings. This barrel is axially symmetric and has two narrow (~ 10 Å) entry pores on each side of the symmetry plain (for comprehensive figures, see I. T. Malik *et al*. 2017 later in the Introduction section). The substrate is translocated by the Clp-ATPase through either of the two entry pores and subsequently degraded within the lumen of ClpP where 14 catalytic Ser-His-Asp triads perform peptide hydrolysis. This sequestered space within the ClpP barrel is inaccessible to cytosolic proteins to prevent uncontrolled degradation (11–14). In the case of *B. subtilis* ClpP (BsClpP) *in vitro*, a lower oligomeric state renders BsClpP inactive and ClpP-ATPases are required to assemble the active ClpP tetradecamer. While the oligomeric state of ClpP has not been investigated *in vivo* so far, the requirement of tetradecamer assembly might pose an additional layer of protective safeguards against harmful self-digest. Finally, substrates require recognition via regulated modifications and/or with the help of adapters and unfolding by Clp-ATPases. Collectively, the mechanisms in place to protect the cell from uncontrolled protein degradation illustrate the sensitivity of this crucial cellular degradation process.

ClpP interacts with its partner Clp-ATPase at either or both of its two poles where the narrow entrance pores are located (15, 16). Mutational and modelling studies identified hydrophobic pockets (H-pockets) as the binding site where Clp-ATPases make contact with ClpP via flexible loops containing conserved tripeptide motifs (17, 18). A total of 14 of these H-pockets are located on the surface of ClpP, seven per heptameric ring at each pole. They are located between two adjacent ClpP subunits within the tetradecameric complex and are composed of amino acid residues from each. Hence, the formation of hydrophobic and hydrogen bonds with the H-pockets confers intra-ring stability (19, 20).

This interaction interface between Clp-ATPase and ClpP on the apical surface of ClpP presents a hot spot for inhibitors of protein-protein-interaction. Acyldepsipeptide antibiotics of the ADEP class (ADEPs) present the best characterized ClpP binder and also dock at the H-pockets (20–23). These compounds are derived from the natural

product ADEP1 ('factor A') isolated from *Streptomyces hawaiiensis* (24). Medicinal chemistry optimization efforts yielded several synthetic congeners with high efficacy against a panel of enterococci, streptococci as well as *S. aureus* and *B. subtilis* with minimal inhibitory concentrations (MIC) of well under 1 µg/ml, in some cases by several orders of magnitude (21, 25). By binding the H-pocket, ADEPs prevent communication between ClpP and the Clp-ATPase and thereby inhibit all natural functions of the Clp protease (26, 27). Since the Clp protease is non-essential for viability in most bacteria, inhibition of the Clp protease does not lead to growth inhibition in these organisms (28, 29). In accordance, ADEPs kill firmicutes not by inhibition but over-activation. The mode of action of ADEPs was first described in the non-pathogenic model organism *B. subtilis*, where ADEP treatment leads to cell death by unregulated proteolysis (21). Also, ADEP enables ClpP to degrade the full-length model substrate casein *in vitro* (21). A major target protein of ADEP-activated ClpP (ADEP/ClpP) is the cell division protein FtsZ, a homologue of the eukaryotic cytoskeleton element tubulin, important for Z-ring formation during bacterial cell division (30). The uncontrolled degradation of FtsZ leads to filamentation in *B. subtilis* and cell death. Furthermore, ADEP/ClpP degrades nascent peptide chains at the ribosome and prolonged exposure to elevated ADEP levels led to a multitude of non-native protein fragments (19, 31). In the pathogenic model organism *S. aureus*, it was shown that the addition of ADEP in combination with rifampin leads to the eradication of persister cells (31). Crystal structures of ADEP/ClpP showed an increased diameter of the entry pores (20, 22, 23). This increased accessibility to the proteolytic core of ClpP is most likely responsible for the ability of ADEP/ClpP to degrade full-length proteins without the need for previous unfolding by an ATPase.

While ADEP antibiotics efficiently kill firmicutes by ClpP over-activation, ClpP is not essential for survival in these organisms and resistant mutants can be generated at frequencies of ~10^{-6} *in vitro* (21). In contrast, functional ClpP is essential for survival in mycobacteria (32). ADEPs show significantly higher MICs against mycobacteria, which might be attributed to reduced uptake and efflux but potentially also to a different mode of ClpP deregulation in this genus (33). In the presence of efflux pump inhibitors, the ADEP antitubercular MIC is reduced by half but still much higher than observed for firmicutes. Furthermore, the molecular organization of mycobacterial ClpP is significantly different. Here, the proteolytic core component of the Clp protease

consists of two ClpP paralogues, ClpP1 and ClpP2. Independently purified ClpP1 and ClpP2 elute as structures of heptameric or lower oligomeric state in size-exclusion chromatography and when mixed stoichiometrically, they can assemble to form inactive tetradecamers (34, 35). *In vitro*, the assembly of the active ClpP1P2 particle is dependent on the addition of accessory N-terminally blocked dipeptides like benzyloxycarbonyl-leucyl-leucine (Z-LL) (36, 37). In the presence of Z-LL, ClpP1 and ClpP2 each form pure heptamers. Upon mixing Z-LL treated ClpP1 and ClpP2, they associate to form the active ClpP1P2 complex which is composed of a homo-heptameric ClpP1 ring and a homo-heptameric ClpP2 ring. This unique composition of ClpP1P2 and the Z-LL requirement *in vitro* further sets the mycobacterial Clp protease apart from other organisms.

The Clp protease is essential for temperature tolerance in many bacterial organisms where *clpP* mutants show severe growth inhibition at extreme temperatures (38, 39). Additionally, in the pathogen *S. aureus*, deletion of ClpP leads to severely attenuated virulence. Here, *clpP* deletion led to a strong decrease in the expression of extracellular proteases and α-haemolysin resulting in a non-proteolytic and non-haemolytic phenotype (1, 28). Furthermore, the *S. aureus clpP* knock-out mutant displayed strongly reduced pathogenesis in a murine abscess model (28). β-lactone inhibitors targeting ClpP have been successful in neutralising haemolysis and proteolysis in an agar plate based assay and in decreasing intracellular virulence of *Listeria monocytogenes* in mouse macrophages (29, 40). Furthermore, treatment with β-lactones led to amelioration of an *S. aureus* skin infection in mice (41). These compounds covalently bind to the active site serine of ClpP and abolish its degradation capabilities. Hence, ClpP presents an attractive target for anti-bacterial as well as anti-virulence agents. The latter approach might offer a means to combat critical infections without bestowing too much selective pressure towards resistance development through mutations in ClpP (41, 42). Alongside ADEPs, which form a tool to investigate the implications of binding the H-pocket, β-lactones are instrumental for the direct investigation of ClpP catalysis.

Aims and rational of individual publications

Chapter 1: Mode of activation of mycobacterial ClpP by Z-LL

In principle, ClpPs from *B. subtilis*, *S. aureus* and *E. coli* exhibit a similar *in vitro* activity profile insofar as they possess intrinsic peptide degradation capabilities (BsClpP only when purified as tetradecamers) and they can be activated by ADEPs to degrade the full-length proteins casein and FtsZ. They differ merely in their respective catalysis rates *in vitro*. Mycobacterial ClpP on the other hand shows a different molecular organization as well as significantly different *in vitro* behaviour. While tetradecamer formation is sufficient to switch on intrinsic *B. subtilis* ClpP, tetradecamer assembly is not sufficient for activity in mycobacteria, at least under *in vitro* assay conditions (27, 36, 37). The requirement of the agonist molecule Z-LL for functional assembly or reassembly, even when tetradecameric ClpP1P2 particle has been obtained, is unique to mycobacterial ClpP.

At the time of our publication, that is presented in chapter 1 of this thesis, neither the binding site of Z-LL nor its mode of activation of mycobacterial ClpP were known. Originally, N-terminally blocked peptides were employed as substrate analogues to inhibit catalysis. Hence, binding to the active sites was expected (36). With the discovery of the agonistic behaviour of Z-LL in mycobacterial ClpP by increasing its catalysis rate over 1000-fold, it was speculated that Z-LL might target a distinct allosteric binding site (36). Since the H-pocket had already been shown to serve as a binding site for the ClpP activator ADEP, we set out to investigate whether Z-LL might also bind there. With the finding that mycobacterial ClpP1P2 activity is also contingent upon the Z-LL activating effect in the presence of the partner Clp-ATPase ClpC1, an involvement of the H-pocket in Z-LL binding became less likely (36). Thus, we turned our attention towards the active sites. However, a role of the active sites as potential binding sites is difficult to investigate. Since Z-LL is mandatory for activity in mycobacteria, a putative competitive inhibition would not show by classical biochemical approaches. Hence, we decided to further investigate the role of Z-LL in ClpP activity in the background of *B. subtilis*. Using our model organism, where ClpP function is well understood, I performed competition assays with Z-LL, substrate and ADEP and ClpP and could clearly show that Z-LL binds to the active site of ClpP (27).

Chapter 2: ADEP regulates ClpP of *S. aureus* and *B. subtilis* by conformational control

In chapter 2, the activating effect of ADEPs was combined with the inhibitory effects of β-lactones to study the interrelationship between conformation and activity of ClpP. β-lactones offered an elegant tool to turn off the catalytic capabilities of ClpP. In combination with ADEPs, these compounds were instrumental in identifying the effect of ADEPs on the active site of ClpP. Until then, pore enlargement had been deemed the sole effect of ADEPs responsible for ClpP activation. In order to investigate active site function isolated from pore enlargement, an assay had to be devised that disregards the increased accessibility to the ClpP lumen because of pore enlargement. Therefore, a set of β-lactones with side chains of varying bulkiness was employed to study the effect on the hydrolysis rate in the absence and presence of ADEPs. Consequently, dissociation of covalently bound β-lactone inhibitors in the presence and absence of ADEPs provided further insight into the direct effect of ADEP binding on the active sites within ClpP. This study provided a comprehensive and thorough biochemical assessment of the *in vitro* effects of ADEPs on *S. aureus* ClpP (SaClpP) including affinity, thermal stability, conformation and GFP degradation by SaClpXP. This work was performed by our collaboration partner from the group of Stephan Sieber (Munich).

My task in this context was to extend the results obtained for SaClpP to ClpP from *B. subtilis* and to draw general conclusions on the molecular operation mode of ClpP (see Supplementary Figures and Methods for Chapter 2, page 160). These findings cumulated in a review article that dissected the information obtained with the help of several agonist molecules targeting either ClpP or the Clp-ATPases and summarized the inner workings of this complex machinery in great detail (Chapter 2; “Conformational control of the bacterial Clp protease by natural product antibiotics”).

Chapter 3: Lasso peptides mutated to mimic IGF-loops activate ClpP and are C-pocket sensitive

ADEP antibiotics have been instrumental in elucidating the ClpP gating mechanism (20, 22, 23, 43). Structure-activity-relationship (SAR) investigations of ADEP fragments showed that the *N*-acyldifluorophenylalanine moiety (fragment **5**) is necessary and sufficient for (albeit low) activity, while the macrolactone backbone

conveys potency (44). The *N*-acyldifluorophenylalanine was speculated to present the pharmacophore of the ADEP structure. It also superimposed nicely with the conserved tripeptide motif of partner Clp-ATPases in modelling studies which resulted in the prevalent notion that ADEPs mimic Clp-ATPase binding (22, 43–45). Still, while ADEPs are the most suitable Clp-ATPase mimetics available, a more profound contribution of the macrolactone backbone on the ADEP activity cannot be excluded. In fact, a cryo-EM structure of ClpAP, the only co-structure of a Clp-ATPase bound to ClpP available today, does not show a significant increase in pore diameter (46). Also, a linear peptide carrying the IGF tripeptide motif found in a cognate Clp-ATPase did not activate ClpP (18). Thus, the ADEP effect most likely extends beyond simple mimicry of the IGF-loops of the Clp-ATPases. In order to investigate the effects of presenting ClpP with a conserved tripeptide motif as part of a flexible loop, we constructed microcin J25 (MccJ25) mutants. MccJ25 is a ribosomally synthesized peptide of the class II of lasso peptides (47). Lasso peptides show a unique topology with an N-terminal intramolecular peptide bond resulting in a ring structure and the C-terminal end threaded through the N-terminal ring. The resulting structure is reminiscent of a lariat knot where the C-terminal tail describes a loop. This structure served as a suitable template to introduce the three conserved motifs IGF (*B. subtilis*, *E. coli*, and S. *aureus* ClpX), IGL (*E. coli* ClpA), VGF (*B. subtilis* ClpC) at three different positions within the MccJ25 loop which yielded nine different compounds. *In vitro* characterization of the acquired loop mutant panel and comparison with ADEP activity provided further insight into the ClpP activation mechanism and helped define ADEP-specific effects in demarcation to natural effects mediated by Clp-ATPases.

Chapter 1

Acyldepsipeptide antibiotics kill mycobacteria by preventing the physiological functions of the ClpP1P2 protease

Kirsten Famulla[1], Peter Sass[1], Imran Malik[1], Tatos Akopian[2], Olga Kandror[2], Marina Alber[3], Berthold Hinzen[4], Helga Ruebsamen-Schaeff[5], Rainer Kalscheuer[3], Alfred L. Goldberg[2], and Heike Brötz-Oesterhelt[1,*]

[1]Department of Microbial Bioactive Compounds, Interfaculty Institute of Microbiology and Infection Medicine, University of Tuebingen, Germany; [2]Department of Cell Biology, Harvard Medical School, Boston, MA; [3]Institute for Medical Microbiology and Hospital Hygiene, University of Duesseldorf; [4]Bayer Pharma AG, Wuppertal, Germany; [5]AiCuris GmbH & Co. KG, Wuppertal, Germany.

*For correspondence: heike.broetz-oesterhelt@uni-tuebingen.de

Famulla, K. *et al*. Acyldepsipeptide antibiotics kill mycobacteria by preventing the physiological functions of the ClpP1P2 protease. *Molecular Microbiology* (2016) 101(2), 194–209
doi:10.1111/mmi.13362

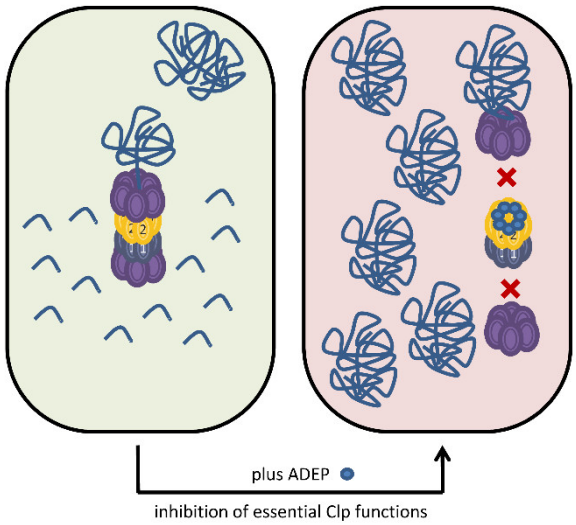

Abbreviated Summary

The mechanism of action of antibiotic acyldepsipeptides (ADEP) has been commonly accepted to function by activating unregulated protease activity of bacterial ClpP peptidase. Here, we show enhanced killing by ADEP upon depletion of the ClpP1P2 level in a conditional *Mycobacterium bovis* BCG mutant. Our data reveal killing of mycobacteria by ADEPs through abrogating the interaction between ClpP and its cognate Clp-ATPases rather than ClpP activation like in many other bacteria.

Summary

The Clp protease complex in Mycobacterium tuberculosis is unusual in its composition, functional importance, and activation mechanism. While most bacterial species contain a single ClpP protein that is dispensable for normal growth, mycobacteria have two ClpPs, ClpP1 and ClpP2, which are essential for viability and together form the ClpP1P2 tetradecamer. Acyldepsipeptide antibiotics of the ADEP class inhibit the growth of Gram-positive firmicutes by activating ClpP and causing unregulated protein degradation. Here we show that, in contrast, mycobacteria are killed by ADEP through inhibition of ClpP function. Although ADEPs can stimulate purified M. tuberculosis ClpP1P2 to degrade larger peptides and unstructured proteins, this effect is weaker than for ClpP from other bacteria and depends on the presence of an additional activating factor (e.g. the dipeptide benzyloxycarbonyl-leucyl-leucine in vitro) to form the active ClpP1P2 tetradecamer. The cell division protein FtsZ, which is a particularly sensitive target for ADEP-activated ClpP in firmicutes, is not degraded in mycobacteria. Depletion of the ClpP1P2 level in a conditional Mycobacterium bovis BCG mutant enhanced killing by ADEP unlike in other bacteria. In summary, ADEPs kill mycobacteria by preventing interaction of ClpP1P2 with the regulatory ATPases, ClpX or ClpC1, thus inhibiting essential ATP-dependent protein degradation.

Introduction

Mycobacterium tuberculosis (MTB), the causative infectious agent of tuberculosis, is a major threat in hospital and community settings worldwide. Mycobacteria are intrinsically resistant to most antimicrobial agents essentially due to their thick, hydrophobic cell wall, with mycolic acids and phthiocerol-lipids, diverse ABC drug exporters and the expression of enzymes that modify antibiotics or their targets (Daffe and Draper, 1998; Buriankova *et al.*, 2004; Louw *et al.*, 2009). Multidrug resistant (MDR) strains of *M. tuberculosis* are already widespread and extensively drug resistant (XDR) as well as totally drug resistant (TDR) strains have emerged (Goldman *et al.*, 2007; Calligaro *et al.*, 2014). Moreover, clinically applied antibiotics only act against actively growing mycobacteria, but not persisters (Robertson *et al.*, 2012; Fattorini *et al.*, 2013), further emphasizing the need for new treatment strategies to target this pathogen (Balganesh *et al.*, 2008).

The *M. tuberculosis* Clp protease complex is an attractive novel target for antitubercular drugs because it is essential for growth and virulence (Sassetti *et al.*, 2003; Schmitt *et al.*, 2011; Griffin *et al.*, 2011; Ollinger *et al.*, 2012; Raju *et al.*, 2012a; Raju *et al.*, 2012b; Vasudevan *et al.*, 2013; Gavrish *et al.*, 2014; Raju *et al.*, 2014). ClpP forms the proteolytic core of the Clp protease complex, with fourteen subunits assembled into two heptameric rings around a spacious chamber that encloses the 14 catalytic triads. Small apical and distal entrance pores of the ClpP tetradecamer restrict access of substrates to the active sites (Alexopoulos *et al.*, 2013; Brötz-Oesterhelt and Sass, 2014; Liu *et al.*, 2014). Thus, ClpP alone is either dormant or limited to the degradation of small peptides (Yu and Houry, 2007; Kress *et al.*, 2009; Molière and Turgay, 2009). For efficient protein degradation, ClpP strictly depends on the assistance of cognate Clp-ATPases, which widen the entrance pores for substrate passage, unfold the proteins and thread them through the pores into the degradation chamber (Lee *et al.*, 2010; Li *et al.*, 2010; Baker and Sauer, 2012).

While most bacterial species possess a single *clpP* gene, mycobacteria encode two copies, *clpP1* and *clpP2*, which are organized in a single operon and are co-transcribed (Cole *et al.*, 1998; Personne *et al.*, 2013). Initial attempts to characterize the MTB ClpP proteins *in vitro* yielded inactive ClpP1 and ClpP2 oligomers of heptameric or lower order (Ingvarsson *et al.*, 2007; Benaroudj *et al.*, 2011) and even

when homo-tetradecamers were obtained (Ingvarsson *et al.*, 2007; Akopian *et al.*, 2012), they did not exhibit any peptidase activity (Akopian *et al.*, 2012). The active form of the enzyme was characterized only after the discovery of particular N-terminally blocked dipeptide activators such as benzyloxycarbonyl-leucyl-leucine (Z-LL) that promote the dissociation of the homo-tetradecamers into heptamers *in vitro* and their re-association into the active mixed ClpP1P2 tetradecamer, which is composed of one ClpP1 and one ClpP2 ring (Akopian *et al.*, 2012). These rings influence each other's conformations, and their interaction is indispensable for both peptidase activity and ATP-dependent degradation of proteins in collaboration with an AAA^+-ATPase (Akopian *et al.*, 2012; Schmitz and Sauer, 2014; Schmitz *et al.*, 2014). *In vivo*, ClpP1P2 functions together with Clp-ATPases ClpC1 or ClpX, both of which are also essential for viability in mycobacteria (Sassetti *et al.*, 2003; Griffin *et al.*, 2011; Gavrish *et al.*, 2014).

Here, we set out to investigate the effects of the novel class of acyldepsipeptide antibiotics called ADEP against mycobacteria in order to evaluate their potential use against this major pathogen. In previous studies, ADEPs have shown substantial antibacterial activity against several Gram-positive pathogens including multidrug-resistant *Staphylococcus aureus in vitro* and in rodent infection models (Brötz-Oesterhelt *et al.*, 2005; Hinzen *et al.*, 2006; Conlon *et al.*, 2013), and even persisters were eradicated by ADEP treatment (Conlon *et al.*, 2013). The mode of action of ADEP is distinct from all other antibiotics and it is important to note that it is based on a dual molecular mechanism (Brötz-Oesterhelt *et al.*, 2005): 1) The binding of ADEP to hydrophobic pockets at the ClpP surface induces a conformational change that widens the gated pores for substrate entry (Kirstein *et al.*, 2009; Lee *et al.*, 2010; Li *et al.*, 2010), thereby allowing uncontrolled ATP-independent degradation of nascent polypeptides and unstructured proteins in the absence of regulatory Clp-ATPases (Kirstein *et al.*, 2009; Conlon *et al.*, 2013); 2) in addition, by binding to these hydrophobic pockets, ADEPs prevent the interaction of ClpP with its regulatory ATPases (Kirstein *et al.*, 2009; Lee *et al.*, 2010), thereby precluding the selective degradation by the Clp protease machinery of its physiological substrates. In firmicutes, where ClpP is not essential for growth under moderate conditions, ADEP-mediated cell death is primarily a consequence of the nonselective degradation of indispensable proteins by activated ClpP alone. One such substrate is the essential

cell division protein FtsZ, which is particularly sensitive to proteolysis by ADEP-activated ClpP in *S. aureus* and *Bacillus subtilis* (Sass *et al.*, 2011). Although inhibition of ClpP's physiological functions probably contributes somewhat to ADEP efficacy against pathogenic firmicutes, (e.g. *Staphylococcus* and *Streptococcus*) in which this protease contributes to virulence (Frees *et al.*, 2014), this mechanism is not the primary cause of cell death and has received little attention.

ADEPs were shown to possess antibacterial activity against *M. tuberculosis* (Ollinger *et al.*, 2012), although the mechanism of ADEP's antitubercular activity was not investigated. We therefore set out to characterize the effects of ADEP on the function of purified *M. tuberculosis* ClpP1 and ClpP2 in the absence and presence of Z-LL using both peptide and protein substrates. In addition, we tackled the question of the primary killing event in mycobacteria. Because a functional Clp protease is essential for viability of *M. tuberculosis* under all conditions, it is *a priori* unclear whether ADEP kills primarily by activating nonselective proteolysis or by blocking the physiological functions of ClpP1P2 and its associated ATPases. To this end, we constructed a conditional *clpP1P2* knock-down strain of *Mycobacterium bovis* BCG Pasteur and determined the growth inhibitory activity of ADEP with different cellular levels of ClpP.

Recently, an independent study was published describing the effects of ADEP on the activity of purified MTB ClpP1P2 as well as the crystal structure of ADEP bound to the active ClpP1P2 tetradecamer (Schmitz *et al.*, 2014). Those observations on the structure of ClpP1P2/ADEP and our present results from substrate degradation assays confirm that ADEP opens the pore for substrate entry. Nonetheless, our findings also indicate that it is not excessive nonspecific protein degradation that kills mycobacteria, but the inability of the Clp protease complex to perform its essential physiological functions in eliminating potentially toxic proteins. A coherent picture of the antibacterial mechanism of ADEPs in mycobacteria has now emerged.

Table 1. MIC determinations (µg ml^{-1}) of ADEP derivatives against mycobacteria and *B. subtilis.*

Strain / Medium	ADEP2	ADEP4	ADEP7	ADEP8	apramycin	isoniazid
Minimal medium						
M. smegmatis mc²155	64	>64	>64	>64	nd	4
M. bovis BCG Pasteur	16 (8)	>64 (16)	>64 (16)	32	1	0.06
M. tuberculosis H37Rv	32 (16)	>64	>64	32	1	nd
7H9 medium						
M. bovis BCG Pasteur	64	>64	>64	32	nd	0.06
Mueller-Hinton broth						
B. subtilis 168 fresh ADEP [a]	0.06	0.13	0.25	0.03	nd	nd
B. subtilis 168 preincubated ADEP [b]	8	1	2	1	nd	nd

Data in brackets represent the concentration where partial growth inhibition was observed.
nd, not determined.
[a] MIC determinations using freshly diluted ADEP2.
[b] MIC determinations using ADEP2, which had been pre-incubated for 9 days in Mueller-Hinton broth.

Results

Antibacterial activity of ADEP against mycobacteria

Moderate activity against *M. tuberculosis* was reported for ADEPs, with ADEP2 being the most active (minimal inhibitory concentration, MIC of 25 µg ml^{-1}) among a small series of congeners tested (Ollinger *et al.*, 2012). We corroborate this result for ADEP2 using a BSA free minimal medium and determined a slightly higher susceptibility for the closely related slow growing *M. bovis* BCG as well as slightly lower susceptibility for the fast-growing *Mycobacterium smegmatis* (Table 1). Broadening the range of ADEP congeners to the ones depicted in figure 1, ADEP2 remained the most active. This finding is notable because ADEP4, which is particularly potent against *S. aureus* and other Gram-positive bacteria (Brötz-Oesterhelt *et al.*, 2005; Conlon *et al.*, 2013), was less effective than ADEP2 against mycobacteria. All ADEP congeners tested so far are less active against mycobacteria than against other Gram-positive bacteria, where MICs were generally in the nanomolar range (Brötz-Oesterhelt *et al.*, 2005; Carney *et al.*, 2014). One reason could be a lower uptake of ADEPs into the mycobacterial cell, as the computer model mycpermcheck (Merget *et al.*, 2013) predicts 0% probability of ADEP passage across the mycobacterial cell wall. In addition, the activity of efflux pumps in *M. tuberculosis* was shown to reduce ADEP2 activity 2 to 4-fold (Ollinger *et al.*, 2012). Alternatively, the cause for the comparably

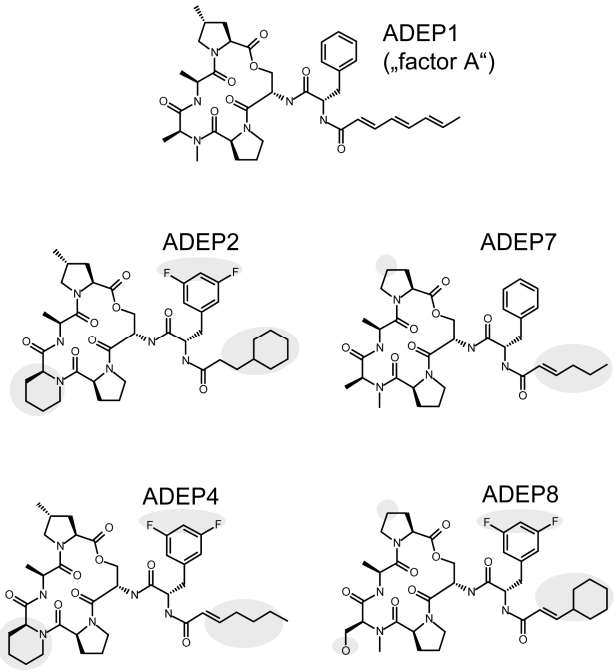

Figure 1. Structure of the natural product ADEP1 and its synthetic congeners used in this study. ADEP1 was originally isolated from a fermentation broth of *Streptomyces hawaiiensis* NRRL 15010 and briefly described as “factor A” in a patent (Michel and Kastner, 1982). The synthetic congeners ADEP2, 4 and 7 have been reported previously (Brötz-Oesterhelt *et al.*, 2005; Hinzen *et al.*, 2006), whereas ADEP8 represents an additional derivative that was synthesized by a previously described procedure (Hinzen *et al.*, 2006). Regions where the synthetic congeners deviate from the natural product ADEP1 are highlighted.

low MIC values of mycobacteria could be a technical problem rather than a physiological difference. While MIC determinations for most bacteria are based on an overnight incubation of cells with the antibiotic, the corresponding assay for slow growing *M. tuberculosis* and *M. bovis* takes 10 days and even for the faster growing *M. smegmatis* still takes 2 days, which demands a certain stability of the antibiotic over time in the medium. In *B. subtilis,* we observed that while freshly dissolved ADEP2 yielded an MIC of 0.06 µg ml^{-1} in the regular overnight assay, pre-incubation of ADEP2 in medium for 9 days prior to performing the same procedure resulted in a MIC of 8 µg ml^{-1} (Table 1). Following the time course of ADEP2 degradation under MIC assay conditions by HPLC revealed the degradation of 75 - 90% ADEP2 within a single day (Fig. S1).

ADEP alone fails to activate purified ClpP1, ClpP2 or mixed ClpP1P2

Assuming that the antibacterial activity of ADEP against mycobacteria is based on ClpP as the target, we performed a series of experiments with purified ClpP1 and ClpP2 of *M. tuberculosis*. First, we investigated, whether ADEP might produce active tetradecamers from purified ClpP1, ClpP2 or a combination of both in the absence of the activating dipeptide Z-LL. Using the fluorogenic peptide substrate benzyloxycarbonyl-Gly-Gly-Leu-7-amino-4-methylcoumarin (Z-GGL-amc), no peptidase activity could be detected during 40 minutes of incubation in the presence of ADEP up to 100 µg ml^{-1}. The experiment was repeated using fluorescein isothiocyanate (FITC)-casein as a model protein substrate, but still no protease activity

was observed with ADEP alone, in clear contrast to the strong stimulation of casein degradation observed with ADEP-activated homo-tetradecameric ClpP proteins from *B. subtilis* and *E. coli* (Kirstein *et al.*, 2009). These differences highlight the unique nature and activation process of MTB ClpP.

ADEP and Z-LL synergistically stimulate peptidase activity of ClpP1P2

We next determined the effect of ADEPs on the peptidase activity of the mixed MTB ClpP1P2 tetradecamer, formed and pre-activated by Z-LL. ClpP1P2 activated by Z-LL alone was able to degrade the fluorogenic peptide substrate Z-GGL-amc (Fig. 2A). Pre-formation and pre-activation of ClpP1P2 by Z-LL was indispensable for ClpP1P2 to show activity in our assays. Consequently, Z-LL pre-treated ClpP1P2 was used in all experiments described below. Nonetheless, several of our collection of ADEP derivatives (Fig. 1) caused a slight but reproducible increase in peptidase activity of Z-LL pre-activated ClpP1P2, with ADEP4, 7, and 8 being the most effective (Fig. 2B).

Next, we tested the degradation of longer peptides, using the “FRETs 25 Xaa peptide library” (Peptides International), which contains a collection of diverse quenched peptides containing 11 amino acids. These fluorogenic peptides were also cleaved by ClpP1P2 and again ADEPs stimulated this process weakly (Fig. 2C and D). We also studied a branched peptide (Buckley *et al.*, 2011) consisting of a hexapeptide core with an N-terminally linked amc moiety and a C-terminal lysine branch (Fig. 2E). ADEPs markedly stimulated degradation of the branched peptide and led to an up to threefold higher degradation rate compared to the situation without antibiotic (Fig. 2F and G) in accord with the established ADEP mechanism of increasing the diameter of ClpP entrance pores.

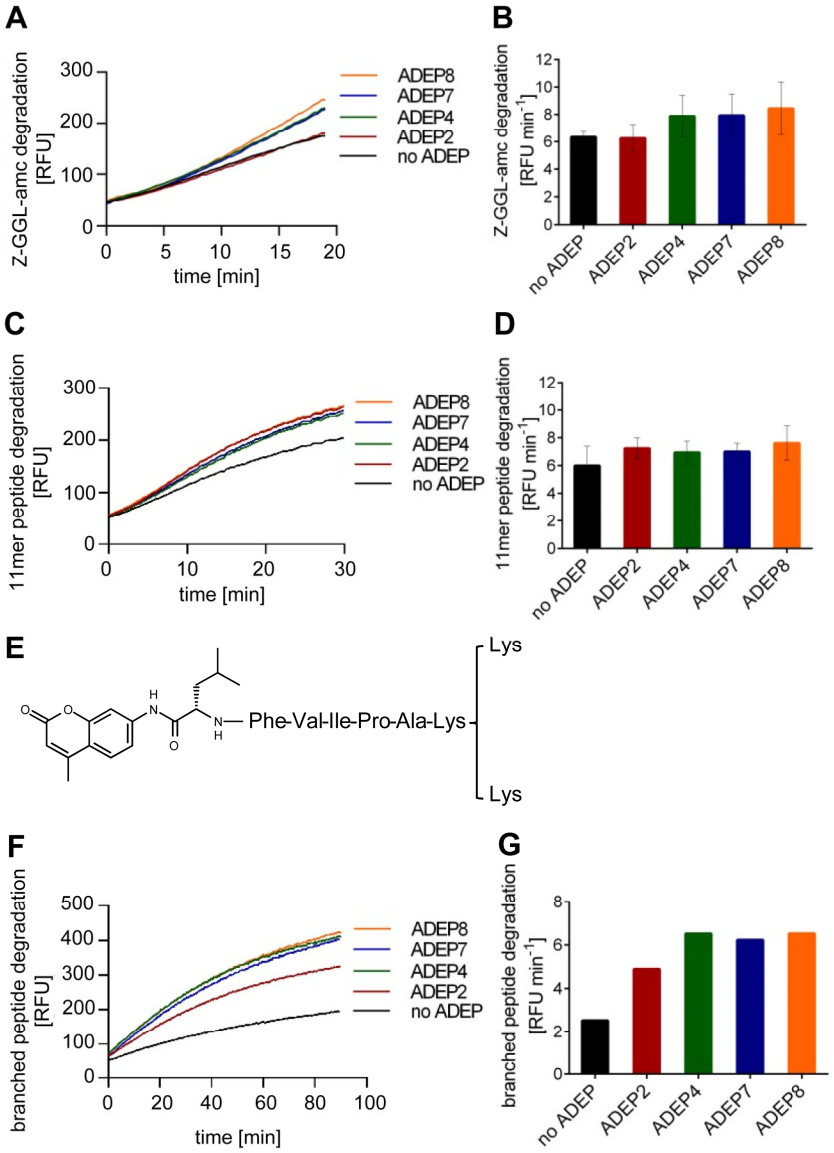

Figure 2. Peptide degradation assays using purified MTB ClpP1P2.
A. Time course of degradation of the tripeptide substrate Z-GGL-amc in the presence of different ADEP derivatives.
B. Reaction rates (increase in relative fluorescence units, RFU, per minute) during the initial linear 5 min of the Z-GGL-amc degradation reaction in A.
C. Time course of degradation of 11-mer peptides from the "FRET 25 Xaa peptide library" in the presence of different ADEP derivatives.
D. Reaction rates (increase in RFU min^{-1}) during the initial linear 5 min of the 11-mer peptide library degradation reaction in C.
E. Chemical structure of the branched peptide used in this study.
F. Time course of degradation of the branched peptide in the presence of different ADEP derivatives. G. Reaction rates (increase in RFU min^{-1}) during the initial linear period (5 min) of enzyme activity in F. All data sets were reproduced in three independent experiments. In A, C, F and G, one representative experiment is shown. B and D show mean values of at least three independent experiments and error bars indicate standard deviations.

Effects of ADEP on protein degradation by ClpP1P2 and its interaction with ClpC1

We next investigated, whether ADEP can also stimulate degradation of the model protein substrate FITC-casein. Addition of ADEPs significantly enhanced this process, with ADEP4, 7 and 8 increasing the degradation rate approximately five-fold and ADEP2 about two-fold (Fig. 3A). The effect of ADEPs was concentration-dependent as exemplified here by ADEP8, which showed half-maximal activation at 25 µM (Fig. 3B). Monitoring the degradation of unlabeled casein by SDS-PAGE confirmed the results of the fluorogenic assay (Fig. 3C). To test whether ADEP-activated ClpP1P2 is also able to degrade other unstructured proteins, we employed the microtubule-associated protein Tau, which is natively unfolded. ADEPs also significantly increased

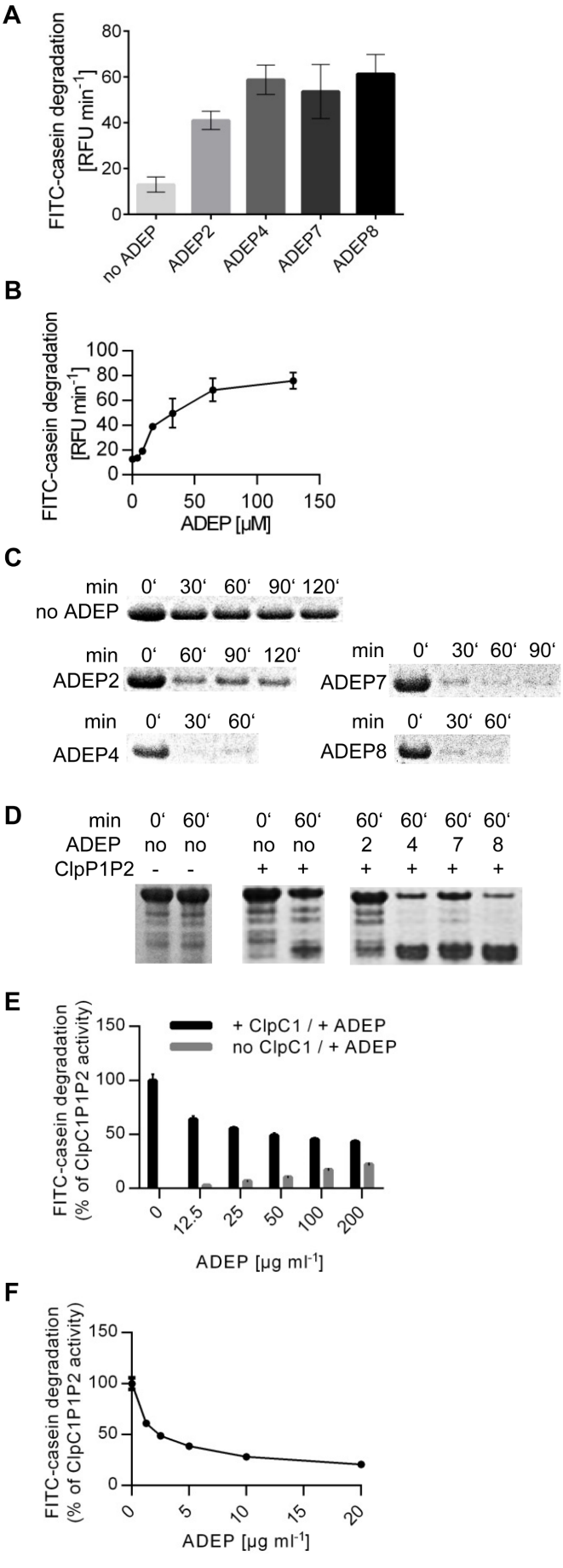

Figure 3. Degradation of unfolded proteins using purified MTB ClpP1P2.
A. FITC-casein degradation rates (increase in RFU min^{-1}) in the presence of ADEP calculated from the initial linear period of enzyme activity (5 min).
B. Reaction rates of FITC-casein degradation at increasing ADEP8 concentrations.
C. Time course of proteolysis of unlabeled casein analyzed by SDS-PAGE.
D. Degradation of the eukaryotic model protein substrate Tau analyzed by SDS-PAGE.
E. FITC-casein degradation by ClpP1P2 in the presence of competing amounts of ClpC1 *versus* ADEP2. Black bars indicate combined activation of ClpP1P2 by ClpC1 and increasing amounts of ADEP. Two-fold molar excess of ClpC1 over ClpP1P2 was kept constant, which in the absence of ADEP ensures efficient ClpC1P1P2 tetradecamer formation. ClpC1P1P2 activity in the absence of ADEP was taken as 100%. Grey bars indicate activating activity of ADEP in the absence of ClpC1 (as determined in parallel reactions).
F. Inhibition of ClpC1P1P2 proteolytic activity by ADEP. Reaction rates for ClpC1P1P2 calculated from the values presented in E. The contribution of ADEP (grey bars in panel E) was subtracted from the combined reaction rates (black bars in panel E). In A, B, E, and F data represents the mean values of three experiments and error bars indicate the respective standard deviations.

the digestion of Tau by ClpP1P2 (Fig. 3D), which, however, caused also some degradation of this substrate alone (Fig. 3D).

The hexameric ATPase ClpC1 *in M. tuberculosis* catalyzes ATP-dependent degradation of casein by ClpP1P2 (Akopian *et al.*, 2012). Although ADEP activated casein hydrolysis by ClpP1P2, it was not as efficient as ClpC1. The degradation rate of casein in the presence of 200 µg ml^{-1} ADEP2 did not exceed 20% of the rate in the presence of ClpC1 (Fig. 3E). This large difference in their stimulatory activities allowed us to

monitor the effect of ADEP on the interaction of ClpC1 with ClpP1P2. Adding ADEP to the ClpC1P1P2 complex in the presence of ATP substantially reduced the degradation of casein. Thus, ADEP competed with ClpC1 for ClpP1P2 binding and blocked ATP-dependent proteolysis (Fig. 3F).

Binding mode of Z-LL to ClpP

Even though we could measure activation of MTB ClpP1P2 by ADEP, the magnitude of stimulation was much lower than with *B. subtilis* ClpP (BS ClpP) (Fig. S2) or as reported for *E. coli* ClpP (Kirstein *et al.*, 2009; Li *et al.*, 2010; Leung *et al.*, 2011). One obvious difference is the presence of Z-LL in the mycobacterial system, which was indispensable for forming the active conformation of the ClpP1P2 tetradecamer. The mechanism of activation of Z-LL and related dipeptides is unclear. As Z-LL is a hydrophobic dipeptide, it could potentially bind to the active sites and interfere with the catalytic activity of MTB ClpP1P2. Alternatively, Z-LL could bind to the hydrophobic ATPase-binding pockets and stimulate in a similar way as ADEP. To distinguish these possibilities directly with MTB ClpP1P2 was not possible *in vitro*, as we did not obtain catalytically active protein in the absence of Z-LL. However, using BS ClpP as a model, we were able to observe an inhibitory effect of Z-LL on catalytic activity. In order to focus on catalysis and to minimize effects of ADEP-mediated pore opening, we measured the hydrolysis of the small fluorogenic peptide substrate *N*-succinyl-Lys-Tyr-amc (suc-LY-amc) by BS ClpP in the presence and absence of either Z-LL or ADEP2, as well as both compounds together. While ADEP2 and Z-LL were non-competitive (Fig. 4A and B), suc-LY-amc and Z-LL showed typical competitive behavior (i.e. nearly constant V_{Max} values and increasing K_M values with increasing Z-LL concentrations) (Fig. 4C and D). Thus, Z-LL binds to the active sites and decreases hydrolysis of the fluorogenic substrate. We further tested whether Z-LL does not only bind, but also may be hydrolyzed by BS ClpP. Our HPLC analyses showed that it is not a substrate, as the amount of Z-LL was not reduced after 3 hours incubation with BS ClpP, under typical assay conditions (Fig. S3). Thus, at concentrations used typically, Z-LL has the potential to interact with the active site but not with the hydrophobic pocket, where ADEPs and Clp-ATPases bind. The question, whether the presence of Z-LL in addition to its special activating function also affects hydrolysis by

MTB ClpP1P2 remains uncertain. These results are in line with the published ClpP1P2-ADEP Z-Ile-Leu crystal structure (Schmitz *et al.*, 2014), and our recent X-ray analysis of MTB ClpP1P2-CBZ-LL (Li *et al.*, 2016), which shows the activating peptide benzoyl-Leu-Leu in all 14 active sites and not in the hydrophobic pockets.

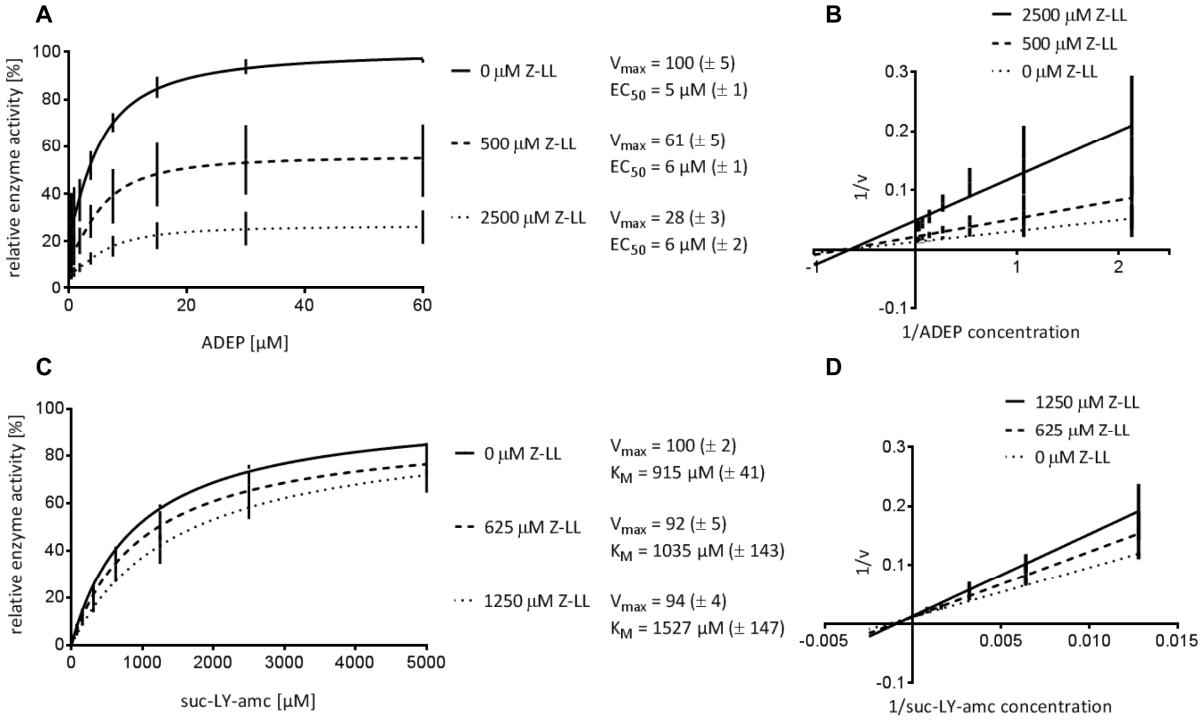

Figure 4. Inhibition of BS ClpP by Z-LL. Z-LL is non-competitive with ADEP (A and B) but competitive with suc-LY-amc (C and D). Mean values of at least three independent experiments are presented. Standard deviations are indicated in brackets. Reaction rates are given in % of the maximum value in the absence of Z-LL. EC_{50} = ADEP concentration where half of the maximum activation is reached. The activating effect of ADEP on peptide hydrolysis by BS ClpP is based on stabilization of the active tetradecameric conformation as reported previously (Lee *et al.*, 2010).

In mycobacteria FtsZ is not degraded in the presence of ADEP

We had previously observed that ADEPs inhibit bacterial cell division in *B. subtilis* and *S. aureus* by stimulating the degradation of the essential cell division protein FtsZ by ClpP (Sass *et al.*, 2011). Therefore, we tested whether ADEPs can activate MTB ClpP1P2 to digest mycobacterial FtsZ (MTB FtsZ). MTB ClpP1P2 alone degraded a small fraction of our MTB FtsZ preparation (Fig. 5A), which might represent a residual amount of insufficiently folded FtsZ protein. However, the presence of ADEPs did not increase degradation further (Fig. 5A, panel 1). By contrast, MTB FtsZ was rapidly and completely hydrolyzed by ADEP-activated BS ClpP in a control sample (Fig. 5A, panel 2), whereas ADEPs could not activate MTB ClpP1P2 to degrade *B. subtilis* FtsZ (BS FtsZ) (Fig. 5A, panel 3). Thus, these results reflect the unique properties of MTB

ClpP1P2 rather than structural differences between the FtsZ proteins from the different species.

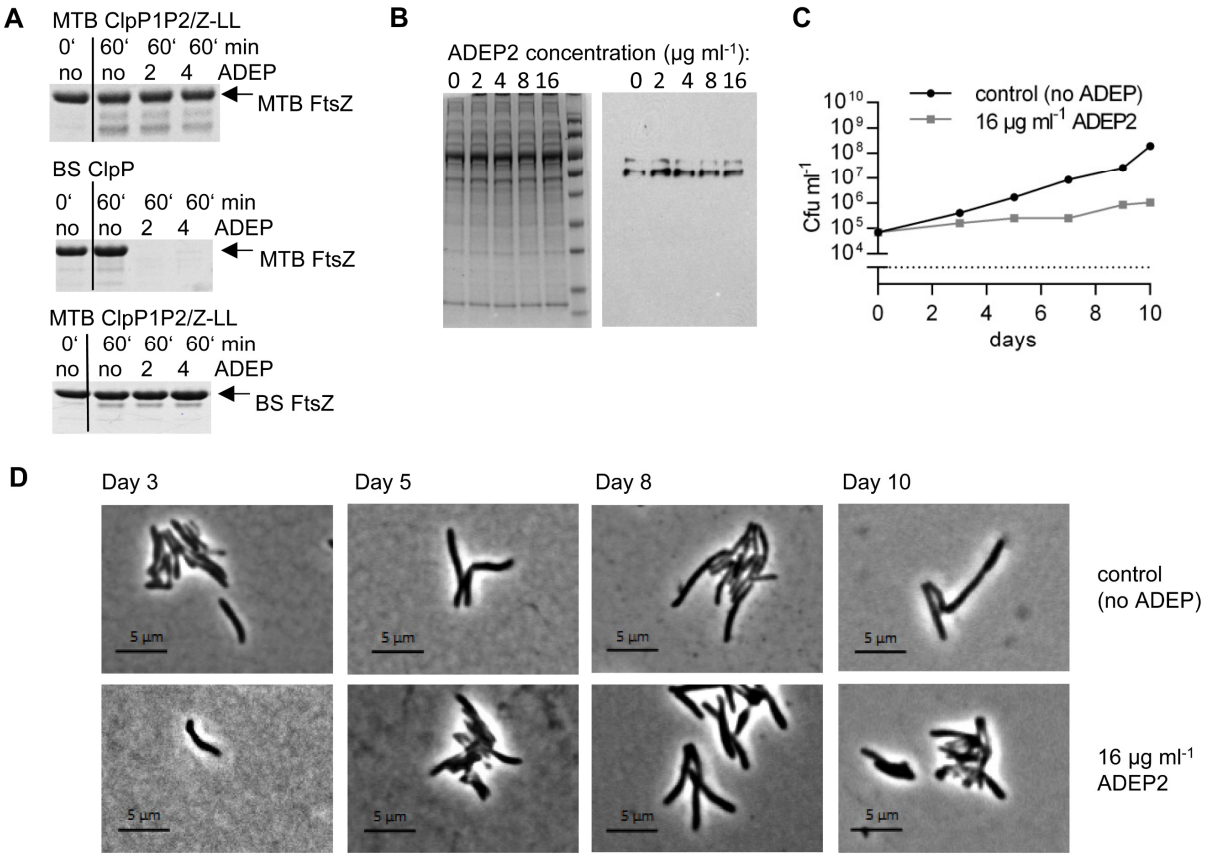

Figure 5. Growth of *M. bovis* BCG is inhibited by ADEP2, but FtsZ is not degraded.
A. *In vitro* degradation of FtsZ from *M. bovis* BCG (MTB FtsZ) or *B. subtilis* 168 (BS FtsZ) with ClpP proteins from *M. tuberculosis* or *B. subtilis* in the absence or presence of ADEP2 and ADEP4.
B. Lysates of *M. bovis* BCG wildtype (wt), grown for 10-12 days in the presence of rising ADEP2 concentrations. SDS page (left), Western blot using an anti-MTB FtsZ antibody (right).
C. Growth curve of *M. bovis* BCG wt in the absence or presence of ADEP2.
D. Phase contrast images of *M. bovis* BCG wt without ADEP (upper lane) or with 16 µg ml^{-1} ADEP2 (lower lane) at distinct points in time.

To make sure that we did not overlook potential effects on MTB FtsZ due to limitations of the *in vitro* assay, we also monitored the FtsZ concentration in ADEP-treated *M. bovis* BCG by Western blotting cell extracts and probing with polyclonal antiserum against MTB FtsZ. At an ADEP2 concentration corresponding to the MIC (16 µg ml^{-1}), FtsZ was present in the extract at the same levels as in untreated controls (Fig. 5B), even though bacterial growth was strongly impaired (Fig. 5C). Because degradation of FtsZ in *B. subtilis* causes filamentation (Sass *et al.*, 2011), we recorded the shape of *M. bovis* BCG in the presence of ADEP2 at different points of the growth curve, but never observed filamented mycobacteria (Fig. 5D). These data further confirm that in mycobacteria, FtsZ is not degraded by ADEP-activated ClpP1P2.

Down-regulation of clpP1P2 expression increases ADEP susceptibility of M. bovis

To focus on the question of the primary killing event in mycobacteria, we constructed the conditional *clpP1P2* knock-down strain *M. bovis* BCG *clpP1-tetoff* (Fig. 6A, S4 and S5) that allows for *clpP1* gene silencing in the presence of anhydrotetracycline (ATc). As shown for *M. tuberculosis*, *clpP1* and *clpP2* are co-transcribed (Personne *et al.*, 2013) and ATc-induced down-regulation of *clpP1* concomitantly silences gene expression of *clpP2* (Raju *et al.*, 2014). The use of *M. bovis* BCG allowed us to avoid the safety containment required for *M. tuberculosis*, while profiting from the particularly high homology between the two species (overall homology 95 - 99%, (Behr *et al.*, 1999)). Of note, *clpP1*, *clpP2*, and *ftsZ* genes as well as the promoter region and operon structure of the bicistronic *clpP1P2* operon show 100% sequence identity between the two species and genes of the AAA^+-ATPases *clpC1* and *clpX* 99%. A concentration as low as 0.1 ng ml^{-1} ATc slowed down the growth rate of the *clpP1-tetoff* strain (Fig. 6B) and at 0.5 ng ml^{-1} ATc the cells were dying (Fig. 6C), confirming that ClpP is also essential in *M. bovis*. In contrast, the growth curve of *M. bovis* wildtype (wt) was not affected at 2 ng ml^{-1} ATc (Fig. 6D) and even 25 ng ml^{-1} did not impede growth of the wildtype strain as indicated by the MIC growth controls (Table 2). Western blot analyses using an anti-ClpP2 antiserum proved that protein levels of ClpP2 were indeed decreased upon addition of ATc in a concentration-dependent manner in the conditional mutant and demonstrated that the ClpP1P2 protein level could be efficiently regulated from a wildtype-like level in the absence of ATc to a considerably reduced level at 0.1 µg ml^{-1} ATc (Fig. 6E). MIC determinations of the *clpP1-tetoff* strain showed that the presence of ATc caused a strong increase in ADEP2 sensitivity (Fig. 6F, 6G and Table 2). This ATc-effect was restricted to ADEP and did not occur with other antibiotics like apramycin or isoniazid, the mechanisms of which are unrelated to ClpP (Table 2). The synergy between ADEP2 and ATc was specific for the *clpP1-tetoff* mutant and was not observed with the wildtype and can, thus, be linked to the reduced ClpP1P2 protein level. Improved activity of an antibacterial agent upon target down-regulation is a widely accepted means of validating that the compound acts through inhibition of a particular target (Chen *et al.*, 2000; Haas *et al.*, 2001; Ji *et al.*, 2004). Consequently, our data reveal 1) that ClpP is the target for ADEP also in mycobacteria and 2) that preventing the essential natural

functions of the ClpP1P2/Clp-ATPase complex by ADEP is responsible for mycobacterial death.

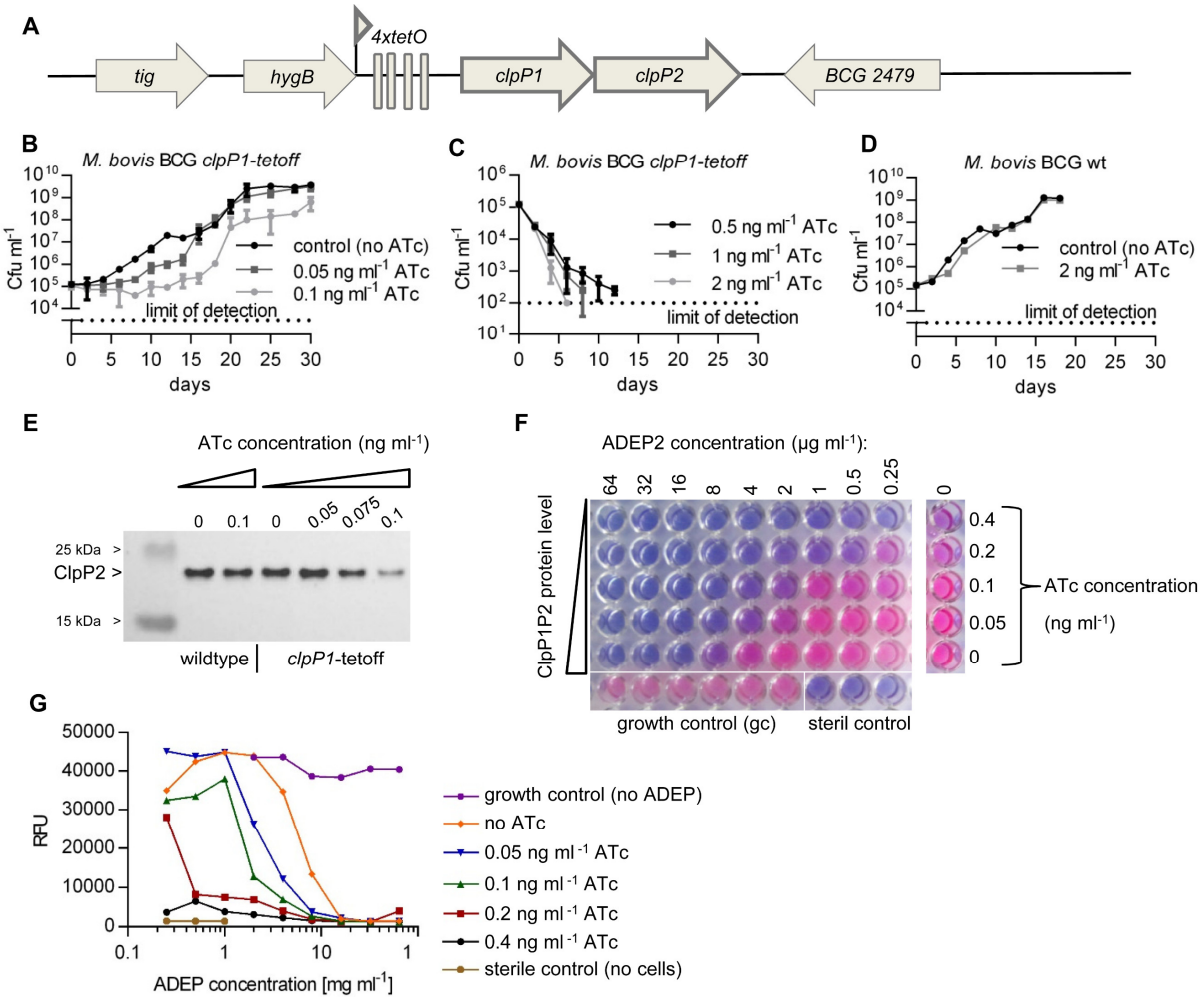

Figure 6. Impact of *clpP1P2* down-regulation on growth and ADEP sensitivity of *M. bovis* BCG.
A. Genomic organization of the *clpP* region in *M. bovis* BCG *clpP1-tetoff*. The original promoter in front of *clpP1* was replaced by the P*myc1* promoter from *M. smegmatis* engineered to contain four *tetO* operator sites. In the presence of anhydrotetracycline (ATc) a Tet-repressor binds to TetO, thereby shutting down transcription of the bicistronic *clpP1P2* operon.
B. and C. Growth of *M. bovis* BCG *clpP1-tetoff* is inhibited with increasing ATc concentrations.
D. Growth of *M. bovis* BCG wildtype (wt) is not affected by ATc.
E. ClpP2 protein levels in *M. bovis* BCG *clpP1-tetoff* compared to wildtype in the absence and presence of increasing ATc concentrations. Immunodetection of ClpP2 with anti-MTB ClpP2 antiserum.
F. Down-regulation of clpP1P2 sensitizes M. bovis BCG clpP1-tetoff to ADEP. Titration of ClpP1P2 protein levels against ADEP2 concentration. Photograph shows the microtiter plate after 10 days of incubation in the presence of ADEP. In living, metabolically active cells the blue, non-fluorescent resazurin dye is reduced to the pink, fluorescent resorufin.
G. Graphical presentation of RFU values of all wells from F. The data show mean values and standard deviations of at least three independent experiments (B, C, D, and E) or one representative experiment of at least three independent biological replicates (F and G).

Our conclusions for mycobacteria became even clearer, when we compared the situation described above with that in *B. subtilis.* Using a conditional *B. subtilis* pX2-*clpP* strain, where *clpP* expression can be regulated by xylose (Gerth *et al.*, 2004) (Fig. S5), we found that in *B. subtilis* – unlike in mycobacteria – down-regulation of

clpP expression led to ADEP resistance (Table 3). In accordance with our previous finding that *B. subtilis* primarily suffers from cell division inhibition due to FtsZ degradation by ADEP-deregulated ClpP (Sass *et al.*, 2011), our current results confirm that in *B. subtilis,* ADEP strictly depends on sufficiently high ClpP levels in order to exert its lethal action. In summary, while in *Bacillus* and other firmicutes (based on our previous data (Sass *et al.*, 2011)), ADEP kills by causing non-specific proteolysis by ClpP, mycobacteria cannot cope with the consequences of ADEP's preventing ClpP1P2 from binding its cognate ATPases, ClpX (Schmitz *et al.*, 2014) and ClpC1 (Fig. 3F).

Table 2. Down-regulation of *clpP1P2* increases susceptibility of *M. bovis* BCG *clpP1-tetoff* to ADEP2.

	no ATc	0.05 ng ml^{-1} ATc	0.1 ng ml^{-1} ATc	0.2 ng ml^{-1} ATc	25 ng ml^{-1} ATc
MIC (µg ml^{-1}) against *M. bovis* BCG *clpP1-tetoff*					
ADEP2	16 (8)	8 (4)	4 (2)	2 (0.5)	no growth
apramycin	1	1	nd	1	no growth
isoniazid	0.03	0.03	0.03	0.03	no growth
MIC (µg ml^{-1}) against *M. bovis* BCG wt					
ADEP2	16	Nd	nd	nd	16
apramycin	1	Nd	nd	nd	1
isoniazid	0.06	Nd	nd	nd	0.06

MIC values against *M. bovis* BCG Pasteur wildtype (wt) and *M. bovis* BCG Pasteur *clpP1-tetoff* in the presence of increasing ATc concentrations. In this conditional system *clpP1P2* expression is suppressed by ATc resulting in decreased ClpP1P2 protein levels (for further information on strain regulation compare figure S5A). For ease of comparison with table 3, data are arranged with decreasing ClpP levels from left to right. Data in brackets represent the concentration where partial growth inhibition was observed. nd, not determined.

Discussion

In this study, we demonstrate that ADEPs target ClpP1P2 of mycobacteria, and exert their antibacterial action by abrogating the interaction between ClpP1P2 and its cognate Clp-ATPases. There are two likely reasons for this unique effect on mycobacteria, one related to the unusual mechanism of activation of ClpP1P2 in mycobacteria and the second related to its essential role in eliminating certain proteins, whose accumulation is toxic.

The enzymatic activation of mycobacterial ClpP proteins is exceptional because it requires the association of a ClpP1 and a ClpP2 ring, while either ClpP variant alone

is inactive, even when present as tetradecamers. Simply mixing ClpP1 and ClpP2 is not sufficient for significant peptidase activity, which *in vitro* was only demonstrable in the presence of N-terminally blocked hydrophobic peptides (such as Z-LL used in this study), related peptides or peptide derivatives (Akopian *et al.*, 2012; Schmitz *et al.*, 2014). It is presently unclear whether *in vivo*, a similar activating peptide, a non-peptidic low molecular weight compound, or an assembly chaperone, serves this essential activating function. In a recent study by Schmitz and Sauer ClpP1P2 activity was also observed when the cognate AAA^+-partner ClpX translocated a folded protein substrate through the pores into the mixed tetradecamer (Schmitz and Sauer, 2014). They suggested that the ATP-driven substrate delivery into the degradation chamber by a bound AAA^+-ATPase provides the necessary stimulus for ClpP1P2 activation in the mycobacterial cell, and that sub-stoichiometric active-site occupancy by substrate peptides stabilizes the active conformation (Schmitz and Sauer, 2014).

In vitro, these two roles, activating and stabilizing, are served by the hydrophobic dipeptides, such as Z-LL used here and previously (Akopian *et al.*, 2012) or Z-IL (Schmitz *et al.*, 2014), at rather high concentrations (1 to 5 mM). Our kinetic measurements demonstrating competitive inhibition of peptide hydrolysis by Z-LL are in accord with the crystal structure of ClpP1P2-ADEP displaying Z-IL within the active sites (Schmitz *et al.*, 2014) and a structure of ClpP1P2 in the presence of benzoyl-LL but without ADEP (Li *et al.*, 2016). It is impressive how occupancy of active sites by Z-LL or related compounds can induce these major conformational changes in ClpP1 and ClpP2. In the present study, the response to ADEP was completely dependent on Z-LL-mediated formation of active ClpP1P2, just as we previously observed with ClpC1, which only stimulated casein degradation in the presence of the dipeptide activator (Akopian *et al.*, 2012). The inability of ADEP to substitute for Z-LL in activating ClpP1P2 is consistent with the fact that in crystal structures ADEPs were never seen within the proteolytic chamber of ClpP (Lee *et al.*, 2010; Li *et al.*, 2010; Schmitz *et al.*, 2014). The antibiotics bind to the hydrophobic pockets at the ClpP periphery in a position, where the subunits join, and where under physiological conditions the I/LGF/L loops of the cognate Clp-ATPases dock. The additivity between activation by Z-LL and ADEP that we observed in our assays indicates that both types of activators serve a different function in MTB ClpP1P2.

Table 3. Down-regulation of *clpP* reduces susceptibility of *B. subtilis* 168-pX2-*clpP* to ADEP2.

	10%	8%	5%	4%	3%	2%	1%	no xylose
ADEP2 MIC (µg ml^{-1}) in LB medium								
B. subtilis 168 wt	0.5	nd	nd	nd	nd	nd	nd	0.5
B. subtilis 168-pX2-*clpP*	0.25	1	4	8	16	16	>32	>32
B. subtilis 168Δ*clpP*	>32	nd	nd	nd	nd	nd	nd	>32
apramycin MIC (µg ml^{-1}) in LB medium								
B. subtilis 168 wt	2	nd	nd	nd	nd	nd	nd	4
B. subtilis 168-pX2-*clpP*	4	4	2	4	2	2	1	2
B. subtilis 168Δ*clpP*	1	nd	nd	nd	nd	nd	nd	2

MIC values against *B. subtilis* 168 wildtype (wt), *B. subtilis* 168-pX2-*clpP* and *B. subtilis* 168*ΔclpP* in the presence of different xylose concentrations. In this conditional system *clpP* expression is induced by xylose (for further information on strain regulation compare figure S5B). For ease of comparison with table 2, data are arranged with decreasing ClpP levels from left to right. nd, not determined.

While ADEP occupied all 14 hydrophobic pockets in the homo-tetradecameric ClpP from *B. subtilis* and *E. coli* (Lee *et al.*, 2010; Li *et al.*, 2010; Schmitz *et al.*, 2014), the antibiotic was only found at ClpP2 in the structure of MTB ClpP1P2 (Lee *et al.*, 2010; Li *et al.*, 2010; Schmitz *et al.*, 2014). Interestingly, even with this partial occupancy at ClpP2 the pores of both rings, ClpP1 and ClpP2, were open (Schmitz *et al.*, 2014). Our findings that ADEP stimulated the degradation of longer and branched peptides as well as of the unstructured proteins casein and Tau by Z-LL activated ClpP1P2 more strongly than the degradation of small peptides is in accordance with such widened pores. However, in the mycobacterial system with its special activation requirements pore opening is not sufficient for ClpP deregulation. ADEPs neither hydrolyze ATP nor actively translocate proteins into the proteolytic chamber. If this ATP-dependent translocation process conducted by the Clp-ATPase partners contributes to activation of ClpP1P2, as proposed by Schmitz and Sauer (Schmitz and Sauer, 2014), then it may explain why ADEPs do not unleash non-specific protein degradation in mycobacteria as they do in firmicutes and proteobacteria. Our observation that ADEPs do not stimulate mycobacterial ClpP1P2 to degrade FtsZ, unlike they do with ClpP from other bacteria (Sass *et al.*, 2011), supports the notion that ADEP does not over-activate mycobacterial ClpP as severely as it does with other ClpP homologs. Although, without proteome analyses, we cannot exclude that other proteins might become targeted and degraded in mycobacteria by deregulated

ClpP1P2/ADEP, especially at elevated ADEP concentrations, our current results exclude this as the primary cause of mycobacterial death.

In mycobacteria ADEP toxicity results primarily from prevention of the physiological functions of the ClpP1P2/Clp-ATPase complex. When ADEP occupies the hydrophobic pockets of ClpP, the Clp-ATPases can no longer bind. Even pre-assembled ClpP/Clp-ATPase complexes were shown to disassemble upon ADEP addition (Kirstein *et al.*, 2009), because of competition between ADEP and the I/LGF/L loops for the same ClpP binding sites. Consequently, ADEP prevents ClpP and Clp-ATPases from interacting to degrade their folded protein substrates. Decreased interaction was described for *B. subtilis* ClpCP and ClpXP, *E. coli* ClpAP and ClpXP (Kirstein *et al.*, 2009; Lee *et al.*, 2010; Leung *et al.*, 2011) as well as for *M. tuberculosis* ClpXP1P2 (Schmitz *et al.*, 2014). Here, we show that ADEPs also block the interaction between ClpC1 and ClpP1P2. While in all bacteria investigated thus far, ADEPs can prevent the Clp-ATPase/peptidase systems from performing their physiological functions, in most species, this does not cause growth defects. For instance, in *B. subtilis clpP* deletion has pleiotropic effects, including impaired sporulation, loss of genetic competence and motility, heat sensitivity and reduced survival in stationary phase (Msadek *et al.*, 1998; Gerth *et al.*, 1998; Gerth *et al.*, 2004), while in *S. aureus* virulence is strongly reduced in the absence of functional ClpP (Frees *et al.*, 2014). However, under moderate growth conditions in rich media, ClpP is dispensable in these firmicutes, although it might rapidly lead to suppressor mutations such as in *spx*, a toxic ClpP substrate in *B. subtilis* (Nakano *et al.*, 2002a; Nakano *et al.*, 2002b).

In contrast, in *M. tuberculosis* all components of the Clp protease machinery, i.e. ClpP1, ClpP2, ClpC1, and ClpX, are essential for growth (Sassetti *et al.*, 2003; Griffin *et al.*, 2011; Ollinger *et al.*, 2012; Raju *et al.*, 2012b) probably by proteolytically preventing the accumulation of global transcription factors and other toxic proteins (Raju *et al.*, 2014). One such important ClpP substrate in mycobacteria is the transcription factor WhiB1, whose accumulation was shown to be lethal to *M. tuberculosis* (Raju *et al.*, 2014). A second likely substrate for ClpP1P2 is CarD (Raju *et al.*, 2014). Although CarD accumulation is not directly lethal, it was shown to play a role in the stringent response controlling rRNA transcription (Stallings *et al.*, 2009) and could, thus, slow down vegetative growth. Evidence that disturbing the function of the Clp protease complex leads to cell death in mycobacteria comes also from the studies

of three cyclic peptide antibiotics, all of which target ClpC1. Cyclomarin, by binding to the ATPase, increased hydrolysis of a model protein in *M. smegmatis* by a still unknown mechanism (Schmitt *et al.*, 2011), while lassomycin (Gavrish *et al.*, 2014) and ecumicin (Gao *et al.*, 2014) were shown to stimulate ATP-hydrolysis by ClpC1, while uncoupling it from protein degradation by ClpP1P2.

In summary, by docking to the hydrophobic pockets of ClpP, the ADEPs 1) release ClpP from its regulatory constraints in e.g. firmicutes, setting ClpP free to work as an independent protease, but 2) they also prevent the physiological functions of the Clp protease system in protein homeostasis, which leads to cell death in species where Clp-mediated proteolysis is essential for viability. The present findings further validate prior indications that mycobacterial ClpP is a promising antitubercular drug target (Schmitt *et al.*, 2011; Akopian *et al.*, 2012; Raju *et al.*, 2012b; Gavrish *et al.*, 2014; Gao *et al.*, 2014) and demonstrate that ClpP1P2 is druggable, i.e. that its function can be blocked by a chemical agent to prevent mycobacterial growth. Development of ADEPs as potential antitubercular agents will require compound optimization including improved stability, solubility, oral bioavailability, and reduced efflux. Our data indicate that among our small collection of congeners, the most potent derivatives against the isolated mycobacterial enzyme (ADEP4, 7 and 8) were inferior to ADEP2 against whole cells. As in most other drug optimization programs, target affinity is only one critical parameter. Reaching sufficient intracellular concentrations is equally important and ADEP2 might have an advantage here due to better uptake or lower efflux compared to the other congeners. In general, ADEPs will probably benefit from the combination approach that is widely used in tuberculosis therapy. Rifampicin, which was shown to act synergistically with ADEP against *S. aureus* (Conlon *et al.*, 2013), is widely used against *M. tuberculosis* and another interesting option could be a combination of ADEP with streptomycin, as down-regulation of *clpP1P2* expression in *M. smegmatis* increased susceptibility against aminoglycosides (Raju *et al.*, 2012b).

Experimental procedures

Bacterial strains and growth conditions

B. subtilis 168 (Anagnostopoulos and Spizizen, 1961), *B. subtilis* Δ*clpP* (Msadek *et al.*, 1998) and *B. subtilis* pX2-*clpP* (Gerth *et al.*, 1998) were cultured in Mueller-Hinton broth or on Mueller-Hinton agar plates at 37 °C. Liquid cultures of *M. smegmatis* mc^2155 (Snapper *et al.*, 1990), *M. tuberculosis* H37Rv, *M. bovis* BCG Pasteur (Institute Pasteur) and *M. bovis* BCG *clpP1-tetoff* (this study) were cultured in 10 ml minimal medium (Yam *et al.*, 2009) at 37 °C and 80 rpm. Selection pressure in *M. bovis* BCG *clpP1-tetoff* was applied by 50 µg ml^{-1} hygromycin B (Roth) and 20 µg ml^{-1} kanamycin (Sigma). Mycobacteria were also cultured on Middlebrook 7H10 (BD) agar plates containing ADS (50 mg ml^{-1} BSA, 8.1 mg ml^{-1} NaCl, 20 mg ml^{-1} glucose) and OADC Enrichment (BD). Agar plates streaked with *M. smegmatis* were incubated for 2 days and agar plates with *M. bovis* BCG and *M. bovis* BCG *clpP1-tetoff* were incubated for 3 weeks and 5 weeks, respectively, at 37 °C and 5% CO_2.

Construction of the conditional M. bovis BCG clpP1-tetoff mutant

For establishing regulated expression of the *clpP1* gene, a synthetic gene cassette (*hyg*-P*myc1*-4x*tetO*; M. Alber and R. Kalscheuer, unpublished results) comprising a hygromycin resistance gene and the P*myc1* promoter from *M. smegmatis* engineered to contain four *tetO* operator sites (serving as the DNA binding sites for the cognate repressor protein TetR) was inserted immediately upstream of the *clpP1* start codon in *M. bovis* BCG Pasteur. Targeted gene knock-in was achieved by specialized transduction employing temperature-sensitive mycobacteriophages essentially as described previously (Bardarov *et al.*, 2002). Briefly, for generation of allelic exchange constructs for site-specific insertion in *M. bovis* BCG of the *hyg*-P*myc1*-4x*tetO* cassette, upstream- and downstream DNA regions flanking the *clpP1* start codon were amplified by PCR employing the primer *clpP1*-F1-fwd and *clpP1*-F1-rev as well as *clpP1*-F2-fwd and *clpP1*-F2-rev (Table S1). Subsequently, the upstream and downstream flanks were digested with the indicated restriction enzymes, and ligated with *Van*91I-digested pcRv1327c-4x*tetO* vector arms (M. Alber and R. Kalscheuer,

unpublished results). The resulting knock-in plasmid was then linearized with *Pac*I and cloned and packaged into the temperature-sensitive phage phAE159 (J. Kriakov and W. R. Jacobs, Jr., unpublished results), yielding a knock-in phage which was propagated in *M. smegmatis* at 30 °C. Allelic exchange in *M. bovis* BCG using the knock-in phage at the non-permissive temperature of 37 °C was achieved by specialized transduction using hygromycin (50 µg ml^{-1}) for selection, resulting in site-specific insertion of the *hyg*-P*myc1*-4x*tetO* cassette (Fig. S4). The obtained BCG knock-in mutant c-*clpP1* was verified by PCR, using the primer pair c-*clpP1*-fwd and c-*clpP1*-rev followed by sequencing of the PCR product with the primer seq-*clpP1*-fwd and seq-*clpP2*-rev. For achieving controlled gene expression of the target gene *clpP1*, a synthetic gene (*rev-tetR*) derived from Tn10 *tetR* encoding a mutated TetR protein with reversed binding affinity to *tetO* sites upon binding of tetracycline (Klotzsche *et al.*, 2009) was heterologously expressed in the knock-in mutant. For this, the *rev-tetR* gene was amplified by PCR employing the primer pair *rev-tetR*-fwd and *rev-tetR*-rev (Table S1) and using the plasmid pTC-28S15-0X (Addgene plasmid 20316) as a template and cloned using the restriction enzymes *Eco*RI and *Hin*dIII into the episomal *E. coli*-mycobacterium shuttle plasmid pMV261-RBS-D, which is a derivative of plasmid pMV261 (Stover *et al.*, 1991) harbouring a mutated ribosome binding site (M. Alber and R. Kalscheuer, unpublished results). The resulting plasmid pMV261::*rev-tetR*-RBS-D providing constitutive gene expression from the HSP60 promoter in mycobacteria was transformed by electroporation into the *M. bovis* BCG c-*clpP1* knock-in mutant using solid medium containing 50 µg ml^{-1} hygromycin and 20 µg ml^{-1} kanamycin for selection. This yielded the conditional mutant BCG c-*clpP1* pMV261::*rev-tetR*-RBS-D (here referred to as *M. bovis* BCG *clpP1-tetoff*).

Growth analyses

M. bovis BCG wt and *M. bovis* BCG *clpP1-tetoff* were grown as described above with increasing ATc concentrations (0, 0.05, 0.075, 0.1, 0.2, 0.5, 1 and 2 ng ml^{-1}). At distinct points in time 30 µl samples were retrieved and serial dilutions were plated on Middlebrook 7H10 plates, containing ADS and OADC. After 3 - 5 weeks incubation at 37 °C and 5% CO_2, colony forming units were counted.

MIC determination

MICs were determined by broth microdilution in 96-well plates using minimal medium (Yam *et al.*, 2009) for mycobacteria and Mueller-Hinton broth (BD) for *B. subtilis*. ADEPs were diluted in DMSO. Isoniazid or apramycin were diluted in H_2O. ADEPs were synthesized as described previously (Hinzen *et al.*, 2006). Colonies of *B. subtilis* 168 or *M. smegmatis* mc^2155 were diluted in 0.9% NaCl and the optical density at 600 nm (OD_{600nm}) was measured.

Pre-cultures of *M. tuberculosis* H37Rv, *M. bovis* BCG wt and *M. bovis* BCG *clpP1-tetoff* were grown as described above, containing either no ATc or 0.1 ng ml^{-1} ATc, until an OD_{600nm} of 0.6 - 1 was reached. All bacteria were diluted in medium to $1x10^5$ cfu ml^{-1} and 50 µl of the inoculum was added per well. The cells were incubated for 9 days (*M. bovis* and *M. tuberculosis*) or 2 days (*M. smegmatis*) at 37 °C and 5% CO_2 followed by addition of resazurin (10 µl; 100 µg ml^{-1}) (AppliChem) and fluorescence measurement (560 nm_{ex}, 600 nm_{em}) at day 10. *B. subtilis* was incubated for 16 - 18 h at 37 °C in ambient air and the MIC was determined as the absence of visible bacterial growth according to CLSI (Clinical and Laboratory Standards Institute) standards (CLSI M07-09, 2012).

Isolation of total RNA

Cultures (10 ml) of *M. bovis* BCG wt or *clpP1-tetoff* (OD_{600nm} 0.7 - 1), both grown either in the absence or in the presence of 0.1 ng ml^{-1} ATc, were pelleted and incubated overnight in 1 ml RNA protect (Qiagen) at room temperature (RT). After storing the samples at -80 °C, RNA was isolated with the RNeasy Kit (Qiagen), including on column DNase I digestion. Further DNA digestion was performed with the Turno DNase (Life Technologies) followed by concentration of the samples with the NucleoSpin RNA Clean-up Kit XS (Macherey-Nagel). Quality and quantity of the RNA were controlled by gel electrophoresis (3% agarose) and by absorption spectra measurements using the Nanodrop spectrophotometer (Thermo Scientific).

Preparation of cell lysates and Western blotting

Cultures of *M. bovis* BCG (8 ml, OD_{600nm} 0.7 - 1) was pelleted and lysed in 500 µl PBS buffer containing 0.05% Tween 80 and glass beads (150 - 212 µm, Sigma-Aldrich) using the Precellys 24 homogenizer (Belkin/Peqlab). Protein concentration of the lysate was determined by measuring the absorbance at 280 nm using the Nanodrop spectrophotometer. Lysates were diluted, mixed with 4x LDS sample buffer (Thermo Scientific) and incubated for 10 min at 99 °C. Equal protein concentrations of all lysates were confirmed by SDS-PAGE. Proteins were transferred to an Amersham Hybond-ECL membrane (GE Healthcare) via semi-dry blotting. The membrane was incubated with polyclonal antiserum against FtsZ (Dziadek *et al.*, 2002) or ClpP2 of *M. tuberculosis* followed by incubation with anti-rabbit IgG horse radish peroxidase-linked antibody (Cell signaling) as secondary antibody. Detection was performed with Amersham ECL prime western blotting detection reagent (GE Healthcare).

Protein expression and purification

MTB ClpP1 and MTB ClpP2 were expressed separately in *M. smegmatis* mc²155 and purified as previously described (Akopian *et al.*, 2012). BS ClpP and BS FtsZ were expressed in *E. coli* and were purified as described earlier (Sass *et al.*, 2011). MTB Fts*Z* was cloned via *Nco*I and *Hin*dIII restriction sites into the IPTG-inducible expression vector pET22bΔ*pelB* (Sass and Bierbaum, 2007) and was expressed in *E. coli* BL21 (DE3) with a C-terminal 6xHis tag. Genomic DNA from *M. bovis* BCG was used as PCR template, as the *ftsZ* gene of this non-pathogenic model organism shows 100% nucleotide sequence identity to *ftsZ* of *M. tuberculosis*. MTB *ftsZ*-fwd and MTB *ftsZ*-rev (Table S1) served as primers. Protein expression was induced at an OD_{600} of 0.6 with 1 mM IPTG for 5 h at 37 °C. Cells were lysed in 50 mM NaH_2PO_4, 300 mM NaCl, 10 mM imidazole, pH 8 using a French Press. FtsZ-His6 was purified by Ni-NTA column chromatography and eluted with 50 mM NaH_2PO_4, 300 mM NaCl, 250 mM imidazole. For storage 5% glycerol was added to the eluate.

Formation of the MTB ClpP1P2 tetradecamer

For the formation of catalytically active MTB ClpP1P2, equal volumes of MTB ClpP1 and MTB ClpP2 were mixed with 5 mM Z-LL and were then incubated for 4 h at RT. After confirming peptidase activity, the active enzyme was stored at 4 °C.

Degradation of fluorescent peptides and proteins

Degradation assays were performed in 96-well plates as previously described (Akopian *et al.*, 2012). For short peptide substrates, 0.1 mM Z-GGL-amc or 0.1 mM suc-LY-amc (Enzo life science, USA) were used with 1.5 µg ml^{-1} MTB ClpP1P2. For more complex peptide model substrates, 10 µM of the three-generation peptides were used with 0.8 µg ml^{-1} MTB ClpP1P2. Fluorescence of amc was measured in a SpectraMax M5 plate reader (Molecular Devices) at 380 nm_{ex} and 460 nm_{em}. As protein substrate, 4 µg ml^{-1} FITC-casein (Mobitec) was employed with either 6.25 µg ml^{-1} MTB ClpP1P2 or 2 µg ml^{-1} BS ClpP. Here, fluorescence was measured at 492 nm_{ex} and 518 nm_{em}. All assays were performed in 80 µl buffer A (50 mM phosphate buffer, pH 7.6; 100 mM KCl, 5% glycerol). Z-LL was used at a concentration of 5 mM. If not indicated otherwise ADEP was applied at 100 µg ml^{-1}.

Competitive assays with BS ClpP

To investigate potential kinetic interactions between Z-LL and either peptide substrate or ADEP we used BS ClpP and suc-LY-amc in 96-well plates with 3 µM BS ClpP-His6 in a previously described activity buffer (50 mM TrisHCl, pH8; 100 mM KCl, 25 mM $MgCl_2$, 2 mM DTT) (Turgay *et al.*, 1998). To study Z-LL in competition with a substrate, mixtures were prepared in activity buffer containing 0, 500 or 2500 µM Z-LL, each supplemented with a constant amount of 3 µM BS ClpP. A serial dilution of suc-LY-amc with final concentrations ranging from 0 - 5000 µM was added to start the reaction. To study Z-LL together with ADEP2 a serial dilution of ADEP2 with final concentrations ranging from 0 - 60 µM was mixed with a constant amount of 3 µM BS ClpP in activity buffer. Premixes of 0, 500 or 2500 µM Z-LL and a constant amount of 30 µM of suc-LY-amc were added to start the reaction. Fluorescence was measured using the

Infinite M200pro plate reader (Tecan) with 380 nm_{ex} and 430 nm_{em}. The data was analyzed via Michaelis Menten fittings using Graph Pad Prism software.

Degradation of unlabeled protein substrates

Degradation assays with unlabeled proteins were performed using either 6.25 µg ml^{-1} MTB ClpP1P2 or 2 µg ml^{-1} BS ClpP in 30 µl of buffer A as described above. As substrates, 8 µg ml^{-1} Tau, 7.5 µg ml^{-1} FtsZ, or 7.5 µg ml^{-1} casein were used. Samples were incubated for 30 - 120 min at 37 °C in the absence or presence of 50 µg ml^{-1} ADEP before stopping the reaction with 4x LDS sample buffer 5.0. The degradation of substrates was analyzed by SDS-PAGE.

HPLC analyses

To determine Z-LL stability in the presence of ClpP, Z-LL (1 mM) was incubated with 3 µM BS ClpP in 1 ml activity buffer at 37 °C. Immediately and after 3 h aliquots of 50 µl were analyzed using a 1100 series HPLC (Agilent) with an EC 250/3 Nucleodur C18 HTec column of 5 µm diameter (Macherey-Nagel) and the following gradient of methanol (solvent A) and water (solvent B): 0 - 10 min 10% solvent A; 10 - 40 min 10 to 100% solvent A; 40 - 50 min 100% solvent A. To determine ADEP stability in aqueous culture broth over time, 16 µg ml^{-1} ADEP2 was incubated in 2 ml minimal medium (Yam *et al.*, 2009) for 10 days at 37 °C. At distinct points in time 100 µl aliquots were analyzed via HPLC using the following gradient of methanol (solvent A) and water (solvent B): 0 - 5 min 0% solvent A; 5 - 10 min 0 to 60% solvent A; 10 - 40 min 60 to 100% solvent A; 40 - 50 min 100% solvent A. The data was analyzed via ChemStation software (Agilent).

Acknowledgements

We thank Anne Wochele for expert technical assistance. We are grateful to Holger Paulsen and Siegfried Raddatz (Bayer Pharma AG, Wuppertal) for ADEP synthesis, to Craig M. Crews (Yale University, New Haven) for providing the branched peptide, to Eckhard Mandelkow (DESY, Hamburg) for sharing Tau protein, to Malini

Rajagopalan (University of Texas Health Science Center) for providing the polyclonal antiserum against MTB FtsZ, to D. Schnappinger (Weill Cornell Medical College, NY) for sharing plasmid pTC-28S15-0X, and to U. Gerth (University of Greifswald) for providing pX2-*clpP*. This work was supported by a grant of the German Research Foundation (DFG; FOR854, BR 3783/1-2) to H.B.O. and P.S. and by a grant of the Jürgen Manchot Foundation to R.K. H.R.S. reports holding stock options in AiCuris; all other authors declare no competing financial interests.

References

Akopian, T., Kandror, O., Raju, R.M., Unnikrishnan, M., Rubin, E.J., and Goldberg, A.L. (2012) The active ClpP protease from M. tuberculosis is a complex composed of a heptameric ClpP1 and a ClpP2 ring. EMBO J 31: 1529-1541.

Alexopoulos, J., Ahsan, B., Homchaudhuri, L., Husain, N., Cheng, Y.Q., and Ortega, J. (2013) Structural determinants stabilizing the axial channel of ClpP for substrate translocation. Mol Microbiol 90: 167-180.

Anagnostopoulos, C., and Spizizen, J. (1961) Requirements for transformation in Bacillus subtilis. J Bacteriol 81: 741-746.

Baker, T.A., and Sauer, R.T. (2012) ClpXP, an ATP-powered unfolding and protein-degradation machine. Biochim Biophys Acta 1823: 15-28.

Balganesh, T.S., Alzari, P.M., and Cole, S.T. (2008) Rising standards for tuberculosis drug development. Trends Pharmacol Sci 29: 576-581.

Bardarov, S., Bardarov Jr S Jr, Pavelka Jr, M.S.J., Sambandamurthy, V., Larsen, M., Tufariello, J. *et al.* (2002) Specialized transduction: an efficient method for generating marked and unmarked targeted gene disruptions in Mycobacterium tuberculosis, M. bovis BCG and M. smegmatis. Microbiology 148: 3007-3017.

Behr, M.A., Wilson, M.A., Gill, W.P., Salamon, H., Schoolnik, G.K., Rane, S., and Small, P.M. (1999) Comparative genomics of BCG vaccines by whole-genome DNA microarray. Science 284: 1520-1523.

Benaroudj, N., Raynal, B., Miot, M., and Ortiz-Lombardia, M. (2011) Assembly and proteolytic processing of mycobacterial ClpP1 and ClpP2. BMC Biochem 12: 61.

Brötz-Oesterhelt, H., Beyer, D., Kroll, H.P., Endermann, R., Ladel, C., Schroeder, W. *et al.* (2005) Dysregulation of bacterial proteolytic machinery by a new class of antibiotics. Nat Med 11: 1082-1087.

Brötz-Oesterhelt, H., and Sass, P. (2014) Bacterial caseinolytic proteases as novel targets for antibacterial treatment. Int J Med Microbiol 304: 23-30.

Buckley, D.L., Corson, T.W., Aberle, N., and Crews, C.M. (2011) HIV protease-mediated activation of sterically capped proteasome inhibitors and substrates. J Am Chem Soc 133: 698-700.

Buriankova, K., Doucet-Populaire, F., Dorson, O., Gondran, A., Ghnassia, J.C., Weiser, J., and Pernodet, J.L. (2004) Molecular basis of intrinsic macrolide resistance in the Mycobacterium tuberculosis complex. Antimicrob Agents Chemother 48: 143-150.

Calligaro, G.L., Moodley, L., Symons, G., and Dheda, K. (2014) The medical and surgical treatment of drug-resistant tuberculosis. J Thorac Dis 6: 186-195.

Carney, D.W., Schmitz, K.R., Truong, J.V., Sauer, R.T., and Sello, J.K. (2014) Restriction of the conformational dynamics of the cyclic acyldepsipeptide antibiotics improves their antibacterial activity. J Am Chem Soc 136: 1922-1929.

Chen, D.Z., Patel, D.V., Hackbarth, C.J., Wang, W., Dreyer, G., Young, D.C. *et al.* (2000) Actinonin, a naturally occurring antibacterial agent, is a potent deformylase inhibitor. Biochemistry 39: 1256-1262.

CLSI M07-09 (2012) Methods for dilution antimicrobial susceptibility tests for bacteria that grow; approved standard - ninth edition.

Cole, S.T., Brosch, R., Parkhill, J., Garnier, T., Churcher, C., Harris, D. *et al.* (1998) Deciphering the biology of Mycobacterium tuberculosis from the complete genome sequence. Nature 393: 537-544.

Conlon, B.P., Nakayasu, E.S., Fleck, L.E., LaFleur, M.D., Isabella, V.M., Coleman, K. *et al.* (2013) Activated ClpP kills persisters and eradicates a chronic biofilm infection. Nature 503: 365-370.

Daffe, M., and Draper, P. (1998) The envelope layers of mycobacteria with reference to their pathogenicity. Adv Microb Physiol 39: 131-203.

Dziadek, J., Madiraju, M.V., Rutherford, S.A., Atkinson, M.A., and Rajagopalan, M. (2002) Physiological consequences associated with overproduction of Mycobacterium tuberculosis FtsZ in mycobacterial hosts. Microbiology 148: 961-971.

Fattorini, L., Piccaro, G., Mustazzolu, A., and Giannoni, F. (2013) Targeting dormant bacilli to fight tuberculosis. Mediterr J Hematol Infect Dis 5: e2013072.

Frees, D., Gerth, U., and Ingmer, H. (2014) Clp chaperones and proteases are central in stress survival, virulence and antibiotic resistance of Staphylococcus aureus. Int J Med Microbiol 304: 142-149.

Gao, W., Kim, J.Y., Chen, S.N., Cho, S.H., Choi, J., Jaki, B.U. *et al.* (2014) Discovery and characterization of the tuberculosis drug lead ecumicin. Org Lett 16 (23): 6044-6047.

Gavrish, E., Sit, C.S., Cao, S., Kandror, O., Spoering, A., Peoples, A. *et al.* (2014) Lassomycin, a ribosomally synthesized cyclic peptide, kills mycobacterium tuberculosis by targeting the ATP-dependent protease ClpC1P1P2. Chem Biol 21: 509-518.

Gerth, U., Kirstein, J., Mostertz, J., Waldminghaus, T., Miethke, M., Kock, H., and Hecker, M. (2004) Fine-tuning in regulation of Clp protein content in Bacillus subtilis. J Bacteriol 186: 179-191.

Gerth, U., Kruger, E., Derre, I., Msadek, T., and Hecker, M. (1998) Stress induction of the Bacillus subtilis clpP gene encoding a homologue of the proteolytic component of the Clp protease and the involvement of ClpP and ClpX in stress tolerance. Mol Microbiol 28: 787-802.

Goldman, R.C., Plumley, K.V., and Laughon, B.E. (2007) The evolution of extensively drug resistant tuberculosis (XDR-TB): history, status and issues for global control. Infect Disord Drug Targets 7: 73-91.

Griffin, J.E., Gawronski, J.D., Dejesus, M.A., Ioerger, T.R., Akerley, B.J., and Sassetti, C.M. (2011) High-resolution phenotypic profiling defines genes essential for mycobacterial growth and cholesterol catabolism. PLOS Pathog 7: e1002251.

Haas, M., Beyer, D., Gahlmann, R., and Freiberg, C. (2001) YkrB is the main peptide deformylase in Bacillus subtilis, a eubacterium containing two functional peptide deformylases. Microbiology 147: 1783-1791.

Hinzen, B., Raddatz, S., Paulsen, H., Lampe, T., Schumacher, A., Häbich, D. *et al.* (2006) Medicinal chemistry optimization of acyldepsipeptides of the enopeptin class antibiotics. ChemMedChem 1: 689-693.

Ingvarsson, H., Mate, M.J., Hogbom, M., Portnoi, D., Benaroudj, N., Alzari, P.M. *et al.* (2007) Insights into the inter-ring plasticity of caseinolytic proteases from the X-ray structure of Mycobacterium tuberculosis ClpP1. Acta Crystallogr D Biol Crystallogr 63: 249-259.

Ji, Y., Yin, D., Fox, B., Holmes, D.J., Payne, D., and Rosenberg, M. (2004) Validation of antibacterial mechanism of action using regulated antisense RNA expression in Staphylococcus aureus. FEMS Microbiol Lett 231: 177-184.

Kirstein, J., Hoffmann, A., Lilie, H., Schmidt, R., Rübsamen-Waigmann, H., Brötz-Oesterhelt, H. *et al.* (2009) The antibiotic ADEP reprogrammes ClpP, switching it from a regulated to an uncontrolled protease. EMBO Mol Med 1: 37-49.

Klotzsche, M., Ehrt, S., and Schnappinger, D. (2009) Improved tetracycline repressors for gene silencing in mycobacteria. Nucleic Acids Res 37: 1778-1788.

Kress, W., Maglica, Z., and Weber-Ban, E. (2009) Clp chaperone-proteases: structure and function. Res Microbiol 160: 618-628.

Lee, B.G., Park, E.Y., Lee, K.E., Jeon, H., Sung, K.H., Paulsen, H. *et al.* (2010) Structures of ClpP in complex with acyldepsipeptide antibiotics reveal its activation mechanism. Nat Struct Mol Biol 17: 471-478.

Leung, E., Datti, A., Cossette, M., Goodreid, J., McCaw, S.E., Mah, M. *et al.* (2011) Activators of cylindrical proteases as antimicrobials: identification and development of small molecule activators of ClpP protease. Chem Biol 18: 1167-1178.

Li, D.H., Chung, Y.S., Gloyd, M., Joseph, E., Ghirlando, R., Wright, G.D. *et al.* (2010) Acyldepsipeptide antibiotics induce the formation of a structured axial channel in ClpP: A model for the ClpX/ClpA-bound state of ClpP. Chem Biol 17: 959-969.

Li, M., Kandror, O., Akopian, T., Dharkar, P., Wlodawer, A., Maurizi, M.R., and Goldberg, A.L. (2016) Structure and functional properties of the active form of the proteolytic complex, ClpP1P2, from Mycobacterium tuberculosis. J. Biol. Chem. doi/10.1074/jbc.M115.700344.

Liu, K., Ologbenla, A., and Houry, W.A. (2014) Dynamics of the ClpP serine protease: A model for self-compartmentalized proteases. Crit Rev Biochem Mol Biol 49: 400-412.

Livak, K.J., and Schmittgen, T.D. (2001) Analysis of relative gene expression data using real-time quantitative PCR and the 2(-Delta C(T)) Method. Methods 25: 402-408.

Louw, G.E., Warren, R.M., Gey van Pittius, N.C., McEvoy, C.R., van Helden, P.D., and Victor, T.C. (2009) A balancing act: efflux/influx in mycobacterial drug resistance. Antimicrob Agents Chemother 53: 3181-3189.

Merget, B., Zilian, D., Muller, T., and Sotriffer, C.A. (2013) MycPermCheck: the Mycobacterium tuberculosis permeability prediction tool for small molecules. Bioinformatics 29: 62-68.

Michel, K.H., and Kastner, R.E. (1982) A54556 antibiotics and process for production thereof. US patent 4492650.

Molière, N., and Turgay, K. (2009) Chaperone-protease systems in regulation and protein quality control in Bacillus subtilis. Res Microbiol 160: 637-644.

Msadek, T., Dartois, V., Kunst, F., Herbaud, M.L., Denizot, F., and Rapoport, G. (1998) ClpP of Bacillus subtilis is required for competence development, motility, degradative enzyme synthesis, growth at high temperature and sporulation. Mol Microbiol 27: 899-914.

Nakano, M.M., Nakano, S., and Zuber, P. (2002a) Spx (YjbD), a negative effector of competence in Bacillus subtilis, enhances ClpC-MecA-ComK interaction. Mol Microbiol 44: 1341-1349.

Nakano, S., Zheng, G., Nakano, M.M., and Zuber, P. (2002b) Multiple pathways of Spx (YjbD) proteolysis in Bacillus subtilis. J Bacteriol 184: 3664-3670.

Nde, C.W., Toghrol, F., Jang, H.J., and Bentley, W.E. (2011) Toxicogenomic response of Mycobacterium bovis BCG to peracetic acid and a comparative analysis of the M. bovis BCG response to three oxidative disinfectants. Appl Microbiol Biotechnol 90: 277-304.

Ollinger, J., O'Malley, T., Kesicki, E.A., Odingo, J., and Parish, T. (2012) Validation of the essential ClpP protease in Mycobacterium tuberculosis as a novel drug target. J Bacteriol 194: 663-668.

Personne, Y., Brown, A.C., Schuessler, D.L., and Parish, T. (2013) Mycobacterium tuberculosis ClpP proteases are co-transcribed but exhibit different substrate specificities. PLoS One 8: e60228.

Raju, R.M., Goldberg, A.L., and Rubin, E.J. (2012a) Bacterial proteolytic complexes as therapeutic targets. Nat Rev Drug Discov 11: 777-789.

Raju, R.M., Jedrychowski, M.P., Wei, J.R., Pinkham, J.T., Park, A.S., O'Brien, K. *et al.* (2014) Post-translational regulation via Clp protease is critical for survival of Mycobacterium tuberculosis. PLOS Pathog 10: e1003994.

Raju, R.M., Unnikrishnan, M., Rubin, D., Krishnamoorthy, V., Kandror, O., Akopian, T. *et al.* (2012b) Mycobacterium tuberculosis ClpP1 and ClpP2 function together in protein degradation and are required for viability in vitro and during infection. PLOS Pathog 8 (2): e1002511.

Robertson, B.D., Altmann, D., Barry, C., Bishai, B., Cole, S., Dick, T. *et al.* (2012) Detection and treatment of subclinical tuberculosis. Tuberculosis (Edinb) 92: 447-452.

Sass, P., and Bierbaum, G. (2007) Lytic activity of recombinant bacteriophage phi11 and phi12 endolysins on whole cells and biofilms of Staphylococcus aureus. Appl Environ Microbiol 73: 347-352.

Sass, P., Josten, M., Famulla, K., Schiffer, G., Sahl, H.G., Hamoen, L., and Brötz-Oesterhelt, H. (2011) Antibiotic acyldepsipeptides activate ClpP peptidase to degrade the cell division protein FtsZ. Proc Natl Acad Sci U S A 108: 17474-17479.

Sassetti, C.M., Boyd, D.H., and Rubin, E.J. (2003) Genes required for mycobacterial growth defined by high density mutagenesis. Mol Microbiol 48: 77-84.

Schmitt, E.K., Riwanto, M., Sambandamurthy, V., Roggo, S., Miault, C., Zwingelstein, C. *et al.* (2011) The natural product cyclomarin kills Mycobacterium tuberculosis by targeting the ClpC1 subunit of the caseinolytic protease. Angew Chem Int Ed Engl 50: 5889-5891.

Schmitz, K.R., Carney, D.W., Sello, J.K., and Sauer, R.T. (2014) Crystal structure of Mycobacterium tuberculosis ClpP1P2 suggests a model for peptidase activation by AAA+ partner binding and substrate delivery. Proc Natl Acad Sci U S A 111: E4587-E4595.

Schmitz, K.R., and Sauer, R.T. (2014) Substrate delivery by the AAA+ ClpX and ClpC1 unfoldases activates the mycobacterial ClpP1P2 peptidase. Mol Microbiol 93: 617-628.

Snapper, S.B., Melton, R.E., Mustafa, S., Kieser, T., and Jacobs, Jr.W.R. (1990) Isolation and characterization of efficient plasmid transformation mutants of Mycobacterium smegmatis. Mol Microbiol 4: 1911-1919.

Stallings, C.L., Stephanou, N.C., Chu, L., Hochschild, A., Nickels, B.E., and Glickman, M.S. (2009) CarD is an essential regulator of rRNA transcription required for Mycobacterium tuberculosis persistence. Cell 138: 146-159.

Stover, C.K., de la Cruz, V.F., Fuerst, T.R., Burlein, J.E., Benson, L.A., Bennett, L.T. *et al.* (1991) New use of BCG for recombinant vaccines. Nature 351: 456-460.

Turgay, K., Hahn, J., Burghoorn, J., and Dubnau, D. (1998) Competence in Bacillus subtilis is controlled by regulated proteolysis of a transcription factor. EMBO J 17: 6730-6738.

Vasudevan, D., Rao, S.P., and Noble, C.G. (2013) Structural basis of mycobacterial inhibition by cyclomarin A. J Biol Chem 288: 30883-30891.

Yam, K.C., D'Angelo, I., Kalscheuer, R., Zhu, H., Wang, J.X., Snieckus, V. *et al.* (2009) Studies of a ring-cleaving dioxygenase illuminate the role of cholesterol metabolism in the pathogenesis of Mycobacterium tuberculosis. PLOS Pathog 5: e1000344.

Yu, A.Y., and Houry, W.A. (2007) ClpP: a distinctive family of cylindrical energy-dependent serine proteases. FEBS Lett 581: 3749-3757.

Chapter 2

AAA+ chaperones and acyldepsipeptides activate the ClpP protease via conformational control

Malte Gersch[1,*], Kirsten Famulla[2,*], Maria Dahmen[1], Christoph Göbl[1,3], Imran Malik[2], Klaus Richter[1], Vadim s. Korotkov[1], Peter Sass[2], Helga Rübsamen-Schaeff[4], Tobias Madl[1,3,5], Heike Brötz-Oesterhelt[2,§] & Stephan A. Sieber[1,§]

[1]Department of Chemistry and Center for Integrated Protein Science Munich (CIPSM), Technische Universität München, Lichtenbergstraße 4, 85748 Garching, Germany. [2]Institute for Pharmaceutical Biology and Biotechnology, University of Düsseldorf, Universitätsstraße 1, 40225 Düsseldorf, Germany. [3]Institute of Structural Biology, Helmholtz Zentrum München, 85764 Neuherberg, Germany. [4]AiCuris GmbH & Co. KG, Friedrich-Ebert-Straße 475, 42117 Wuppertal, Germany. [5]Institute of Molecular Biology & Biochemistry, Center of Molecular Medicine, Medical University of Graz, 8010 Graz, Austria. *These authors contributed equally to this work. § These authors jointly supervised this work. Correspondence and requests for materials should be addressed to H.B.-O. (email: heike.broetz-oesterhelt@uni-tuebingen.de) or to S.A.S. (email: Stephan.sieber@mytum.de).

Gersch, M. *et al*. AAA+ chaperones and acyldepsipeptides activate the ClpP protease via conformational control. *Nat. Commun.* 6:6320 doi: 10.1038/ncomms7320 (2015).

Abstract

The Clp protease complex degrades a multitude of substrates, which are engaged by a AAA+ chaperone such as ClpX and subsequently digested by the dynamic, barrel-shaped ClpP protease. Acyldepsipeptides (ADEPs) are natural product-derived antibiotics that activate ClpP for chaperone-independent protein digestion. Here we show that both protein and small-molecule activators of ClpP allosterically control the ClpP barrel conformation. We dissect the catalytic mechanism with chemical probes and show that ADEP in addition to opening the axial pore directly stimulates ClpP activity through cooperative binding. ClpP activation thus reaches beyond active site accessibility and also involves conformational control of the catalytic residues. Moreover, we demonstrate that substoichiometric amounts of ADEP potently prevent binding of ClpX to ClpP and, at the same time, partially inhibit ClpP through conformational perturbance. Collectively, our results establish the hydrophobic binding pocket as a major conformational regulatory site with implications for both ClpXP proteolysis and ADEP-based anti-bacterial activity.

Introduction

The proper balance of protein synthesis and protein degradation on a cellular level is of pivotal importance in all kingdoms of life and its perturbation is currently intensively investigated for therapeutic application in the context of cancer, inflammation and infectious diseases[1–3]. Recently, two opposite strategies based on the chemical stimulation or inhibition of protein degradation have been shown to either kill bacteria or silence their pathogenesis[4]. β-lactones are covalent inhibitors of the bacterial serine protease ClpP[5,6]. Inhibition of ClpP enzymatic activity halts the degradation of proteins involved in virulence regulation, which results in attenuated pathogenesis[7,8]. In contrast, ADEPs are a class of natural product-derived cyclic acyldepsipeptides that act as potent antibiotics through the dysregulation and activation of ClpP[9,10]. In an unperturbed cell, proteolysis occurs through binding of a AAA+ chaperone such as ClpX to the apical sides of the barrel-shaped, proteolytic component ClpP whereupon a functional ClpXP protease complex with a continuous substrate channel is formed[11–15]. In this complex, ClpX engages substrate proteins prone to degradation, unfolds them and threads them into the ClpP proteolytic chamber where they are subsequently

degraded[16–18]. Crystal structures of the ClpP barrel in different conformations have been solved, including an active extended and an inactive compressed conformation, however, how the associated structural dynamics are regulated is currently not known[6,13,19,20]. ClpP alone is able to cleave only small peptides, with binding of ClpX being strictly required for the degradation of proteins[21]. ADEPs eliminate this regulation by binding at the junction of the ClpP subunits in a hydrophobic pocket that is also used by ClpX[22,23]. Binding of ADEPs causes a conformational change in the N-terminal region of ClpP whereupon the axial pore of the protease is enlarged allowing proteins to access the ClpP active sites within the degradation chamber (Fig. 1a)[24,25]. Proteomic experiments showed that this uncontrolled proteolysis leads to the depletion of several essential proteins such as the bacterial cytoskeleton protein FtsZ, which in turn causes impaired cell division and ultimately cell death[26,27]. Since this unique antibiotic mechanism exploits a cellular machinery and activates it for destruction, ADEPs were recently shown to be active also against bacterial persister cells and established biofilms of pathogenic *Staphylococcus aureus*[27].

Here we show that the conformation of the ClpP barrel is controlled through the hydrophobic pocket on the protease surface. ClpP is arrested in the active, extended conformation on engagement with ADEP or chaperone, which leads to a stimulation of catalytic activity. Our results reveal an additional layer of regulation in the ClpXP system: the link between ClpP barrel conformation and occupation of the allosteric sites. This demonstrates that the allosteric binding pocket of ClpP functions as a conformational switch that not only controls the accessibility of the active sites but also their activity.

Results

Characterization of the SaClpP–ADEP interaction. We set out to investigate the activation of ClpP from *S. aureus* (SaClpP) by ADEPs and to analyze the corresponding effects on protease function and conformation. We started by screening a small compilation of ADEP derivatives[28], which we found to be equally potent in inducing SaClpP proteolysis (Supplementary Fig. 1a–c). All biochemical and structural assays were performed with ADEP7 (Fig. 1b) unless noted otherwise, which showed a slightly higher affinity than the widely used reference compound ADEP4 towards

both C-terminally Strep-tagged and native SaClpP protein (Supplementary Fig. 1d–f). Wild-type SaClpP was purified as a tetradecamer with 14 identical ADEP binding sites. A detailed concentration-dependent analysis of ADEP7-induced fluorescein isothiocyanate (FITC)–casein degradation by SaClpP exhibited a sigmoidal behaviour and was thus adequately described by the Hill equation (Fig. 1c)[25,29]. Data analysis yielded an affinity constant of 3.1 μM and a Hill parameter of 2.0, indicative of positive cooperativity and consistent with previous studies on *Escherichia coli* ClpP[25,29]. Isothermal titration calorimetry (ITC) experiments in which ADEP7 was added to a solution of SaClpP showed nonstandard behaviour[30] (Fig. 1d) with the reaction becoming more exothermic during the initial increase of the ADEP7:SaClpP ratio. This can be explained by a lower binding affinity of the initial ADEP molecules and thus confirms positive cooperativity. We next reverted the conditions and titrated SaClpP into a solution of ADEP7 thereby starting with a fully saturated SaClpP (Fig. 1e). Here data analysis yielded an ADEP7:SaClpP molar ratio of 1.0 and a K_d of 2.1 mM, which likely describes the binding of an ADEP7 molecule to a SaClpP tetradecamer that already has several ADEP molecules bound (see Supplementary Fig. 2 for replicate and control experiments and Supplementary Table 1 for a compilation of parameters obtained from ITC experiments).

We further determined the degree of stabilization in a thermal shift assay (Fig. 1f). Addition of ADEP7 led to a drastic increase in the protein melting temperature and thus SaClpP folding stability with a half-maximal effective concentration of 2.7 μM. Collectively, these data confirm an affinity of ADEP7 to SaClpP in the 2–3 μM range, slightly higher than the values of 0.82 and 0.37 μM determined for *Bacillus subtilis* ClpP (BsClpP, Supplementary Fig. 3a) and *E. coli* ClpP (EcClpP)[25], respectively. We therefore compared the binding sites based on available structure and sequence data and identified three residues that were different in SaClpP (Supplementary Fig. 3b,c). We generated SaClpP mutant proteins where these three residues were replaced by the corresponding amino acids of BsClpP/EcClpP and found that exchanging histidine 83 for phenylalanine was sufficient for increasing the affinity of SaClpP for ADEP7 to a level comparable to BsClpP (Supplementary Fig. 3d–f). Notably, the mutation also caused partial heptamer formation as evidenced by size exclusion chromatography. Importantly, this oligomerization defect was completely abrogated by ADEP7 binding, indicating that ADEPs exhibit conformational control over ClpP. The basis for this

conformational control as well as for the observed cooperativity was unknown and we therefore decided to carry out a series of in-depth structural and functional studies.

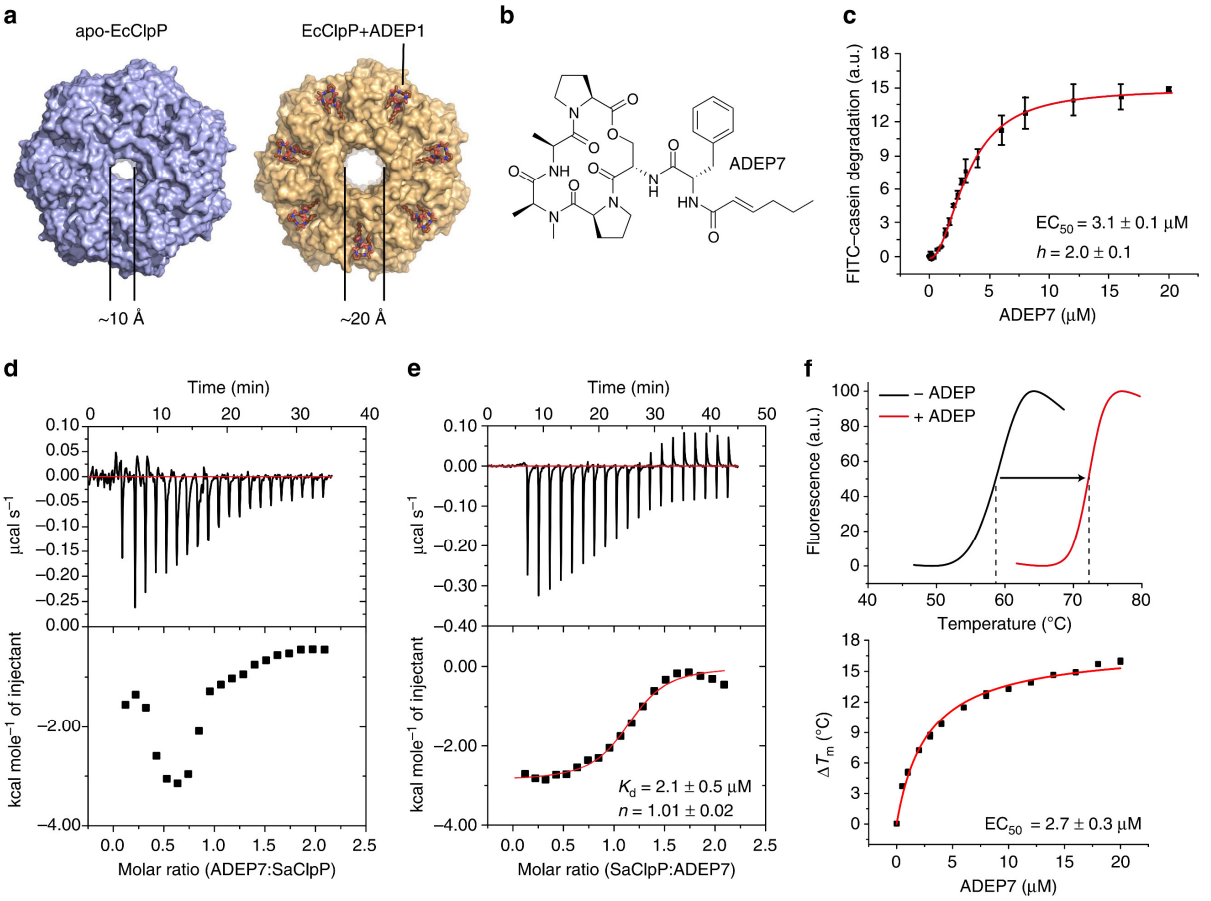

Figure 1 | ADEP cooperatively binds and stabilizes SaClpP. (**a**) Binding of ADEP to the hydrophobic pocket on the apical surface of ClpP causes a conformational change that opens the axial substrate entry pore of ClpP (PDB IDs: 1TYF, 3MT6). (**b**) Structure of ADEP7. (**c**) ADEP7-induced degradation of FITC-casein by SaClpP (0.5 µM) indicates positive cooperativity (Hill coefficient h = 2.0 ± 0.1; EC_{50} = 3.1 ± 0.1 µM). (**d**) ITC titration of ADEP7 (500 µM) into a solution of SaClpP (50 µM) shows positive cooperative binding, which prevents standard data analysis. (**e**) ITC titration of SaClpP (617 µM) into a solution of ADEP7 (62 µM). Parameters obtained from this experiment are: stoichiometry factor n = 1.01 ± 0.02; K_d = 2.1 ± 0.5 µM; ΔH = -3369 ± 100 cal mol^{-1}; ΔS = 13.8 cal mol^{-1} K^{-1}. The stoichiometry factor refers to the ratio of monomeric SaClpP folding by ADEP7. A value of 1 is equivalent to 14 ADEP molecules binding per $SaClpP_{14}$. (**f**) Thermal shift assays reveal strong stabilization of SaClpP folding by ADEP7 in a concentration-dependent manner (melting temperature of free SaClpP: 58.3 °C; ADEP7 concentration in upper panel: 12 µM; EC_{50} = 2.7 ± 0.3 µM). Plotted data in **c** and **f** are mean ± s.d. (N = 3). Parameters determined from curve fits in **c**, **e** and **f** are given with fitting errors.

ADEP accelerates ClpP catalysis. At first, we investigated how binding of ADEP to SaClpP influences protease catalysis. In a simplified view, the cleavage of a peptide substrate can be described as a two-step process in which first the catalytic serine is acylated by a nucleophilic attack at the scissile amide bond, and second the acyl-ester intermediate is hydrolyzed by a water molecule to regenerate the free enzyme (Fig. 2a). To dissect the mechanism of catalysis, we made use of customized β-lactones that were previously described and characterized as SaClpP inhibitors[5,31]. These compounds can be viewed as electrophilic, stripped-down substrate mimetics

in which the R^1 substituent resembles the S1 amino acid side chain and which otherwise lack an amide backbone or prime site substituents[32].

The nucleophilic attack of the active site serine at the β-lactone carbonyl leads to ring opening and acylation. We quantified this step by measuring catalytic efficiencies (that is, observed rate constant per inhibitor concentration values, $k_{obs}/[I]$) for five different β-lactones both in the presence and absence of ADEP7 (Fig. 2b,c, Supplementary Fig. 4). The values spanned a range of 3 orders of magnitude and correlated well with the length of the R^1 substituent as established previously[31]. In addition, we confirmed the site of modification by peptide mass spectrometry to be the catalytic serine 98 (Fig. 2d). Comparing the catalytic efficiencies in the presence of a saturating amount of ADEP7 to the respective value of free SaClpP yielded a general increase of a factor of 2, irrespective of the size of the β-lactone (Fig. 2c). Previous structural studies have revealed that ADEP enlarges the axial pore of ClpP from a diameter of roughly 10 to 20 Å, and pore opening is currently viewed as the sole reason for ADEP activity[24,25]. Our data suggest an additional stimulation of catalytic turnover since the increase in catalytic efficiency was found to be independent of the size of the β-lactone inhibitor and was also obtained with the smallest compound VK292, which has a maximum diameter of ~7 Å.

To quantitatively assess the second reaction step, the hydrolysis of the acyl-enzyme intermediate, we incubated SaClpP with high concentrations of lactones D3 and U1, diluted the reaction mixture and followed the hydrolysis of the acyl-ester intermediate by intact-protein mass spectrometry both in the presence and absence of ADEP7 (Fig. 2e). ADEP again dramatically increased the reaction velocity roughly by twofold by decreasing the half-life time ($T_{1/2}$) of the hydrolysis of D3 from 11.1 to 4.8 h. The behaviour of lactone U1 is different in that it reacts more slowly with the enzyme, but once acylation has occurred it exhibits particularly slow hydrolysis ($T_{1/2} > 40$ h). While the reason for this β-lactone-inherent difference is unknown, ADEP7 released this impediment and caused even faster hydrolysis with a $T_{1/2}$ of 2.38 h. Since the hydrolysis reaction occurs within the catalytic chamber, the state of the N-terminal residues (that is, the diameter of the axial pore) is not expected to affect the hydrolysis velocity (for coordinated conformational changes, see the Discussion section). Hence these results unequivocally demonstrate allosteric stimulation of ClpP catalytic activity by ADEP, independent of axial pore enlargement.

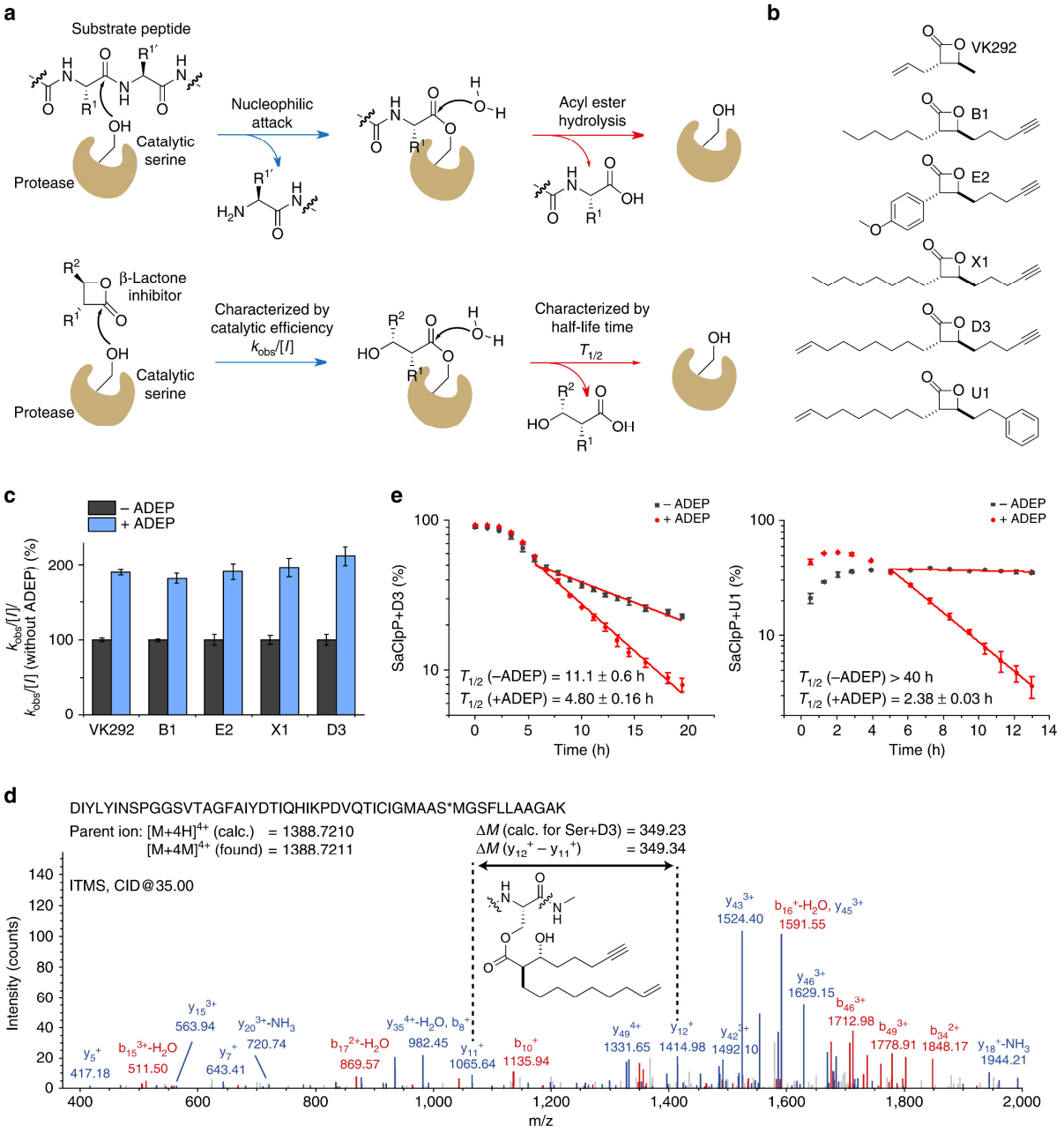

Figure 2 | ADEP accelerates ClpP catalysis. (**a**) Simplified schematic representations of the reactions of the SaClpP active site serine with a substrate peptide (upper panel) and with a β-lactone (lower panel). (**b**) Structures of β-lactones used in this study. (**c**) Catalytic efficiencies for the reactions of SaClpP (0.5 μM) with five β-lactones in the presence or absence of saturating ADEP7 (12 μM). For each lactone, values were normalized to the respective catalytic efficiency in the absence of ADEP7 for easy comparison. See Supplementary Fig. 4 for raw data, error bars denote fitting errors. (**d**) CID fragmentation spectrum of the peptide indicated bearing a covalent modification of β-lactone D3 at the catalytic serine 98 of SaClpP (y ions, blue; b ions, red). For a complete list of identified fragments, refer to Supplementary Table 2. (**e**) ADEP7 accelerated the acyl-ester hydrolysis step. SaClpP (10 μM) was incubated for 5 min with saturating concentrations of lactone D3 and U1 (50 μM), then diluted fivefold and treated with ADEP7 (12 μM) or DMSO, followed by incubation at 37 °C. The degree of covalent modification of SaClpP was quantified via intact-protein mass spectrometry after several time points (three independent experiments, mean ± s.d.). CID, Collision-Induced Dissociation.

We next examined if this stimulation of activity is accompanied by functional changes of the active site. To this end, we analyzed the turnover of a fluorogenic substrate peptide (Suc-LY-AMC) and observed that saturating ADEP only affected the catalytic

rate constant $k_{cat,app}$, while the affinity constant $K_{M,app}$ remained unchanged (Supplementary Fig. 5a). Moreover, we screened a variety of β-lactones with diverse substituents for their potential to acylate SaClpP in the presence and absence of ADEP7; however, ADEP did not apparently change the preference of SaClpP for specific β-lactone probes (Supplementary Fig. 5b,c). In addition, we synthesized all four stereoisomers of lactone U1 and looked for changes in binding through intact-protein mass spectrometry. Only the (*S*,*S*)-configured lactone reacted with SaClpP with both *cis*-configured lactones showing marginal modification of the protease (Supplementary Fig. 5d,e). These results indicate that the ADEP-induced increase of catalytic activity is not due to a change in geometry of the ClpP substrate pocket. Consistent with this, previous co-crystal structures of both BsClpP and EcClpP revealed no difference in the orientation of the active site catalytic triad on ADEP1 binding and ascribed the effect of ADEP binding to a change in the nearby N-terminal region[24,25]. These observations excluded that ADEP binding induces a reorientation of active site residues and raises the question of the molecular mechanism of enhanced catalysis.

ADEP allosterically controls ClpP barrel conformation. An explanation for the unusual ADEP-induced activation in line with all previous experiments would be a stimulation of ClpP through conformational restriction of the complex into a more active form. The ClpP protease is known to be highly dynamic[20] and structural information on SaClpP is available for an active extended[19], an inactive compact[33] and an inactive compressed[6] conformation[34]. These conformations differ in the height of the barrel (~10 nm for the extended and ~9 nm for the compact and compressed conformations), in the alignment of the catalytic triad residues and in the orientation of the E-helix in the handle region (Fig. 3a and Supplementary Fig. 6a). Protein NMR studies with EcClpP[35] have revealed the presence of at least two states in solution, which is supported by molecular dynamics simulations[36] and normal mode analysis[37] suggesting that ClpP samples different conformations. We sought to elucidate the structural basis of ADEP allostery by studying a panel of mutant proteins, which adopt different conformational states. We introduced mutations at all residues of the catalytic triad - S98, H123 and D172 (H123A and H123N proteins showed an increased tendency to aggregation and were therefore excluded from further studies). We also mutated the oligomerization sensor residues R171 and D170 (as well as nearby T169),

which engage in inter-ring salt bridging depending on the conformational state and thereby facilitate a functional coupling of tetradecamer formation to the catalytic triad[19,38,39]. Analytical size exclusion chromatography showed a clustering of these mutants into three distinct groups (Fig. 3b). While the R171A and T169A proteins were clearly heptameric as reported previously[19,31], the D172N and D170A proteins migrated only slightly slower than wild-type, tetradecameric SaClpP. We confirmed the integrity of all protein samples by a Coomassie gel as well as by intact-protein mass spectrometry to exclude abnormal autocatalytic processing (Supplementary Table 3). We also confirmed the assigned oligomerization states by size exclusion chromatography–multiangle light scattering (SEC–MALS) analysis (Supplementary Fig. 6b). In addition, we validated these data by analytical ultracentrifugation, which also indicated a different sedimentation of the D172N mutant compared with wild-type SaClpP (Fig. 3c). With the molecular masses of the subunits as well as the oligomerization unchanged, the smaller appearance in the size exclusion experiment of D172N proteins could result from a more compact/compressed tetradecameric conformation.

To correlate ClpP conformations with both peptidase and proteolytic activity, we functionally characterized the mutant enzymes in the presence of ADEP (Fig. 3d,e). Both mutants of the active site aspartate (D172A and D172N) containing a weakened charge-relay system of the catalytic triad were catalytically inactive alone. Unexpectedly, they gained proteolytic activity in the presence of ADEP, with undistinguishable activity of D172N and wild type in a FITC–casein degradation assay. Moreover, ADEP stimulated hydrolysis of the fluorogenic peptide Suc-LY-AMC in the D172N but not in the D172A mutant.

We speculated that subtle changes near the oligomerization sensor residues of ClpP such as D172N might trigger the adoption of a compacted conformation as the lowest energy state. To investigate the mutation- and ADEP-induced changes in more detail on a structural level, we applied small angle X-ray scattering (SAXS; Fig. 3f,g). A comparison of the inter-atomic pair distance distribution functions (PDDF, *P(R)*) of wild-type and D172N SaClpP clearly showed a more compacted conformation of the D172N protein. The data also demonstrate that the oligomeric assemblies in wild-type and D172N SaClpP have the same mass (identical integral of the *P(R)* in Fig. 3f, see Table 1), confirming different conformations rather than oligomerization states.

Addition of either ADEP4 or ADEP7 led to an increase in the size of both the wild-type and the D172N protein as revealed by a shift in the *P(R)* function, and the conformations became virtually indistinguishable in the ADEP-bound state. The ADEP-induced shift of the *P(R)* function as well as of the radius of gyration, R_g, in the D172N sample is fully in agreement with the shift predicted by analyzing the structures of the compressed and the extended conformation (Fig. 3h; $\Delta R_g^{(\text{compressed->extended}),\ \text{calculated}} = 1.8$ Å; $\Delta R_g^{(\text{SaClpP-D172N-> +ADEP4}),\ \text{observed}} = 1.7$ Å). Moreover, low-resolution models inferred from the data support the conclusion of an ADEP-mediated shift from a compressed to an extended conformation in the D172N protein (Fig. 3i). Notably, also the wild-type protein either bound to ADEP4 or ADEP7 showed a small increase in size. The inter-ring bridge mutants T169A and R171A were clearly heptameric in SAXS analysis and failed to assemble to functional tetradecameric complexes on addition of ADEP, which is in line with their lack of catalytic activity (Supplementary Fig. 6c–f). SAXS data were recorded three times with independently purified protein samples including tag-free and C-terminally Strep-tagged protein, and the described changes were consistently visible.

It has been speculated that the compressed conformation precludes ADEP binding due to a closed binding pocket[33]. Consistently, we found a rough threefold lower affinity of SaClpP-D172N for ADEP7 by ITC while the affinity towards SaClpP-S98A was less affected (Supplementary Fig. 2e,f). In addition, we validated the SAXS results with dynamic light scattering (DLS), which significantly showed a small ADEP-induced increase in the wild-type protein radius and a larger ADEP-induced increase in the D172N sample, with both ADEP-bound proteins being equal in size (Fig. 3j). Since it is difficult to correlate static crystal structures to the data inferred from solution-based methods, the possibility remains that the compressed structure we are observing in solution may not entirely represent that described by X-ray crystallography. However, when taken together, these data clearly demonstrate how binding of ADEP exhibits conformational control on the ClpP barrel. Occupation of the regulatory allosteric site reverts the catalytically incompetent, compressed conformation of the D172N mutant and locks the wild-type protein in an extended conformation, explaining the ADEP-induced increase in catalytic activity.

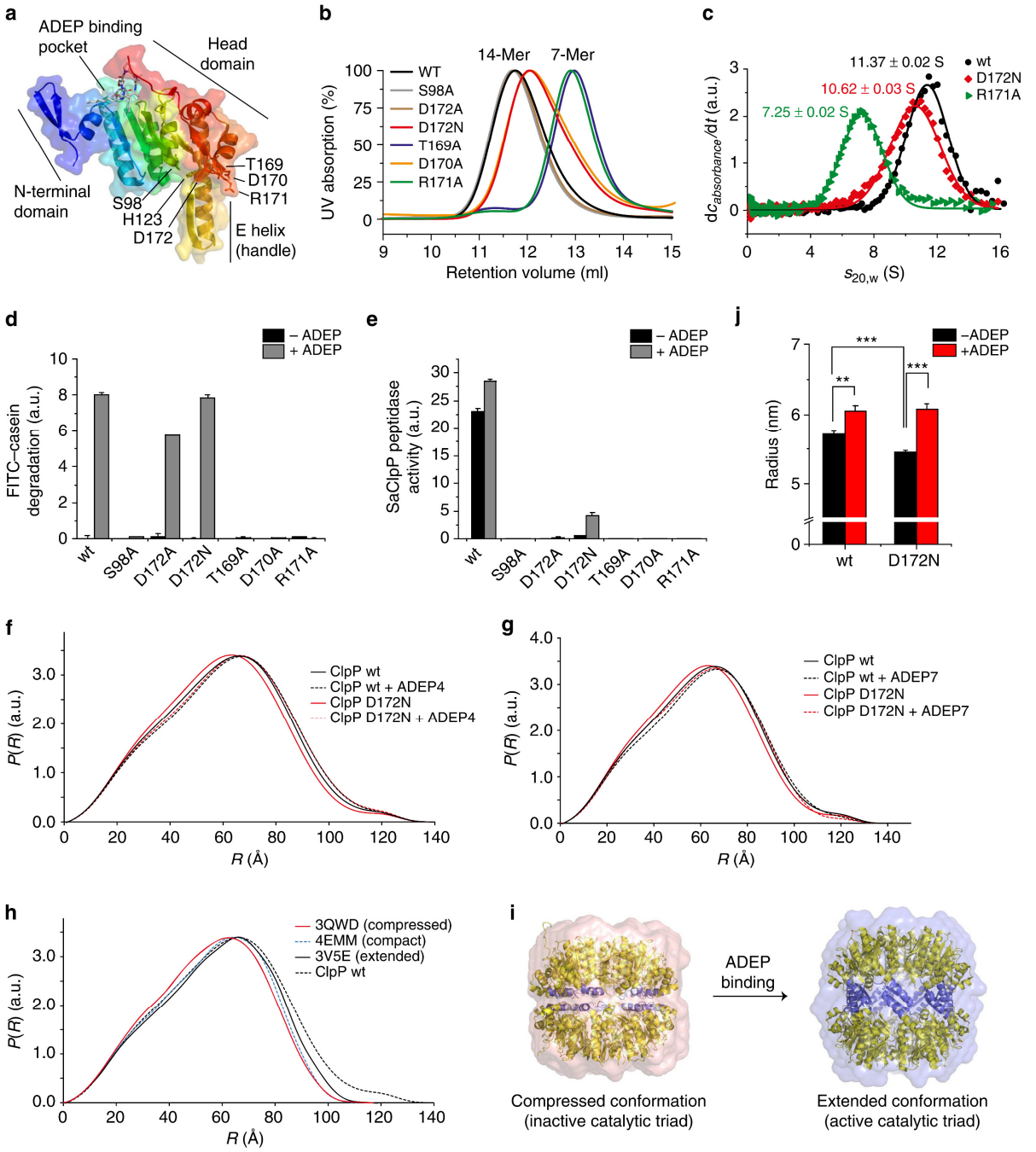

Figure 3 | Binding of ADEP to ClpP induces a conformational switch to the active, extended ClpP barrel conformation. (**a**) Cartoon representation of a ClpP monomer showing the position of the ADEP binding site, the catalytic triad (S98, H123, D172) and the oligomerization sensor R171 (PDB ID: 3MT6). (**b**) Analytic size exclusion chromatograms of wilt-type and mutant SaClpP. (**c**) Analytical ultracentrifugation results for selected mutants. Sedimentation coefficients were obtained as the centres of Gauss functions whose fitting errors are given. (**d**) FITC-casein degradation activity of wild-type and mutant SaClpP (1 µM) in the presence or absence of ADEP7 (12 µM). Mean ± s.d. of initial slopes are given. (**e**) Peptidase activity of wild-type and mutant SaClpP (0.5 µM) in the presence or absence of ADEP7 (12 µM). Mean ± s.d. of initial slopes are given. (**f**) Inter-atomic pair distance distribution functions (PDDF) of tag-free SaClpP proteins treated with either DMSO or ADEP4 (1:1 mixture, 380 µM, 0.6% DMSO). (**g**) PDDF of tag-free SaClpP with/without ADEP7 (1:1 mixture, 380 µM, 0.6% DMSO). (**h**) Comparison of measured (ClpP wt) and predicted (3QWD, 4EMM, 3V5E) inter-atomic pair distance distribution functions. (**i**) *Ab initio* low-resolution models of SAXS scattering curves from SaClpP-D172N superimposed with SaClpP in the compressed conformation (left), as well as from SaClpP-D172N + ADEP4 superimposed with SaClpP in the extended conformation (right). (**j**) Dynamic light scattering results of wild-type and D172N SaClpP treated with either DMSO or ADEP7 (1:1 mixture, 310 µM, 3% DMSO). Please note the axis break. Mean ± s.e.m.; ***P*<0.01, ****P*<0.001 (independent two sample *t*-tests, *N* = 10, with each of the 10 results established from 10 technical replicates, equal variances not assumed). UV, ultraviolet.

Substoichiometric occupation leads to partial inhibition. When we analyzed the concentration-dependent response of SaClpP peptidase activity to ADEP7, we unexpectedly found biphasic behaviour. While saturating amounts of ADEP stimulated SaClpP peptidase activity as described above, small ADEP concentrations corresponding to three to four ADEP molecules per $SaClpP_{14}$ showed partial inhibition (Fig. 4a). This partial inhibition was also observed with ADEP4, as well as with tag-free SaClpP protein (Supplementary Fig. 7a–c). Moreover, a similar phenomenon was observed with the D172N mutant whose low residual peptidase activity was further diminished by adding a small amount of ADEP (Fig. 4b). Consistent with the wild-type SaClpP data, no such effect was observed during proteolysis (Fig. 4c). We analyzed

Table 1 | SAXS data and analysis of SaClpP proteins.

Sample	Stoichiometry	R_g (Å)	Molecular mass (kDa)*
SaClpP wt	—	46.4 ± 0.1	292
SaClpP wt + ADEP4	1:1	46.7 ± 0.1	305
SaClpP wt + ADEP7	1:1	46.3 ± 0.1	296
SaClpP-D172N	—	44.7 ± 0.1	303
SaClpP-D172N + ADEP4	1:1	46.4 ± 0.1	300
SaClpP-D172N + ADEP7	1:1	45.6 ± 0.1	296
SaClpP wt (Strep)	—	49.0 ± 0.1	320
SaClpP wt (Strep) + ADEP7	1:1	49.2 ± 0.1	330
SaClpP-D172N (Strep)	—	47.4 ± 0.1	324
SaClpP-D172N (Strep) + ADEP7	1:1	48.8 ± 0.1	330
SaClpP T169A	—	40.7 ± 0.1	167
SaClpP T169A + ADEP7	1:1	41.8 ± 0.1	160
SaClpP R171A	—	39.5 ± 0.1	170
SaClpP R171A + ADEP7	1:1	40.2 ± 0.1	180

Samples were treated either with ADEP or with the respective amount of DMSO.
*The molecular mass was determined from the scattering intensity at zero angle ($I(0)$) using BSA as reference. Expected molecular masses of native SaClpP and Strep-tagged SaClpP are 301 kDa and 316 kDa, respectively.
ADEP, acyldepsipeptide; BSA, bovine serum albumin; DMSO, dimethylsulphoxide; *Rg*, radius of gyration; SaClpP, ClpP from *Staphylococcus aureus*; SAXS, small angle X-ray scattering; wt, wild type.

the respective SaClpP:ADEP ratios via analytical ultracentrifugation and found that a substoichiometric amount of ADEP slightly decreased the sedimentation coefficient of wild-type ClpP, whereas this effect was reverted at higher ADEP concentrations (Fig. 4d). Similarly, the sedimentation coefficient of D172N first decreased with small amounts of ADEP and increased to a higher value than the free protein on further addition of ADEP (Fig. 4e). We hypothesize that binding of the initial ADEP molecules to a tetradecameric ClpP induces structural perturbations owing to a conformationally heterogeneous assembly, which would also account for the observed positive cooperativity.

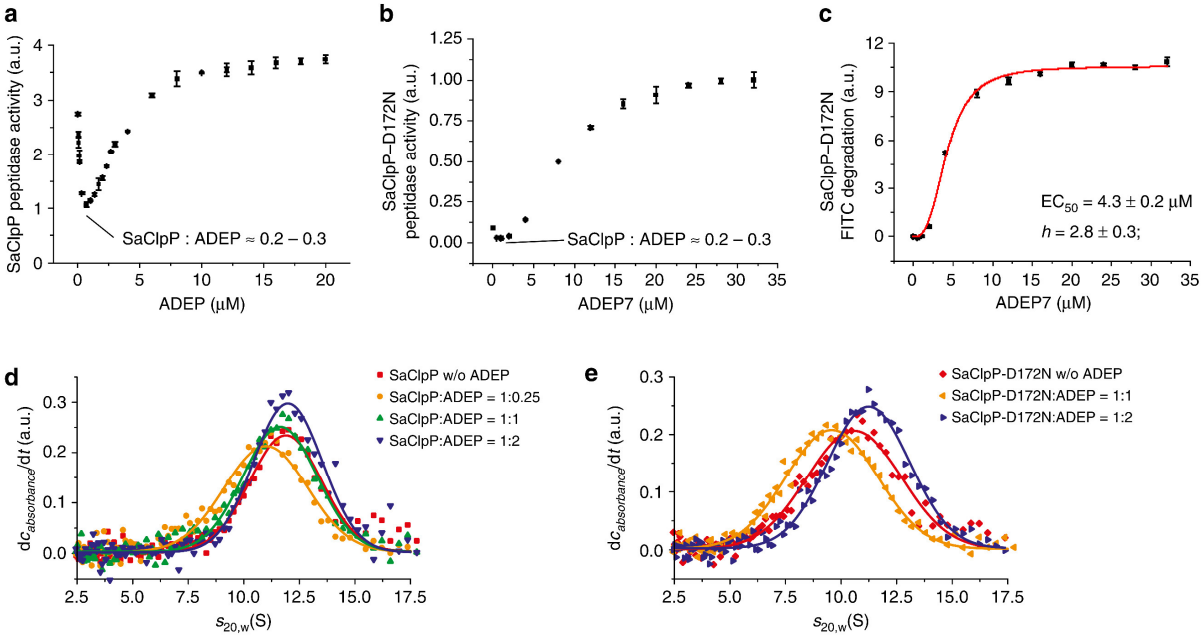

Figure 4 | Substoichiometric amounts of ADEP cause partial inhibition of ClpP. (**a**) Concentration-dependent partial inhibition or stimulation of wild-type SaClpP peptidase activity by ADEP7. The ratio of ADEP bound to ClpP was estimated from the concentrations at the minimum and a K_d of 2.1 μM. A ratio of 0.2-0.3 corresponds to 2.8-4.2 ADEP molecules per $SaClpP_{14}$. (**b**) Concentration-dependent inhibition or stimulation of SaClpP-D172N peptidase activity by ADEP7. In line with the compressed conformation of SaClpP-D172N, the initial peptidase activity is lower than that of the wild-type protein. The ration of ADEP bound to ClpP was estimated from a K_d of 6.1 μM. (**c**) FITC-casein degradation by SaClpP-D172N indicates positive cooperativity (h = 2.8 ± 0.3; EC_{50} = 4.3 ± 0.2 μM). (**d**) Analytical ultracentrifugation results of SaClpP (7.5 μM) treated with DMSO (0.6% (v/v)) or ADEP7 (7.5 and 15 μM). Plotted data in **a**-**c** are mean ± s.d. (N = 3). Parameters determined from curve fits in **c** are given with fitting errors.

Despite a sequence homology of ~60% (Supplementary Fig. 3b), ClpP proteins from different species are remarkably different in their oligomerization behaviour. We studied BsClpP, which under our purification conditions using affinity and size exclusion chromatography in glycerol containing buffer yielded a tetradecameric and a monomeric fraction (Supplementary Fig. 7d–i)[10]. In analogy to SaClpP, the intrinsically active tetradecameric BsClpP showed partial inhibition of peptidase activity at low ADEP concentrations while the monomeric BsClpP was inactive in the

absence of ADEP and was activated with an even lower ADEP concentration than the tetradecameric BsClpP (Supplementary Fig. 7e–g). Similar results were obtained with *Listeria monocytogenes* ClpP2 (LmClpP2) tetradecamer and heptamer (Supplementary Fig. 7h,i)[40]. These data provide evidence that the hydrophobic ADEP binding pocket acts as a major conformational regulatory site across organisms, which allows for differential regulation of protease activity depending on the degree of occupation per tetradecamer.

SaClpX and ADEP share a ClpP activation mechanism. The ADEP-bound conformation of ClpP has been suggested to serve as a model for the Clp–ATPase-bound state of ClpP since ADEP and the IGF loop of ClpX are assumed to share the same binding site. We therefore reasoned that ClpX might be able to exert conformational control on ClpP in a similar way. We thus tested all protein mutants in a SaClpXP assay in which we monitored the fluorescence of a green fluorescent protein (GFP) variant to which a C-terminal degradation tag (SsrA tag) was appended (Fig. 5a,b)[17]. To differentiate between GFP unfolding and degradation, the assay mixture was analyzed by Coomassie gel after 3 h. The D172N mutant showed GFP degradation activity similar to the wild-type enzyme, which is in full agreement with the results of ADEP-induced casein degradation, indicating that SaClpX is also able to revert the compressed conformation of the D172N protein. The intermediate assay signal of the S98A mutant protein was assigned as unfolding activity without proteolysis[41], whereas the heptameric oligomerization of the T169A and R171A mutants consistent with the SAXS data precluded activation by SaClpX and thus GFP unfolding. In a competition assay, ADEP7 and ADEP4 inhibited GFP unfolding by SaClpXP and thus binding of SaClpX to ClpP with IC_{50} values of 225 and 221 nM (Fig. 5c). This value is in the range of the assay concentration of tetradecameric SaClpP (200 nM), consistent with a shared binding site of ADEP and ClpX[10]. The IC_{50}, furthermore, suggests that the binding of a single ADEP molecule to only one SaClpP apical surface is sufficient to reduce SaClpXP proteolysis by half (Fig. 5e).

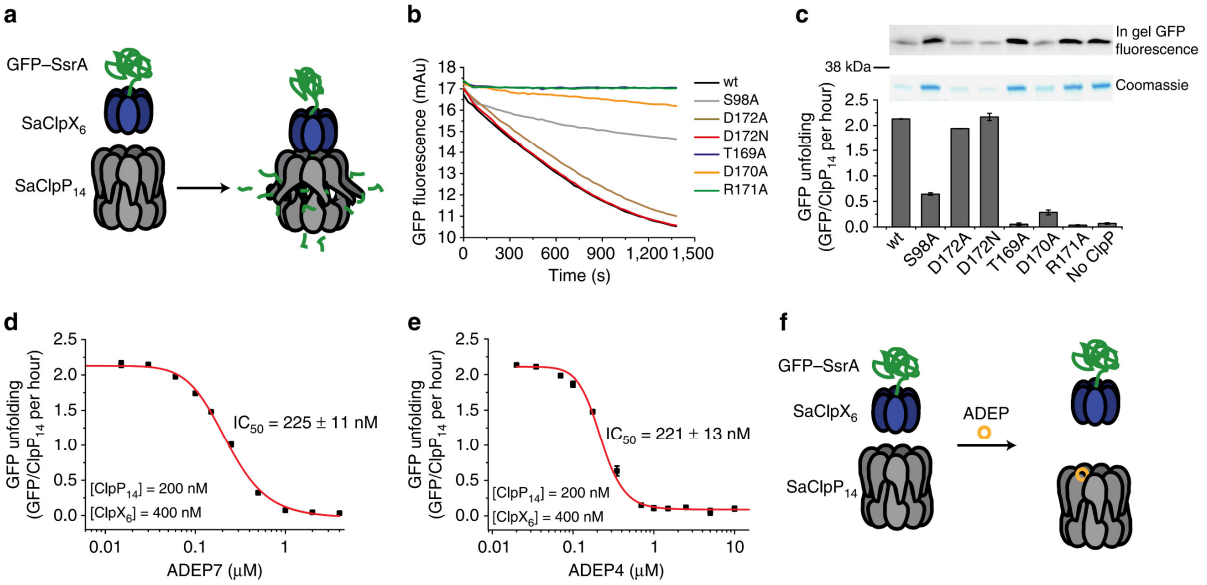

Figure 5 | ClpX activates ClpP in a similar manner and is competed by ADEP. (**a**) Schematic of the SaClpX-mediated unfolding of SsrA-tagged GFP and its subsequent degradation by SaClpP. (Note, the precise path of product peptide release is unclear and under debate.) (**b**) SaClpX-GFP assay. The initial slopes of the decrease in GFP fluorescence of the fluorescence-time courses were quantified and are displayed in the bar graph. A Coomassie-stained gel of these samples showing GFP after 3 h at 30 °C indicates that wild-type, D172A, D172N, and D170A SaClpP are capable of protein degradation, while S98A, T169A and R171A are not. This is consistent with in-gel GFP fluorescence measurements. See Supplementary Fig. 7n,o for uncropped gel images. (**c**,**d**) ADEP7 and ADEP4 disrupt SaClpXP-mediated GFP unfolding with an IC_{50} value comparable to the concentration of $SaClpP_{14}$. (**e**) Schematic showing how the binding of ADEP to $SaClpP_{14}$ prevents the binding of $ClpX_6$ and thus GFP unfolding. Mean ± s.d. are given in all panels (N = 3). IC_{50} values are given with fitting errors.

Discussion

Multicomponent protease complexes require the precise coordination of several processes including substrate engagement, unfolding, degradation and product release. To this end, the different parts of the complexes need to be functionally coupled in an accurate and versatile manner. Moreover, information must be coded in structural form and transmitted through allosteric binding events. Since uncontrolled proteolysis poses a threat to cellular viability, reliable and multi-layered regulation is essential for these machineries.

The ClpXP protease is a prime example of such a complex since the dynamics of its components have been studied and a framework of reference structures exist[42,43], though a structure of the entire complex is lacking[34,44–46]. Biochemical experiments have shown that ClpX interacts with ClpP primarily through docking of its IGF loop into a hydrophobic pocket on the surface of ClpP that is also used by ADEPs to dysregulate ClpP[22–24]. The N-termini of ClpP have been shown to gate the entry into the degradation chamber by adopting different conformations, where the ‘down’

conformation as a hydrophobic plug closes and the 'up' conformation opens the entry portal[47,48]. Although ADEPs have already been shown to regulate these gated pores, further activating influences of the antibiotic had not been considered. Here we show that ADEPs additionally stimulate ClpP catalysis through cooperative binding. In previously published studies on ADEP-ClpP co-crystal structures this allosteric activation had been missed, since it is not based on changes of active site geometry but on conformational dynamics. We find that ADEPs are able to revert the catalytically incompetent compressed conformation of the D172N ClpP mutant through switching its conformation to the extended state, which exhibits an aligned catalytic triad (contrary to the compressed conformation, where the triad is not aligned). Similarly, ClpX activates ClpP-D172N for proteolysis, implicating that a chaperone is also able to induce the conformational switch of the ClpP-D172N barrel conformation necessary for catalysis. Importantly, we observe that also wild-type ClpP adopts an extended state by addition of ADEP. Our biochemical and structural data thus converge at the view that occupation of the hydrophobic pocket arrests the dynamic ClpP barrel in its catalytically competent conformation, which contributes to sustained peptidase as well as proteolytic activity.

Conformational arrest[49,50] is a strong regulation principle in ClpP as it even compensates for the lack of a catalytic D172 residue and facilitates proteolytic processing with a Ser–His catalytic dyad. This interpretation is corroborated by a previous study on functional coupling in the ClpXP complex, where occupation of the ClpP active site by a covalent inhibitor increased the affinity of the peptidase for the ATPase[22]. Our results now establish the bidirectionality of this cross-talk and implicate ClpP conformations and catalytic activity in this regulation. Studies on the human ClpP[51,52] showed that hClpP is heptameric in solution and that its catalytically competent tetradecameric state can be triggered by addition of ClpX from *E. coli*[53]. These data suggested a conformational coupling of the hydrophobic pocket with the handle domain. Our data structurally expand this finding, showing that this conformational control is also present within tetradecameric ClpP. Further indications came from hydrogen-exchange mass spectrometry experiments where ADEPs were used as ClpX mimetics and ADEP binding induced rigidification of ClpP in the equatorial handle region[48]. Moreover, mutations in the N-terminal region were used to propose that substrate access might coordinate with protease active site reactivity[54].

Most recently, ADEP was shown to contribute to ClpP activation in the heterooligomeric ClpP1P2 system from *Mycobacterium tuberculosis*, but only in the presence of an additional activating peptide[55].

ClpX interacts with ClpP via two distinct loop structures. ADEP is an IGF-loop model that demonstrates the sophisticated mechanism by which the ATPase exerts conformational control on the peptidase. The hydrophobic pocket at the surface of ClpP serves as the major regulatory 'button' that the IGF loop presses to stabilize the extended, catalytically active conformation of ClpP and simultaneously to put the N-terminal loops of ClpP in the upward position[56], thereby opening the gated pore. Shielding the open ClpP pore with its own pore-2 loops, ClpX establishes a secluded channel for substrate passage into the catalytic cavity. Coupling the two conformational movements to the same allosteric site and regulatory event ensures that catalytic triads are only active, when the pore is securely covered.

The ClpXP complex is not homogeneous during operation. In addition to the symmetry mismatch of hexameric ClpX and the axially heptameric ClpP, ClpX was shown to exhibit conformational heterogeneity based on the nucleotide state of the ATPase domain where coordinated hydrolysis by two to four subunits is coupled to substrate translocation[57,58]. While we provide evidence that full occupation of the allosteric site on ClpP leads to activation, we also show that a smaller degree of occupation causes partial inhibition through conformational perturbation. It is currently unclear how the symmetry-mismatched interaction of ClpX and ClpP is mediated and how many hydrophobic pockets on one apical side of a ClpP heptamer are occupied by one ClpX hexamer. We find it intriguing that in a SaClpXP assay with concentrations corresponding to two ClpX hexamers bound to the two apical sides of ClpP (that is, a $ClpX_6$:$ClpP_{14}$:$ClpX_6$ complex as observed with electron microscopy)[53,59,60], the addition of one ADEP molecule per ClpP tetradecamer was sufficient to reduce the substrate unfolding activity by half (Fig. 5c,d). This suggests that occupation of already one of the seven hydrophobic pockets on a ClpP ring is incompatible with ClpX binding, either through cooperativity-induced conformational heterogeneity or through direct collision with ClpX. Moreover, we are fascinated by the unexpected finding that an allosteric activator molecule is also capable of reducing the activity of the catalytic complex when binding at substoichiometric conditions. This allows for a putative model in which ClpP activity is differentially regulated dependent on the respective ClpX binding state.

While the relevance of this phenomenon in ClpXP proteolysis is unclear, we find it important to note that low concentrations of ADEP in a medicinal setting may lead to partial ClpP inhibition and thus bacteria with reduced pathogenicity[7].

Collectively, our results shed light on the way ClpP reciprocates activation by ClpX and ADEP. We provide mechanistic insights into how ADEPs and chaperones exhibit conformational control on ClpP and how this interaction goes beyond active site accessibility, but also influences protease catalysis. We provide evidence that the hydrophobic pocket acts as a major regulatory site of ClpP and that the binding of ADEP or ClpX to this site allows for differential regulation of protease activity and conformation depending on the degree of occupation per tetradecamer. Further experiments should investigate if this allosteric layer of regulation is present also in other multicomponent proteases such as the proteasome.

Methods

Cloning and protein purification. C-terminally Strep-tagged ClpP from *S. aureus* NCTC 8325 (SaClpP)[19] and ClpP from *L. monocytogenes* (LmClpP2)[40] were purified through affinity and size exclusion chromatography from expression in *E. coli* BL21(DE3). Tag-free wild-type SaClpP was purified through anion exchange, hydrophobic interaction and size exclusion chromatography[39]. Expression constructs of mutant proteins were created using the QuikChange methodology using primers listed in the Supplementary Table 4 (refs 19,39). Expression was carried out in BL21(DE3) or SG1146a cells and purification proceeded as described for the wild-type proteins. Strain SG1146a was a gift from S. Gottesman (NIH, Bethesda, USA). Monomeric concentrations of ClpP are given unless otherwise noted.

BsClpP was expressed and purified as follows. *E. coli* SG1146a was transformed with pClpP11 (ref. 61). Cultures (1 l) were grown at 37 °C until an OD_{600} of 0.4–0.6 was reached. Then expression of the C-terminally His-tagged fusion protein was induced with 1 mM isopropyl-β-D-thiogalactoside and cultures were grown at 28 °C over night. Cells were lysed in buffer A (50 mM sodium phosphate, 300 mM NaCl, 20% (v/v) glycerol, 20 mM imidazole; pH 8.0) using a Precellys homogenizer (PeqLab). Supernatants were mixed with Ni-NTA matrix (Qiagen) at 4 °C over night and subjected to plastic columns (Thermo Scientific). ClpP was eluted with buffer B (50 mM sodium phosphate, 300 mM NaCl, 20% (v/v) glycerol, 250 mM imidazole; pH 8.0). The eluted proteins were concentrated with Amicon Ultra Centrifugal Filters with 10 kDa cutoff (Merck-Millipore) and subjected to gel filtration on an ÄKTA purifier system with a Superdex 200 16/60 column (GE Healthcare). Tetradecamers and monomers of ClpP were eluted with buffer C (50 mM sodium phosphate, 300 mM NaCl, 20% (v/v) glycerol; pH 8.0). Our reported purifications of BsClpP in the absence of glycerol and in the presence of dithiothreitol (DTT)[61] yielded predominately monomeric ClpP[62]. In the presence of glycerol, both tetradecameric and monomer species were obtained (Supplementary Fig. 7d). Monomeric BsClpP could be converted to tetradecameric BsClpP through addition of ADEP (Supplementary Fig. 7h,i).

Enhanced GFP tagged for ClpXP degradation, enhanced GFP–ssrA (eGFP–ssrA), originates from eGFP (protein ID C5MKY7) and was cloned as a fusion protein with a ssrA tag (AANDENYALAA) at the C terminus. An expression clone was assembled

using the Gateway cloning strategy (Invitrogen) with pDonr201 as donation vector and pDest007 (ref. 63) as expression vector. The expression construct was transformed into *E. coli* KY2266 cells. Expression was carried out in 4 l LB media after induction with anhydrotetracycline (0.2 mg/l) at an OD_{600} of 0.5 for 4 h at 37 °C. The pellet was washed with PBS and resuspended in ice-cold lysis/wash buffer (100 mM Tris, 150 mM NaCl, 1 mM EDTA, pH 8.0). The cells were lysed using a Constant Cell Disruption system. The lysate was cleared via centrifugation (38,000 g, 45 min, 4 °C). Protein purification was achieved on an Äkta Purifier 10 system (GE Healthcare). Affinity chromatography was carried out with a StrepTrap HP 5 ml column. eGFP–ssrA containing elution fractions were pooled, concentrated and purified with a HiLoad 16/60 Superdex 200 pg gel filtration column in GF buffer (100 mM NaCl, 20 mM Tris, 10% (v/v) glycerol, pH 7.0).

Tag-free ClpX from *S. aureus* NCTC 8325 (SaClpX) was used in all experiments and obtained as follows. The gene encoding ClpX (geneID 3919696) was amplified using primers listed in Supplementary Table 4. An expression construct was assembled using the Gateway cloning strategy with pDonr207 as donation vector and pET300 as expression vector. The expression construct encoding N-terminally His_6-tagged, full-length SaClpX with an N-terminal TEV site was transformed into chemically competent BL21(DE3) cells. Expression was carried out in 1 l LB media after induction with isopropyl-β-D-thiogalactoside (0.5 mM) at an OD_{600} of 0.6 for 15 h at 25 °C. The cell pellet was washed with PBS and resuspended in ice-cold lysis buffer (50 mM Hepes pH 7.5, 300 mM KCl, 15% (v/v) glycerol, 1 mM DTT). The cells were lysed with a Constant Cell Disruption system and subsequent sonification (3 x 30 s, 80%, Bandelin sonoplus). $MgCl_2$ (5 mM) was added and the suspension was cleared through centrifugation (36,000g, 30 min, 4 °C). Affinity purification was carried out on an ÄKTA Purifier 10 chromatography system with a Ni-NTA Superflow cartridge (5 ml). The column was equilibrated in lysis buffer (+5 mM $MgCl_2$), the lysate was loaded and it was washed with 10 column volumes lysis buffer (+5 mM $MgCl_2$, +40 mM imidazole). Elution was carried out with a steep gradient in elution buffer (lysis buffer + 5 mM $MgCl_2$ + 500 mM imidazole). EDTA (2 mM) and TEV protease (500 ml of 1.7 mg ml^{-1} stock) were added to the pooled elution fractions and it was incubated at 4 °C over night. Cleavage was monitored by intact-protein mass spectrometry and SDS–PAGE. If necessary, a second addition of TEV protease was carried out followed by incubation

at 4° C over night. The sample was concentrated with a 10 kDa Amicon ultra centrifugal filter to reduce the imidazole content, diluted in breaking buffer (10 ml final volume, final imidazole: 40 mM). $MgCl_2$ (2 mM) was added and the solution was passed through a pre-equilibrated Ni-NTA column. The flow-through was collected, three times buffer-exchanged with a 10 kDa Amicon ultracentrifugation device in lysis buffer (+2 mM $MgCl_2$) and frozen in aliquots. A gel filtration step was omitted since analytical runs showed no signs of aggregated protein.

Catalytic efficiency measurements. Serial β-lactone inhibitor dilutions (1 µl of 100x stock in DMSO) were added to wells and Suc-LY-AMC (50 µl, 2x, final concentration: 200 µM) in assay buffer A was added. ADEP (12 µM from 10 mM stock) or the respective amount of DMSO was added to a SaClpP solution (2x, final concentration: 1 µM) in assay buffer A and everything was brought to 32 °C. Subsequently, 50 µl of the protein solution was added to the wells and fluorescence was recorded as described above with a 20-s interval. Kinetic constants were obtained assuming pseudo-first-order kinetics by fitting the curves to

$$F(t) = F_0 + A(1 - e^{-k_{obs}t})$$

wherein $F(t)$ denotes the fluorescence-time course, F_0 denotes the initial fluorescence, A denotes the saturation limit and k_{obs} denotes the rate constant. Catalytic efficiencies were determined as slopes from $k_{obs}/[I]$ plots[31].

FITC–casein assay. ADEP (1 µl of 100x stock in DMSO) was added to wells of black flat-bottomed 96-well plates. Protein dilution (80 µl, 1.2x, final concentration: 1 µM) was added and incubated at 37 °C for 15 min. Casein mix (20 µl, 5x, final concentration of mixed casein: 0.24 mg ml^{-1}, final concentration of FITC–casein: 0.048 mg ml^{-1}) was added and the reaction was followed in an infinite M200Pro plate reader with excitation at 494 nm and detection at 521 nm at 37 °C. Initial slopes (usually 0–300 s) were used for data analysis. All data were referenced against the slope of casein solution without addition of protease. Fitting was performed with OriginPro (MicroCal) using the Michaelis–Menten equation, wherein instead of a K_M the half-maximal effective concentration EC_{50} was used.

Isothermal titration calorimetry. All ITC experiments were performed on a MicroCal iTC200 system (GE Healthcare) in 20 mM Hepes pH 7.0, 100 mM NaCl with a maximum of 2% (v/v) DMSO at 25 °C and with constant stirring at 1,000 rpm. Prior to

experiments, the protein was gel filtrated into 20 mM Hepes pH 7.0, 100 mM NaCl, concentrated if necessary using 10 kDa Nanosep centrifugational devices (Pall) and the ligand was dissolved in the exact same buffer from a 50 mM stock in DMSO. DMSO concentrations of syringe and cell samples were matched if necessary by addition of pure DMSO. The experiment was started after equilibration for 300 s with a first injection of 0.4 µl that was discarded during the analysis. A typical experiment consisted of 20 subsequent injections with a 2 µl injection volume into a cell filled with 200 µl sample. Each injection was made over a period of 4 s with a 2–3-min interval between subsequent injections. Power was recorded at 'high' gain setting, with a reference power of 10 µcal s^{-1} and a 5-s filter period. Data analysis including baseline correction and evaluation was carried out with OriginPro 8.5ITC. Due to cooperativity and thus the nonstandard form of some ITC curves, no fits based on simplified models were obtained for ligand into protein experiments. In the case of protein into ligand experiments, fits were carried out taking into account all injections until the maximum heat occurred and the two subsequent injections. We assume this to reflect the binding of ADEP to a ClpP protein with already some ADEP molecules bound. The binding characteristics of the initial ADEP molecules binding to free ClpP are likely to be different.

Thermal shift assay. ADEP (0.5 µl of 100x stocks in DMSO) was placed into wells of white 96-well PCR plates. Sypro Orange (1x) was added to a SaClpP (1 µM) solution in buffer D and 50 µl were added to each well. The plate was sealed and fluorescence was recorded in a CFX96 Real-Time System (Bio-Rad) while heating from 20 to 80 °C in 0.3 °C steps. Data analysis was performed with CFX Manager software and OriginPro. Melting temperatures were referenced against the melting temperature of DMSO-treated SaClpP.

Intact-protein mass spectrometry. Samples were diluted down to 1–2 µM protein concentration in buffer D. Aliquots (4–2 µl) were desalted with a Massprep online desalting cartridge (Waters) according to the manufacturer's procedure on a Dionex UltiMate 3000 HPLC system and subsequently measured on a Thermo LTQ FT Ultra mass spectrometer with electron spray ionization. Promass Deconvolution software (Thermo Scientific) was used for data analysis and deconvolution (input range: 500–2,000 *m*/*z*; output range: 20,000–30,000 Da; peak width = 3; merge width = 0.3; smooth width = 7; number of smooths = 2). Thermo Scientific Xtract software was

used for verification. For the time-course experiments, SaClpP (10 μM) was incubated for 5 min at room temperature with saturating concentrations of lactone D3 and U1 (50 μM). It was then diluted fivefold and treated with ADEP7 (12 μM) or DMSO, followed by incubation at 37 °C. The degree of covalent modification of SaClpP was quantified via intact-protein mass spectrometry after several time points (three independent experiments). Mass intensities were normalized against the sum of intensities of the free protein and the modified protein. $T_{1/2}$ was calculated from linear fits of the logarithmic plots.

SEC–MALS. Analytical size exclusion chromatography was carried out on an ÄKTA Purifier 10 chromatography system with a calibrated Superdex 200 10/300 GL column in buffer D (20 mM Hepes pH 7.0, 100 mM NaCl) at 4 °C with a flow of 0.5 ml min^{-1}. Samples (300 μl of a 1 mg ml^{-1} SaClpP solution or 1 ml of a 250 μg ml^{-1} solution) were loaded into a 500 μl or 1 ml sample loop and elution was monitored by ultraviolet absorption at 280 nm. Ultraviolet traces were referenced against the salt peak in the conductivity trace and normalized to the highest signal for easy comparison. SEC–MALS analysis was carried out on an Agilent 1200 Series chromatography system equipped with a Superdex 200 10/300 GL column and coupled to a DAWN Heleos II MALS detector as well as an Optilab rEX refractive index detector (Wyatt Technology). Samples (100 μl of 2 mg ml^{-1} protein solutions) were loaded from an autosampler and analyzed in buffer D (20 mM Hepes pH 7.0, 100 mM NaCl; used for SaClpP proteins and LmClpP2) with a flow of 0.5 ml min^{-1} or in buffer F (50 mM Tris pH 8.0, 200 mM NaCl, 20% glycerol; used for LmClpP2 + glycerol and BsClpP proteins) with a flow of 0.4 ml min^{-1}. Masses and errors were derived from analysis in Astra 6.1 (Wyatt Technology) and calibration with BSA.

Analytical ultracentrifugation. Sedimentation velocity experiments were performed in a ProteomeLab XL-A (Beckman Coulter, USA) instrument equipped with an ultraviolet/visible-detection unit. Protein was detected at 280 nm. Runs were performed at 34,000 rpm. (93,220g) at 20 °C. Proteins were spun in a Ti50 rotor equipped with seven sample cells and one reference counterbalance cell. Samples of mutant and wild-type SaClpP were analyzed in buffer D with different concentrations (7.5–80 μM). Samples of mutant and wild-type SaClpP with ADEP were analyzed in buffer D + 0.6% (v/v) DMSO with a protein concentration of 7.5 μM. Scanning intervals were set to 0.003 cm. All data were verified by at least two

independent experiments. Data analysis was performed using the 'Time Course' function of the SedView programme. In addition, all the sedimentation experiments were evaluated with the UltraScan II software.

Small angle X-ray scattering. SAXS data for solutions of SaClpP wild-type and mutant samples free and bound to ADEP were recorded on an in-house SAXS instrument (SAXSess mc2, Anton Paar, Graz, Austria) equipped with a Kratky camera, a sealed X-ray tube source and a two-dimensional Princeton Instruments PI · SCX:4300 (Roper Scientific) CCD detector. The scattering patterns were measured with a 90-min exposure time (540 frames, each 10 s) for several solute concentrations in the range 1.8–8.2 mg ml^{-1}. Data for each sample was recorded at three different concentrations, that is, undiluted, at half concentration and one-fourth concentration. As no changes in the shape of the SAXS curves were observed for all samples recorded at different dilutions, the highest concentration with the best signal-to-noise ratio was selected to prepare the figures and for further analysis. Tag-free or C-terminal Strep-tagged proteins were purified by size exclusion chromatography prior to measurement. Samples were taken from the central peak fractions and treated with either ADEP4/7 (50 mM stocks in DMSO, final concentration range: 84–380 µM corresponding to a 1:1 ratio of ADEP:SaClpP) or the respective amount of DMSO (0.6% (v/v) max). Radiation damage was excluded based on a comparison of individual frames of the 90-min exposures, where no changes were detected. A range of momentum transfer of $0.012 < s < 0.63$ $Å^{-1}$ was covered ($s = 4\pi\sin(\theta)/\lambda$, where 2θ is the scattering angle and $\lambda = 1.5$ Å is the X-ray wavelength). All SAXS data were analyzed with the package ATSAS (version 2.5). The data were processed with the SAXSQuant software (version 3.9), and desmeared using the programmes GNOM[64] and GIFT[65]. The forward scattering, $I(0)$, the radius of gyration, R_g, the maximum dimension, D_{max}, and the inter-atomic distance distribution functions, ($P(R)$), were computed with the programme GNOM. The masses of the solutes were evaluated by comparison of the forward scattering intensity with that of a human serum albumin reference solution (molecular mass 69 kDa). To generate *ab initio* shape models, a total number of 20 models were calculated using the programme DAMMIF[66] and aligned and averaged using the programme DAMAVER[67]. C72 and C7 symmetry was defined for tetradecameric and heptameric SaClpP, respectively. The *ab initio* shape

models were aligned with crystal structures of SaClpP (PDB IDs 3V5E and 3QWD) using the programme SUPCOMB[68].

Dynamic light scattering. Protein samples in buffer D (322 µM) with ADEP (322 µM) or DMSO (3%) were loaded into disposable plastic cuvettes. DLS was measured on a Wyatt DynaPro Nanostar laser photometer (662.3 nm) at 25 °C. For each sample, 10 measurements were performed, which consisted of 10 acquisitions each with an acquisition time of 5 s. Data were fit with Dynamics version 7 software to a multimodal spheric model. *P* values were calculated in OriginPro using an independent two-sample *t*-test (N = 10) with equal variances not assumed.

SaClpXP assay. Degradation assays were performed in PZ buffer (25 mM Hepes, 200 mM KCl, 5 mM $MgCl_2$, 1 mM DTT, 10% (v/v) glycerol, pH 7.6) with 60 µl reaction volume at 30 °C. GFP fluorescence was monitored in white, flat-bottom well plates (Greiner) by exciting at 465 nm and measuring emission at 535 nm using an Infinite F200 Pro (Tecan). Degradation reactions contained 0.4 µM $SaClpX_6$, 0.2 µM $ClpP_{14}$, 0.36 µM GFP–ssrA and an ATP regeneration system (4 mM ATP, 16 mM creatine phosphate, 20 U ml^{-1} creatine phosphokinase). 0.6 µl (1% of reaction volume) ADEP was added in different concentrations in DMSO. All reaction partners except the substrate were pre-incubated for 10 min at 30 °C. GFP–ssrA was added to start the reaction. All data were recorded in triplicate measurements. GFP unfolding activity was derived as initial slopes in fluorescence time courses. Reactions were quenched after 3 h by addition of SDS sample buffer, and samples were analyzed both by denaturing and weakly denaturing SDS–PAGE for Coomassie and in-gel GFP fluorescence analysis, respectively.

Binding site identification. SaClpP (10 µM) was treated with β-lactone D3 (100 µM) in buffer D and incubated for 1 h at 25 °C. It was checked by protein mass spectrometry for complete modification and the sample was then buffer-exchanged to 50 mM ammonium bicarbonate (pH 7.3). Following a trypsin digest, peptides were analyzed on a LTQ Orbitrap XL mass spectrometer (Thermo Scientific)[39]. Data analysis was performed with the SEQUEST algorithm and the *S. aureus* NCTC 8325 proteome via Bioworks software allowing for covalent modification with D3 (monoisotopic mass: 262.1933 amu) on serine, threonine, cysteine, histidine and lysine residues.

***In vitro* activity-based protein profiling.** SaClpP (1 mM) was incubated with alkyne-tagged β-lactones (50 µM) in buffer D for 1 h at room temperature in a total volume of 100 µl, and the entire procedure of click-chemistry-mediated attachment of a fluorophore, separation via SDS–PAGE and fluorescence scanning have been described previously[39]. See the Supplementary Methods and Supplementary Figs 8–12 for the synthesis of the four stereoisomers of β-lactone U1.

Acknowledgements

We are grateful to Deutsche Forschungsgemeinschaft [(Emmy Noether program MA 5703/1-1, to T.M.), FOR 854 (to H.B.-O. and P.S.), SFB 1035 (to S.A.S)], CIPSM (to S.A.S.) and the European Research Council (ERC starting grant to S.A.S.) for funding the research. This work was further supported by the Bavarian Ministry of Sciences, Research and the Arts (Bavarian Molecular Biosystems Research Network to T.M.). We acknowledge the Leibniz Supercomputing Centre (LRZ, www.lrz.de) for providing computing time on the Linux Cluster. We thank Mona Wolff and Katja Bäuml for technical assistance; Hamed Kooshapur and Michael Sattler for access to the ITC calorimeter; Michael Groll for access to the DLS laser photometer; as well as Berthold Hinzen, Holger Paulsen and Siegfried Raddatz for ADEP synthesis.

Author contributions

M.G., K.F., M.D., I.M., P.S. produced the proteins and performed the biochemical experiments. C.G. and T.M. performed SAXS measurements and modelling; M.G. and V.S.K. synthesized β-lactones; K.R. performed ultracentrifugation experiments; H.R.-S. provided ADEPs. S.A.S., H.B.-O. and M.G. designed the experiments and wrote the manuscript. All authors analyzed the data, discussed the results and provided input for the preparation of the manuscript.

References

1. Drag, M. & Salvesen, G. S. Emerging principles in protease-based drug discovery. *Nat. Rev. Drug Discov.* **9**, 690–701 (2010).
2. Huber, E. M. & Groll, M. Inhibitors for the immuno- and constitutive proteasome: current and future trends in drug development. *Angew. Chem. Int. Ed.* **51**, 8708–8720 (2012).
3. Turk, B. Targeting proteases: successes, failures and future prospects. *Nat. Rev. Drug Discov.* **5**, 785–799 (2006).
4. Brötz-Oesterhelt, H. & Sass, P. Bacterial caseinolytic proteases as novel targets for antibacterial treatment. *Int. J. Med. Microbiol.* **304**, 23–30 (2014).
5. Böttcher, T. & Sieber, S. A. β-Lactones as specific inhibitors of ClpP attenuate the production of extracellular virulence factors of *Staphylococcus aureus*. *J. Am. Chem. Soc.* **130**, 14400–14401 (2008).
6. Geiger, S. R., Böttcher, T., Sieber, S. A. & Cramer, P. A conformational switch underlies ClpP protease function. *Angew. Chem. Int. Ed.* **50**, 5749–5752 (2011).
7. Frees, D., Qazi, S. N., Hill, P. J. & Ingmer, H. Alternative roles of ClpX and ClpP in *Staphylococcus aureus* stress tolerance and virulence. *Mol. Microbiol.* **48**, 1565–1578 (2003).
8. Böttcher, T. & Sieber, S. A. Structurally refined β-lactones as potent inhibitors of devastating bacterial virulence factors. *Chembiochem* **10**, 663–666 (2009).
9. Brötz-Oesterhelt, H. *et al*. Dysregulation of bacterial proteolytic machinery by a new class of antibiotics. *Nat. Med.* **11**, 1082–1087 (2005).
10. Kirstein, J. *et al*. The antibiotic ADEP reprogrammes ClpP, switching it from a regulated to an uncontrolled protease. *EMBO Mol. Med.* **1**, 37–49 (2009).
11. Katayama-Fujimura, Y., Gottesman, S. & Maurizi, M. R. A multiple-component, ATP-dependent protease from *Escherichia coli*. *J. Biol. Chem.* **262**, 4477–4485 (1987).
12. Maurizi, M. R. *et al*. Sequence and structure of ClpP, the proteolytic component of the ATP-dependent Clp protease of *Escherichia coli*. *J. Biol. Chem.* **265**, 12536–12545 (1990).
13. Wang, J., Hartling, J. A. & Flanagan, J. M. The structure of ClpP at 2.3 Å resolution suggests a model for ATP-dependent proteolysis. *Cell* **91**, 447–456 (1997).
14. Sauer, R. T. *et al*. Sculpting the proteome with AAA(+) proteases and disassembly machines. *Cell* **119**, 9–18 (2004).
15. Sauer, R. T. & Baker, T. A. AAA+ proteases: ATP-fueled machines of protein destruction. *Annu. Rev. Biochem.* **80**, 587–612 (2011).
16. Gottesman, S., Roche, E., Zhou, Y. & Sauer, R. T. The ClpXP and ClpAP proteases degrade proteins with carboxy-terminal peptide tails added by the SsrA-tagging system. *Genes Dev.* **12**, 1338–1347 (1998).
17. Weber-Ban, E. U., Reid, B. G., Miranker, A. D. & Horwich, A. L. Global unfolding of a substrate protein by the Hsp100 chaperone ClpA. *Nature* **401**, 90–93 (1999).
18. Martin, A., Baker, T. A. & Sauer, R. T. Protein unfolding by a AAA+ protease is dependent on ATP-hydrolysis rates and substrate energy landscapes. *Nat. Struct. Mol. Biol.* **15**, 139–145 (2008).
19. Gersch, M., List, A., Groll, M. & Sieber, S. A. Insights into the structural network responsible for oligomerization and activity of the bacterial virulence regulator caseinolytic protease P (ClpP). *J. Biol. Chem.* **287**, 9484–9494 (2012).
20. Liu, K., Ologbenla, A. & Houry, W. A. Dynamics of the ClpP serine protease: a model for self-compartmentalized proteases. *Crit. Rev. Biochem. Mol. Biol.* **49**, 400–412 (2014).
21. Maurizi, M. R., Thompson, M. W., Singh, S. K. & Kim, S. H. Endopeptidase Clp: ATP-dependent Clp protease from *Escherichia coli*. *Methods Enzymol.* **244**, 314–331 (1994).
22. Joshi, S. A., Hersch, G. L., Baker, T. A. & Sauer, R. T. Communication between ClpX and ClpP during substrate processing and degradation. *Nat. Struct. Mol. Biol.* **11**, 404–411 (2004).
23. Kim, Y. I. *et al*. Molecular determinants of complex formation between Clp/Hsp100 ATPases and the ClpP peptidase. *Nat. Struct. Mol. Biol.* **8**, 230–233 (2001).
24. Lee, B.-G. *et al*. Structures of ClpP in complex with acyldepsipeptide antibiotics reveal its activation mechanism. *Nat. Struct. Mol. Biol.* **17**, 471–478 (2010).
25. Li, D. H. S. *et al*. Acyldepsipeptide antibiotics induce the formation of a structured axial channel in ClpP: a model for the ClpX/ClpA-bound state of ClpP. Chem. Biol. 17, 959–969 (2010).
26. Sass, P. *et al*. Antibiotic acyldepsipeptides activate ClpP peptidase to degrade the cell division protein FtsZ. *Proc. Natl Acad. Sci. USA* **108**, 17474–17479 (2011).
27. Conlon, B. P. *et al*. Activated ClpP kills persisters and eradicates a chronic biofilm infection. *Nature* **503**, 365–370 (2013).
28. Hinzen, B. *et al*. Medicinal chemistry optimization of acyldepsipeptides of the enopeptin class antibiotics. *ChemMedChem* **1**, 689–693 (2006).
29. Leung, E. *et al*. Activators of cylindrical proteases as antimicrobials: identification and development of small molecule activators of ClpP protease. *Chem. Biol.* **18**, 1167–1178 (2011).
30. Freiburger, L. A., Auclair, K. & Mittermaier, A. K. Elucidating protein binding mechanisms by variable-c ITC. *Chembiochem* **10**, 2871–2873 (2009).
31. Gersch, M. *et al*. The mechanism of caseinolytic protease (ClpP) inhibition. *Angew. Chem. Int. Ed.* **52**, 3009–3014 (2013).
32. Gersch, M., Kreuzer, J. & Sieber, S. A. Electrophilic natural products and their biological targets. *Nat. Prod.*

Rep. **29**, 659–682 (2012).
33. Zhang, J. *et al*. Structural switching of *Staphylococcus aureus* Clp protease—a key to understanding protease dynamics. *J. Biol. Chem.* **286**, 37590–37601 (2011).
34. Alexopoulos, J. A., Guarne, A. & Ortega, J. ClpP: a structurally dynamic protease regulated by AAA+ proteins. *J. Struct. Biol.* **179**, 202–210 (2012).
35. Sprangers, R., Gribun, A., Hwang, P., Houry, W. & Kay, L. E. Quantitative NMR spectroscopy of supramolecular complexes: dynamic side pores in ClpP are important for product release. *Proc. Natl Acad. Sci. USA* **102**, 16678–16683 (2005).
36. Ye, F. *et al.* Helix unfolding/refolding characterizes the functional dynamics of *Staphylococcus aureus* Clp protease. *J. Biol. Chem.* **288**, 17643–17653 (2013).
37. Kimber, M. S. *et al.* Structural and theoretical studies indicate that the cylindrical protease ClpP samples extended and compact conformations. *Structure* **18**, 798–808 (2010).
38. Gribun, A. *et al*. The ClpP double ring tetradecameric protease exhibits plastic ring-ring interactions, and the N termini of its subunits form flexible loops that are essential for ClpXP and ClpAP complex formation. *J. Biol. Chem.* **280**, 16185–16196 (2005).
39. Gersch, M., Kolb, R., Alte, F., Groll, M. & Sieber, S. A. Disruption of oligomerization and dehydroalanine formation as mechanisms for ClpP protease inhibition. *J. Am. Chem. Soc.* **136**, 1360–1366 (2014).
40. Zeiler, E. *et al.* Vibralactone as a tool to study the activity and structure of the ClpP1P2 complex from *Listeria monocytogenes*. *Angew. Chem. Int. Ed.* **50**, 11001–11004 (2011).
41. Kim, Y. I., Burton, R. E., Burton, B. M., Sauer, R. T. & Baker, T. A. Dynamics of substrate denaturation and translocation by the ClpXP degradation machine. *Mol. Cell* **5**, 639–648 (2000).
42. El Bakkouri, M. *et al.* Structural insights into the inactive subunit of the apicoplast-localized caseinolytic protease complex of *Plasmodium falciparum*. *J. Biol. Chem.* **288**, 1022–1031 (2013).
43. Lee, B. G., Kim, M. K. & Song, H. K. Structural insights into the conformational diversity of ClpP from *Bacillus subtilis*. *Mol. Cell* **32**, 589–596 (2011).
44. Stinson, B. M. *et al*. Nucleotide binding and conformational switching in the hexameric ring of a AAA+ machine. *Cell* **153**, 628–639 (2013).
45. Martin, A., Baker, T. A. & Sauer, R. T. Distinct static and dynamic interactions control ATPase-peptidase communication in a AAA+ protease. *Mol. Cell* **27**, 41–52 (2007).
46. Glynn, S. E., Martin, A., Nager, A. R., Baker, T. A. & Sauer, R. T. Structures of asymmetric ClpX hexamers reveal nucleotide-dependent motions in a AAA+ protein-unfolding machine. *Cell* **139**, 744–756 (2009).
47. Bewley, M. C., Graziano, V., Griffin, K. & Flanagan, J. M. The asymmetry in the mature amino-terminus of ClpP facilitates a local symmetry match in ClpAP and ClpXP complexes. *J. Struct. Biol.* **153**, 113–128 (2006).
48. Sowole, M. A., Alexopoulos, J. A., Cheng, Y. Q., Ortega, J. & Konermann, L. Activation of ClpP protease by ADEP antibiotics: insights from hydrogen exchange mass spectrometry. *J. Mol. Biol.* **425**, 4508–4519 (2013).
49. Boehr, D. D., Nussinov, R. & Wright, P. E. The role of dynamic conformational ensembles in biomolecular recognition. *Nat. Chem. Biol.* **5**, 789–796 (2009).
50. Zorn, J. A. & Wells, J. A. Turning enzymes ON with small molecules. *Nat. Chem. Biol.* **6**, 179–188 (2010).
51. Kang, S. G., Maurizi, M. R., Thompson, M., Mueser, T. & Ahvazi, B. Crystallography and mutagenesis point to an essential role for the N-terminus of human mitochondrial ClpP. *J. Struct. Biol.* **148**, 338–352 (2004).
52. Kang, S. G. *et al*. Functional proteolytic complexes of the human mitochondrial ATP-dependent protease, hClpXP. *J. Biol. Chem.* **277**, 21095–21102 (2002).
53. Kang, S. G., Dimitrova, M. N., Ortega, J., Ginsburg, A. & Maurizi, M. R. Human mitochondrial ClpP is a stable heptamer that assembles into a tetradecamer in the presence of ClpX. *J. Biol. Chem.* **280**, 35424–35432 (2005).
54. Jennings, L. D., Bohon, J., Chance, M. R. & Licht, S. The ClpP N-terminus coordinates substrate access with protease active site reactivity. *Biochemistry* **47**, 11031–11040 (2008).
55. Schmitz, K. R., Carney, D. W., Sello, J. K. & Sauer, R. T. Crystal structure of *Mycobacterium tuberculosis* ClpP1P2 suggests a model for peptidase activation by AAA+ partner binding and substrate delivery. *Proc. Natl Acad. Sci. USA* **111**, E4587–E4595 (2014).
56. Effantin, G., Maurizi, M. R. & Steven, A. C. Binding of the ClpA unfoldase opens the axial gate of ClpP peptidase. *J. Biol. Chem.* **285**, 14834–14840 (2010).
57. Maya, S. *et al*. The ClpXP protease unfolds substrates using a constant rate of pulling but different gears. *Cell* **155**, 636–646 (2013).
58. Maillard, R. A. *et al*. ClpX(P) generates mechanical force to unfold and translocate its protein substrates. *Cell* **145**, 459–469 (2011).
59. Grimaud, R., Kessel, M., Beuron, F., Steven, A. C. & Maurizi, M. R. Enzymatic and structural similarities between the *Escherichia coli* ATP-dependent proteases, ClpXP and ClpAP. *J. Biol. Chem.* **273**, 12476–12481 (1998).
60. Ortega, J., Lee, H. S., Maurizi, M. R. & Steven, A. C. Alternating translocation of protein substrates from both ends of ClpXP protease. *EMBO J.* **21**, 4938–4949 (2002).
61. Turgay, K., Hahn, J., Burghoorn, J. & Dubnau, D. Competence in *Bacillus subtilis* is controlled by regulated proteolysis of a transcription factor. *EMBO J.* **17**, 6730–6738 (1998).
62. Kirstein, J. *et al*. Adaptor protein controlled oligomerization activates the AAA+ protein ClpC. *EMBO J.* **25**, 1481–1491 (2006).
63. Ober, M., Muller, H., Pieck, C., Gierlich, J. & Carell, T. Base pairing and replicative processing of the formamidopyrimidine-dG DNA lesion. *J. Am. Chem. Soc.* **127**, 18143–18149 (2005).
64. Svergun, D. I. Determination of the regularization parameter in indirect-transform methods using perceptual

criteria. *J. Appl. Crystallogr.* **25**, 495–503 (1992).
65. Bergmann, A., Fritz, G. & Glatter, O. Solving the generalized indirect Fourier transformation (GIFT) by Boltzmann simplex simulated annealing (BSSA). *J. Appl. Crystallogr.* **33**, 1212–1216 (2000).
66. Franke, D. & Svergun, D. I. DAMMIF, a program for rapid ab-initio shape determination in small-angle scattering. *J. Appl. Crystallogr.* **42**, 342–346 (2009).
67. Volkov, V. V. & Svergun, D. I. Uniqueness of ab initio shape determination in small-angle scattering. *J. Appl. Crystallogr.* **36**, 860–864 (2003).
68. Kozin, M. B. & Svergun, D. I. Automated matching of high- and low-resolution structural models. *J. Appl. Crystallogr.* **34**, 33–41 (2001).

Conformational control of the bacterial Clp protease by natural product antibiotics

I. T. Malik and H. Brötz-Oesterhelt*

*Department of Microbial Bioactive Compounds, Interfaculty Institute of Microbiology and Infection Medicine, University of Tuebingen, Germany. E-mail: heike.broetz-oesterhelt@uni-tuebingen.de

Imran Malik *et al.*, Conformational control of the bacterial Clp protease by natural product antibiotics.
Natural Product Reports (2017) 34(7), 815-831
doi: 10.1039/c6np00125d

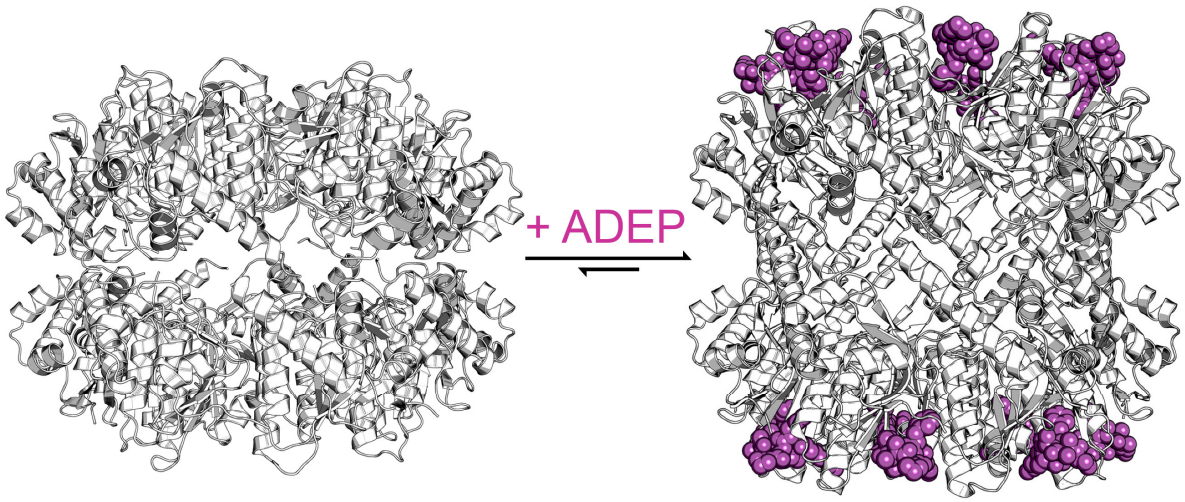

Natural products dysregulate the Clp protease by allosteric activation and opening the gated pore.

Abstract

The bacterial Clp protease is a highly conserved and structurally versatile machine. It has gained a lot of recognition during the last decade as a novel antibacterial drug target with an unprecedented mechanism of action. Due to its complexity, there are distinct means of interfering with its natural functions and several compounds targeting this machine have been identified. In this review, we summarize the current state of knowledge about natural products deregulating Clp proteolysis, a crucial and delicate process within the cell. Among those, acyldepsipeptide antibiotics of the ADEP class (ADEPs) are characterized best. The molecular mechanism of ADEP-mediated deregulation sheds light on the inner workings of the Clp protease.

1 Introduction

Bacterial resistances towards antibiotics pose a huge problem for the treatment of infectious diseases.[1,2] Until recently, antibiotic development largely relied on synthetic modifications of established antibiotic classes to overcome resistances by compound derivatization. However, this source is running dry and new antibiotic classes with unprecedented core structures are urgently needed to overcome the plethora of resistance mechanisms spreading through the bacterial population. Antibacterial agents with unrelated chemical scaffolds often act by novel mechanisms of bacterial growth inhibition and are less affected by widespread resistance traits. New means of killing multi-drug resistant bacteria must be found.

Microbial natural products are a privileged source of antibacterial lead structures. Being produced by microorganisms themselves and optimized through co-evolution with bacterial competitors for billions of years, they often surpass synthetic comparators with regard to cell entry and complex target interactions.[3,4] Most antibiotics in therapeutic use to date inhibit essential functions in DNA, RNA, protein or cell wall syntheses, whereas daptomycin and polymyxins interfere with membrane integrity, but rarely is a completely unrelated mode of action described for a novel antibacterial agent with good tolerance and promising efficacy in infection models.

During the last decade, a bacterial protease has emerged as an unprecedented antibacterial target in the course of mode of action studies on acyldepsipeptide

antibiotics (ADEPs). Isolated from the fermentation broth of *Streptomyces hawaiiensis*, the natural products A54556 A and B (factor A and B) showed good antibiotic activity *in vitro* without mechanism-based cross-resistance to other known antibiotics.[5,6] Identification of the resistance-mediating mutation within an ADEP-resistant *Escherichia coli* mutant and affinity chromatography with an immobilized ADEP congener lead to ClpP as the direct target.[6] Medicinal chemistry campaigns established the structure-activity relationship and led to a number of derivatives with enhanced *in vitro* potency and stability.[7–10] Furthermore, ADEP treatment proved successful in lethal bacterial infections in rodents, including deep-seated biofilm infections, and, in combination with e.g. rifampicin, eradicated persister cells of methicillin-resistant *Staphylococcus aureus*.[6,7,11]

ClpP is a serine peptidase with active sites shielded within its barrel shaped proteolytic chamber. It can only degrade peptides on its own but is capable of protein degradation when partnering with a cognate Clp/Hsp100 chaperone (Clp-ATPase). As ClpP can act in conjunction with several Clp-ATPases, the resulting proteolytic complexes differ in their respective Hsp100 module. However, as they uniquely contain ClpP as the proteolytic core, we will refer to the complex consisting of ClpP and any corresponding Clp-ATPase as the "Clp protease". The Clp protease system has a multitude of functions in bacteria, including protein quality control and homeostasis, stress management, virulence factor expression, and regulation of cell differentiation programmes.[12–14] Its function is also essential for viability in actinobacteria including *Mycobacterium tuberculosis*.[15]

Following the first reports on ADEP, other natural products were recently discovered to modulate, i. e. inhibit or activate, either the proteolytic core ClpP or its Hsp100 partners. In this review, while briefly touching on the promising biological activities of these compounds, we will focus on the intriguing mechanistic interaction between the Clp protease system and its natural product modulators. Among those, ADEP is best understood. The interplay between ClpP and ADEP stands representative for a new principle of killing bacteria by targeting and deregulating a protease system. Furthermore, ADEPs are instrumental in understanding the molecular operation mode of the complex Clp protease machinery.

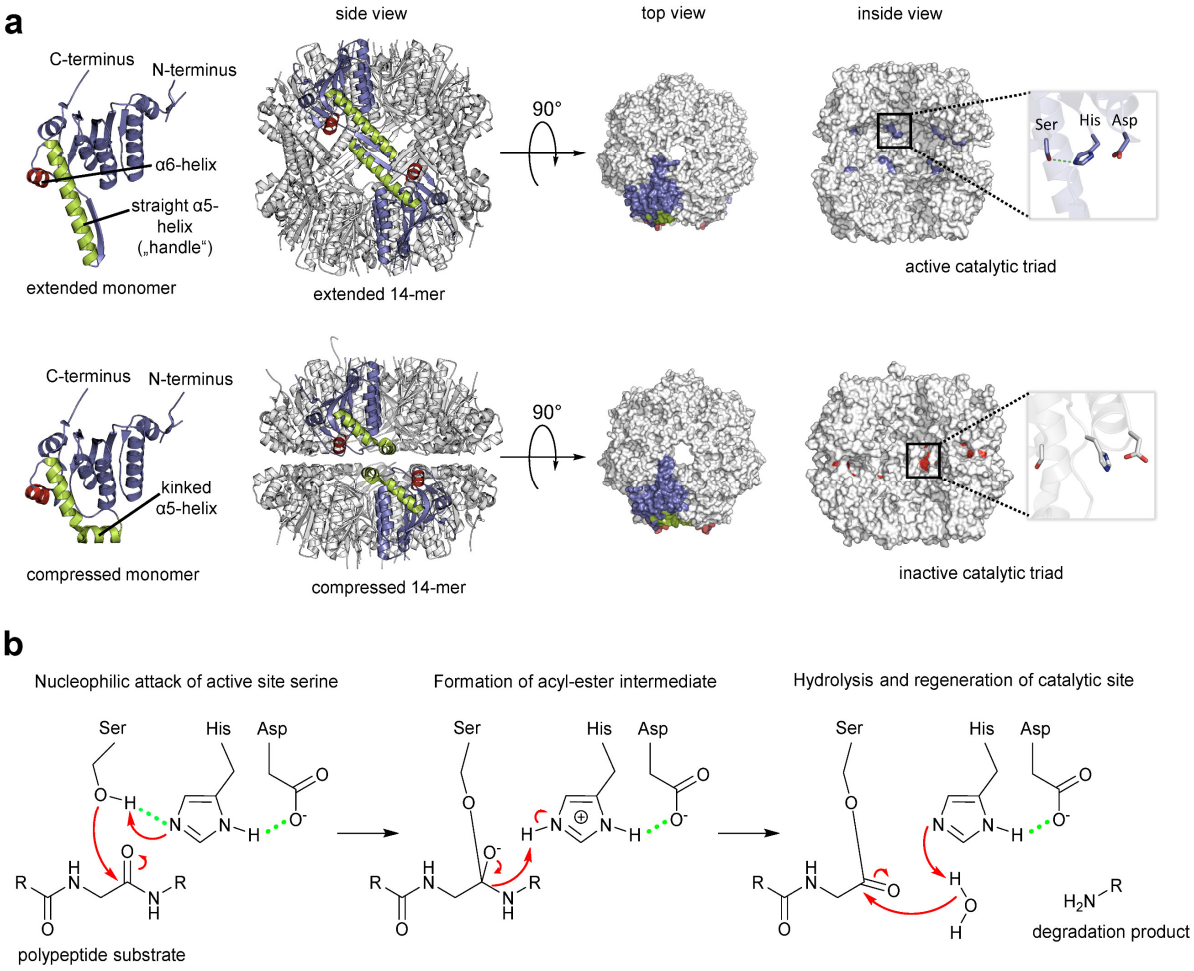

Fig. 1 The proteolytic core of the Clp protease, ClpP. (a) Crystal structures of ClpP from *S. aureus*. Overview of the ClpP architecture both in active extended (PDB code: 3V5E) and in inactive compressed conformation (PDB code: 3QWD). Two opposing subunits are highlighted in colour. The α5- and α6-helices responsible for the ring-ring connection are coloured in green and red, respectively. The top and inside views are depicted in a surface fill model representation. The inside view reveals the catalytic sites within the barrel and the orientations of the residue side chains. The histidine side chain imidazole is rotated away from the hydrolytic serine hydroxyl function in the inactive arrangement and cannot form a hydrogen bond. The hydrogen bond network required to stabilize the reaction intermediate cannot be formed. (b) Catalytic mechanism of the model serine protease ClpP. Key interactions within the catalytic triad during peptide bond cleavage are indicated (reaction details are given in the text).

2 ClpP structure and function

2.1 ClpP and AAA+ chaperones regulate protein homeostasis, stress response, cellular differentiation, and virulence

The Clp protease system is widely conserved within the bacterial domain and is functionally organized in two separate compartments. The Clp/Hsp100 enzymes of the AAA+ super family of chaperones (Clp-ATPases) select substrates for degradation, unfold and thread them into the proteolytically active ClpP in an ATP-dependent fashion. There is a number of different Clp-ATPases that associate with ClpP for

protein degradation, e. g. ClpX and ClpA in *E. coli*, ClpX and ClpC in *Staphylococcus aureus*, ClpX and ClpC1 in *Mycobacterium tuberculosis*, to name a few. Each shows distinct substrate specificities and performs different cellular functions, albeit there are some redundancies. In the beginning, the characterization of the Clp protease took place primarily in non-pathogenic *E. coli* and *Bacillus subtilis* strains. In *E. coli*, loss-of-function of ClpP or Clp-ATPases causes only a mild phenotype, as here, the Clp system shares functions in protein homoeostasis with the Lon protease.[16,17] In *B. subtilis*, *clpP* deletion prevents motility, sporulation and genetic competence.[18] Heat tolerance and stationary phase survival are also reduced and accumulation of the stress regulator Spx in a *clpP* or *clpX* mutant is toxic and impairs growth.[18,19] Trapping experiments with a proteolytically inactive ClpP variant revealed protein substrates with important functions in global stress, cell division, global transcription regulation, DNA damage repair, and protein synthesis.[13,20] Meanwhile, the Clp protease is validated as a drug target in pathogenic organisms, as recently reviewed.[21–23] For instance, in *S. aureus*, the Clp protease is responsible for stress tolerance and involved in virulence regulation.[24,25] *ClpP* and *clpX* deletions were shown to attenuate *S. aureus* in a murine skin abscess model and a *Staphylococcus epidermidis clpP* deletion mutant proved less virulent in a catheter infection in rats.[26,27] A synthetic β-lactone acting as a covalent suicide inhibitor of ClpP was effective in treating staphylococcal skin abscesses in mice, demonstrating druggability of ClpP's catalytic triad.[28] *ClpP* deletions further prevented *Streptococcus pneumoniae* from colonizing the nasopharynx and infecting lungs of mice, and reduced survival of *Listeria monocytogenes* within macrophages.[29,30] While the Clp-ATPases and the ClpP peptidase work together in general degradation of misfolded and aggregated proteins as well as in directed regulatory proteolysis, Clp-ATPases also possess chaperone activity independently of the peptidase.[31,32] They can actively induce structural changes within their substrates altering their biological activity. For instance, one of the first characterized substrates of *E. coli* ClpX was the Mu transposase.[33] ClpX alters its conformation and thereby initiates the transition from recombination to Mu phage replication without the need of a partner peptidase.[33,34] Secondly, expression of *spa*, the gene encoding protein A in *S. aureus*, is nearly abolished in a *clpX* but not a c*lpP* mutant.[26] Protein A is a virulence factor expressed in the early growth phase and hampers detection by the host immune system. It is under negative regulatory control of the accessory gene regulator (*agr*) quorum sensing system, which is activated in

the late exponential phase of growth and down-regulates protein A expression by post-transcriptional inhibiton.[35,36] The repression of *spa* in a *clpX* mutant works independently of *agr* and counteracts the normally occurring derepression in an *agr* negative strain.[24] ClpC in *S. aureus* plays an important role in acetate catabolism and has been further characterized as a global regulator in late growth phase carbon metabolism.[37,38] In *M. tuberculosis*, the entire Clp protease system including the chaperones ClpX, ClpC1 and ClpB as well as the two ClpP paralogs, ClpP1 and ClpP2, is essential for growth.[15,39–42] Compounds targeting the ClpC1 ATPase in mycobacteria display potent antibacterial activity. In Gram-negatives, the Clp protease is implicated with the type III secretion system and a lack of functional ClpX results in severely attenuated or abolished virulence.[43–45] Reviewed examples and similar reports established the Clp protease as a promising novel drug target.

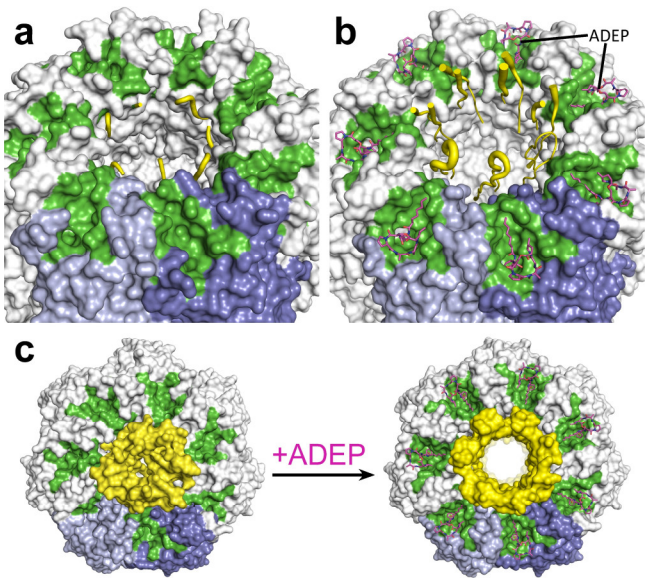

Fig. 2 View on the apical side of a ClpP tetradecamer from *E. coli*. (a) "Down"-conformation of the N-terminus of ClpP (PDB code: 1YG6): Two neighbouring ClpP subunits are coloured in shades of blue, the hydrophobic pockets, each spanning two ClpP subunits, are highlighted in green. The N-terminal loops (yellow) surrounding the axial pore are disordered and close the channel by serving as a hydrophobic plug. (b) "Open gate"-conformation of the N-terminus of the ClpP/ADEP-complex (PDB code: 3MT6). In the representation of the N-terminal loops, strength of the ribbon correlates with flexibility. Three loops are completely resolved and show a β-hairpin structure that points upwards. Flexibility of the N-terminal loops increases towards the rip region, indicated by unresolved structures in the four other loops. In contrast to the "up"-conformation reported for apo-ClpP, this structure has an increased pore diameter of 20 Å. (c) Top view of the structured axial channel in the apo form of ClpP in the "up"-conformation (left) and the widened pore of ClpP in complex with ADEP (right).

2.2 ClpP forms the proteolytic core of a compartmentalized protease

Fourteen ClpP protomers arrange themselves to form a tetradecameric barrel-shaped complex in a stack of two heptameric rings (Fig. 1a). The catalytic residues are located within the sequestered space of the barrel. Seven hydrophobic pockets on both sides of the barrel serve as anchors for partner Clp-ATPases during translocation of substrates into the proteolytic chamber of ClpP (Fig. 2).[46,47] Several crystal structures of ClpP from different species have revealed distinct barrel conformations, namely compressed, compact and extended state.[48–52] Based on molecular dynamics (MD) simulation experiments, the compact conformation has been speculated to represent

a stable intermediate state between extended and compressed, showing a local energy minimum during transitions between extended and compressed conformations.[48] Here, we focus only on the two end-points of this transition (Fig. 1a). The compressed conformation, about 80 Å in height, is deemed to be inactive because of the arrangement of the active site residues with an increased distance between the serine and the histidine side chain, whereas crystal structures of extended conformations, where the barrel is elongated by approximately 10 Å along the rotational axis, show the active site residues in reduced distance (Fig. 1a).[49,53–55] In the course of the nucleophilic attack of the active site serine on the electron deficient carbonyl carbon of the peptide bond, the proton of the serine hydroxyl group is abstracted by the histidine imidazole and the positive charge thereby generated at the histidine imidazole is stabilized by the carboxyl function of the aspartate (Fig. 1b). The resulting acyl-ester intermediate then undergoes hydrolysis and the serine side chain is regenerated to undergo the next cycle of catalysis. In the catalytically competent conformation, these three side chains are in the correct distance to form hydrogen bonds (see green dotted lines in Fig. 1b), which strongly enhance nucleophilicity of the serine. This competent conformation has so far only been observed in crystal structures that captured ClpP in the extended conformation, but never in crystals containing compressed conformations. Notably, other key structural elements show considerable shifts between the two conformations in X-ray crystallography structures. These shifts correlate with predicted residue flexibility from MD simulation experiments.[55] The most flexible domains of a ClpP protomer are the N-terminal loop and the α5-helix. The latter is associated with the ring-ring interface in the equatorial plane and is also known as the handle region.[50] The handle of each ClpP subunit adopts a straight orientation in the extended conformation while it is kinked in the compressed structure (Fig. 1a). The physiological significance of these conformations and their regulation are still subject to investigation.[49,51] A crystal structure of ClpP with an inhibitor covalently bound to the active site displayed a slightly more compacted conformation, corroborating the idea of a functional link between conformation and catalysis.[56] One model proposes an exit route for peptide products *via* transient equatorial pore openings in the compressed situation with the compression motion being part of a natural cycle of ClpP dynamics.[57–61] Introducing covalent cross-links between handle regions of neighbouring ClpP subunits resulted in decreased handle flexibility and displayed increased substrate retention times within the ClpP lumen.[59]

This finding strongly supports the idea of an involvement of the handle region in product release. Nonetheless, product release *via* the axial pores or a combination of both cannot be ruled out, yet. While most compressed crystal structures of ClpP show a disordered tip of the α5-helix, two structures from *S. aureus* reveal a kinked orientation.[49,55] In this state, the handle is stabilized by hydrogen bonds within its own subunit.[48] In the extended state, a straight α5-helix is involved in a network of hydrogen bonds stabilizing the ring-ring connection between the two heptamers.[55] This network of hydrogen bonds connects the tip of the extended helix of one ClpP subunit (Fig. 1a, green helix) to amino acid residues in the α6-helix of the opposing ClpP subunit (Fig. 1a, red helix). Mutation studies of these amino acid residues termed “oligomerization sensors” showed defects in oligomeric state formation and catalytic capabilities, stressing the importance of the handle to make contact to the opposing ring.[51] Interestingly, MD simulations indicate a tendency towards the compressed state in the absence of the hydrogen bond network due to favourable thermodynamics.[48,55] Therefore, it can be assumed that control over the conformational state is part of a protection system in the cell that requires the proteolytic extended form to be actively promoted.

2.3 The apical side of the ClpP barrel harbours interaction sites for the cognate Clp-ATPases

In the absence of a cognate Clp-ATPase, ClpP can only degrade small peptides.[62,63] The axial channels are the only opening into the catalytic chamber of ClpP.[64,65] These channels are bordered by the respective N-termini of the ClpP subunits (Fig. 2). A crystal structure of *E. coli* ClpP in the apo form displayed an “up”-conformation of the N-terminus at one apical side and a “down”-conformation at the opposite side suggesting a gating functionality of the N-terminus for substrate entry.[66] Although the N-terminal residues of the “down”-conformation are unresolved, it has been proposed that in this conformation, clustering of hydrophobic residues within the axial channel serves as a hydrophobic plug and presents the closed gate of ClpP.[67] Interestingly, the observation that only six out of seven N-terminal loops were in the “up”-conformation led the authors to speculate about a pseudo-6-fold symmetry matching the 6-fold symmetry of the partner Clp-ATPase.[66] Cryo-EM studies with a ClpP tetradecamer bound to a ClpA hexamer at one apical side only, showed an open

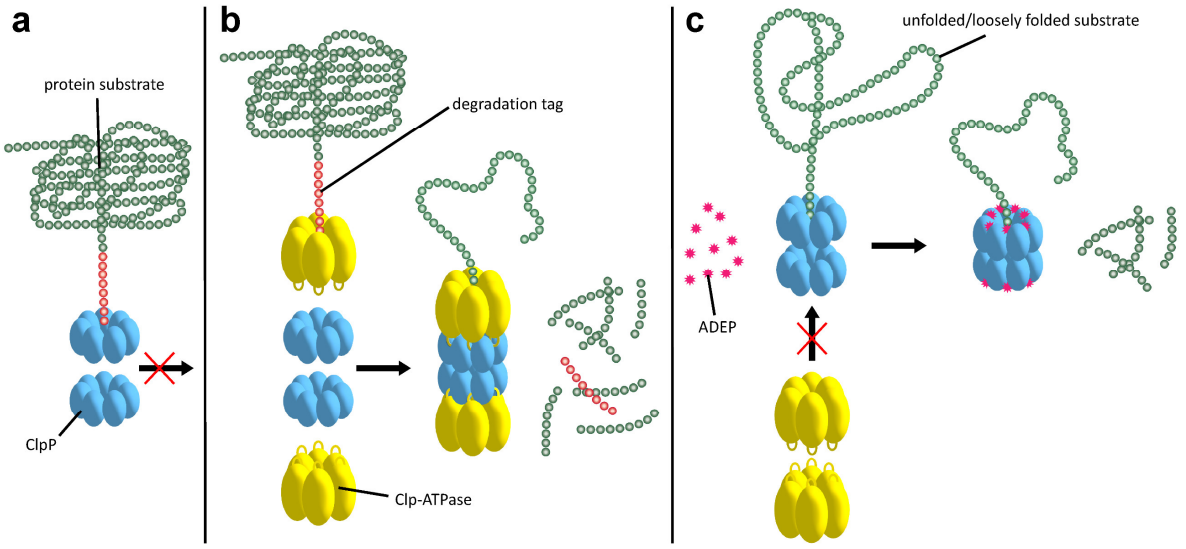

Fig. 3 Operation of the Clp protease system and deregulation by ADEP. (a) In the dormant, inactive state the ClpP barrel is either not assembled or, if already assembled, the axial pores are closed. Proteins are not degraded by ClpP when on its own. (b) In the natural context, substrates are recognized by the Clp-ATPase *via* specific degradation tags and with the aid of adapter proteins. The Clp-ATPase docks to the "hydrophobic pockets" of ClpP *via* surface loops presenting a conserved tripeptide signal, thereby initiating assembly of the ClpP tetradecamer in a conformation competent for catalysis. Furthermore, the Clp-ATPase actively unfolds the protein substrate using ATP hydrolysis and threads it into the entry pores of the catalytic chamber. (c) ADEP binding to the "hydrophobic pockets" of ClpP also assembles the ClpP barrel in a catalytically competent state. By steric hindrance, ADEP efficiently prevents the interaction of ClpP with the Clp-ATPases. As one consequence, none of the natural protein substrates can be degraded anymore. As a second consequence, ClpP pores open and some protein substrates and nascent polypeptide chains necessary for bacterial growth and survival are now degraded (dual mechanism). Degradation tags are not required for ADEP-mediated protein degradation.

channel with a diameter of 12 Å at the apical side facing ClpA, forming a continuous channel with the Clp-ATPase.[68] The N-terminal domain of ClpP on the ClpA-free side was blocked. Whether the "up"-conformation observed in the *E. coli* ClpP crystal (i. e. the state with upraised N-termini yet narrow pore diameter) resembles the open gate in the natural context when bound to Clp-ATPases, is still controversially discussed. Alexopoulos *et al.* argue that the "up"-conformation as observed in the *E. coli* structure (i. e. the state with upraised N-termini yet narrow pore diameter) might not be identical to the Clp-ATPase-bound open conformation in the substrate feeding process.[69] For more details on N-terminal gating, refer to reference 69. Structural investigations with the help of ADEP activators, which mimic binding of Clp-ATPases by employing the same binding pocket, have been instrumental in addressing the question of how these conformations are related to pore gating (compare section 3.2).[53,69,70] Furthermore, is was suggested that the "up"-conformation stabilizes the intermediate substrate-bound form of ClpP while the "down"-conformation facilitates substrate hydrolysis, thus directly involving the N-terminus in the catalytic cycle of ClpP.[71]

2.4 Proteolysis by ClpP is tightly regulated

Substrates tagged with a degradation signal like the C-terminal ssrA-tag for incomplete translation of nascent polypeptide chains are recognized and bound by ClpX.[72,73] Subsequently, ClpX assembles into hexamers and makes contact with ClpP by binding to the hydrophobic pockets *via* loops containing highly conserved (L/I/V)-GF tripeptide motifs necessary for association with ClpP and by binding the N-terminal stem loop of ClpP *via* its pore-2-loops.[46,47,74] ATP binding and hydrolysis by ClpX then provides the energy to mechanically unfold and translocate linearized protein into ClpP.[75–78] Within the proteolytic chamber, substrate is cleaved into small peptide fragments of around 6-8 residues (Fig. 3).[79,80] Thus, substrate specificity is not defined by the amino acid sequence rather than by Clp-ATPases that recognize specific degradation signals and interact with certain adapter proteins.[20,73,81–83] Exposure to the active site residues is sufficient for cleavage with no strict specificity, albeit a preference for certain amino acids at the P1 position exists.[84,85]

The Clp protease is a paradigm of self-compartmentalized proteases and shares typical architectural features with other compartmentalized proteases like HslUV or the 26S proteasome. The term self-compartmentalized expresses that the active sites reside within a proteolytic chamber (“compartment”), which is shielded from the cytoplasm and inaccessible to potential protein substrates (Fig. 3a). Cleavage is performed in this sequestered space only after active unfolding and translocation of substrate through the narrow axial pores by Clp-ATPases (Fig. 3b). These in turn select substrates by either decisive degradation signals, through contacts mediated by specific adaptor proteins, or a combination of both. Furthermore, binding of Clp-ATPases to ClpP initiates structural reorganizations within ClpP that render substrate cleavage possible.[68,86] Findings derived from the interaction of ClpP with ADEPs strongly contributed to our understanding of these reorganizations (see below).[53,67,69,70,87] In the case of *B. subtilis* ClpP, protomers do not assemble to a barrel *in vitro* unless either ClpX or ClpC is active to bind and deliver substrate.[88] These architectural restrictions are common among these proteolytic machines; they prohibit uncontrolled substrate processing and serve as safeguards against potentially harmful self-digest.[89]

3 Deregulation of the Clp protease by natural products

3.1 Uncontrolled ClpP activity is bactericidal

ADEP mimics binding of Clp-ATPases to the hydrophobic pockets. This event inhibits association of ClpP with Clp-ATPases, and thereby abolishes all natural functions of the Clp protease that require Clp-ATPase mediated degradation (Fig. 3c).[90,91] The affinity of ADEP for ClpP with a K_D of approximately 2 µM is much stronger compared to the Clp-ATPases, as a single ADEP molecule is sufficient for displacing of a full ClpX hexamer.[91] Clp protease function is essential for stress regulation and virulence in firmicutes. But, disturbing the ClpP – Clp-ATPase interaction under non-stressing *in vitro* conditions alone does not result in cell death as exemplified by *clpP* and *clpX* deletion mutants.[12,21,22] Covalent β-lactone inhibitors of ClpP lead to decreased virulence factor excretion in *S. aureus* but show no growth inhibition in *in vitro* assays for antibacterial activity.[92]

The ADEP mode of killing in firmicutes is uncontrolled proteolysis by the ClpP/ADEP complex, i. e. proteins that are not tagged for degradation are still unspecifically targeted by ClpP. ADEP binding circumvents the above mentioned safeguards and initiates structural shifts that enable ClpP to degrade the loosely folded model substrate casein and nascent polypeptide chains in an unregulated fashion.[2,37,70] The over-activated ClpP causes degradation of bacterial cell division protein FtsZ, as demonstrated in *B. subtilis*, *S. aureus*, and *Wolbachia* sp., resulting in cell division inhibition and eventually cell death.[93,94] Furthermore, Conlon *et al.* performed proteomic analysis of non-replicating methicillin-resistant *S. aureus* after long-term exposure to ADEP and identified decreased abundance in 417 proteins compared to a non-treated control.[11]

Besides acyldepsipeptide antibiotics, a number of compounds have been described to target the Clp protease (Fig. 4). A non-peptide-based natural product activator of ClpP, sclerotiamide, has recently been identified in a screening for β-casein degradation.[95] As of yet, there is no available data on neither the mechanism of ClpP binding nor antibacterial activity of this compound. In comparison to the natural product ADEP1, casein degradation was slow and rather high concentrations of sclerotiamide were required. Furthermore, sclerotiamide activity was restricted to ClpP from *E. coli*

and ClpP from *B. subtilis* could not be activated. So far, ADEP is the only natural product activator that is confirmed to target ClpP from a wide variety of organisms.

3.2 ClpP in complex with ADEP molecules adopts an "open-gate"-conformation

The ClpP/ADEP complex adopts a proteolytically active conformation strongly resembling the extended form of apo-ClpP, yet distinct, because of an increased diameter of the axial pores (Fig. 2).[53,70] The crystal structure of *E. coli* ClpP in complex with ADEPs shows the N-terminal loop pointing upwards, similar to the "up"-conformation of apo ClpP, but with a widened axial pore of 20 Å in diameter, henceforth referred to as the "open gate"-conformation (Fig. 2b).[70] It is not yet known, if such an increased diameter which was not observed in the cryo-EM structure of the

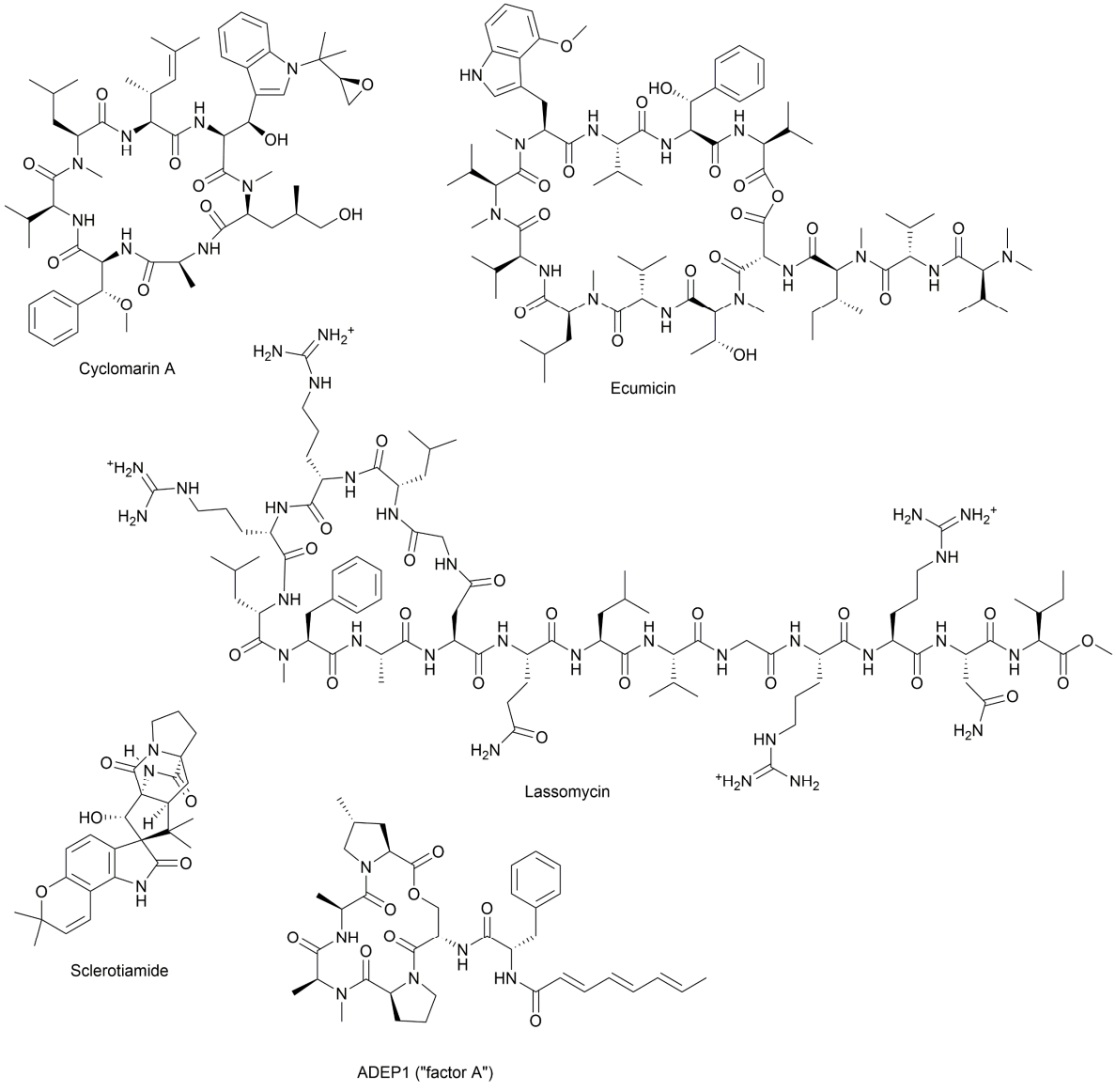

Fig. 4 Natural product modulators of the Clp protease.

E. coli ClpP/ClpA complex ('ClpAP') might present a special case exclusive to the ClpP/ADEP complex or if it occurs in a similar form also during the ClpP/Clp-ATPase interaction. In contrast to the structured terminal β-hairpins of the *E. coli* ClpP/ADEP crystals, the axial pores seemed unstructured in ClpP crystals from *B. subtilis* in complex with ADEP. This difference was attributed to tight packing of the *B. subtilis* ClpP/ADEP complexes in the crystals, while the *E. coli* crystals showed less tight packing in the N-terminal region. Thus, it was proposed that the N-terminal loops of ClpP/ADEP indeed form a structured channel (Fig. 2b).[69,96] Bound ADEP molecules provide additional hydrophobic anchor points for the N-terminal tail of ClpP.[67] The whole ClpP/ADEP complex displays reduced structural flexibility, as displayed in hydrogen/deuterium exchange experiments.[67] In this study, ClpP was incubated in a deuterated solution both in absence and in presence of ADEP1. Hydrogen/deuterium exchange as a measure of flexibility occurred to a lesser extent in the presence of ADEP1, especially in the equatorial plane where the α5-helices are located.[67] This finding underlines the allosteric nature of the ClpP/ADEP interaction. Structural dynamics in regions of the ClpP macromolecule that lie distant from the ADEP binding site are affected. For some years, pore gating has been considered to be the only structural determinant of ADEP-mediated activation. However, recent data reveal additional activating rearrangements (see below).

3.3 Disruption of the functional ClpP – Clp-ATPase interaction kills mycobacteria

3.3.1 Cyclomarine A

A non-ribosomal cyclic heptapeptide called cyclomarin A (CymA, Fig. 4) was isolated from a marine streptomycete.[97] It was later found to show potent bactericidal activity against a panel of multidrug-resistant *M. tuberculosis* suggesting a novel mechanism of action.[98] Subjecting non-replicating persisters to 2.5 μM of CymA killed 90% of the initial inoculum within 5 days. The resistance frequency was below 10^{-9} and attempts to select for a resistant mutant failed.[98] The antibacterial activity of CymA was specific to mycobacteria whereas five other strains, Gram-positive and Gram-negative alike, were non-susceptible. Affinity chromatography with an immobilized cyclomarin A derivative was performed and revealed the mycobacterial Clp/Hsp100 chaperone ClpC1 as the molecular target. Expression of selective domains of ClpC1 showed that CymA binds to the N-terminal domain.[99] In *B. subtilis* ClpC, substrate specificity and

recognition is mediated by either adapter proteins like MecA or arginine phosphorylation of substrate by McsB.[88,100–102] Both MecA and phosphate-marked substrates bind to the N-terminal domain of ClpC. A requirement for adaptor-mediated substrate delivery has not been reported for mycobacterial ClpC1, so far, and ClpP1P2 is capable of *in vitro* casein degradation with the help of ClpC1 alone. There is evidence, however, that PknB-mediated phosphorylation is a determinant of substrate binding by ClpC1 in mycobacteria.[103] Crystal structures demonstrate that CymA binding to ClpC1 occurs close to a region that corresponds to the MecA interacting site of ClpC from *B. subtilis*.[99,104] The precise mode of action is still to be investigated, but an involvement of CymA in ClpC1 substrate recognition is discussed. Vasudevan *et al.* proposed that CymA binding decreases flexibility in the ClpC1 N-terminal domains, rendering its substrate entry pore more accessible.[99] They furthermore interpreted a decreased GFP signal in *Mycobacterium smegmatis* upon treatment with CymA as an increased *in vivo* GFP degradation activity of the CymA stimulated Clp protease.[98] On a cautionary note, decrease of GFP fluorescence has also been observed *in vitro* as a result of *E. coli* Clp-ATPase mediated unfolding activity, independent of degradation.[46,105] Therefore, it has been rightly stated that uncoupling the Clp-ATPase from proteolysis, as is the case for other compounds binding to ClpC1 (see below), is also an option for the CymA mode of action.[23] On a side note, the natural congener cyclomarin C, which has been co-isolated with cyclomarin A, also displays potent antitubercular activity with a minimal inhibitory concentration (MIC) value of 0.1 µg/ml.

Other natural compounds that specifically target the mycobacterial ClpC1 chaperone are lassomycin, ecumicin and a recently reported rufomycin analogue.[106–108]

3.3.2 Lassomycin

Lassomycin (Fig. 4) is a ribosomally synthesized peptide and consists of 16 amino acids. After posttranslational modification, an intramolecular amide bond is formed between the N-terminus and the carboxyl side chain of aspartic acid at position 8 resulting in a “lasso”-like structure. MIC values specifically for *Mycobacterium tuberculosis* are in the range of 0.8-3 µg/ml including multidrug-resistant strains.[106] Genome sequencing of six resistant mutants showed mutations in the *clpC*1 gene.[106] Like cyclomarin A, lassomycin binds the N-terminal domain of ClpC1, which results in

two functional anomalies. Firstly, ATP hydrolysis rate is increased and, secondly, degradation of the model substrate casein by the ClpC1P1P2 complex is abolished. Whether cell death stems from increased unfolding activity in the wake of pronounced ATP hydrolysis or from attenuated substrate degradation by ClpP1P2 is still unknown.

3.3.3 Ecumicin and RUF-I

Ecumicin (Fig. 4) is a non-ribosomal cyclic tridecapeptide, originating from a *Nonomuraea* strain with strong antitubercular activity against resistant mycobacteria with MICs in the range of marketed antibiotics and no detected cytotoxicity.[107,109,110] Resistant mutants revealed mutations in the N-terminal region of ClpC1. Like lassomycin, ecumicin uncouples ClpC1 from ClpP1P2 proteolysis and increases ATPase activity severalfold.[110]

The effort to find new antitubercular compounds also led to the discovery of RUF-I, an analogue of the natural product rufomycin, with so far undisclosed structure.[108] RUF-I was also reported to target ClpC1, but so far, little information is available on this compound.[108] An initial study showed no cross-resistance between ecumicin and rufomycin and resistant clones generated by exposure to either ecumicin or rufomycin, showed distinct single point mutations in *clpC1,* implicating different binding modes.

3.3.4 Acyldepsipeptides

Unlike the ClpC1 binders, ADEPs display only a moderate antitubercular activity with an MIC of 25 µg/ml for ADEP2, the strongest congener, which is in strong contrast to the nanomolar MIC values that ADEPs show against firmicutes.[40] Ollinger *et al.* argued, that efflux in mycobacteria might strongly effect ADEP potency, but the efflux-mediated effects measured were mild and even combining two efflux pump inhibitors, reserpine and verapamil, did only improve ADEP activity about twofold.[40] Although some contribution of efflux cannot be disregarded, impaired uptake through the mycobacterial cell envelope and a different mode of action of ADEP in mycobacteria compared to firmicutes might more strongly account for the difference in potency. A conditional *clpP1P2* knockdown strain in *Mycobacterium bovis* revealed an increased susceptibility to ADEP at reduced ClpP1P2 levels.[111] This behavior is in stark contrast to *B. subtilis*, where down-regulation of ClpP leads to increased resistance, and indicates that ADEP acts through inhibition of Clp protease function in mycobacteria.[111] Furthermore, while ADEP was able to activate mycobacterial

ClpP1P2 to degrade casein *in vitro*, this was only possible when agonist peptides, such as carboxybenzyl-leucyl-leucine (Z-LL), were also present, and ADEP was inferior to ClpC1 in activating ClpP1P2. Mycobacterial ClpP1P2 is special in its requirement for certain N-blocked agonist peptides for activation *in vitro*.[87,112] It was suggested that ClpP1P2 activation within the mycobacterial cell requires binding of the partner Clp-ATPase in combination with active delivery of protein substrate.[113] In accordance, ADEP induced *in vitro* casein digestion by ClpP1P2 only when the substrate mimetic Z-LL was also present and could not activate ClpP1P2 independently.[111] In contrast, ADEP alone efficiently suppressed association of ClpP1P2 with both ClpC1 and ClpX *in vitro*.[87,111] Unlike firmicutes, Clp protease activity is essential for growth of mycobacteria under all conditions and proteomic studies in a ClpP1P2 knockout strain showedClpX solltest Du auch nenneni Raju et al.ranscription factor WhiB.ns of the Clp protease.n ADEP effectively abrogated the interashowed the accumulation of the toxic transcription factor WhiB.[114] Based on the mode of action data available, ADEP kills mycobacteria by abrogating the communication of ClpP1P2 with its partnering Clp-ATPases and consequently by inhibiting the natural functions of the Clp protease system. ClpC1 binders like ecumicin or lassomycin also disturb communication between ClpC1 and ClpP1P2, but they additionally affect ATPase activity of ClpC1 which probably also perturbs ClpP1P2-independent functions of the chaperone. The higher potency of these compounds might, at least in part, be attributed to this additional mechanistic effect. In addition, increased uptake might occur.

4 Molecular interaction between ADEP and ClpP

4.1 ADEP structure-activity-relationship (SAR)

4.1.1 ADEP4

The main component of the acyldepsipeptide A54556 natural product complex termed ADEP1 (A54556 factor A, Fig. 5) consists of a peptidolactone macrocyclic core coupled to an *N*-acylphenylalanine moiety *via* an amid bond.[5,6] Importantly, the structure suggested in the original patent from 1985 was not correct as it indicated a methyl group at the proline moiety which is coloured in black in Fig. 5.[5] Fig. 4 and 5 depict the structure that was later revised, carrying the methyl group at the other

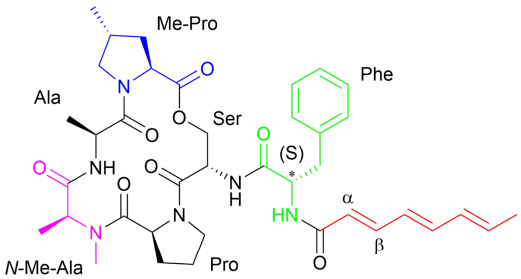

ADEP1 ("factor A")

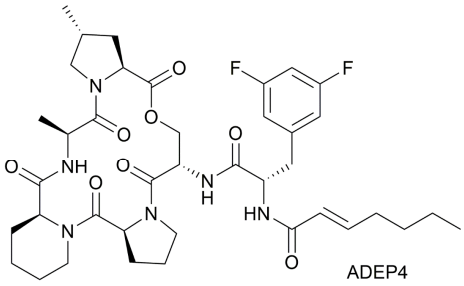

ADEP4

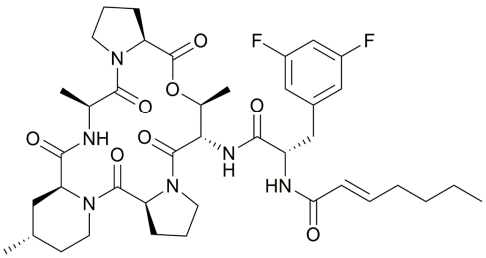

ADEP B315

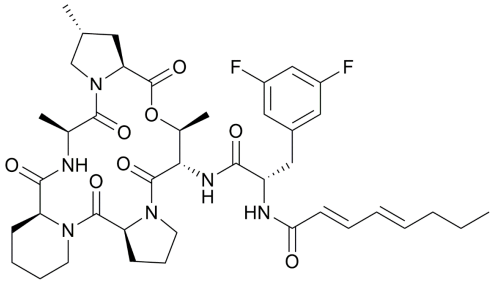

Goodreid *et al.* 2016, compound **26**

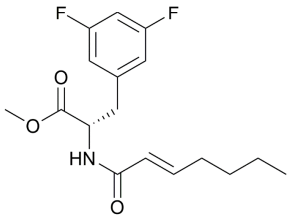

Carney *et al.* 2014, fragment **5**

proline residue (blue in Fig. 5).[7] ADEP1 showed already good antibacterial activity *in vitro* against enterococci, including vancomycin-resistant strains (VRE), streptococci, including penicillin-resistant *Streptococcus pneumonia* (PRSP), as well as moderate activity against staphylococci, including methicillin-resistant *S. aureus* (MRSA).[6] Limitations in potency and chemical as well as metabolic stability were addressed in a derivatization program.[7] In the course of this medicinal chemistry optimization, several structural requirements were revealed: the aliphatic side chain (red in Fig. 5) does not tolerate polar substituents, the α,β double bond is crucial for good activity and has to be in trans-configuration, the Cα stereocenter of the phenylalanine moiety (green in Fig. 5) must be S-configured and the alanine (purple in Fig. 5) requires an N-terminally attached methyl group. Furthermore, 3,5-bisfluorination of the phenyl moiety and introduction of pipecolate at the alanine (purple) for increased rigidity led to increased potency. The methyl group of the methylproline residue (blue) is also important for potency (Fig. 5). Substitutions at the phenylalanine benzene ring showed a very tight SAR. Fluorination in position 3 improved activity somewhat and 3,5-bisfluorination led to a strong improvement of MIC values against staphylococci, streptococci and

enterococci. However, introduction of an additional fluorine substituent in position 4 (yielding 3,4,5-fluorination) was detrimental.[7] This is in accordance with the spatial limitations of the narrow binding groove occupied by the benzene ring where 4-fluorination possibly clashes sterically. 3,5-bisfluorination on the other hand is well accommodated by a polar environment of aspartic acid and threonine side chains within the ClpP binding pocket.[53] The poly-unsaturated aliphatic side chain of ADEP1 was susceptible to temperature and light exposure. Removal of the triene functionality led to increased chemical stability while length and hydrophobicity of the alkyl side chain are important for potency. A heptenoyl moiety proved to be ideal in length for activity against staphylococci.[7] Applying these optimizations led to the synthesis of ADEP4, an improved congener with antibacterial *in vitro* and *in vivo* activity superior to natural product ADEP1, and in the range of antibiotics currently in clinical use.[6,7]

4.1.2 ADEP4 *N*-acylphenylalanine moiety

To dissect the relevance of ADEP sub-structures, several fragments were synthesized. Interestingly, the *N*-acylphenylalanine portion by itself is necessary and sufficient for *in vitro* activity even though it is not very potent.[115] Enzymatic assays showed cooperativity similar to full-size ADEP congeners suggesting a similar binding mechanism. The peptidolactone macrocycle adds to potency but is inactive on its own. Thus, the acylphenylalanine part poses the minimal structural requirement for the ADEP effect.[115] Compounds including parts of the macrocyclic core show increased apparent binding constants compared to the mere *N*-acylphenylalanine moiety.[115] By providing additional contacts to the hydrophobic pocket the macrocycle improves affinity to achieve higher potency.

4.1.3 B315

Rigidifying the N-methylalanine region of the macrocycle by incorporating pipecolic acid enhanced potency significantly, as exemplified by the ADEP4 congener (Fig. 5). The search for more rigid compounds becomes self-evident when taking into account that, in principle, a reduced entropic cost of the binding event leads to increased potency. Analogues of ADEP4 with further modifications of the pipecolate moiety were also synthesized.[8] The 4-methylpipecolate congener B315, for

Fig. 5 Natural product ADEP1 and synthetic derivatives. Important structural elements of ADEP1 are colour-coded. Red: aliphatic side chain; green: phenylalanine linker (bisfluorinated for increased potency in the synthetic congeners); blue: methylproline; purple: *N*-methylalanine (modified for increased potency in ADEP4)

instance, showed potent *in vitro* activity against VRE and MRSA.[8] Additional modifications in this position led to 4-isopropylpipecolate (derivative not shown) and the serine residue within the macrocycle was exchanged with *allo*-threonine.[9] In general, rigidifying the peptidolactone backbone in these positions improved antibacterial activity and allowed for stronger ClpP activation with the exception of modifications that challenged the ClpP binding pocket sterically (4-isopropylpipecolate). Interestingly, introduction of a methylpipecolate showed slightly decreased activity against *S. pneumoniae* and *E. faecalis* compared to pipecolate (compound **1c** compared to **1b** in reference 9), but, in combination with the *allo*-threonine, a synergistic effect was reported (compound **1g** compared to **1f** in reference 9).[9] Within the context of congener series compared directly to each other, exchange of the serine residue with *allo*-threonine and 4-methylation of the pipecolate moiety proved to be the macrocycle rigidifications most beneficial for MIC values against staphylococci, streptococci and enterococci as well as for ClpP activation.[9] The resulting ADEP B315 (compound **1g** in reference 9) was later tested *in vivo* and proved effective in mice infected with methicillin-susceptible as well as methicillin-resistant *S. aureus* with des-methyl-ADEP4 and vancomycin as benchmarks.[116] These findings confirm that rigidification as a pharmacological principle can indeed be applied to the ADEP peptidolactone macrocycle for improved ClpP binding. However, it is noteworthy, that Carney *et al.*, who had presented ADEP B315 as the ADEP derivative with strongest *in vitro activity* by then, had not compared it side-by-side to the ADEP4 congener.[9] A more recent study including ADEP4 (compound **7** in reference 10) and ADEP B315 (compound **8** in reference 10) shows ADEP4 to be superior in activity against an MRSA strain and inferior against a VRE strain.[10] A B315 congener including the activity-relevant methyl-proline (compound **22** in reference 10) was also part of this study and did not add to the *in vitro* activity of ADEP B315.

4.1.4 Compound 26

In an attempt to optimize the ADEP structure for activity against Gram-negative bacteria, compound **26** was synthesized, which includes the *allo*-threonine, the methyl-proline, the pipecolic acid modification, and an octanoyl aliphatic side chain containing a diene functionality also present in the natural product factor D.[10] This diene functionality improved stability compared to the natural product triene of factor A at ambient conditions. The increase in length to eight carbons with respect to ADEP4

raises the question whether the spatial limitations for the aliphatic side chain might be related to firmicutes. Compound **26** achieved increased activity compared to ADEP4 against chloramphenicol-resistant *Neisseria gonorrhoeae* and activity against an *E. coli* mutant with a compromised outer membrane but not the wild type.

4.2 ADEP – biological activity

Synthetic ADEP congeners, including ADEP4, B315 and compound **26** (Fig. 4) have MIC values in the low nanomolar range against a broad panel of Gram-positive pathogens.[6,9,10] ADEP4 cured mice with lethal systemic *S. aureus* infections where ADEP1 failed due to limited antibacterial activity, poor chemical stability and high metabolic clearance.[6,7] ADEP4 also outmatched marketed linezolid in murine lethal systemic infections caused by *S. aureus*, *S. pneumoniae* or *E. faecalis* and B315 was more effective than vancomycin in reducing the bacterial load of *S. aureus* in livers and kidneys of mice.[6,116] Furthermore, ADEP4 showed exceptional activity against persister cells of *S. aureus*. In side-by-side experiments with stationary cells, where ciprofloxacin, linezolid, rifampicin and vancomycin were literally inactive, ADEP4 reduced the number of colony forming units of *S. aureus* by 4 log units.[11] When ADEP4 was combined with either ciprofloxacin, or linezolid, or rifampicin, bacteria were eradicated to the level of detection.[11] A combination treatment of ADEP4 and rifampicin also eradicated *S. aureus* from a biofilm that had developed during a deep-seated thigh infection in neutropenic mice.[11] ADEP was also effective in killing a persisting *Enterococcus faecium* strain isolated from a neutropenic patient.[117] ADEP4 at 0.2 µM eradicated this clinical isolate even in a preformed biofilm, while all marketed comparators tested, i. e. vancomycin and daptomycin, failed even at 50 to 256 µg/ml.[117] The antibacterial potency of ADEPs proves the potential of ClpP's hydrophobic pocket as a druggable target site, where bactericidal and anti-persister activity can be achieved covering a broad spectrum of bacteria. ClpP mutations, which were observed in firmicutes during ADEP treatment under moderate growth conditions *in vitro*, should play less of a role under the stressed conditions of the infection process, where ClpP is essential for virulence and fitness.[6,24,25,115] Nonetheless, combination therapy is probably the therapeutic application strategy for ADEP, also considering the observed synergy against persisters.

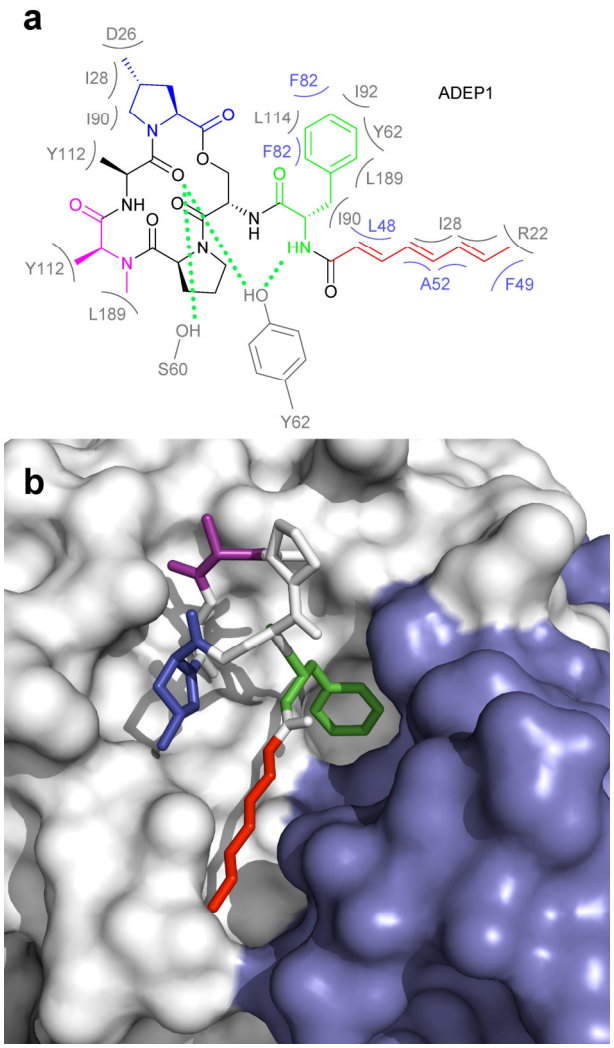

Fig. 6 Interaction between ADEP1 and *B. subtilis* ClpP. (a) Structure of ADEP1 and ClpP amino acid residues involved in binding. Two neighbouring ClpP subunits contribute to ADEP binding with their respective amino acid residues highlighted in grey and blue. Residues coloured in grey belong to the white ClpP subunit in Fig. 3b, blue residues originate from the blue ClpP subunit in Fig. 3b. Hydrophobic interactions are denoted by brackets, hydrogen bonds by green dotted lines. (b) Surface fill model of the *B. subtilis* ClpP crystal structure complexed with ADEP1. Two adjacent ClpP monomers are depicted in white and blue, respectively. The *N*-acylphenylalanine moiety inserts deeply into the hydrophobic pocket and comprises the green (phenylalanine) and red (aliphatic side chain) functional groups. The macrocycle backbone is more solvent-exposed. It contains the *N*-methylalanine (purple) and the methylproline (blue) moieties beneficial for activity.

Specificity of ADEPs for prokaryotes is high and eukaryotic cells are not affected up to the micromolar concentration range.[6,118] Recently, a first organ histology study was published.[116] Histological analyses of liver and kidney sections from healthy mice treated with 50 µg/ml B315 did not indicate any tissue toxicity, whereas vancomycin, which had been run in parallel, showed pronounced kidney toxicity as obvious from vacuolization of kidney cells and protein accumulation. Despite these promising preliminary studies on *in vivo* efficacy, the current leads require further improvement, e. g. with regard to solubility (for intravenous application), metabolism, and chemical stability. When considering combination therapy, pharmacokinetic and pharmacodynamics parameters of the partners must also be compatible and drug-drug interaction must be avoided. Efforts concerning pharmacological optimization are underway.

4.3 Interaction of ADEP with the hydrophobic pocket of ClpP

The ADEP binding pocket ranges over two neighbouring ClpP subunits. In accordance with the minimal structural requirement for ADEP to take effect, the aliphatic side chain and the benzene ring of the phenylalanine are buried deeply within the hydrophobic pocket of ClpP (Fig. 6b). The relevance of this part of the molecule is represented by the number of its hydrophobic interactions (Fig. 6a).[53] As each ADEP

molecule establishes direct contacts with two neighbouring ClpP subunits within the same ring, the stabilizing effects within the heptameric ring are obvious.[53,90] When studying the surface model of *B. subtilis* ClpP with bound ADEP1, the structural confinements of the hydrophobic side-chain in terms of length as well as sterical limitations for substituents at the benzene ring become apparent. Modelling of a superimposition of the *Helicobacter pylori* ClpX LGF-loop extracted from a *Hp*ClpX crystal structure with an ADEP structure from an ADEP-bound *E. coli* ClpP crystal, suggests that the ADEP phenyl moiety and aliphatic side chain mimic binding of the LGF motif (consensus sequence in *E. coli*: IGF).hH*Hhkjldsjfkjsdlfj*[70,119] Both the *N*-acylphenylalanine moiety of ADEP1 and the LGF motif overlap closely (Fig. 7c). The LGF leucine side chain extends into the channel that is otherwise occupied by the ADEP aliphatic side chain. The phenylalanine moiety of ADEP1 closely overlaps with the LGF phenylalanine. This is especially remarkable considering that the *N*-acylphenylalanine moiety, which closely resembles the (L/I)-GF-motif of ClpX, is also the minimal structural requirement for ADEP activity (see section 4.1). Modifications in solvent-exposed regions of the macrocycle are promising for further compound optimization in terms of physiochemistry and ADME, whereas the potential for improvement of the *N*-acylphenylalanine part of ADEP seems limited due to the strict SAR and space limitations of the binding pocket. The ADEP binding pocket presents a hot spot for ClpP modulation and serves as a model target for protein-protein-interaction modulators. Efforts to screen for potential alternative ClpP binders have been undertaken with first positive results.[120]

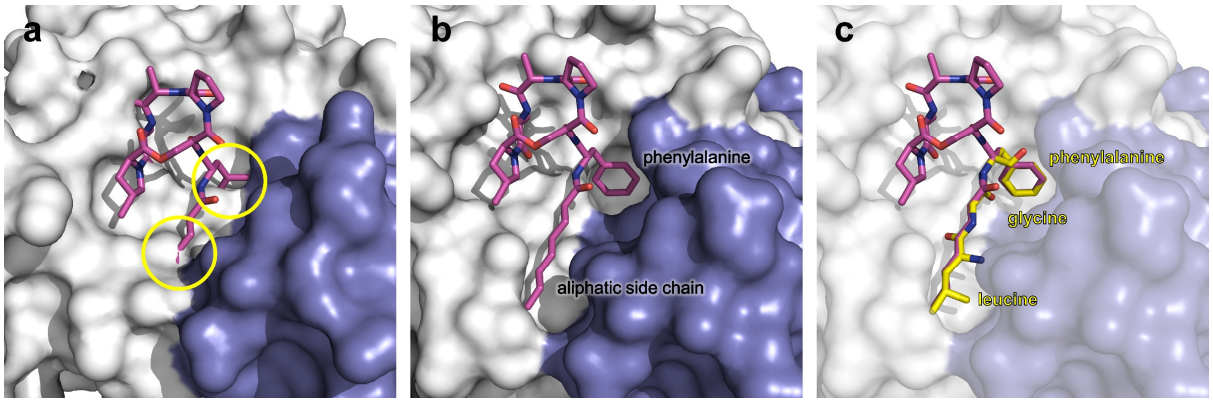

Fig. 7 Surface fill model of the *B. subtilis* ClpP crystal structure in complex with ADEP1. (a) Modelling of an ADEP1 molecule into the ADEP binding pocket of ClpP in the compressed conformation (PDB code: 3TT6) predicts sterical clashes (circles). This is also the case with other ADEP derivatives as well as different compressed ClpP structures. (b) Close-up view of an ADEP1 molecule in the hydrophobic pocket of ClpP in its extended state (PDB code: 3KTI). (c) Superimposition of the LGF motif from *Helicobacter pylori* ClpX (PDB code: 1UM8) with the *N*-acylphenylalanine moiety of ADEP1. The leucine and glycine residues overlap closely with the aliphatic side chain of ADEP1.

Recently, discovery of a gain-of-function ClpP mutant of *S. aureus* provided new insight into the architectural properties of the ADEP binding site.[121] The Tyr62 residue of *B. subtilis* ClpP had already been shown to form two hydrogen bonds and also hydrophobic interactions with ADEP1 (Fig. 6a).[53] The H-bonds are formed between the tyrosine residue and the macrocycle backbone as well as the proximal part of the aliphatic chain. Hydrophobic interactions with the benzene ring of the ADEP phenylalanine residue further anchor the molecule. Upon closer look, Ni *et al.* found that said tyrosine residue was rotated by approximately 90° in the ADEP-bound structures of *Bs*ClpP, *Ec*ClpP, and *Mt*ClpP1P2/agonist when compared to the apo forms of the respective ClpPs.[53,70,87] They argue that the energy barrier for adopting this rotated conformation is probably too high in the apo form of ClpP. Mutating Tyr63 in *S. aureus*, the corresponding tyrosine residue according to *Sa*ClpP nomenclature, to an alanine, however, led to a rotated peptide backbone even in the absence of activator and bestowed β-casein and even FtsZ degradation capability onto ClpP alone. This marked an important step in the elucidation of the ADEP pocket organization and possibly revealed the key switch for turning on the protease.

4.4 ADEPs exert conformational control over the entire ClpP barrel

ADEPs provide an elegant means for investigating the implications of “filling” the hydrophobic binding pocket of ClpP (Fig. 7). N-terminal gate closing serves as a safeguard against uncontrolled digestion of proteins. A gated pore mechanism has long been presumed to be the critical factor in ClpP control. The available data however reveal a more global regulatory principle that includes additional safety measures.

Cumulative evidence indicates that the conformational control of ClpP by ADEP reaches beyond the N-terminal region lining the central entrance pore. Thermal shift assays revealed that ADEP binding increases the overall folding stability of the *S. aureus* ClpP complex.[91] In contrast to wild type ClpP from *S. aureus*, the catalytic site mutant D172N showed no residual peptidase activity in *in vitro* degradation assays but could be successfully activated by addition of either ADEPs or ClpX to degrade full-length protein and small peptides. Small angle X-ray scattering analysis showed a more compacted conformation for the D172N mutant with no difference in oligomeric state. ADEPs promote the extended conformation in this mutant that is otherwise only observed in a compacted conformation.[91] Hydrogen-deuterium exchange experiments

using *E. coli* ClpP showed a remarkable increase in rigidity of the handle region after addition of ADEP.[67] The concept that "filling" the hydrophobic pocket stabilizes the handle in an extended conformation and the catalytic site in a competent conformation is in line with the crystallographic data.[53,70] This is remarkable insofar as the hydrophobic pocket is connected *via* intramolecular relays not just to the N-terminal region but also the more distant handle region. Recent insights into the workings of *M. tuberculosis* ClpP are particularly interesting in this respect. *M. tuberculosis* encodes two ClpP paralogs on a single operon, namely *clpP1* and *clpP2*.[122] In the presence of an agonist peptide, ClpP1 and ClpP2 arrange into heterotetradecameric ClpP1P2 complexes *in vitro*, composed of two homoheptameric ClpP1 and ClpP2 rings, respectively.[123,124] This heterotetradecamer interacts asymmetrically with cognate Clp-ATPases ClpX and ClpC1 which bind only to ClpP2.[125] In accordance, X-ray crystallographic structural data of the ClpP1P2/ADEP complex show ADEP binding only at one ring, ClpP2.[87] Remarkably, pore opening was still triggered at the ClpP1 ring.[87] Thus, the conformation rearrangement that ADEP binding sets in motion must propagate from the hydrophobic pockets of ClpP2 *via* the ring-ring interface to the N-termini of ClpP1 over a distance of approximately 90 Å. This finding implies a long-

distance relay within the complex that extends beyond single subunits.

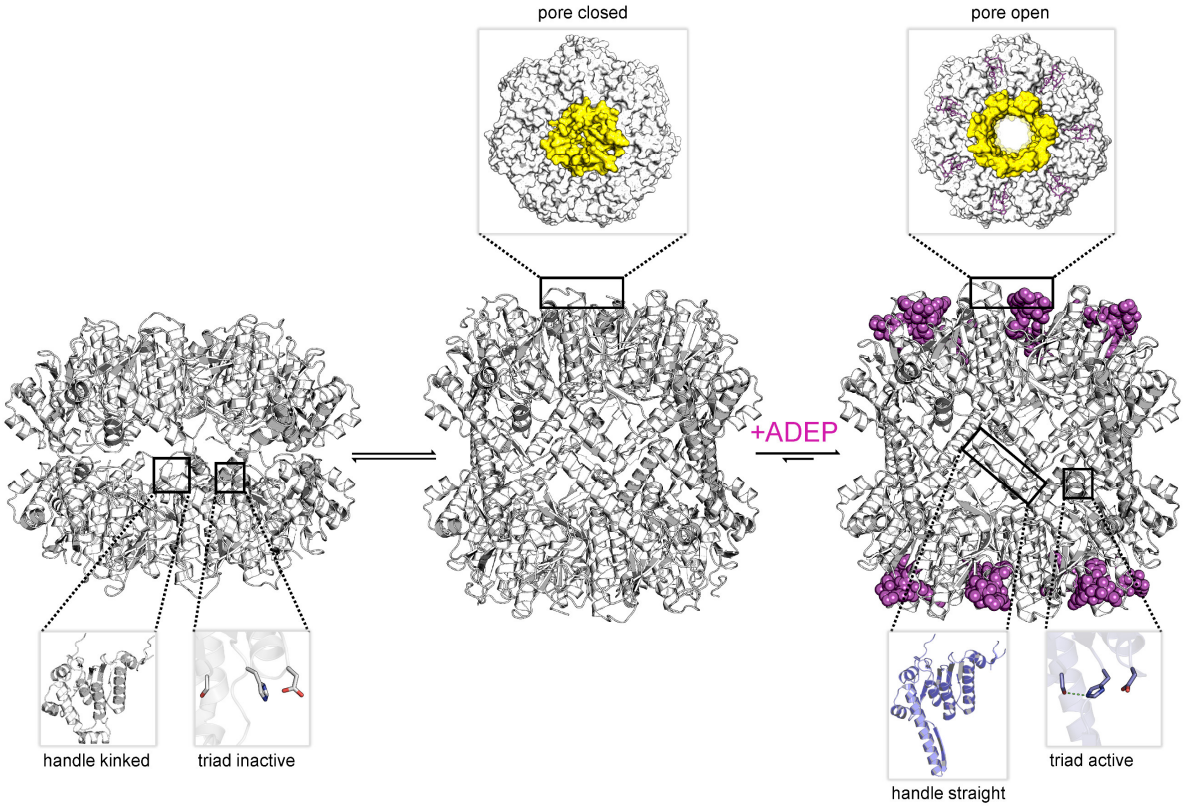

Fig. 8 Current model of ClpP conformational control by ADEPs. ClpP resides in a natural equilibrium between the inactive compressed and the active extended states. None of these are proteolytically competent because the digestion chamber is inaccessible for proteins. ADEP binding shifts this equilibrium towards the active extended state, opens the axial entry pores and, in addition, enhances catalytic efficiency.

To determine whether ADEP binding also effects the catalytic centres of ClpP, known inhibitors have been deployed in combination with ADEP treatment. β-lactones are covalent inhibitors of the ClpP peptidase (suicide inhibitors).[126,127] Instead of a peptide bond, the active site serine attacks the carbonyl atom of the β-lactone ring. This event opens the ring to establish an acyl-ester linkage with the inhibitor which is much more stable than the acyl-ester intermediate in polypeptide degradation.[127] The following hydrolysis reaction regenerating the active site serine is substantially slowed (see catalysis mechanism of serine proteases in Fig. 1b). When ClpP was exposed to ADEP and β-lactone in combination, the catalytic efficiency of the first step, i. e. β-lactone binding, was two-fold accelerated for all β-lactone inhibitors employed despite varying side-chains.[91] Even more striking was the stimulating effect of ADEP on the β-lactone hydrolysis reaction. Hydrolysis rates of the bound inhibitors were stimulated from two-fold to approximately 20-fold depending on the β-lactone structure tested.[91]

Notably, ADEPs affect the hydrolysis activity independently of the open state of the axial pores and stimulate catalysis as allosteric activators.

In conclusion, the hydrophobic pocket serves as a sort of “master switch” to turn the whole complex into an “on”-state. Turning the switch leads to the formation of an active extended conformation of ClpP, accelerated substrate turnover by the catalytic sites, widened axial pores, and an overall more stable and structurally less flexible machine. Taking a closer look at the geometry of the ADEP binding pocket provides a clue as to how ADEPs may achieve this transition. Modelling of ADEP1 (as well as ADEP derivatives) into the binding pocket of the inactive compressed ClpP structure from *B. subtilis* predicts a sterical clash of the aliphatic side chain (Fig. 7a). Thus, ADEPs can be regarded as sterical locks fixing ClpP in the active extended form and restricting transition to the inactive compressed form. This idea is further supported by the complete lack of compressed structures that have been co-crystallized with ADEP. It has been established that ClpP is a highly dynamic macromolecule.[52] We propose a model in which ClpP resides in an equilibrium between an active and inactive state and transiently adopts all of the above-mentioned states. However, ADEP binding strongly shifts this equilibrium towards the active state *via* conformational control (Fig. 8). ClpP functions like a clockwork where each cogwheel is tightly interconnected. Mutation of a single amino acid residue can alter the structural organization of the whole macromolecule, for instance the active site mutation D172N, which results in a more compacted structure.[91] Mutation of the Y63 to alanine enables an otherwise tightly controlled peptidase to degrade a folded protein substrate.[121] Therefore, structural shifts at one position are accompanied by a cascade of structural rearrangements that span the whole macromolecule. This structural interdependency is most vividly demonstrated by the observation that ADEP binding to the ClpP2 ring leads to pore opening in the opposing ClpP1 ring of the mycobacterial ClpP1P2 complex.[87] According to this model, ADEP binding is the equivalent to blocking one cogwheel with an iron rod and, as a consequence, bringing the whole clockwork to a halt.

4.5 Comparison between ADEP-mediated and Clp-ATPase-mediated activation of ClpP

To this day, no co-crystallization of ClpP with any partner Clp-ATPase has been achieved. ADEPs have served as a tool to investigate the interaction between ClpP

and its cognate unfoldases. Some of the findings gained by investigating the interaction between ADEP and ClpP have been transferred to Clp-ATPase/ClpP interaction. But, there are differences. Clp-ATPases actively unfold and thread the unfolded protein strand into the catalytic space of ClpP. In Cryo-EM structures with Clp-ATPases, the axial gate of ClpP appeared smaller than in the “open-gate”-conformation of the ClpP/ADEP crystal structures.[68,69] The α5-helices of ClpP can adopt an unstructured conformation without destroying the oligomeric state and several studies suggest ClpP dynamics to be crucial in the interaction with Clp-ATPases.[58] While this motion of ClpP has been suggested to be part of a natural cycle required for catalysis and product release, dynamics of ADEP-mediated activity might be different.

In hydrogen exchange experiments, ADEP binding has been shown to induce a rigidification of the α5-helices in the equatorial plane.[67] As ADEPs binds to the hydrophobic pockets of ClpP with high affinity, it can be assumed that many, if not all, hydrophobic pockets are occupied by ADEP molecules at the same time. Clp-ATPase binding is comparatively weak and one Clp-ATPase hexamer can never fill more than six hydrophobic pockets at once. In accordance with the notion that “filling” the hydrophobic pocket enforces the active extended state, weak and partial binding by Clp-ATPases might have evolved to ensure ClpP dynamics important for natural functions. Here, we propose that the tight ADEP binding event shifts the dynamic equilibrium of ClpP more strongly towards the active extended conformation than binding of Clp-ATPases does. In that case, equatorial pore opening would occur to a smaller extent due to predominantly extended handles. The widened axial pore of the ClpP/ADEP complex then could not only allow for substrate entry but also, at least partially, accommodate product exit, thus altering the presumed operation mode of the structurally versatile ClpP.

5 Outlook

The bacterial Clp protease is a novel potential drug target that had not been included in the large antibacterial screening campaigns of pharma companies in the 1990s/2000s due to its inessentiality for growth of most pathogens under moderate conditions and due to the fact that mechanism-wise only inhibition but not activation and deregulation of a target were envisioned. It took the study of ADEP as a natural

product to understand the elaborate mechanism by which a protease machine can be taken out of its natural context and misdirected to kill multi-resistant and persisting bacterial pathogens. Bacterial Clp protease activity can be deregulated in a multi-facetted way with two different major consequences. Abrogating the interaction or productive enzymatic cycle between the proteolytic core ClpP and its cognate Clp-ATPases prevents all natural functions of the protease in general and regulated proteolysis. This consequence is achieved by known modulators blocking either the hydrophobic pocket of ClpP (ADEP) or by binding to the N-terminus of the mycobacterial Clp-ATPase ClpC1 (lassomycin, ecumicin, and potentially cyclomarin A). In addition, extensive conformational control of ClpP by ADEP leads to unregulated proteolysis and the degradation of vital bacterial proteins. Notably, it is the latter aspect by which ClpP as a non-essential target in firmicutes leads to bactericidal activity. Since the first report of ClpP as the target of ADEP about ten years ago, four additional and structurally unrelated natural product classes (Fig. 4) have been discovered to act on Clp proteases by either binding to ClpP or the cognate Clp-ATPase partner. It is likely that further natural product modulators of the Clp system remain to be found.

Acknowledgements

The research group of H. B.-O. acknowledges financial support of the German Research Foundation (SFB 766).

References

1 *WHO*, 2014, **ISBN:** 978 92 4 156474 8.
2 J. O'Neill, *AMR Review*, 2014, Antimicrobial Resistance: Tackling a Crisis for the Future Health and Wealth of Nations.
3 T. A. Wencewicz, *Bioorg. Med. Chem.*, 2016, **24**, 6227–6252.
4 L. L. Silver, *Future Microbiol.*, 2015, **10**, 1711–1718.
5 K. H. Michel and R. E. Kastner, *US Pat.*, 1985, **4492650**.
6 H. Brötz-Oesterhelt, D. Beyer, H.-P. Kroll, R. Endermann, C. Ladel, W. Schroeder, B. Hinzen, S. Raddatz, H. Paulsen, K. Henninger, J. E. Bandow, H.-G. Sahl and H. Labischinski, *Nat. Med.*, 2005, **11**, 1082–1087.
7 B. Hinzen, S. Raddatz, H. Paulsen, T. Lampe, A. Schumacher, D. Häbich, V. Hellwig, J. Benet-Buchholz, R. Endermann, H. Labischinski and H. Brötz-Oesterhelt, *ChemMedChem*, 2006, **1**, 689–693.
8 A. M. Socha, N. Y. Tan, K. L. Laplante and J. K. Sello, *Bioorganic Med. Chem.*, 2010, **18**, 7193–7202.
9 D. W. Carney, K. R. Schmitz, J. V. Truong, R. T. Sauer and J. K. Sello, *J. Am. Chem. Soc.*, 2014, **136**, 1922–1929.
10 J. D. Goodreid, J. Janetzko, J. P. Santa Maria, K. S. Wong, E. Leung, B. T. Eger, S. Bryson, E. F. Pai, S. D. Gray-Owen, S. Walker, W. A. Houry and R. A. Batey, *J. Med. Chem.*, 2016, **59**, 624–646.
11 B. P. Conlon, E. S. Nakayasu, L. E. Fleck, M. D. LaFleur, V. M. Isabella, K. Coleman, S. N. Leonard, R. D. Smith, J. N. Adkins and K. Lewis, *Nature*, 2013, **503**, 365–370.
12 D. Frees, U. Gerth and H. Ingmer, *Int. J. Med. Microbiol.*, 2014, **304**, 142–149.
13 J. Feng, S. Michalik, A. N. Varming, J. H. Andersen, D. Albrecht, L. Jelsbak, S. Krieger, K. Ohlsen, M. Hecker, U. Gerth, H. Ingmer and D. Frees, *J. Proteome Res.*, 2013, **12**, 547–558.
14 S. Runde, N. Molière, A. Heinz, E. Maisonneuve, A. Janczikowski, A. K. W. Elsholz, U. Gerth, M. Hecker and K. Turgay, *Mol. Microbiol.*, 2014, **91**, 1036–1052.
15 C. M. Sassetti, D. H. Boyd and E. J. Rubin, *Mol. Microbiol.*, 2003, **48**, 77–84.
16 W. F. Wu, Y. Zhou and S. Gottesman, *J. Bacteriol.*, 1999, **181**, 3681–3687.
17 C. K. Smith, T. A. Baker and R. T. Sauer, *Proc. Natl. Acad. Sci. U. S. A.*, 1999, **96**, 6678–6682.
18 T. Msadek, V. Dartois, F. Kunst, M. L. Herbaud, F. Denizot and G. Rapoport, *Mol. Microbiol.*, 1998, **27**, 899–914.
19 S. Nakano, G. Zheng, M. M. Nakano and P. Zuber, *J. Bacteriol.*, 2002, **184**, 3664–3670.
20 J. M. Flynn, S. B. Neher, Y. I. Kim, R. T. Sauer and T. A. Baker, *Mol. Cell*, 2003, **11**, 671–683.
21 P. Sass and H. Brötz-Oesterhelt, *Curr. Opin. Microbiol.*, 2013, **16**, 522–530.
22 H. Brötz-Oesterhelt and P. Sass, *Int. J. Med. Microbiol.*, 2014, **304**, 23–30.
23 E. Culp and G. D. Wright, *J. Antibiot. (Tokyo).*, 2016.
24 D. Frees, K. Sørensen and H. Ingmer, *Infect. Immun.*, 2005, **73**, 8100–8108.
25 D. Frees, J. H. Andersen, L. Hemmingsen, K. Koskenniemi, K. T. Bæk, M. K. Muhammed, D. D. Gudeta, T. A. Nyman, A. Sukura, P. Varmanen and K. Savijoki, *J. Proteome Res.*, 2012, **11**, 95–108.
26 D. Frees, S. N. A. Qazi, P. J. Hill and H. Ingmer, *Mol. Microbiol.*, 2003, **48**, 1565–1578.
27 C. Wang, M. Li, D. Dong, J. Wang, J. Ren, M. Otto and Q. Gao, *Microbes Infect.*, 2007, **9**, 1376–1383.
28 F. Weinandy, K. Lorenz-Baath, V. S. Korotkov, T. Böttcher, S. Sethi, T. Chakraborty and S. A. Sieber, *ChemMedChem*, 2014, **9**, 710–713.
29 H. Y. Kwon, A. D. Ogunniyi, M. H. Choi, S. N. Pyo, D. K. Rhee and J. C. Paton, *Infect. Immun.*, 2004, **72**, 5646–5653.
30 O. Gaillot, E. Pellegrini, S. Bregenholt, S. Nair and P. Berche, *Mol. Microbiol.*, 2000, **35**, 1286–1294.
31 H. P. Feng and L. M. Gierasch, *Curr. Biol.*, 1998, **8**, R464–R467.
32 J. Porankiewlcz, J. Wang and A. K. Clarke, *Mol. Microbiol.*, 1999, **32**, 449–458.
33 I. Levchenko, L. Luo and T. A. Baker, *Genes Dev.*, 1995, **9**, 2399–2408.
34 R. Kruklitis, D. J. Welty and H. Nakai, *EMBO J.*, 1995, **9**, 935–44.
35 B. Felden, F. Vandenesch, P. Bouloc and P. Romby, *PLoS Pathog.*, 2011, **7**, e1002006.
36 R. Singh and P. Ray, *Future Microbiol.*, 2014, **9**, 669-681
37 I. Chatterjee, P. Becker, M. Grundmeier, M. Bischoff, G. A. Somerville, G. Peters, B. Sinha, N. Harraghy, R. A. Proctor and M. Herrmann, *J. Bacteriol.*, 2005, **187**, 4488–4496.
38 I. Chatterjee, S. Schmitt, C. F. Batzilla, S. Engelmann, A. Keller, M. W. Ring, R. Kautenburger, W. Ziebuhr, M. Hecker, K. T. Preissner, M. Bischoff, R. A. Proctor, H. P. Beck, H. P. Lenhof, G. A. Somerville and M. Herrmann, *Proteomics*, 2009, **9**, 1152–1176.
39 J. E. Griffin, J. D. Gawronski, M. A. DeJesus, T. R. Ioerger, B. J. Akerley and C. M. Sassetti, *PLoS Pathog.*, 2011, **7**, e1002251.
40 J. Ollinger, T. O'malley, E. A. Kesicki, J. Odingo and T. Parish, *J. Bacteriol.*, 2012, **194**, 663–668.
41 R. M. Raju, M. Unnikrishnan, D. H. F. Rubin, V. Krishnamoorthy, O. Kandror, T. N. Akopian, A. L. Goldberg and E. J. Rubin, *PLoS Pathog.*, 2012, **8**, e1002511.
42 D. M. Roberts, Y. Personne, J. Ollinger and T. Parish, *Future Microbiol.*, 2013, **8**, 621–631.
43 M. W. Jackson, E. Silva-Herzog and G. V. Plano, *Mol. Microbiol.*, 2004, **54**, 1364–1378.

44 C. Webb, M. Moreno, M. Wilmes-Riesenberg, R. Curtiss and J. W. Foster, *Mol. Microbiol.*, 1999, **34**, 112–123.
45 R. Hengge-Aronis, *Microbiol. Mol. Biol. Rev.*, 2002, **66**, 373–395.
46 S. A. Joshi, G. L. Hersch, T. A. Baker and R. T. Sauer, *Nat. Struct. Mol. Biol.*, 2004, **11**, 404–411.
47 Y. I. Kim, I. Levchenko, K. Fraczkowska, R. V. Woodruff, R. T. Sauer and T. A. Baker, *Nat. Struct. Biol.*, 2001, **8**, 230–233.
48 F. Ye, J. Zhang, H. Liu, R. Hilgenfeld, R. Zhang, X. Kong, L. Li, J. Lu, X. Zhang, D. Li, H. Jiang, C. G. Yang and C. Luo, *J. Biol. Chem.*, 2013, **288**, 17643–17653.
49 S. R. Geiger, T. Böttcher, S. A. Sieber and P. Cramer, *Angew. Chem. Int. Ed.*, 2011, **50**, 5749–5752.
50 J. Wang, J. A. Hartling and J. M. Flanagan, *Cell*, 1997, **91**, 447–456.
51 M. Gersch, A. List, M. Groll and S. A. Sieber, *J. Biol. Chem.*, 2012, **287**, 9484–9494.
52 K. Liu, A. Ologbenla and W. A. Houry, *Crit. Rev. Biochem. Mol. Biol.*, 2014, **49**, 400–412.
53 B.-G. Lee, E. Y. Park, K.-E. Lee, H. Jeon, K. H. Sung, H. Paulsen, H. Rübsamen-Schaeff, H. Brötz-Oesterhelt and H. K. Song, *Nat. Struct. Mol. Biol.*, 2010, **17**, 471–478.
54 B. G. Lee, M. K. Kim and H. K. Song, *Mol. Cells*, 2011, **32**, 589–595.
55 J. Zhang, F. Ye, L. Lan, H. Jiang, C. Luo and C. G. Yang, *J. Biol. Chem.*, 2011, **286**, 37590–37601.
56 A. Szyk and M. R. Maurizi, *J. Struct. Biol.*, 2006, **156**, 165–174.
57 M. R. Maurizi, S. K. Singh, M. W. Thompson, M. Kessel and A. Ginsburg, *Biochemistry*, 1998, **37**, 7778–7786.
58 A. Gribun, M. S. Kimber, R. Ching, R. Sprangers, K. M. Fiebig and W. A. Houry, *J. Biol. Chem.*, 2005, **280**, 16185–16196.
59 R. Sprangers, A. Gribun, P. M. Hwang, W. A. Houry and L. E. Kay, *Proc. Natl. Acad. Sci. U. S. A.*, 2005, **102**, 16678–16683.
60 Ž. Maglica, K. Kolygo and E. Weber-Ban, *Structure*, 2009, **17**, 508–516.
61 M. S. Kimber, A. Y. H. Yu, M. Borg, E. Leung, H. S. Chan and W. A. Houry, *Structure*, 2010, **18**, 798–808.
62 K. M. Woo, W. J. Chung, D. B. Ha, A. L. Goldberg and C. H. Chung, *J. Biol. Chem.*, 1989, **264**, 2088–2091.
63 M. W. Thompson, S. K. Singh and M. R. Maurizi, *J. Biol. Chem.*, 1994, **269**, 18209–18215.
64 J. Ortega, S. K. Singh, T. Ishikawa, M. R. Maurizi and A. C. Steven, *Mol. Cell*, 2000, **6**, 1515–1521.
65 T. Ishikawa, F. Beuron, M. Kessel, S. Wickner, M. R. Maurizi and A. C. Steven, *Proc. Natl. Acad. Sci. U. S. A.*, 2001, **98**, 4328–4333.
66 M. C. Bewley, V. Graziano, K. Griffin and J. M. Flanagan, *J. Struct. Biol.*, 2006, **153**, 113–128.
67 M. A. Sowole, J. A. Alexopoulos, Y. Q. Cheng, J. Ortega and L. Konermann, *J. Mol. Biol.*, 2013, **425**, 4508–4519.
68 G. Effantin, M. R. Maurizi and A. C. Steven, *J. Biol. Chem.*, 2010, **285**, 14834–14840.
69 J. A. Alexopoulos, A. Guarné and J. Ortega, *J. Struct. Biol.*, 2012, **179**, 202–210.
70 D. H. S. Li, Y. S. Chung, M. Gloyd, E. Joseph, R. Ghirlando, G. D. Wright, Y. Q. Cheng, M. R. Maurizi, A. Guarné and J. Ortega, *Chem. Biol.*, 2010, **17**, 959–969.
71 L. D. Jennings, J. Bohon, M. R. Chance and S. Licht, *Biochemistry*, 2008, **47**, 11031–11040.
72 K. C. Keiler, P. R. Waller and R. T. Sauer, *Science*, 1996, **271**, 990–993.
73 S. Gottesman, E. Roche, Y. Zhou and R. T. Sauer, *Genes Dev.*, 1998, **12**, 1338–1347.
74 A. Martin, T. A. Baker and R. T. Sauer, *Mol. Cell*, 2007, **27**, 41–52.
75 J. A. Kenniston, T. A. Baker, J. M. Fernandez and R. T. Sauer, *Cell*, 2003, **114**, 511–520.
76 B. M. Stinson, V. Baytshtok, K. R. Schmitz, T. A. Baker and R. T. Sauer, *Nat. Struct. Mol. Biol.*, 2015, **22**, 411–416.
77 A. Martin, T. A. Baker and R. T. Sauer, *Nat. Struct. Mol. Biol.*, 2008, **15**, 139–145.
78 A. Martin, T. A. Baker and R. T. Sauer, *Nature*, 2005, **437**, 1115–1120.
79 K. H. Choi and S. Licht, *Biochemistry*, 2005, **44**, 13921–13931.
80 L. D. Jennings, D. S. Lun, M. Médard and S. Licht, *Biochemistry*, 2008, **47**, 11536–11546.
81 I. Levchenko, M. Seidel, R. T. Sauer and T. A. Baker, *Sci.* , 2000, **289**, 2354–2356.
82 J. M. Flynn, I. Levchenko, M. Seidel, S. H. Wickner, R. T. Sauer and T. A. Baker, *Proc. Natl. Acad. Sci. U. S. A.*, 2001, **98**, 10584–10589.
83 J. Kirstein, N. Molière, D. A. Dougan and K. Turgay, *Nat. Rev. Microbiol.*, 2009, **7**, 589–599.
84 M. W. Thompson and M. R. Maurizi, *J. Biol. Chem.*, 1994, **269**, 18201–18208.
85 T. A. Baker and R. T. Sauer, *Biochim. Biophys. Acta - Mol. Cell Res.*, 2012, **1823**, 15–28.
86 S. G. Kang, M. N. Dimitrova, J. Ortega, A. Ginsburg and M. R. Maurizi, *J. Biol. Chem.*, 2005, **280**, 35424–35432.
87 K. R. Schmitz, D. W. Carney, J. K. Sello and R. T. Sauer, *Proc. Natl. Acad. Sci. U. S. A.*, 2014, **111**, E4587-E4595.
88 J. Kirstein, T. Schlothauer, D. A. Dougan, H. Lilie, G. Tischendorf, A. Mogk, B. Bukau and K. Turgay, *EMBO J.*, 2006, **25**, 1481–1491.
89 T. A. Baker and R. T. Sauer, *Trends Biochem. Sci.*, 2006, **31**, 647–653.
90 J. Kirstein, A. Hoffmann, H. Lilie, R. Schmidt, H. Rübsamen-Waigmann, H. Brötz-Oesterhelt, A. Mogk and K. Turgay, *EMBO Mol. Med.*, 2009, **1**, 37–49.
91 M. Gersch, K. Famulla, M. Dahmen, C. Göbl, I. Malik, K. Richter, V. S. Korotkov, P. Sass, H. Rübsamen-Schaeff, T. Madl, H. Brötz-Oesterhelt and S. A. Sieber, *Nat. Commun.*, 2015, **6**, 6320.
92 T. Böttcher and S. A. Sieber, *ChemBioChem*, 2009, **10**, 663–666.

93 P. Sass, M. Josten, K. Famulla, G. Schiffer, H.-G. Sahl, L. Hamoen and H. Brötz-Oesterhelt, *Proc. Natl. Acad. Sci. U. S. A.*, 2011, **108**, 17474–17479.
94 A. Schiefer, J. Vollmer, C. Lämmer, S. Specht, C. Lentz, H. Ruebsamen-Schaeff, H. Brötz-Oesterhelt, A. Hoerauf and K. Pfarr, *J. Antimicrob. Chemother.*, 2013, **68**, 1790-1800.
95 N. P. Lavey, J. A. Coker, E. A. Ruben and A. S. Duerfeldt, *J. Nat. Prod.*, 2016, **79**, 1193–1197.
96 J. Alexopoulos, B. Ahsan, L. Homchaudhuri, N. Husain, Y. Q. Cheng and J. Ortega, *Mol. Microbiol.*, 2013, **90**, 167–180.
97 M. K. Renner, Y. C. Shen, X. C. Cheng, P. R. Jensen, W. Frankmoelle, C. A. Kauffman, W. Fenical, E. Lobkovsky and J. Clardy, *J. Am. Chem. Soc.*, 1999, **121**, 11273–11276.
98 E. K. Schmitt, M. Riwanto, V. Sambandamurthy, S. Roggo, C. Miault, C. Zwingelstein, P. Krastel, C. Noble, D. Beer, S. P. S. Rao, M. Au, P. Niyomrattanakit, V. Lim, J. Zheng, D. Jeffery, K. Pethe and L. R. Camacho, *Angew. Chemie - Int. Ed.*, 2011, **50**, 5889–5891.
99 D. Vasudevan, S. P. S. Rao and C. G. Noble, *J. Biol. Chem.*, 2013, **288**, 30883–30891.
100 K. Turgay, L. W. Hamoen, G. Venema and D. Dubnau, *Genes Dev.*, 1997, **11**, 119–128.
101 T. Schlothauer, A. Mogk, D. A. Dougan, B. Bukau and K. Turgay, *Proc. Natl. Acad. Sci. U. S. A.*, 2003, **100**, 2306–2311.
102 D. B. Trentini, M. J. Suskiewicz, A. Heuck, R. Kurzbauer, L. Deszcz, K. Mechtler and T. Clausen, *Nature*, 2016, **539**, 48-53.
103 S. Barik, K. Sureka, P. Mukherjee, J. Basu and M. Kundu, *Mol. Microbiol.*, 2010, **75**, 592–606.
104 F. Wang, Z. Mei, Y. Qi, C. Yan, Q. Hu, J. Wang and Y. Shi, *Nature*, 2011, **471**, 331–335.
105 E. U. Weber-Ban, B. G. Reid, A. D. Miranker and A. L. Horwich, *Nature*, 1999, **401**, 90–93.
106 E. Gavrish, C. S. Sit, S. Cao, O. Kandror, A. Spoering, A. Peoples, L. Ling, A. Fetterman, D. Hughes, A. Bissell, H. Torrey, T. Akopian, A. Mueller, S. Epstein, A. Goldberg, J. Clardy and K. Lewis, *Chem. Biol.*, 2014, **21**, 509–518.
107 W. Gao, J. Y. Kim, S. N. Chen, S. H. Cho, J. Choi, B. U. Jaki, Y. Y. Jin, D. C. Lankin, J. E. Lee, S. Y. Lee, J. B. McAlpine, J. G. Napolitano, S. G. Franzblau, J.-W. Suh and G. F. Pauli, *Org. Lett.*, 2014, **16**, 6044–6047.
108 M. Choules, Y. Yu, S. H. Cho, J. Anderson, W. Gao, L. Klein, D. C. Lankin, J. Y. Kim, J. Cheng, S. H. Yang, H. Lee, J.-W. Suh, S. G. Franzblau and G. F. Pauli, *Planta Med*, 2015, **81**, CL2.
109 W. Gao, J. G. Napolitano, J. Y. Kim, I.-A. Lee, J. E. Lee, J. Choi, M. F. Rodríguez-Brasco, B. U. Jaki, S. Cho, J. B. McAlpine, G. F. Pauli, J. Kim, J.-W. Suh and S. G. Franzblau, *Planta Med.*, 2012, **78**, PJ134.
110 W. Gao, J. Y. Kim, J. R. Anderson, T. Akopian, S. Hong, Y. Y. Jin, O. Kandror, J. W. Kim, I.-A. Lee, S. Y. Lee, J. B. McAlpine, S. Mulugeta, S. Sunoqrot, Y. Wang, S. H. Yang, T.-M. Yoon, A. L. Goldberg, G. F. Pauli, J.-W. Suh, S. G. Franzblau and S. Cho, *Antimicrob. Agents Chemother.*, 2015, **59**, 880–889.
111 K. Famulla, P. Sass, I. Malik, T. Akopian, O. Kandror, M. Alber, B. Hinzen, H. Ruebsamen-Schaeff, R. Kalscheuer, A. L. Goldberg and H. Brötz-Oesterhelt, *Mol. Microbiol.*, 2016, **101**, 194–209.
112 T. Akopian, O. Kandror, R. M. Raju, M. Unnikrishnan, E. J. Rubin and A. L. Goldberg, *EMBO J.*, 2012, **31**, 1529–1541.
113 K. R. Schmitz and R. T. Sauer, *Mol. Microbiol.*, 2014, **93**, 617–628.
114 R. M. Raju, M. P. Jedrychowski, J.-R. Wei, J. T. Pinkham, A. S. Park, K. O'Brien, G. Rehren, D. Schnappinger, S. P. Gygi and E. J. Rubin, *PLoS Pathog.*, 2014, **10**, e1003994.
115 D. W. Carney, C. L. Compton, K. R. Schmitz, J. P. Stevens, R. T. Sauer and J. K. Sello, *Chembiochem*, 2014, **15**, 2216–2220.
116 M. Arvanitis, G. Li, D. D. Li, D. Cotnoir, L. Ganley-Leal, D. W. Carney, J. K. Sello and E. Mylonakis, *PLoS One*, 2016, **11**, e0153912.
117 E. S. Honsa, V. S. Cooper, M. N. Mhaissen, M. Frank, J. Shaker, A. Iverson, J. Rubnitz, R. T. Hayden, R. E. Lee, C. O. Rock, E. I. Tuomanen, J. Wolf and J. W. Rosch, *MBio*, 2017, **8**, e02124-16.
118 S. Xu, P. Guo, Y. Gao, Q. Shi, D. He, Y. Gao and H. Zhang, *Biochem. Biophys. Res. Commun.*, 2013, **438**, 468–472.
119 D. Y. Kim and K. K. Kim, *J. Biol. Chem.*, 2003, **278**, 50664–50670.
120 E. Leung, A. Datti, M. Cossette, J. Goodreid, S. E. McCaw, M. Mah, A. Nakhamchik, K. Ogata, M. El Bakkouri, Y. Q. Cheng, S. J. Wodak, B. T. Eger, E. F. Pai, J. Liu, S. Gray-Owen, R. A. Batey and W. A. Houry, *Chem. Biol.*, 2011, **18**, 1167–1178.
121 T. Ni, F. Ye, X. Liu, J. Zhang, H. Liu, J. Li, Y. Zhang, Y. Sun, M. Wang, C. Luo, H. Jiang, L. Lan, J. Gan, A. Zhang, H. Zhou and C. G. Yang, *ACS Chem. Biol.*, 2016, **11**, 1964–1972.
122 S. T. Cole, R. Brosch, J. Parkhill, T. Garnier, C. Churcher, D. Harris, S. V Gordon, K. Eiglmeier, S. Gas, C. E. Barry, F. Tekaia, K. Badcock, D. Basham, D. Brown, T. Chillingworth, R. Connor, R. Davies, K. Devlin, T. Feltwell, S. Gentles, N. Hamlin, S. Holroyd, T. Hornsby, K. Jagels, A. Krogh, J. McLean, S. Moule, L. Murphy, K. Oliver, J. Osborne, M. A. Quail, M.-A. Rajandream, J. Rogers, S. Rutter, K. Seeger, J. Skelton, R. Squares, S. Squares, J. E. Sulston, K. Taylor, S. Whitehead and B. G. Barrell, *Nature*, 1998, **393**, 537–544.
123 H. Ingvarsson, M. J. Maté, M. Högbom, D. Portnoï, N. Benaroudj, P. M. Alzari, M. Ortiz-Lombardía and T. Unge, *Acta Crystallogr. D Biol. Crystallogr.*, 2007, **63**, 249–259.
124 N. Benaroudj, B. Raynal, M. Miot and M. Ortiz-Lombardia, *BMC Biochem.*, 2011, **12**, 61.
125 J. Leodolter, J. Warweg and E. Weber-Ban, *PLoS One*, 2015, **10**, e0125345.
126 T. Böttcher and S. A. Sieber, *Angew. Chemie - Int. Ed.*, 2008, **47**, 4600–4603.
127 M. Gersch, F. Gut, V. S. Korotkov, J. Lehmann, T. Böttcher, M. Rusch, C. Hedberg, H. Waldmann, G. Klebe and S. A. Sieber, *Angew. Chemie - Int. Ed.*, 2013, **52**, 3009–3014.

Chapter 3

Lasso peptides modified to mimic ClpX IGF loops activate ClpP and reveal a novel site relevant for ClpX/ClpP interaction

Imran T. Malik[1], Mohamed A. Marahiel[2], Julian D. Hegemann[2,3,*], Heike Brötz-Oesterhelt[1,*]

From the [1]Department of Microbial Bioactive Compounds, Interfaculty Institute of Microbiology and Infection Medicine, University of Tuebingen, Auf der Morgenstelle 28, 72076 Tuebingen, Germany; [2]Department of Chemistry, Philipps-University Marburg, Hans-Meerwein-Strasse 4, 35032 Marburg, Germany; [3]Institute of Chemistry, Technische Universität Berlin, Strasse des 17. Juni 124/TC2, Berlin, 10623, Germany.

Running title: *ClpX IGF loop mimics activate ClpP*

*These authors jointly supervised this work. To whom correspondence should be addressed: Julian D. Hegemann: Institute of Chemistry, Technische Universität Berlin, Strasse des 17. Juni 124/TC2, Berlin, 10623, Germany; email: jdhegemann@googlemail.com. Heike Brötz-Oesterhelt: Department of Microbial Bioactive Compounds, Interfaculty Institute of Microbiology and Infection Medicine, University of Tuebingen, Auf der Morgenstelle 28, 72076 Tuebingen, Germany; email: heike.broetz-oesterhelt@uni-tuebingen.de; Tel. +49 7071 29-74706.

Paper in submission

Keywords: ATP-dependent protease, ATPases associated with diverse cellular activities (AAA+), enzyme kinetics, enzyme mechanism, enzyme mutation, proteolytic enzyme, ClpP, ClpX, MccJ25, acyldepsipeptide antibiotics, ADEP

Abstract

In almost all bacteria, the two-component Clp protease system is responsible for protein homeostasis and quality control. It is involved in important regulatory processes including cell division, host infection, and stress response. To fulfil its natural function, ClpP has to pair up with a Clp-ATPase which feeds substrates targeted for degradation into the proteolytic core of ClpP. This interaction is mediated by conserved tripeptide motifs within flexible loops protruding from the ClpX hexamer which make contact to hydrophobic pockets on the ClpP surface. We constructed mutants of the microcin J25 lasso peptide, a member of the family of ribosomally assembled and post-translationally modified peptides (RiPPs), and introduced the ClpX tripeptide motif into the loop-like structure. These peptides activate ClpP from *Staphylococcus aureus* and *Bacillus subtilis* but do not display the full *in vitro* activation profile of acyldepsipeptide antibiotics of the ADEP class (ADEPs). ADEPs are known ClpP activators that bind to the hydrophobic pockets and enable unregulated full-length protein degradation by ClpP. The MccJ25 loop mutants confer stability and stimulate peptide but not protein degradation. The MccJ25 loop mutants point towards a novel binding site at ClpP that is not targeted by ADEP.

Introduction

The Clp protease is a highly conserved two-component system, which consists of the proteolytic ClpP as well as a regulatory Clp-ATPase. In many bacterial species, the Clp protease was shown to be important for protein homeostasis and quality control, cell differentiation, virulence regulation and stress management (1-3). In pathogenic bacteria, the Clp protease system serves as a promising target for antivirulence and antibacterial treatment (4-6). Several mechanisms of disturbing the Clp system have been devised so far. Regarding the proteolytic ClpP in particular, the following mechanisms can be enumerated: First, the over-activation and deregulation of the proteolytic ClpP which leads to unrestricted access to the proteolytic core and uncontrolled digestion of cytosolic proteins (7-9). Second, disabling the communication between ClpP and the Clp-ATPase and thereby abrogating the natural functions of the Clp system (10-12). Third, functional inhibition of the catalytic site

serine of ClpP with the help of covalent active site inhibitors carrying a β-lactone moiety (5, 13).

ClpP is shaped like a barrel and composed of two heptameric rings that stack upon each other. At the top and bottom of the barrel are narrow entry pores for substrate translocation. The Clp-ATPases are responsible for recognition of substrates and their translocation into the catalytic cavity of ClpP where degradation takes place. In the proteolytically active complex, the two components form a larger stack with the hexameric ring-shaped Clp-ATPases sitting on one or both sides of the ClpP barrel (14, 15). Without the supporting action of a Clp-ATPase like ClpX or ClpC, ClpP alone does not degrade proteins because access to the proteolytic core is limited to small peptides due to the narrow entrance pores (7, 16, 17). Upon a degradation signal, the Clp-ATPase establishes contact to ClpP and actively unfolds and translocates the substrate through the entrance pores. Of particular relevance in this interaction is a flexible loop that protrudes from each Clp-ATPase monomer and carries a conserved (LIV)-G-(FL) hydrophobic tripeptide binding motif at its tip (18, 19). With the help of modelling and mutational studies, hydrophobic binding pockets (H-pocket) at the apical surface of ClpP have been identified to serve as potential anchors for the flexible loop motifs of Clp-ATPases (18, 20, 21). The discovery of acyldepsipeptide antibiotics of the ADEP class (ADEPs) further emphasized the role of the H-pocket (4). By employing the H-pocket, ADEPs over-activate ClpP by increasing the pore diameter and allosterically enhancing catalytic activity which leads to unregulated digest of essential cytosolic proteins and cell death (9, 22-24). In addition, ADEPs competitively disrupt the functional interaction between ClpP and Clp-ATPases and thereby abrogate all natural functions of the Clp protease (10, 24).

ADEP shows potent antibacterial activity against a broad range of Gram-positive bacteria (4, 25-27). Its structure consists of a macrolactone core and a *N*-acylphenylalanine side chain. Analysis of several ADEP fragments revealed that the latter structure is necessary for activity while the macrolactone core is inactive on its own (28). Intriguingly, the *N*-acylphenylalanine fragment necessary for activity closely resembles the tripeptide binding motifs within the protruding loops in Clp-ATPases corroborating ADEP's image as an IGF loop mimic (28-30). However, potency of the *N*-acylphenylalanine fragment was decreased 500-fold compared to the parent ADEP molecule. The macrolactone core is responsible for ADEP's high affinity towards the

H-pocket (28). Thus, although the *N*-acylphenylalanine side-chain of ADEP probably occupies the same binding site as the IGF motif, due to their macrolactone backbone, ADEPs bind a greater surface area of ClpP and establish various additional hydrophobic contacts plus two hydrogen bonds which might produce conformational changes that IGF loop binding cannot achieve.

We set out to generate IGF loop peptides, that resemble the original Clp-ATPase loops. In a previous study, a linear fluorescent peptide containing the IGF motif bound ClpP only very weakly (19). Whether this behaviour is in fact reflecting the poor binding properties of individual IGF loops in the natural context or due to an unfavourable conformation is not known. With the aim to generate a tool peptide that better reflects the Clp-ATPase loop conformation, we introduced the IGF motif into the sequence of microcin J25 (MccJ25), a member of the lasso peptide family that is otherwise not associated with ClpP. Lasso peptides are natural products belonging to the family of ribosomally assembled and post-translationally modified peptides (RiPPs). They are defined by their unique topology, which is reminiscent of a lariat knot and consists of an N-terminal macrolactam ring that is threaded by the linear C-terminal tail section. The lasso structure is maintained by placement of sterically demanding residues in the tail that are positioned above and below where the tail threads the ring. The ring size can vary between 7-9 amino acids and is formed between the N-terminal α-amino group and the carboxylic acid side chain of an Asp or Glu residue (31). This fold confers high proteolytic stability and in many cases is also unaffected by prolonged incubation at high temperatures (31-33). Therefore, lasso peptides are interesting scaffolds for the introduction of peptide epitopes to generate novel and highly stable functional peptides. We reasoned that the loop of a lasso peptide could be converted into a suitable mimic of the Clp-ATPase binding loop. These peptides present an ideal basis for offering the conserved binding epitope of the Clp-ATPase as part of a flexible loop without the higher structural organization of a Clp-ATPase hexamer. Furthermore, they offer high protease stability and the possibility of titrating single IGF loops in order to dissect their binding effect individually. In order to generate such a peptide, the lasso peptide microcin J25 (MccJ25) was chosen, as it can not only be heterologously produced in good yields in *Escherichia coli*, but also has the largest loop amongst known lasso peptides. Additionally, the MccJ25 loop contains a stretch of five residues, Val11-Gly12-Ile-13-Gly14-Thr15, that would allow introduction of the IGL,

IGF, and VGF epitopes without too drastic changes in the peptide sequence. Indeed, all designed lasso peptides could be produced and isolated from *E. coli* and where assessed for *in vitro* activity.

Here we demonstrate that a lasso peptide carrying the tripeptide motif of the partner Clp-ATPase ClpX indeed interacts with ClpP and that its activation mechanism differs from that of ADEP. Unexpectedly, it seems to interact not only with the hydrophobic pocket but, in addition, with a second binding site at ClpP. Our findings may also have implications for the binding mode and activation mechanisms of the Clp-ATPases.

Results

Construction of microcin J25 mutants with canonical tripeptide binding motifs

MccJ25 mutants were generated with the intent to imitate the tripeptide binding motif of cognate Clp-ATPases. Therefore, the three common tripeptide motifs IGL, IGF and VGF found in the respective Clp-ATPases from the model organisms *E. coli* (ClpA), *S. aureus*, *Bacillus subtilis* and *Helicobacter pylori* (ClpX), were introduced each at three positions within the loop of MccJ25 (Fig.1). Thus, a set of nine loop mutants was generated, incorporating IGL, IGF, or VGF starting at either position 11 (11IGL, 11IGF, 11VGF), position 12 (12IGL, 12IGF, 12VGF), or position 13 (13IGL, 13IGF, 13VGF) (Fig. 1).

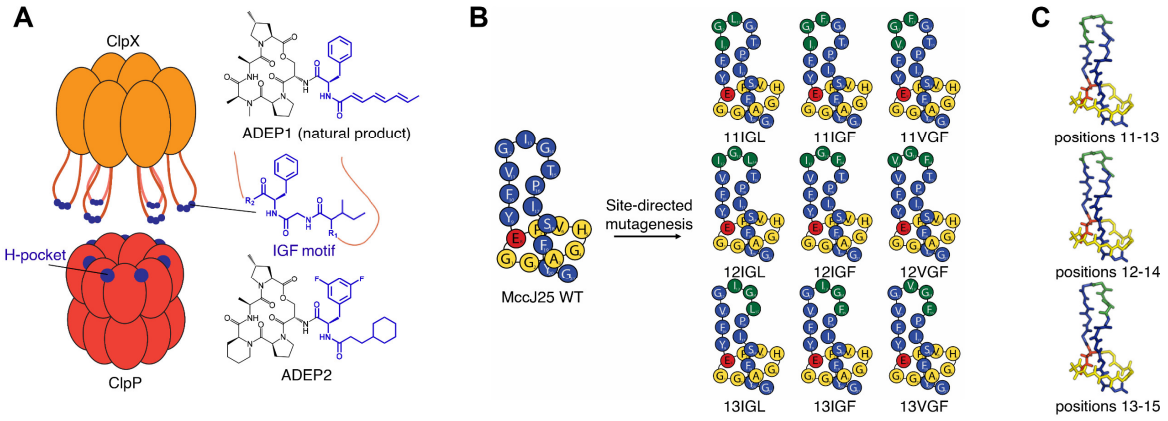

Figure 1. Generation of lasso peptide MccJ25 loop mutants. *A*, schematic of the two components of the Clp protease, ClpP and ClpX. The interaction occurs between protruding flexible loops of ClpX, carrying the conserved tripeptide motif Ile-Gly-Phe, and the H-pockets of ClpP. The H-pockets are located between two adjacent monomers of ClpP. On the right-hand side, the natural product ADEP1 and the synthetic derivative ADEP2 with increased affinity for SaClpP are depicted. The moieties mimicking the IGF motif are highlighted in blue. *B*, generation of MccJ25 loop mutants. Three conserved ClpX tripeptide motifs (IGL, IGF, VGF) from different organisms were introduced into the loop structure of MccJ25 at three different positions, respectively. The macrolactam ring is highlighted in yellow, the N-terminus is coupled to the side-chain of glutamate at position 8 (red) *via* an isopeptide bond. The respective tripeptide motifs are highlighted in green. *C*, crystal structure of MccJ25 (PDB code: 1Q71 (34)) with corresponding colour coding.

MccJ25 loop mutants stabilize the oligomeric state of the *S. aureus* ClpP barrel

In order to assess the different MccJ25 variants, we first chose *S. aureus* ClpP (SaClpP) as a model peptidase and performed *in vitro* degradation assays with the fluorogenic model peptide substrate Suc-LY-AMC. Apo-SaClpP is purified as a stable tetradecamer and thus exhibits intrinsic peptidase activity that can be enhanced weakly by ADEP2 under established assay conditions in a HEPES pH7 buffer (Fig. 2*A*) (24). In order to investigate, whether MccJ25 loop mutants can exert a stabilizing effect on the oligomeric structure of tetradecameric SaClpP, we conducted peptide

degradation assays under destabilizing conditions employing a Tris pH8 buffer. Under these conditions, peptidase activity of apo-SaClpP was almost completely abolished, but we noted that a substantial extent of the original activity (observed in favourable HEPES buffer) was retained in the presence of ADEP2 (Fig. 2*A*). Gel filtration chromatography demonstrated that the detrimental Tris pH8 buffer effect manifests in a breakdown of the oligomeric state of SaClpP (Fig. 2*B*). The full complex consisting of 14 ClpP protomers is roughly 316 kDa in molecular weight, but disassembles in Tris buffer into three fractions, a predominant heptameric fraction and lower oligomeric states in the dimer/trimer range. In the presence of ADEP, SaClpP remains in the active tetradecameric conformation even under unfavourable buffer conditions. This experimental setup was now used to differentiate MccJ25 loop mutants regarding their effect on ClpP stability. In a panel of all nine MccJ25 variants, three loop mutants, all carrying the canonical tripeptide motif at positions 12-14, were able to retain SaClpP activity in Tris buffer, most notably the 12IGF mutant. Gel filtration confirmed, that 12IGF is able to maintain tetradecamer integrity in Tris buffer (Fig. 2*D*). The stabilizing effect of 12IGF is concentration-dependent with an apparent affinity constant of 26 µM (Fig. 2*E*). To exclude that 12IGF serves as a SaClpP substrate, we incubated a mixture of SaClpP and 12IGF under assay conditions for up to 260 min. LC-MS confirmed that 12IGF remained intact (Fig. S1).

To test whether the strongest lasso variant 12IGF was able to interfere with communication between SaClpP and the *S. aureus* model Clp-ATPase ClpX (SaClpX), we also performed a GFP degradation assay, where eGFP carrying the C-terminal degradation tag ssrA is unfolded and translocated into the SaClpP degradation chamber by SaClpX in the presence of ATP. It was shown before that this assay is readily inhibited by small amounts of ADEP due to the strong competition of ADEP and ClpX for the H-pocket which resulted in the abrogation of the interaction between the Clp-ATPase and ClpP (Fig. 2*F*) (24). ADEP (in contrast to an ATP-fuelled Clp-ATPase) cannot activate ClpP to degrade GFP (24). Now, we used the same assay setup for 12IGF and observed that 12IGF interfered with the GFP degradation rate of ClpXP only very slightly (Fig. 2*F*). This was not unexpected, since we had already assumed that the affinity of six individual IGF motifs would not be able to compete with the overall higher avidity of six IGF motifs arranged in a favourable orientation in SaClpX and docking to ClpP simultaneously. Albeit weak, the inhibition

of SaClpXP by 12IGF was nonetheless reproducible and concentration-dependent indicating actual competition with ClpX.

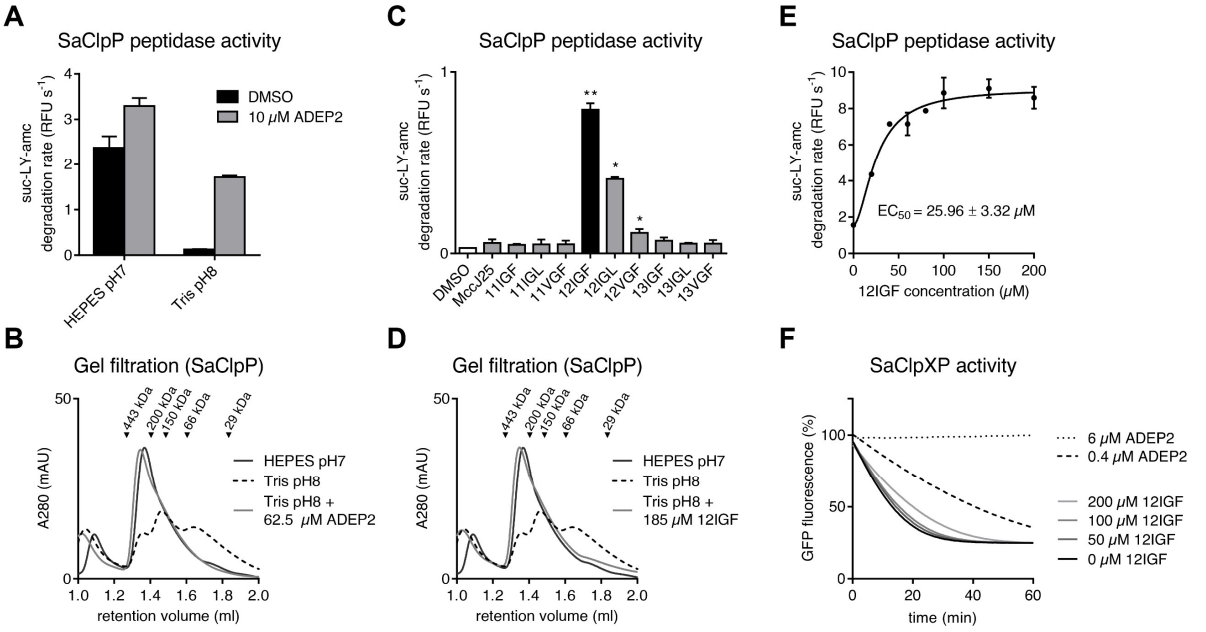

Figure 2. Lasso peptide effect on the Clp system of *S. aureus*. *A and B*, buffer effect on the *in vitro* peptidase activity and oligomeric integrity of SaClpP. Inactivation by oligomeric breakdown in Tris pH8 buffer can be circumvented by addition of ADEP2. Error bars indicate S.D. (three independent experiments). *C and D*, peptidase activity of SaClpP in Tris pH8 buffer in the presence of the MccJ25 loop mutant panel at a concentration of 46 µM. MccJ25 mutations at position 12 are most effective, 12IGF is the most potent variant. Dissociation of SaClpP tetradecamer into lower oligomeric states can be prevented by addition of 12IGF. Error bars indicate S.D. (three independent experiments). *, $p < 0.05$; **, $p < 0.01$. *E*, Stabilizing effect of 12IGF on SaClpP peptidase activity at increasing lasso peptide concentrations with an apparent affinity constant of ~ 26 µM. *F*, time course of GFP-ssrA degradation by SaClpXP in the presence of different concentrations of ADEP2 and 12IGF. 12IGF interferes slightly with SaClpXP activity (three separate experiments, a representative experiment is shown).

MccJ25 loop mutants and ADEPs synergistically stimulate *B. subtilis* ClpP peptidase activity

In previous studies, *B. subtilis* ClpP (BsClpP) had been purified to a large extent in the monomeric form, which was also the predominant conformation under our purification and assay conditions (22, 34). In accordance with its predominantly monomeric state, it exhibited only marginal intrinsic peptidase activity and was strongly stimulated by addition of ADEP (22). This stimulated peptidase activity is achieved first and foremost by the ADEP-induced assembly of the active tetradecameric ClpP complex (7). When we tested the MccJ25 variants for their ability to stimulate BsClpP peptidase activity, stimulation could not be achieved with any of the variants. While in the case of SaClpP, 12IGF was able to stabilize an active tetradecameric complex, it did not achieve the assembly of the BsClpP barrel from monomers. However, in the presence of ADEP2 and thereby fully formed and active BsClpP tetradecameric complexes, certain

MccJ25 loop mutants triggered a further increase in peptidase activity, the 12IGF mutant again showing highest potency (Fig. 3*A*). The activation was concentration-dependent and required much higher overall 12IGF concentrations compared to ADEP2 with an apparent affinity constant of 60 µM (Fig. 3*B*).

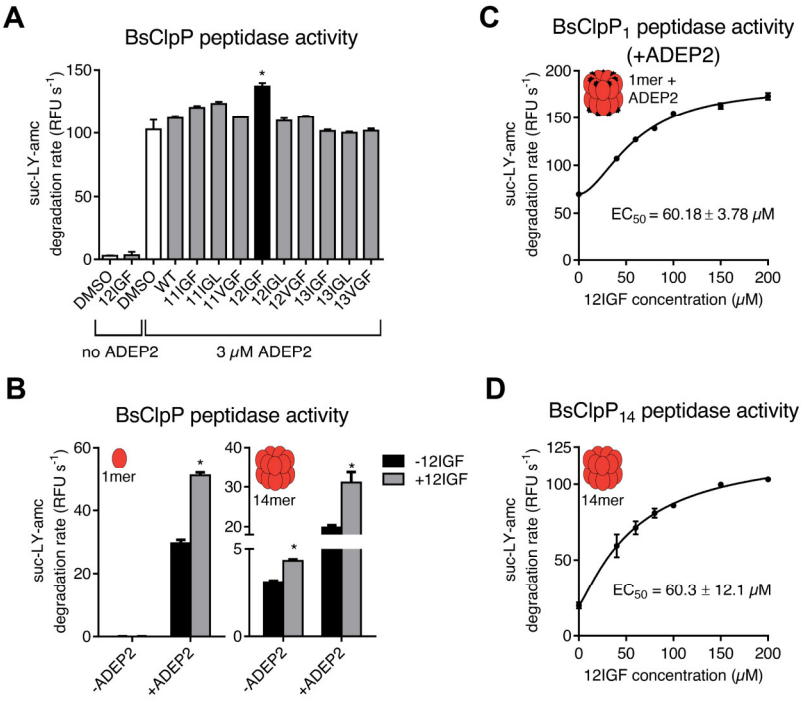

Figure 3. Lasso peptide effect on the Clp system of *B. subtilis*. *A*, peptidase activity of BsClpP in Tris pH8 buffer in the presence of the MccJ25 loop mutant panel at a concentration of 23 µM. This protein preparation was generated by a procedure widely used for BsClpP and contained predominantly monomers (24, see Methods). Error bars indicate S.D. (three independent experiments). *, $p < 0.05$. *B*, peptidase activity of separate pre-purified fractions of either BsClpP monomer (left) or tetradecamer (right) with different combinations of effectors (effector concentrations: 3 µM (ADEP2), 46 µM (12IGF)). Error bars indicate S.D. *, $p < 0.05$. *C*, peptidase activity of pre-purified monomeric BsClpP in the presence of 5 µM of ADEP2 and 12IGF at increasing concentrations. Error bars indicate S.D. (two separate experiments). *D*, peptidase activity of pre-purified tetradecameric BsClpP at increasing 12IGF concentrations. No ADEP was added here. Error bars indicate S.D. (two experiments each).

This finding led us to the hypothesis that lasso peptides are unable to induce the assembly of the active tetradecamer in BsClpP on their own but require a preassembled complex to exert an activating effect. To test this notion, we purified BsClpP under specific buffer conditions that favour tetradecamer assembly and subsequently collected the tetradecameric fraction from a gel filtration column. Immediately after, activity assays were performed with the most potent lasso peptide, MccJ25 12IGF. In fact, 12IGF was able to stimulate peptidase activity of preformed tetradecamers significantly confirming that 12IGF requires a fully assembled BsClpP

barrel for activity (Fig. 3*C*). The apparent affinity of 12IGF for BsClpP was unaffected by the absence or presence of ADEP2 (Fig. 3, *B* and *D*).

While peptidase activity is reliant only on an assembled tetradecameric complex and a functional catalytic triad, degradation of the loosely folded model protein substrate casein requires in addition the opening of the entrance pores as achieved by ADEP binding (22). In contrast to ADEP, the 12IGF loop mutant was not able to activate ClpP, neither SaClpP nor BsClpP, to degrade the fluorogenic protein substrate FITC-casein (Fig. S2).

Lasso peptide-mediated activation is not inhibited by ADEPs

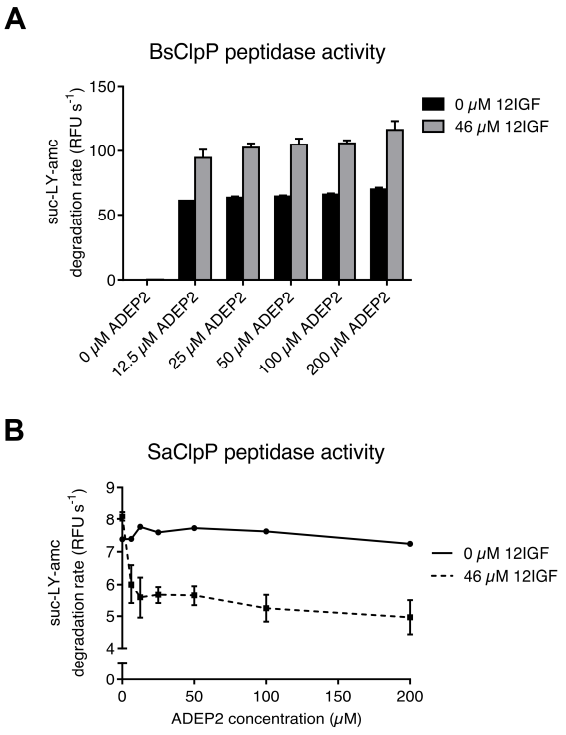

Figure 4. ADEPs and 12IGF show noncompetitivity. *A*, BsClpP *in vitro* peptide degradation assay in the absence and presence of 12IGF at increasing ADEP2 concentrations. The 12IGF synergistic effect remains stable even at high ADEP2 concentrations. Error bars indicate S.D. (three separate experiments). *B*, SaClpP *in vitro* peptide degradation in the absence and presence of 12IGF at increasing ADEP2 concentrations. The combination of ADEP2 and 12IGF lead to a decrease of peptide degradation activity of SaClpP. No converging trend at increasing ADEP2 concentrations can be observed. Error bars indicate S.D. (two separate experiments).

ADEP binds ClpP from different organisms with a comparatively high affinity in the low single-digit micro-molar range, e. g. a K_D value of 2 µM was determined in an isothermal calorimetry experiment for the interaction between SaClpP and ADEP7 (24). Our FITC-casein degradation assays showed apparent affinity constants below 1 µM (Fig. 5*G*). For SaClpP, one ADEP molecule was shown to be sufficient to disturb ClpX binding and inhibit ClpX-mediated GFP degradation by half (24). 12IGF EC_{50} values arrived at 26 and 60 µM in SaClpP and BsClpP peptidase assays, respectively, and thus exceeded the EC_{50} values measured for ADEP by one to two orders of magnitude (Fig. 2*E*; Fig. 3, *B* and *D*). Based on these findings, we expected ADEP to readily displace 12IGF when competing for the same binding site. Therefore, BsClpP competition assays were performed with an increasing concentration of ADEP2 while keeping the 12IGF concentration constant. As a readout, we monitored the surplus of

BsClpP peptidase activity that we had observed in the presence of the 12IGF/ADEP2 combination in relation to ADEP2 alone (Fig. 3*A*) Surprisingly, the additional stimulation of BsClpP by 12IGF in the presence of ADEP2 remained constant even at very high ADEP2 excess (100-fold K_{app} for ADEP; Fig. 4*A*). Interestingly, while 12IGF and ADEP2 co-stimulated the catalytic activity of BsClpP where the tetradecamer first had to be assembled, the lasso peptide reduced the activating potential of ADEP2 in the case of the pre-assembled SaClpP tetradecamer. SaClpP activity reproducibly decreased with rising ADEP2 concentrations in the presence of 12IGF (Fig. 4*B*). The reason for this effect is not known, but this clear consequence of lasso peptide binding to SaClpP could now serve as a readout for our competition assay. Also here, ADEP2 was not able to reduce the lasso effect, even when titrated two orders of magnitude beyond its K_{app} for SaClpP. Both of these findings establish a lack of competitivity between ADEP and 12IGF and suggest a binding mechanism different from ADEP2. Clearly, a high excess of a potent H-pocket binder does not eradicate the 12IGF effect. This came as a surprise since the MccJ25 loop mutants had been designed to mimic IGF loop binding. With a notion that only the H-pocket would serve as a docking point for the IGF motif, we had expected that 12IGF would be limited to the same binding site as ADEP.

12IGF activity is affected by mutations in the C-pocket of ClpP

Leung *et al.* proposed a putative additional ClpP binding pocket termed the ‘C-pocket’ when they identified new activators of cylindrical proteases (ACPs) in a large-scale screening approach of synthetic compound libraries (35). These compounds were tested against *E. coli* ClpP and it was postulated that weaker ACPs were more strongly affected by C-pocket mutations than strong ACPs. The C-pocket is in close vicinity to the H-pocket and constitutes a more polar surface with 50% polar residues compared to 25% of the H-pocket (Fig. 5*A*). Furthermore, like the H-pocket, the C-pocket stretches over two neighbouring ClpP subunits within a barrel. This subunit-spanning feature has accounted for increased inter-ring stability of the ClpP complex when ADEP bound to the H-pocket, so binding of a ligand to the C-pocket could cause the same stabilizing effect. The amino acid residues constituting the C-pocket in EcClpP share 62.5 % identity with the respective SaClpP residues. We exchanged two of the conserved C-pocket residues Y78 and Q82 in SaClpP to alanine as well as the known H-pocket residue M190 to threonine. The M190T mutant had emerged in previous

screenings for ADEP-resistant mutants in our lab and had displayed a reduced affinity for ADEP (Fig. 5*C*, table). Peptidolytic activity of all three SaClpP mutants was in the range of the wildtype (Fig. 5*B*). Both C-pocket mutants Y78A and Q82A displayed casein degradation rates (in the presence of ADEP2) similar to the wildtype and also similar apparent affinities for ADEP2, while the H-pocket mutant M190T showed a 5-fold reduced apparent affinity for ADEP (Fig. 5*C*). Next, we subjected the mutant proteins to the destabilizing Tris pH8 buffer conditions and analysed the fraction of maximum activity (in relation to the favourable HEPES buffer) that is retained with the help of either ADEP2 or 12IGF in each mutant. The C-pocket mutant Q82A retained a similar percentage of its maximum HEPES activity compared to wildtype in the presence of ADEP2 but was more severely affected by the buffer effect in the presence of 12IGF (Fig. 5*D*). *Vice versa*, ADEP2 could not stabilize the H-pocket mutant M190T as well as the wildtype while 12IGF activity was fully competent with this mutant. This finding supports the notion that the C-pocket may serve as a binding site for 12IGF.

Interestingly, the second C-pocket mutant Y78A was not much affected by the Tris buffer. Despite the unfavourable buffer conditions, this mutant displayed peptide degradation capabilities comparable to wildtype SaClpP in favourable HEPES buffer, even in the absence of the stabilizing ligands ADEP2 and 12IGF (Fig. 5*E*). This was also corroborated by gel filtration where the Y78A mutant remained a stable tetradecamer in Tris buffer (Fig. 5*F*). Furthermore, the Y78A mutation conferred stability on SaClpP even in the Q82A background (Fig. 5*E*). This stabilizing effect of the Y78A mutation was remarkable as the wildtype fully decomposed under these conditions.

Since the ClpX mimetic 12IGF showed sensitivity to C-pocket alterations we were wondering whether the same was true for ClpX. To that end, we performed eGFP-ssrA degradation assays. In fact, both the C-pocket mutant Y78A and the H-pocket mutant M190T were no longer able to degrade GFP, and the C-pocket mutant Q82A showed impaired GFP degradation with respect to the wildtype (Fig. 5*G*). This is noteworthy considering that these mutants are functional in both peptide degradation, indicating catalytic capability, as well as casein degradation, indicating pore opening by ADEP2 (Fig. 5*B*,*C*). The Q82A mutant displayed only half of the wildtype peptidase activity but degraded FITC-casein at almost wildtype level and was fully functional in the interaction with ADEP2 as exemplified by the apparent affinity (Fig. 5*C*, table). The

M190T mutant differed from wildtype only in a reduced affinity for ADEP2 which resulted in a higher EC_{50} in ADEP2-dependent casein degradation (Fig. 5*C*, table). Most interestingly, the Y78A C-pocket mutant degraded both peptide (Fig. 5*B*) as well as FITC-casein with the help of ADEP2 (Fig. 5*C*) at wildtype level but was completely inactive in the GFP degradation assay where interaction with SaClpX is required. This finding strongly supports a functional role of the C-pocket in the interaction between SaClpP and SaClpX.

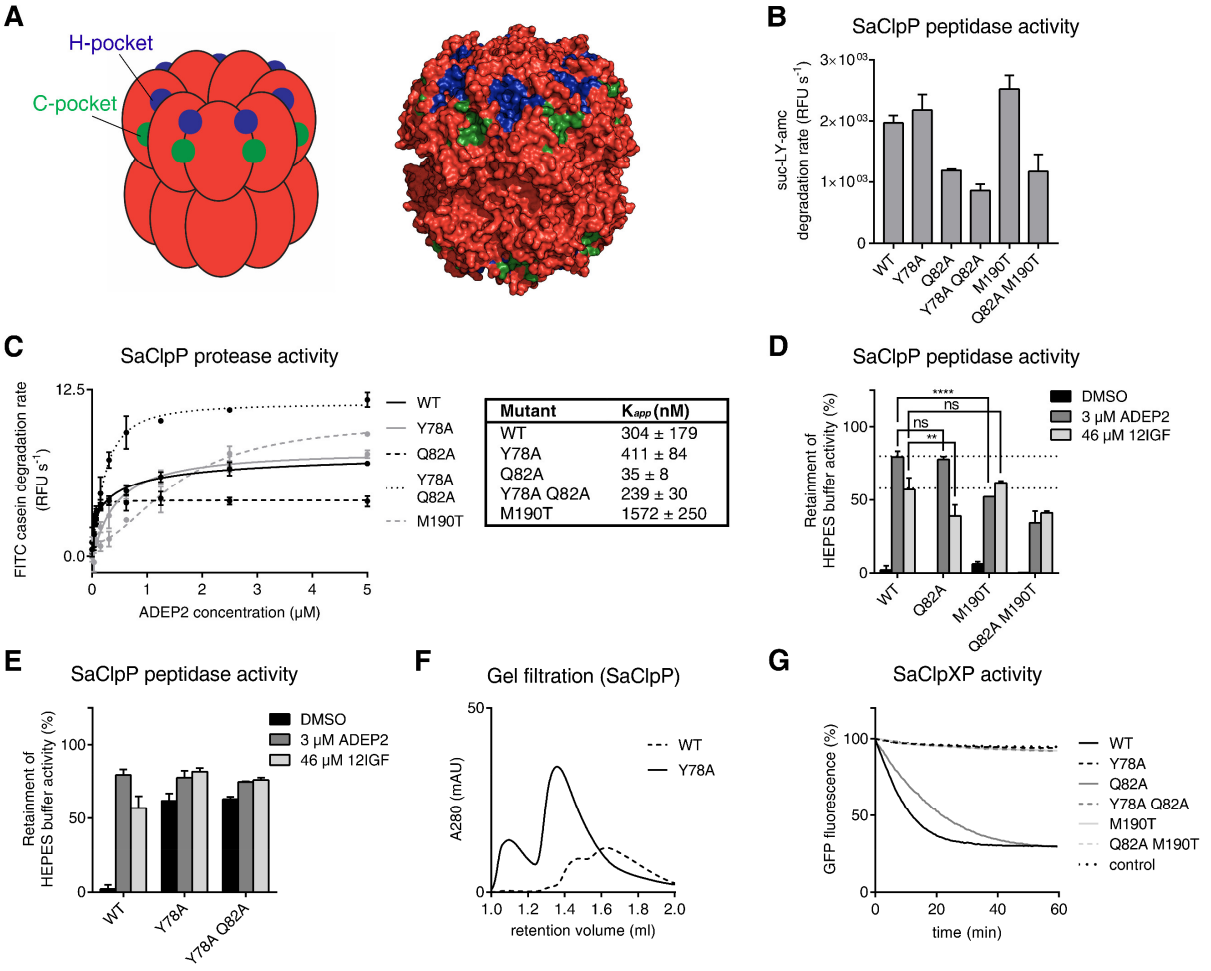

Figure 5. Influence of C-pocket mutations on the effects of ADEP2 and 12IGF. *A*, schematic and crystal structure of SaClpP (Protein Data Bank Code 3V5E (37)) with H-pockets and C-pockets highlighted in *blue* and *green*, respectively. *B*, peptide degradation by SaClpP C- and H-pocket mutants in HEPES buffer. Error bars indicate S.D. (two separate experiments). *C*, casein degradation of 100 nM SaClpP C-pocket (Y78A, Q82A, Y78A Q82A) and H-pocket (M190T) mutants in the presence of increasing concentrations of ADEP2. Error bars indicate S. D. *D*, peptide degradation of SaClpP C- (Q82A) and H-pocket (M190T) mutants in Tris buffer as a percentage of HEPES buffer activity. 12IGF effect is impaired in stabilizing the C-pocket mutant Q82A. Error bars indicate S.D. (three separate experiments were combined) **, $p < 0.01$; ****, $p < 0.0001$. *E*, peptide degradation of the SaClpP C-pocket mutant Y78A and the C-pocket double mutant Y78A Q82A. The mutation confers stability in Tris buffer. Error bars indicate S.D. (two separate experiments). *F*, gel filtration of the SaClpP C-pocket mutant Y78A confirms oligomeric integrity in Tris buffer. *G*, time course of GFP-ssrA degradation by C- and H-pocket mutants of SaClpXP.

Discussion

In comparing the effects of 12IGF with those of ADEP, parallels and also striking differences can be seen. Like ADEP, 12IGF affects ClpP across species, it stabilizes the tetradecameric state of ClpP and it is able to stimulate ClpP's catalytic activity. However, 12IGF lacks ADEP's capacity to assemble the primarily monomeric BsClpP but requires preassembled tetradecamer in order to exert catalytic activation. Apparent affinity constants displayed by 12IGF were one to two orders of magnitude higher than for ADEPs. The low affinity was in accordance with our expectations since even the fully assembled ClpX hexamer had displayed weaker affinities than ADEP (24). ClpX carries six coupled IGF motifs in a rather favourable orientation. Hence, we expected the individual IGF motifs presented by the MccJ25 loop mutants to bind even less strongly than ClpX because the latter benefits from the avidity of six binding sites. SaClpP activation by lasso peptides was specific to the motif IGF, which also occurs naturally in BsClpX as well as SaClpX. Among the series of loop mutants, the IGF motif performed best when starting from position 12 of the MccJ25 sequence, which places it right at the tip of the lasso loop. Thus, we are confident that the loop mutant effect we observe is in fact due to the respective tripeptide motif rather than secondary effects.

A structure-activity relationship study on fragments of the ADEP structure showed that the *N*-acyldifluorophenylalanine moiety of ADEP (designated fragment **5** in reference (28)) is necessary and sufficient to exhibit residual *in vitro* bioactivity against *B. subtilis*, although its antibacterial activity dropped 500-fold compared to intact ADEP (MIC of 8 µg/ml compared to 0.016 µg/ml of the intact ADEP lead structure). The isolated macrolactone core did not show any activity on its own (28). Fragment **5** also superimposed nicely with the resolved LGF tripeptide from a *H. pylori* crystal structure and further substantiated the notion that ADEPs are Clp-ATPase mimetics (23, 29). Based on this data, it was assumed that the *N*-acyldifluorophenylalanine moiety presents the principle pharmacophore of the ADEP molecule while the backbone serves only to confer higher affinity and consequently efficacy through additional molecular interactions. Compared to fragment **5,** a peptide carrying the IGF motif and tested in a previous study was much inferior and showed very little activity (19). Hence, we reasoned that a linear peptide carrying the reserved IGF residues might not adopt the conformation required for effective H-pocket binding. We were intrigued to see that

the IGF motif as part of a loop in fact increases upon the poor apparent affinity of the linear peptide and that the engineered loop peptide was capable of stabilizing ClpP's tetradecameric structure as well as stimulating its catalytic function. Previously, it was shown that for catalysis, ClpP needs to adopt the tetradecameric extended conformation and that ADEP as well as ClpX induce this state in ClpP by exerting conformational control (24). The observation that 12IGF also stimulates catalysis implies corresponding conformational control by the lasso peptide.

12IGF did not enable casein degradation by ClpP which points toward an inability to open the pore sufficiently for entry of the loosely folded protein into the ClpP lumen. Whether the observation that we made for 12IGF reflects on cognate Clp-ATPases and whether also the hexameric IGF loop assembly lacks pore opening capacity, is not known. However, this result is in clear contrast to ADEP whose antibacterial activity depends on pore opening and the resulting deregulated protein and polypeptide degradation in bacterial cells (7, 8). It is notable in this context, that *N*-acylphenylalanine (i. e. ADEP fragment **5** lacking the difluorination) was almost completely inactive against bacterial cells (MIC 64 µg/ml; (28)) and that the difluorination was also shown to strongly improve antibacterial potency in a structural optimization program for ADEP (25). Our current characterization of 12IGF and its distinct effects in relation to ADEP highlights the importance to pay close attention to certain structural features that differentiate ADEP from the (LIV)-G-(FL) motif. The structure of the *N*-acylphenylalanine side-chain of ADEP strongly resembles the IGF tripeptide and it seems reasonable to assume that it addresses the same binding site within the H-pocket of ClpP with consequent catalytic activation by conformational control. However, ADEPs contain further structural elements in form of the macrolactone core and synthetic modifications in form of the difluoro moiety, which are both decisive for antibacterial activity. It is feasible that the additional contacts mediated by the macrolactone core (several hydrophobic interactions as well as two hydrogen bonds (22)) are responsible for ClpP's casein degradation capability based on a wider time-averaged pore diameter and triggered by additional conformational rearrangements in ClpP.

We were surprised to see that 12IGF displayed no competition to ADEP, neither in SaClpP nor in BsClpP. In the case of BsClpP, 12IGF and ADEP2 displayed synergistic behaviour with 12IGF providing additional activity independent of the ADEP2

concentration. In SaClpP, the combination of ADEP2 and 12IGF showed an inhibitory effect that could not be circumvented by applying ADEP2 in high excess. If 12IGF and ADEP2 exclusively shared the same docking site, we would expect ADEP2 excess to successfully displace all of the 12IGF molecules from ClpP and show ADEP2-only activity.

On the search for additional cavities on the ClpP surface, the C-pocket caught our attention as a putative alternative or additional binding site for the loop mutant 12IGF. By employing the stabilizing properties of 12IGF on SaClpP *in vitro*, we were able to show by mutational studies that C-pocket mutants were much more sensitive to oligomeric breakdown in the presence of 12IGF than in the presence of ADEP. *Vice versa*, an H-pocket mutant was less well stabilized by ADEP than by 12IGF. Furthermore, both a fully functional C-pocket and H-pocket were mandatory for full GFP degradation activity and hence functional ClpP-ClpX-interaction. Most noteworthy in this respect is the C-pocket mutant Y78A which showed wildtype-like activity in both peptide degradation assays as well as casein degradation which relies on ADEP binding to a functional H-pocket. Importantly, this mutant was completely inactive in a SaClpXP assay strongly arguing for an interaction of the ClpX IGF loop with the C-pocket.

Based on ClpP mutational and modelling studies as well as assays with the known H-pocket binder ADEP, the H-pocket had been previously established as the major binding site for the (LIV)-G-(FL) loops of cognate Clp-ATPases. The data presented here does not oppose the view that the H-pocket serves as the main docking site of IGF loops, nor does it exclude that 12IGF can bind to this site. However, our data strongly suggest that another cavity on the surface of ClpP can accommodate IGF loops. In contrast to ADEP, which seems to bind to the H-pocket exclusively, a specificity that is probably mediated by the multiple additional interactions formed by the macrolactone core, ClpP-ClpX-interaction requires both a functional H-pocket as well as a functional C-pocket. Regarding the binding site of 12IGF, our data clearly show that in the presence of the strong H-pocket competitor ADEP, 12IGF still affects ClpP activity. While we do not put the interaction between 12IGF and the H-pocket into question, the lack of competitivity between 12IGF and ADEP could well result from 12IGF residing in the C-pocket, while ADEP occupies the H-pocket. Further

investigation is required to confirm a functional role of the C-pocket in the dynamic interaction between ClpP and cognate Clp-ATPases.

Experimental procedures

Mutagenesis of *mcjA* and purification of MccJ25 variants

Mutagenesis of the *mcjA* gene in the MccJ25 production plasmid (pTUC202) (38) was accomplished by using site-directed ligase-independent mutagenesis (SLIM) according to published protocols (39, 40). In short, a set of four primers was used for every mutant. The same two base primers (mcjA_SLIM_FP and mcjA_SLIM_FP; see Table S1) that anneal to the regions flanking the *mcjA* sequence stretch coding for residues 9-18 of MccJ25 were used for every mutant. Another two primers unique for every mutant were employed, which carried the mutated codons for residues 9-18 as 5' overhang on the base primer sequence (see Table X). For every mutation, two 50 µl PCRs were performed using Phusion DNA polymerase (New England Biolabs): One PCR using mcjA_SLIM_FP and the respective overhang reverse primer, the other PCR utilizing the respective overhang forward primer and mcjA_SLIM_RP. Of each reaction, 10 µl were analysed by agarose gel electrophoresis to check if the target DNA was amplified and, if successful, the remainder was treated with DpnI (New England Biolabs) to remove the template DNA (40 µl PCR sample + 4.6 µl CutSmart Buffer + 1.0 µl DpnI, 2 h at 37 °C; followed by DpnI-inactivation for 20 min at 80 °C). DpnI-treated samples were then hybridized. For this, 10 µl of each DNA sample were mixed with 10 µl 5X hybridization buffer (750 mM NaCl, 125 mM Tris, 100 mM EDTA, pH 8.0) and 20 µl of ddH_2O. The mixture was then incubated for 3 min at 99 °C, followed by three cycles of incubation for 5 min at 65 °C and 40 min at 30 °C. For transformation of the hybridized, circular DNA, 10 µl of each hybridization reaction were used and cells carrying the target plasmids were selected for by plating on lysogeny broth (LB) agar plates with 17 µg/ml chloramphenicol. Incorporation of the correct mutations was confirmed by dideoxy sequencing (GATC Biotech AG).

For production of the MccJ25 variants, M9 minimal medium (17.1 g/l $Na_2HPO_4 \cdot 12\ H_2O$, 3 g/l KH_2PO_4, 0.5 g/l NaCl, 1 g/l NH_4Cl, 1 ml/l $MgSO_4$ solution (2 M), 0.2 ml/l $CaCl_2$ solution (0.5 M), pH 7.0; after autoclaving, 10 ml/l sterile glucose solution (40% w/v) and 2 ml/l 500X M9 vitamin mix (Table 1) were added) with 17 µg/ml chloramphenicol was inoculated 1:100 with 37 °C LB overnight cultures also containing 17 µg/ml chloramphenicol and shaken for 3 days at 37 °C in baffled flasks (600 ml medium per 2 l flask).

Table 1. Composition of 500X M9 vitamin mix.

component	amount
choline chloride	1.0 g
folic acid	1.0 g
pantothenic acid	1.0 g
nicotinamide	1.0 g
myo-inositol	2.0 g
pyridoxal hydrochloride	1.0 g
thiamine	1.0 g
riboflavin	0.1 g
disodium adenosine 5'-triphosphate	0.3 g
biotin	0.2 g
	add 300 mL ddH_2O*

*After addition of ddH_2O, a solution of 10 M NaOH was slowly added until a clear solution is obtained (the final pH is usually around 12). After sterile filtration of the clear vitamin mix, it is either stored for short-term at 4 °C or for long-term at -20 °C.

Then, cells were harvested by centrifugation and the supernatant containing the lasso peptides was extracted by stirring with XAD16 resin (20 mL of a suspension of 50 g resin with 200 mL ddH_2O (=250 ml total volume) was added for every liter of culture volume) for 1 h at RT. Afterwards, the resin was collected on filter paper in a funnel, washed three times with 5 ml of ddH_2O and then eluted in a stepwise manner with a total volume of 100 mL of MeOH per liter of original culture volume. The supernatant extract was dried under reduced pressure at 40 °C and resuspended in 8 mL of 50% MeOH in ddH_2O. The resuspended extracts were cleared by centrifugation and subsequent sterile filtration.

For testing if the target lasso peptides were produced, 100 µl of each extract was applied to high-resolution LC-MS employing a 125/2 Nucleosil 300-8 C18 column (Macherey-Nagel) that was connected to microbore 1100 HPLC system (Agilent) and an LTQ-FT ultra-mass spectrometer (Thermo Fisher Scientific). Solvent A (water/0.1% formic acid) and solvent B (MeCN/0.1% formic acid) were used at a column temperature of 40 °C and a flow rate of 0.2 ml/min with the following gradient: Linear increase from 2% to 30% B over 18 min, followed by a linear increase from 30% to 95% B in 15 min and keeping 95% B for another 2 min. Absorbance was recorded at 215 nm. In this way, production of all nine MccJ25 was confirmed.

For purification, the remainders of the extracts were applied to two rounds of preparative HPLC employing a microbore 1100 HPLC system (Agilent) with a VP 250/21 Nucleodur C18 Htec 5 µm column (Macherey-Nagel) at room temperature.

Solvent A and solvent C (MeOH/0.1% formic acid) were used for the first round, and solvent D (water/0.1% trifluoroacetic acid) and solvent E (MeCN/0.1% trifluoroacetic acid) for the second round of purification. The flow rate was set to 18 ml/min and the absorbance was again detected at 215 nm. A gradient starting with a linear increase from 40% to 55% C in 30 min, followed by a linear increase from 55% to 95% C in 2 min and holding 95% for another 3 min was run for the first purification. The fractions containing the target compounds were identified by MS, dried at 40 °C and reduced pressure, dissolved in 8 mL of 20% MeCN and then applied to the second round of purification using a gradient starting with a linear increase from 20% to 40% E in 30 min, followed by a linear increase from 40% to 95% E in 2 min and keeping 95% E for another 3 min. Thereby, pure samples of all MccJ25 variants were obtained for further experiments. Yields ranged from moderate (~0.5-0.6 mg/l for 12IGL, 12IGF, and 12VGF) over good (~5-7 mg/l for 13IGL, 13IGF, and 13VGF) to high (~18-25 mg/ml for 11IGL, 11IGF, and 11VGF). The obtained yields are in good agreement with the extent the lasso peptide scaffold was altered: The more the variant sequence differed from the WT sequence, the worse the production became.

Cloning and protein purification

Expression constructs for C-terminally Strep-tagged ClpP from *S. aureus* were kindly provided by S. Sieber group (TU Munich) (37). Expression of C-terminally Strep-tagged ClpP from *S. aureus* was performed in *E. coli* BL21(DE3). Overnight cultures were transferred into 1 L cultures of LB medium and grown to OD_{600} 0.4 – 0.6 at 37°C. Expression was induced with the addition of 1 mM isopropyl-β-D-galactopyranoside and cells were then harvested and resuspended in ice-cold lysis/wash buffer (150 mM NaCl, 100 mM Tris-HCl pH8, 1 mM EDTA) after 5 h. Cell lysis was performed in a Precellys Homogeniser (Bertin Instruments) and the lysate was cleared by centrifugation for 2 h at 20,000 g and 4 °C. If necessary, DNA digest was performed with DNase I. Purification was conducted via affinity chromatography with subsequent size-exclusion chromatography on an Äkta Start and Äkta Pure system, respectively (GE Healthcare). For affinity chromatography, StrepTrap HP 1 ml columns were used and protein was eluted with an isocratic gradient of lysis/wash buffer + 2.5 mM *d*-desthiobiotin. The protein fraction was applied to a Superdex 200 HiLoad 16/600 preparation grade size-exclusion column (running buffer: 100 mM NaCl, 20 mM

HEPES pH7), concentrated in Amicon Ultra Centrifugal Filters with a molecular weight cut off of 10 kDa and stored at -80 °C.

Expression constructs and expression strains for enhanced GFP carrying a C-terminal ssrA-tag for ClpXP degradation as well as N-terminally His-tagged ClpX from *S. aureus* with an N-terminal TEV site were kindly provided by S. Sieber group. Expression and purification were performed as described previously (24).

C-terminally His-tagged ClpP from *B. subtilis* was expressed in *E. coli* BL21 (DE3) cells and purified via HisTrap HP 1 ml affinity chromatography columns on an Äkta Start system (GE Healthcare). For experiments that required a separation of monomeric and tetradecameric forms, purification was conducted using different buffers with an additional size-exclusion chromatography step and the respective fractions collected. The exact procedure and the buffers are described in (24).

The respective C- and H-Pocket mutants were constructed according to the Quikchange mutagenesis protocol (Agilent) with the primers listed in Table S2. Expression and purification were carried out as described above.

Peptide degradation assay

Peptide degradation assays were performed in black flat-bottom 96-well plates with a total reaction volume of 100 µl and reaction temperatures of 32 °C and 37 °C for SaClpP and BsClpP, respectively. Stock solutions of ADEP2 and MccJ25 agonist peptides were dissolved in DMSO and pre-diluted to 100x the final concentration. Accordingly, 1 µl was placed at the bottom of the wells to a final DMSO concentration of 1 %. Kinetic assays in which final MccJ25 concentrations of 200 µM were employed, 50x pre-dilutions were necessary due to a limited solubility of the lasso peptides, resulting in a total DMSO concentration of 2 %. 50 µl of a 2x enzyme solution (final concentration: 1 µM) in activity buffer was added to the plate and incubated for 15 min at 32 °C and 37 °C for SaClpP and BsClpP activity assays, respectively. The enzyme reaction was started by addition of 49 µl of a solution of fluorogenic model peptide substrate Suc-Leu-Tyr-AMC in activity buffer at a final concentration of 200 µM. For SaClpP assays, the activity buffer was comprised of 100 mM NaCl, 100 mM HEPES pH7. BsClpP activity buffer (50 mM Tris-HCl pH8, 25 mM $MgCl_2$, 200 mM KCl, 2 mM DTT) was used in BsClpP as well as SaClpP assays where the buffer leads to oligomeric breakdown and the activity retaining effect of ClpP agonists was

demonstrated. Fluorescence read-out was performed in a Tecan M200Pro plate reader (excitation/emission: 380/460 nm) every 30 – 60 s for 1h. Enzyme velocity was determined by linear regression of the initial segment of the fluorescence-time plot in GraphPad Prism 5. All assays were performed in triplicate and repeated at least two times.

Casein degradation assay

Casein degradation assays were in principle performed analogous to peptide degradation assays. Fluorescein labelled casein (FITC-casein) was employed at final concentrations of 20 µM in the respective activity buffers (see peptide degradation assay). 1 µl of 100x stock solutions of ADEP2 in DMSO were placed at the bottom of the wells followed by the addition of a 2x SaClpP or BsClpP enzyme solution (1 µM final concentration unless otherwise notified). The mixture was incubated at 32 °C or 37 °C for 15 min and the reaction was started by the addition of a 2x FITC-casein solution in the corresponding activity buffer. Fluorescence read-out was performed in a Tecan M200Pro plate reader with excitation wavelength at 485 nm and emission measured at 535 nm. Enzyme velocity was acquired by linear regression of the initial segment of the fluorescence graph and plotted against ADEP2 concentration. All assays were performed in duplicate or triplicate.

GFP degradation assay

A reaction mixture of SaClpP (2.8 µM), SaClpX (2.4 µM), GFP-ssrA (0.36 µM) and an ATP regeneration system (4mM ATP, 16mM creatine phosphate, 20 U ml^{-1} creatine phosphokinase) were incubated in PZ buffer (25 mM HEPES pH 7.6, 200 mM KCl, 5 mM $MgCl_2$, 1 mM DTT, 10 % (v/v) glycerol) at 30 °C in a Tecan M200Pro plate reader. The reaction volume was set at 100 µl and the reaction was performed in white flat-bottom 96-well plates. GFP-ssrA was added to the reaction mix after a 10 min pre-incubation and fluorescence was monitored at an emission wavelength of 535 nm (excitation: 465 nm).

Analytical gel filtration

Analytical gel filtration chromatography was carried out on an ÄKTA Pure chromatography system with a Superdex 200 3.2 Increase column. Protein samples were diluted 10x in either SaClpP activity (100 mM HEPES pH7, 100 mM NaCl) or

BsClpP activity buffer (50 mM Tris-HCl pH8, 25 mM $MgCl_2$, 200 mM KCl, 2 mM DTT). 40 µl of sample were injected into a 10 µl sample loop. Isocratic elution was carried out at a flow rate of 0.075 ml/min and absorption detected at 280 nm.

Acknowledgments

We would like to thank Andreas Kulik for performing LC/MS-analysis.

Conflicts of interest

The authors declare that they have no conflicts of interest with the contents of this article.

Author Contributions

I. T. M., J. D. H., M. A. M. and H. B.-O. conceptualization; I. T. M. and J. D. H. data curation; I. T. M., J. D. H., and H. B.-O. formal analysis; I. T. M. and J. D. M. investigation; I. T. M. and J. D. M. visualization; I. T. M. writing-original draft; I. T. M., J. D. H., and H. B.-O. writing-review and editing; I. T. M., J. D. H. methodology; M. A. M., H. B.-O. funding acquisition; M. A. M., H. B.-O. project administration; I. T. M., J. D. H. sample preparation.

References

1. Frees, D., Gerth, U., and Ingmer, H. (2014) Clp chaperones and proteases are central in stress survival, virulence and antibiotic resistance of Staphylococcus aureus. *Int. J. Med. Microbiol.* **304**, 142–149
2. Feng, J., Michalik, S., Varming, A. N., Andersen, J. H., Albrecht, D., Jelsbak, L., Krieger, S., Ohlsen, K., Hecker, M., Gerth, U., Ingmer, H., and Frees, D. (2013) Trapping and proteomic identification of cellular substrates of the ClpP protease in staphylococcus aureus. *J. Proteome Res.* **12**, 547–558
3. Runde, S., Molière, N., Heinz, A., Maisonneuve, E., Janczikowski, A., Elsholz, A. K. W., Gerth, U., Hecker, M., and Turgay, K. (2014) The role of thiol oxidative stress response in heat-induced protein aggregate formation during thermotolerance in Bacillus subtilis. *Mol. Microbiol.* **91**, 1036–1052
4. Brötz-Oesterhelt, H., Beyer, D., Kroll, H.-P., Endermann, R., Ladel, C., Schroeder, W., Hinzen, B., Raddatz, S., Paulsen, H., Henninger, K., Bandow, J. E., Sahl, H.-G., and Labischinski, H. (2005) Dysregulation of bacterial proteolytic machinery by a new class of antibiotics. *Nat. Med.* **11**, 1082–1087
5. Böttcher, T., and Sieber, S. A. (2008) β-lactones as specific inhibitors of ClpP attenuate the production of extracellular virulence factors of Staphylococcus aureus. *J. Am. Chem. Soc.* **130**, 14400–14401
6. Böttcher, T., and Sieber, S. A. (2009) β-lactones decrease the intracellular virulence of Listeria monocytogenes in macrophages. *ChemMedChem*. **4**, 1260–1263
7. Kirstein, J., Hoffmann, A., Lilie, H., Schmidt, R., Helga, R. W., Heike, B. O., Mogk, A., and Turgay, K. (2009) The antibiotic ADEP reprogrammes ClpP, switching it from a regulated to an uncontrolled protease. *EMBO Mol. Med.* **1**, 37–49

8. Sass, P., Josten, M., Famulla, K., Schiffer, G., Sahl, H.-G., Hamoen, L., and Brötz-Oesterhelt, H. (2011) Antibiotic acyldepsipeptides activate ClpP peptidase to degrade the cell division protein FtsZ. *Proc. Natl. Acad. Sci. U. S. A.* **108**, 17474–9
9. Conlon, B. P., Nakayasu, E. S., Fleck, L. E., LaFleur, M. D., Isabella, V. M., Coleman, K., Leonard, S. N., Smith, R. D., Adkins, J. N., and Lewis, K. (2013) Activated ClpP kills persisters and eradicates a chronic biofilm infection. *Nature*. **503**, 365–370
10. Famulla, K., Sass, P., Malik, I., Akopian, T., Kandror, O., Alber, M., Hinzen, B., Ruebsamen-Schaeff, H., Kalscheuer, R., Goldberg, A. L., and Brötz-Oesterhelt, H. (2016) Acyldepsipeptide antibiotics kill mycobacteria by preventing the physiological functions of the ClpP1P2 protease. *Mol. Microbiol.* **101**, 194–209
11. Vasudevan, D., Rao, S. P. S., and Noble, C. G. (2013) Structural basis of mycobacterial inhibition by Cyclomarin A. *J. Biol. Chem.* **288**, 30883–30891
12. Schmitt, E. K., Riwanto, M., Sambandamurthy, V., Roggo, S., Miault, C., Zwingelstein, C., Krastel, P., Noble, C., Beer, D., Rao, S. P. S., Au, M., Niyomrattanakit, P., Lim, V., Zheng, J., Jeffery, D., Pethe, K., and Camacho, L. R. (2011) The natural product cyclomarin kills mycobacterium tuberculosis by targeting the ClpC1 subunit of the caseinolytic protease. *Angew. Chemie - Int. Ed.* **50**, 5889–5891
13. Gersch, M., Gut, F., Korotkov, V. S., Lehmann, J., Böttcher, T., Rusch, M., Hedberg, C., Waldmann, H., Klebe, G., and Sieber, S. A. (2013) The mechanism of caseinolytic protease (ClpP) inhibition. *Angew. Chemie - Int. Ed.* **52**, 3009–3014
14. Maurizi, M. R., Singh, S. K., Thompson, M. W., Kessel, M., and Ginsburg, A. (1998) Molecular properties of ClpAP protease of Escherichia coli: ATP- dependent association of ClpA and ClpP. *Biochemistry*. **37**, 7778–7786
15. Ortega, J., Lee, H. S., Maurizi, M. R., and Steven, A. C. (2002) Alternating translocation of protein substrates from both ends of ClpXP protease. *EMBO J.* **21**, 4938–4949
16. Woo, K. M., Chung, W. J., Ha, D. B., Goldberg, A. L., and Chung, C. H. (1989) Protease Ti from Escherichia coli requires ATP hydrolysis for protein breakdown but not for hydrolysis of small peptides. *J. Biol. Chem.* **264**, 2088–2091
17. Thompson, M. W., Singh, S. K., and Maurizi, M. R. (1994) Processive degradation of proteins by the ATP-dependent Clp protease from Escherichia coli: Requirement for the multiple array of active sites in ClpP but not ATP hydrolysis. *J. Biol. Chem.* **269**, 18209–18215
18. Kim, Y. I., Levchenko, I., Fraczkowska, K., Woodruff, R. V, Sauer, R. T., and Baker, T. a (2001) Molecular determinants of complex formation between Clp/Hsp100 ATPases and the ClpP peptidase. *Nat. Struct. Biol.* **8**, 230–233
19. Joshi, S. A., Hersch, G. L., Baker, T. A., and Sauer, R. T. (2004) Communication between ClpX and ClpP during substrate processing and degradation. *Nat. Struct. Mol. Biol.* **11**, 404–411
20. Bewley, M. C., Graziano, V., Griffin, K., and Flanagan, J. M. (2006) The asymmetry in the mature amino-terminus of ClpP facilitates a local symmetry match in ClpAP and ClpXP complexes. *J. Struct. Biol.* **153**, 113–128
21. Effantin, G., Maurizi, M. R., and Steven, A. C. (2010) Binding of the ClpA unfoldase opens the axial gate of ClpP peptidase. *J. Biol. Chem.* **285**, 14834–40
22. Lee, B.-G., Park, E. Y., Lee, K.-E., Jeon, H., Sung, K. H., Paulsen, H., Rübsamen-Schaeff, H., Brötz-Oesterhelt, H., and Song, H. K. (2010) Structures of ClpP in complex with acyldepsipeptide antibiotics reveal its activation mechanism. *Nat. Struct. Mol. Biol.* **17**, 471–478
23. Li, D. H. S., Chung, Y. S., Gloyd, M., Joseph, E., Ghirlando, R., Wright, G. D., Cheng, Y. Q., Maurizi, M. R., Guarné, A., and Ortega, J. (2010) Acyldepsipeptide antibiotics induce the formation of a structured axial channel in ClpP: A model for the ClpX/ClpA-bound state of ClpP. *Chem. Biol.* **17**, 959–969
24. Gersch, M., Famulla, K., Dahmen, M., Göbl, C., Malik, I., Richter, K., Korotkov, V. S., Sass, P., Rübsamen-Schaeff, H., Madl, T., Brötz-Oesterhelt, H., and Sieber, S. a (2015) AAA+ chaperones and acyldepsipeptides activate the ClpP protease via conformational control. *Nat. Commun.* **6**, 6320
25. Hinzen, B., Raddatz, S., Paulsen, H., Lampe, T., Schumacher, A., Häbich, D., Hellwig, V., Benet-Buchholz, J., Endermann, R., Labischinski, H., and Brötz-Oesterhelt, H. (2006) Medicinal chemistry optimization of acyldepsipeptides of the enopeptin class antibiotics. *ChemMedChem*. **1**, 689–693
26. Carney, D. W., Schmitz, K. R., Scruse, A. C., Sauer, R. T., and Sello, J. K. (2015) Examination of a Structural Model of Peptidomimicry by Cyclic Acyldepsipeptide Antibiotics in Their Interaction with the ClpP Peptidase. *ChemBioChem*. **16**, 1875–1879
27. Goodreid, J. D., Janetzko, J., Santa Maria, J. P., Wong, K. S., Leung, E., Eger, B. T., Bryson, S., Pai, E. F., Gray-Owen, S. D., Walker, S., Houry, W. A., and Batey, R. A. (2016) Development and Characterization of Potent Cyclic Acyldepsipeptide Analogues with Increased Antimicrobial Activity. *J. Med. Chem.* **59**, 624–646
28. Carney, D. W., Compton, C. L., Schmitz, K. R., Stevens, J. P., Sauer, R. T., and Sello, J. K. (2014) A simple fragment of cyclic acyldepsipeptides is necessary and sufficient for ClpP activation and antibacterial activity. *Chembiochem*. **15**, 2216–2220
29. Alexopoulos, J. A., Guarné, A., and Ortega, J. (2012) ClpP: A structurally dynamic protease regulated by AAA+ proteins. *J. Struct. Biol.* **179**, 202–210
30. Malik, I. T., and Brötz-Oesterhelt, H. (2017) Conformational control of the bacterial Clp protease by natural product antibiotics. *Nat. Prod. Rep.* 10.1039/c6np00125d
31. Hegemann, J. D., Zimmermann, M., Xie, X., and Marahiel, M. A. (2015) Lasso Peptides: An Intriguing Class

of Bacterial Natural Products. *Acc. Chem. Res.* **48**, 1909–1919
32. Jeanne Dit Fouque, K., Afonso, C., Zirah, S., Hegemann, J. D., Zimmermann, M., Marahiel, M. A., Rebuffat, S., and Lavanant, H. (2015) Ion Mobility–Mass Spectrometry of Lasso Peptides: Signature of a Rotaxane Topology. *Anal. Chem.* **87**, 1166–1172
33. Hegemann, J. D., Zimmermann, M., Zhu, S., Steuber, H., Harms, K., Xie, X., and Marahiel, M. A. (2014) Xanthomonins I-III: A New Class of Lasso Peptides with a Seven-Residue Macrolactam Ring. *Angew. Chemie Int. Ed.* **53**, 2230–2234
34. Rosengren, K. J., Clark, R. J., Daly, N. L., Göransson, U., Jones, A., and Craik, D. J. (2003) Microcin J25 has a threaded sidechain-to-backbone ring structure and not a head-to-tail cyclized backbone. *J. Am. Chem. Soc.* **125**, 12464–12474
35. Kirstein, J., Schlothauer, T., Dougan, D. a, Lilie, H., Tischendorf, G., Mogk, A., Bukau, B., and Turgay, K. (2006) Adaptor protein controlled oligomerization activates the AAA+ protein ClpC. *EMBO J.* **25**, 1481–1491
36. Leung, E., Datti, A., Cossette, M., Goodreid, J., McCaw, S. E., Mah, M., Nakhamchik, A., Ogata, K., El Bakkouri, M., Cheng, Y. Q., Wodak, S. J., Eger, B. T., Pai, E. F., Liu, J., Gray-Owen, S., Batey, R. A., and Houry, W. A. (2011) Activators of Cylindrical Proteases as Antimicrobials: Identification and Development of Small Molecule Activators of ClpP Protease. *Chem. Biol.* **18**, 1167–1178
37. Gersch, M., List, A., Groll, M., and Sieber, S. A. (2012) Insights into structural network responsible for oligomerization and activity of bacterial virulence regulator caseinolytic protease P (ClpP) protein. *J. Biol. Chem.* **287**, 9484–9494
38. Solbiati, J. O., Ciaccio, M., Parías, R. N., and Salomón, R. A. (1996) Genetic analysis of plasmid determinants for microcin J25 production and immunity. *J. Bacteriol.* **178**, 3661–3663
39. Chiu, J., March, P. E., Lee, R., and Tillett, D. (2004) Site-directed, Ligase-Independent Mutagenesis (SLIM): a single-tube methodology approaching 100% efficiency in 4 h. *Nucleic Acids Res.* **32**, e174–e174
40. Chiu, J., Tillett, D., Dawes, I. W., and March, P. E. (2008) Site-directed, Ligase-Independent Mutagenesis (SLIM) for highly efficient mutagenesis of plasmids greater than 8kb. *J. Microbiol. Methods*. **73**, 195–198

Footnotes

Funding to the research group of H. B.-O. was provided by the Deutsche Forschungsgemeinschaft (SFB 766). Funding to J. D. H. was provided by the Deutsche Forschungsgemeinschaft (DFG Research Fellowship 309199717).

The abbreviations used are: ATP, adenosine 5'-triphosphate; ATPase, adenosine triphosphatase; C-terminal, carboxy-terminal; DMSO, dimethyl sulfoxide; DTT, dithiothreitol; EC_{50}, half-maximal effective concentrations; FITC, fluorescein isothiocyanate; GFP, green fluorescent protein; HEPES, 4-(2-hydroxyethyl)-1-peperazineethanesulfonic acid; HPLC, high-performance/pressure liquid chromatography; kDa, kilodalton; LC/MS, liquid chromatography/mass spectrometry; MIC, minimal inhibitory concentration; N-terminal, amino-terminal; PCR, polymerase chain reaction; Tris, tris(hydroxymethyl)aminomethane; WT, wildtype.

General discussion

With the discovery of ADEPs, ClpP has gained increased recognition due to its potential as an antibacterial drug target. The ADEP mechanism of action is unique amongst all known antibiotics and opened up an additional branch in antibiotic research: The dysregulation of bacterial proteases as a means of bacterial growth inhibition. Furthermore, the information on structural and molecular determinants of ClpP activity we possess today is derived in large part from scientific studies involving ADEPs. In the course of this thesis project, several additional agonist molecules that affect ClpP conformation and activity have been analyzed. Alongside ADEPs, these compounds were instrumental in gaining new insight into the molecular organization of the Clp proteases from different organisms (19, 20, 22, 26, 43, 45, 48, 49). Furthermore, the data presented in this study challenge the established notion that ADEPs are mere IGF-loop mimetics and expand upon the interaction between ClpP and the Clp-ATPases.

The Clp protease is a paradigm of self-compartmentalized proteases with several safeguards in place to protect the cell from self-digest. In order for ClpP to become proteolytic, a sequence of events has to occur: First, a substrate tagged and/or bound to an adapter or otherwise modified (and thereby marked for degradation) has to be recognized by a Clp-ATPase. Optionally, this recognition initiates Clp-ATPase assembly (as is the case for BsClpC). Second, the substrate/(adapter/)Clp-ATPase complex has to associate with ClpP. For *B. subtilis* ClpP *in vitro*, this process is required for the assembly of the active ClpP tetradecamer, although the requirement for ClpP assembly has not been demonstrated *in vivo*, yet. In other organisms, e. g. *S. aureus*, ClpP can be purified in the assembled tetradecameric form. Third, ATP hydrolysis provides the energy to unfold the substrate and feed it into the proteolytic lumen of ClpP. This lumen is otherwise inaccessible and free ClpP is not proteolytic, hence the term “self-compartmentalized”. Only when these criteria are met, degradation of proteins can occur. It is therefore remarkable to see that a single small molecule can interfere with this highly regulated and safeguarded process. ADEPs bind the ‘master switch’ of both ClpP conformational control and ClpP/Clp-ATPase communication. The latter is abolished by ADEPs competitively binding the H-pocket.

By addition of ADEPs, even preassembled ClpP/Clp-ATPase complexes dissociate (19). Consequently, ADEPs display a much stronger affinity for the H-pocket than the respective V/IGF/L-loops of cognate Clp-ATPases. For example, a single ADEP molecule is sufficient to reduce SaClpXP-dependent *in vitro* GFP degradation by half (26). Interference with the assembled Clp proteases was also shown for ClpCP and ClpXP in *B. subtilis*, ClpAP and ClpXP in *E. coli*, and ClpXP1P2 in *M. tuberculosis* (19, 20, 22, 23, 50). The latter presents a special case in many respects.

Z-LL is required for the *in vitro* assembly of the active mycobacterial ClpP1P2 tetradecamer and targets the active sites

In contrast to the ClpP homo-tetradecamers of *B. subtilis*, *E. coli*, and *S. aureus*, active mycobacterial ClpP is organized in a hetero-tetradecameric structure that consists of two ClpP1 and ClpP2 heptameric rings, respectively (36). These elute as low oligomeric state species from a size-exclusion chromatography column and, when mixed, assemble to form only inactive homo-tetradecamers consisting of either ClpP1 or ClpP2 subunits (35, 36). Upon addition of an N-terminally blocked dipeptide like Z-LL, they reassemble to form two respective ClpP1 and ClpP2 homo-heptameric rings which associate to form the active ClpP1P2 hetero-tetradecamer (36). This came as a surprise since Z-LL amongst other peptides carrying an N-terminal benzyloxycarbonyl (Cbz) group were originally employed as substrate analogues that function as competitive inhibitors of catalysis (36). When testing several N-terminally blocked dipeptide and tripeptide agonists for their ability to activate mycobacterial ClpP, the correlation could be made that strong activators served as poor substrates and *vice versa* (36). This finding led to the hypothesis that peptides that serve as agonists might bind an allosteric site distinct from the active sites.

In studies conducted by Kirsten Famulla from our group in the laboratory of Alfred Goldberg (Boston), activation of mycobacterial ClpP1P2 by ADEP or the cognate Clp-ATPase ClpC1 was always dependent on the presence of Z-LL. It is still not known how the assembly of ClpP1P2 is orchestrated *in vivo* and whether an additional unknown factor facilitates the reorganization of the ClpP1P2 tetradecamer. It has been speculated that mere exposition of the active sites to peptide substrate by a functional Clp-ATPase initiates the transition to an active ClpP1P2 conformation in the natural context (23). *In vitro*, activity of ClpC1P1P2 however always required the addition of

Z-LL or related blocked peptides (see chapter 1). Unlike ClpPs from other organisms, ADEPs alone neither assemble ClpP1P2 tetradecamers to enable peptidase activity nor over-activate them to enable protein degradation. ADEP-accelerated peptide and casein hydrolysis always depended on preceding Z-LL addition *in vitro* (27).

The mechanism of action of these agonistic N-terminally blocked peptides is still unknown. A possible role of Z-LL as a competitive inhibitor could not be investigated in MtbClpP1P2 by biochemical assays because Z-LL is necessary for activity. Therefore, I conducted competition assays in a *B. subtilis* background. Also, the molecular mode of action of ADEP had been clearly demonstrated in BsClpP with the help of crystal structures and therefore a potential role of the H-pocket in Z-LL binding could be addressed as well. Like in mycobacteria, treatment with Z-LL in a BsClpP assay led to inhibition of catalysis. Furthermore, I was able to show that Z-LL in fact binds to the active sites of BsClpP by competitively interfering with Suc-LY-AMC peptide substrate hydrolysis rather than ADEP binding (chapter 1, figure 4). These findings were also confirmed in mycobacteria by a published crystal structure of ClpP1P2 complexed with ADEP and another established MtbClpP1P2 agonistic activator peptide Z-Ile-Leu (Z-IL) (23). In this crystal structure, ClpP adopts an extended state with the catalytic sites in an active position. The orientation of Z-IL is flipped with respect to natural substrates and the C-terminal leucyl end point towards the active site residues (23). This reversed orientation explains why these activating agonists do not serve as substrates. Binding of a pseudo substrate could be responsible for the rearrangement of the active sites into a catalytically favourable position. Based on the structural dynamics of the ClpP tetradecamer where catalysis is tightly coupled to the conformational state and the active catalytic triad orientation being predicated on an overall extended conformation, the binding of Z-LL could initiate the conversion from an inactive to an active ClpP1P2 particle. However, a possible or even probable inhibitory effect of the agonist peptide due to spatial interference cannot be dismissed. The full catalytic potential of MtbClpP1P2 might exceed the one observed *in vitro* with the help of agonistic peptides.

With the help of a conditional ClpP knockdown strain that allowed for the adjustment of intracellular ClpP1 and ClpP2 levels, we could further show that ADEPs kill mycobacteria by inhibition rather that activation. Since ClpP as well as the other components of the Clp protease are essential for survival in mycobacteria, inhibition

of the functional association of ClpP with the partner Clp-ATPase leads to cell death. ADEPs exert their antitubercular effect via inhibition of the natural functions of the mycobacterial Clp protease and act as inhibitors of protein-protein interaction.

Meanwhile, a number of antitubercular compounds have been described that also act through inhibition of ClpP/Clp-ATPase communication, like cyclomarin A or lassomycin (51–53). In contrast to ADEPs, these do not target the interface between ClpP and the Clp-ATPase but the N-terminal domain (NTD) of the Clp-ATPase ClpC1. The NTD is most likely responsible for the interaction with tagged substrates or adapters because mutational studies revealed the target domain of cyclomarin A to be closely related to the *B. subtilis* ClpC domain responsible for MecA binding (7, 54). While the requirement for adapter binding has not been demonstrated for mycobacterial ClpC1, it provides an explanation for the observed inhibitory effect of these compounds. The amounted data demonstrates the druggability of the Clp protease in mycobacteria by means of inhibiting ClpP/Clp-ATPase association.

ADEPs and β-lactones as tools to investigate the link between H-pocket and active site

While the inhibitory effect of ADEPs on ClpP is straightforward because it simply blocks the ability of Clp-ATPases to make contact to their binding site on the ClpP surface, over-activation is more complex. ClpP from different organisms can adopt different oligomeric states in physiological buffers from low oligomeric states in the mono-/di-/trimer range to heptameric rings. For example, human ClpP elutes as heptamers *in vitro* but still displays low peptidase activity, suggesting an equilibrium between the active tetradecamer and the heptamer with a strong preference for the heptamer (55). SaClpP primarily takes tetradecameric form and thus displays full *in vitro* peptidase activity that can be increased only slightly by addition of ADEP. In turn, ClpP tetradecamers adopt both inactive and active conformations. In the inactive conformation, the catalytic triads within the ClpP barrel are misaligned, the overall structure is compressed, and the α5-helices responsible for inter-ring-contact are disordered (or resolved but kinked in some crystal structures) (56). The active conformation adopts an extended shape with aligned active sites and stretched α5-helices. Both the assembly of lower oligomeric states of ClpP to tetradecamers as well

as the structural shift to the active extended state are mediated by ADEPs binding to the H-pocket (20, 22, 23, 48, 57). However, the effects of ADEP binding go beyond.

β-lactone inhibitors have been described to covalently bind the active site serine of ClpP (58). These compounds carry the eponymous β-lactone moiety which is a biologically privileged structure. Some show antibacterial activity like obafluorin (59) and hymeglusin (60) and a number of targets were identified in an activity-based protein profiling (ABPP) approach which allows for fishing of target molecules by proteomics (61). Here, it was shown that β-lactones effectively bind ClpP among other proteins and that covalently blocking the ClpP active site inhibits virulence markers in *S. aureus* like haemolysis and proteolysis (29). Apart from its biological implications, the ability to selectively block the active site serine provides a useful tool to investigate ClpP catalysis. This is especially interesting in combination with ADEPs. With the help of these two agonist molecules, we were able to dissect the interplay between the hydrophobic pocket and the catalytic sites.

The β-lactone inhibition mechanism is comprised of two major steps. The first step is the formation of a long-lived acyl-ester intermediate which is the rate-limiting step and characterized by the catalytic efficiency of the reaction. To investigate the effect of ADEPs on this first step, several synthetic β-lactone derivatives of varying bulkiness were employed. Catalytic efficiencies were quantified by the effectivity of inhibition of peptide substrate (suc-LY-amc) degradation by these compounds. It was shown that the respective catalytic efficiencies correlate well with the dimensions of the different derivatives (26, 62). Furthermore, ADEPs significantly accelerate the formation of the acyl-ester intermediate. While this ADEP effect might be attributed to pore opening, the fact that ADEP increased k_{obs}/[I] twofold irrespective of the dimensions of the observed β-lactone strongly supports an allosteric activation mechanism of the catalytic centres by ADEP.

The second mechanistic step of β-lactone inhibition consists in the subsequent hydrolysis of the acyl-ester intermediate which results in dissociation of the β-lactone and regeneration of the active site serine and is characterized by the bound half-time ($T_{1/2}$). Again, ADEPs significantly accelerated this process. Collectively, these results clearly demonstrate that ADEP binding directly accelerates catalysis of ClpP independent of its pore gating effect.

ADEPs orchestrate ClpP function by conformational control

While the compressed and extended conformations occur seemingly randomly in different crystal structures of ClpP, ADEP/ClpP complexes exclusively crystallized in the extended state (see review article in chapter 2 for more detail). Computational modelling, protein NMR, and hydrogen-deuterium-mass exchange experiments already established that ClpP samples different conformations and that ADEPs play a role in ClpP conformational control. It could be shown that binding of ADEPs introduces structural rigidity at functionally important regions of the ClpP barrel, most notably the equatorial interface (ring-ring-contact) and the N-terminal region (pore gating) (48, 57). These regions display increased flexibility in the absence of ADEP (48, 57, 63). To address this stabilizing effect of ADEPs further, we performed thermal shift assays with SaClpP in the presence or absence of ADEP and saw a drastic increase in melting temperature upon ADEP addition. We then examined ClpP mutants with known oligomerization or conformation defects. Interestingly, *in vitro* degradation assays showed that a certain active site mutation (D172N) abolished SaClpP *in vitro* FITC-casein degradation activity but could be restored to wild-type level by ADEP addition. Although still tetradecameric, the D172N mutant showed a more compacted conformation illustrated by the inter-atomic pair distance distribution functions from SAXS experiments. Crystal structures of compressed ClpP conformations predicted sterical clashes with ADEP binding at the H-pocket. Consequently, the D172N mutant displayed a threefold lower affinity for ADEP compared to wild-type. In addition, dynamic light scattering experiments confirmed the SAXS results where D172N ClpP resembles the compressed conformation in the absence and the extended conformation in the presence of ADEP. Binding of ADEP initiated a structural shift that made the D172N conformation appear virtually indistinguishable from ADEP-bound wild-type while the apo-enzymes differed significantly. Collectively, these results show the (naturally occurring) conformational sampling of ClpP is strongly shifted towards the active extended state which directly affects catalysis and stability. I was able to reproduce the effects of the D172N mutation on the SaClpP degradation capabilities in BsClpP. These results suggested that conformational control is a general mechanism of ClpP activation that is exerted by binding the hydrophobic pocket.

In conjunction with previous experiments, the effects of H-pocket binding by ADEPs amount to: ClpP assembly (dependent on originating species), pore opening, and locking ClpP in an active extended state accompanied by allosteric activation of catalysis.

Artificial IGF-loops activate ClpP and are sensitive to C-pocket mutations

Since Clp-ATPases make contact to the H-pockets via their IGF-loops, a tripeptide motif strongly resembling the putative pharmacophore of ADEPs, the ADEP-induced effects have been translated to mechanisms of conformational control in the natural context. However, the IGF motif resembles the part of the ADEP structure necessary for activity, the macrolactone backbone of ADEPs also forms numerous contacts with the H-pocket based on the present ADEP/ClpP co-crystal structures (20, 22, 23, 43, 44). In a SAR study with ADEP fragments, this macrolactone ring was found to be completely inactive on its own but to convey increased affinity for the target site as part of the ADEP structure (44). So far, it is established that ADEPs compete with Clp-ATPases for ClpP binding and that it is much more affine. Clp-ATPases form numerous contacts in parallel and its avidity is necessary for efficient binding to ClpP due to low individual affinities of the IGF-loops (64). Deleting more than one IGF loop within the ClpX hexamer eliminates binding to ClpP (64). Therefore, the increased affinity of ADEP mediated by its macrolactone backbone is necessary to ensure functional binding of a single small molecule. Whether the macrolactone ring also produces conformational changes within ClpP that are distinct to the ADEP structure is still unknown.

By using the Microcin J25 (MccJ25) lasso peptide as a lead structure, we constructed loop mutants that could serve as IGF-loop mimetics. MccJ25 has a unique topology with amino acids 9 – 21 forming a loop and its C-terminal end threaded through the N-terminal ring. Within this loop, three positions were chosen to introduce the three conserved Clp-ATPase tripeptide motifs IGL, IGF, and VGL resulting in a total of nine loop mutants. When tested for *in vitro* activity, the lasso peptide loop mutants showed a stabilizing effect on oligomeric integrity of SaClpP under buffer conditions that normally result in oligomeric breakdown. The IGF mutant at position 12 (12IGF) was the most potent by far, allowing peptide degradation at roughly 50% of the maximum

enzyme velocity in Tris pH8 buffer where SaClpP is not peptidolytic on its own. The stabilizing effect of 12IGF was confirmed via gel filtration chromatography. Here, we observed lower oligomeric states in the heptameric and dimeric range in Tris buffer rather than a single tetradecameric fraction. In the presence of 12IGF, the oligomeric breakdown could be prevented and a single tetradecameric peak was visible.

In non-assembled BsClpP fractions, 12IGF was unable to assemble the active BsClpP tetradecamer. Nonetheless, BsClpP activated by ADEP2 showed a further increase in peptidase activity upon addition of 12IGF. This synergistic effect was unexpected as it suggests simultaneous binding of ADEP2 and 12IGF. To test whether the lack of 12IGF activity on its own was the result of its inability to assemble the active BsClpP complex, peptidase assays were performed with monomeric and tetradecameric BsClpP fractions. Indeed, 12IGF readily activated pre-formed BsClpP tetradecamers but not lower oligomeric states. Thus, 12IGF is unable to assemble BsClpP tetradecamers on its own but requires either pre-assembled tetradecamers or ADEP to show an activating effect.

The observed synergism between 12IGF and ADEP2 in stimulating BsClpP activity challenged the conception that these two molecules exclusively share the same binding site. To approach this question, competition assays were performed with increasing ADEP2 concentrations up to high excess while keeping 12IGF constant. In SaClpP, 12IGF led to an ADEP2-dependent decrease of *in vitro* peptidase activity. Since 12IGF was designed to compete with ADEP2 for the H-pocket, high concentrations of the tight binder ADEP2 (K_D ~ 2 µM) of up to 200 µM were expected to fully displace the low affinity binder 12IGF (K_{app} ~ 26 µM). Regardless, the inhibitory effect of 12IGF on ADEP-activated SaClpP remained even at a high excess of ADEP2. These findings established, firstly, that 12IGF indeed binds to ClpP and, secondly, that the binding mode and mechanism of action are different from ADEPs and most likely includes an alternative or additional binding site. The lack of competitivity between 12IGF and ADEP2 was further corroborated by experiments with BsClpP where the synergistic effect of 12IGF remained constant over a range of ADEP2 concentrations up to 200 µM.

Casein degradation by ADEP-activated SaClpP is the result of an increased pore diameter of the entrance pores. However, casein degradation could not be achieved

with the help of 12IGF mutants. Therefore, 12IGF does not seem to open the pore, at least not sufficiently to allow for casein degradation. This was not unexpected, as so far, there is no indication in literature that IGF-loops initiate pore opening in a natural context. For example, ATP-dependent casein degradation by a complex of ClpP with a cognate Clp-ATPase as reported e. g. for the *E. coli* ClpAP complex (65), does not display pore opening to an extent similar to ADEP/ClpP. The pore diameter of the ClpAP complex was roughly 12 Å (46). A crystal structure of *E. coli* ClpP complexed with ADEP1 shows a structured axial channel with a pore diameter of about 20 Å (22). In the natural context, protein substrates are actively unfolded by Clp-ATPases and the ClpP entrance pore only has to accommodate the translocation of a linear peptide chain for which 12 Å of pore diameter are sufficient. The different diameters of the ClpP pores in the ADEP versus ClpX-bound state considered, the strong pore opening seems a particular trait of ADEP binding and might be due to additional bonding between the ADEP molecule and the N-terminal amino acids lining the entrance pore of ClpP (20). While the *N*-acylphenylalanine side-chain of ADEP represents a good mimic of the V/IGF/L-loop of a Clp-ATPase and can be expected to establish similar interactions with the H-pocket of ClpP, ADEP contains a prominent further structural element, the macrolactone core that is crucial for tight binding and a corresponding structure is missing in ClpX IGF-loops. The macrolactone core provides a number of additional hydrophobic and H-bond contacts to the H-pocket of ClpP. It is feasible that either the increased number of interactions in an extended surface area of ClpP or the increased affinity of ADEP, which reduces flexibility in this area, might result in a wider time-averaged pore diameter. In the natural context, IGF-loop affinity in the range of that of ADEP molecules would most likely be undesirable because the ClpP-ClpX-interaction has to maintain a certain degree of dynamics and must be reversible. In conclusion, ADEPs and IGF-loop mutants have to be regarded separately due to differences in their activation profile and their molecular makeup. Furthermore, the loop mutant data presented here are in agreement with the available data on the interaction between Clp-ATPases and ClpP. Like 12IGF in our study, Clp-ATPases were shown to stabilize the ClpP barrel (55). Like 12IGF, they were affected by C-pocket alterations and neither are able to gate the pore to allow casein degradation.

Comparison of H- and C-pocket architecture and outlook

The clear lack of competitivity between 12IGF and ADEP2 demonstrated in both BsClpP and SaClpP suggested a different binding mode of 12IGF. Based on literature data, a putative additional binding site on the surface of ClpP termed the C-pocket caught our attention (50). With the help of mutational studies, it could be clearly shown, that activation by 12IGF is more sensitive to mutations in the C-pocket while activation by ADEP2 is more sensitive to H-pocket mutations. In fact, the C-pocket mutations did not affect the ADEP2-dependent degradation of casein but led to decreased peptidase activity in Tris pH8 buffer in the presence of 12IGF. Furthermore, like H-pocket alterations, mutations in the C-pocket abolished ClpX-dependent GFP-degradation with the exception of the Q82A mutant which showed a 50% decrease in GFP-degradation. Collectively, the data demonstrate that the interaction between ClpP and ClpX is dependent on a functional H- as well as C-pocket while the interaction between ADEP2 and ClpP is H-pocket-dependent. Since the *N*-acylphenylalanine moiety of ADEP molecules closely resembles the IGF motif on a molecular level, this H-pocket specificity of ADEP is probably based on the additional interactions contributed by the macrolactone backbone. *In vitro* assays with C-pocket mutants in the presence of the isolated *N-acylphenylalanine* fragment will allow to test this hypothesis.

The H-pocket and the C-pocket are located in close proximity and share a remarkable architectural similarity. Both pockets feature a central tyrosine residue within their deepest indentation with the side chain hydroxyl function pointing outwards. The Y63 residue of *S. aureus* ClpP (Y62 in *B. subtilis* ClpP) is one of two H-pocket residues that forms a hydrogen bond with ADEP (20). Furthermore, mutational studies showed that the Y63 residue might serve as handle within the H-pocket (66). The *S. aureus* ClpP Y63A mutant displayed a gain-of-function phenotype where the protein backbone was rotated by roughly 90°. This rotation initiates a cascade of structural shifts that turns ClpP into an unregulated protease that degrades casein and even the cell division protein FtsZ. The same kind of rotation of the Y63 residue can be observed in co-crystal structures of ClpP with ADEP (20, 22, 23). *In vivo*, the *S. aureus* Y63A mutant did not form a persister phenotype and was completely killed upon rifampin treatment in line with the ADEP-promoted killing of persister cells (31, 66). Due to the high conservation of this tyrosine residue among ClpPs from different species, the

authors claimed to have uncovered a principle activation mechanism of ClpP and that the Y63 residue might present the point of attack for ADEP antibiotics.

Similarly, the C-pocket also carries a tyrosine residue in its central cavity and we were able to show that this residue is indispensable for the functional interaction with ClpX. Y78A ClpP displayed an intriguing phenotype which served as a clear distinguishing feature between the two pockets. While the activity of ADEP was not impaired in this mutant, ClpX-mediated GFP degradation was abolished completely. Furthermore, the Y78A mutant displayed peptidase activity in Tris buffer in the absence of stabilizing agonists such as ADEP2 or 12IGF. Gel filtration confirmed that this mutant was unsusceptible to the destabilizing effects of the Tris buffer and a single tetradecameric fraction and no lower oligomeric states were detected. This leads to the intriguing hypothesis that this central residue might serve as an “instability factor” that prevents uncontrolled assembly of ClpP which might be safeguarding the cell from accidental ClpP activity. Consequently, mutating Y78 to alanine might relieve ClpP from the requirement of interacting with a stabilizing Clp-ATPase for functional activation. Phenotypic whole cell studies of a genomic ClpP Y78A mutant are required to functionally characterize this critical site.

The fundamental conclusions for the ClpP architecture are: 1.) The conformational state of ClpP and its activity are strongly interconnected. 2.) The H-pocket serves as the master switch of conformational control. 3.) The C-pocket plays a crucial role in Clp-ATPase communication and is supplemental in maintaining oligomeric stability.

Taken together, the findings about the functional importance of the C-pocket uncovered an additional layer of ClpP/Clp-ATPase-communication. This communication interface is critical in maintaining regulated and safe proteolysis and interfering at this junction can have devastating effects on ClpP function and, thus, on key Clp protease mediated functions and even viability in certain bacteria. Understanding the relationship between architecture und function of the C-pocket in ClpP will enable a more refined approach to the development of therapeutics that are targeted at this hot spot.

References

1. Feng, J., Michalik, S., Varming, A. N., Andersen, J. H., Albrecht, D., Jelsbak, L., Krieger, S., Ohlsen, K., Hecker, M., Gerth, U., Ingmer, H., and Frees, D. (2013) Trapping and proteomic identification of cellular substrates of the ClpP protease in staphylococcus aureus. *J. Proteome Res.* **12**, 547–558

2. Frees, D., Gerth, U., and Ingmer, H. (2014) Clp chaperones and proteases are central in stress survival, virulence and antibiotic resistance of Staphylococcus aureus. *Int. J. Med. Microbiol.* **304**, 142–149

3. Runde, S., Molière, N., Heinz, A., Maisonneuve, E., Janczikowski, A., Elsholz, A. K. W., Gerth, U., Hecker, M., and Turgay, K. (2014) The role of thiol oxidative stress response in heat-induced protein aggregate formation during thermotolerance in Bacillus subtilis. *Mol. Microbiol.* **91**, 1036–1052

4. Trentini, D. B., Suskiewicz, M. J., Deszcz, L., and Mechtler, K. (2015) Arginine phosphorylation marks proteins for degradation by the ClpCP protease. *Nature*. **539**, 1–41

5. Sauer, R. T., and Baker, T. A. (2011) AAA+ proteases: ATP-fueled machines of protein destruction. *Annu. Rev. Biochem.* **80**, 587–612

6. Schlothauer, T., Mogk, A., Dougan, D. A., Bukau, B., and Turgay, K. (2003) MecA, an adaptor protein necessary for ClpC chaperone activity. *Proc. Natl. Acad. Sci. U. S. A.* **100**, 2306–11

7. Wang, F., Mei, Z., Qi, Y., Yan, C., Hu, Q., Wang, J., and Shi, Y. (2011) Structure and mechanism of the hexameric MecA-ClpC molecular machine. *Nature*. **471**, 331–335

8. Kirstein, J., Molière, N., Dougan, D. a, and Turgay, K. (2009) Adapting the machine: adaptor proteins for Hsp100/Clp and AAA+ proteases. *Nat. Rev. Microbiol.* **7**, 589–599

9. Kirstein, J., Schlothauer, T., Dougan, D. a, Lilie, H., Tischendorf, G., Mogk, A., Bukau, B., and Turgay, K. (2006) Adaptor protein controlled oligomerization activates the AAA+ protein ClpC. *EMBO J.* **25**, 1481–1491

10. Wah, D. A., Levchenko, I., Baker, T. A., and Sauer, R. T. (2002) Characterization of a Specificity Factor for an AAA+ ATPase: Assembly of SspB Dimers with ssrA-Tagged Proteins and the ClpX Hexamer. *Chem. Biol.* **9**, 1237–1245

11. Woo, K. M., Chung, W. J., Ha, D. B., Goldberg, A. L., and Chung, C. H. (1989) Protease Ti from Escherichia coli requires ATP hydrolysis for protein breakdown but not for hydrolysis of small peptides. *J. Biol. Chem.* **264**, 2088–2091

12. Kang, S. G., Maurizi, M. R., Thompson, M., Mueser, T., and Ahvazi, B. (2004) Crystallography and mutagenesis point to an essential role for the N-terminus of human mitochondrial ClpP. *J. Struct. Biol.* **148**, 338–352

13. Ortega, J., Singh, S. K., Ishikawa, T., Maurizi, M. R., and Steven, A. C. (2000) Visualization of substrate binding and translocation by the ATP-dependent protease, ClpXP. *Mol. Cell*. **6**, 1515–1521

14. Ishikawa, T., Beuron, F., Kessel, M., Wickner, S., Maurizi, M. R., and Steven, A. C. (2001) Translocation pathway of protein substrates in ClpAP protease. *Proc. Natl. Acad. Sci. U. S. A.* **98**, 4328–33

15. Maurizi, M. R., Singh, S. K., Thompson, M. W., Kessel, M., and Ginsburg, A. (1998) Molecular properties of ClpAP protease of Escherichia coli: ATP- dependent association of ClpA and ClpP. *Biochemistry*. **37**, 7778–7786

16. Ortega, J., Lee, H. S., Maurizi, M. R., and Steven, A. C. (2002) Alternating translocation of protein substrates from both ends of ClpXP protease. *EMBO J.* **21**, 4938–4949

17. Kim, Y. I., Levchenko, I., Fraczkowska, K., Woodruff, R. V, Sauer, R. T., and Baker, T. a (2001) Molecular determinants of complex formation between Clp/Hsp100 ATPases and the ClpP peptidase. *Nat. Struct. Biol.* **8**, 230–233

18. Joshi, S. A., Hersch, G. L., Baker, T. A., and Sauer, R. T. (2004) Communication between ClpX and ClpP during substrate processing and degradation. *Nat. Struct. Mol. Biol.* **11**, 404–411

19. Kirstein, J., Hoffmann, A., Lilie, H., Schmidt, R., Helga, R. W., Heike, B. O., Mogk, A., and Turgay, K. (2009) The antibiotic ADEP reprogrammes ClpP, switching it from a regulated to an uncontrolled protease. *EMBO Mol. Med.* **1**, 37–49

20. Lee, B.-G., Park, E. Y., Lee, K.-E., Jeon, H., Sung, K. H., Paulsen, H., Rübsamen-Schaeff, H., Brötz-Oesterhelt, H., and Song, H. K. (2010) Structures of ClpP in complex with acyldepsipeptide antibiotics reveal its activation mechanism. *Nat. Struct. Mol. Biol.* **17**, 471–478

21. Brötz-Oesterhelt, H., Beyer, D., Kroll, H.-P., Endermann, R., Ladel, C., Schroeder, W., Hinzen, B., Raddatz, S., Paulsen, H., Henninger, K., Bandow, J. E., Sahl, H.-G., and Labischinski, H. (2005) Dysregulation of bacterial proteolytic machinery by a new class of antibiotics. *Nat. Med.* **11**, 1082–1087

22. Li, D. H. S., Chung, Y. S., Gloyd, M., Joseph, E., Ghirlando, R., Wright, G. D., Cheng, Y. Q., Maurizi, M. R., Guarné, A., and Ortega, J. (2010) Acyldepsipeptide antibiotics induce the formation of a structured axial channel in ClpP: A model for the ClpX/ClpA-bound state of ClpP. *Chem. Biol.* **17**, 959–969

23. Schmitz, K. R., Carney, D. W., Sello, J. K., and Sauer, R. T. (2014) Crystal structure of Mycobacterium tuberculosis ClpP1P2 suggests a model for peptidase activation by AAA+ partner binding and substrate delivery. *Proc. Natl. Acad. Sci. U. S. A.* **111**, E4587-95

24. Michel, K. H., and Kastner, R. E. (1985) AS4556 antibiotics and process for production thereof. *US Pat.* [online] http://en.zl50.com/920130321768369056.html (Accessed October 7, 2014)

25. Hinzen, B., Raddatz, S., Paulsen, H., Lampe, T., Schumacher, A., Häbich, D., Hellwig, V., Benet-Buchholz, J., Endermann, R., Labischinski, H., and Brötz-Oesterhelt, H. (2006) Medicinal chemistry optimization of acyldepsipeptides of the enopeptin class antibiotics. *ChemMedChem*. **1**, 689–693

26. Gersch, M., Famulla, K., Dahmen, M., Göbl, C., Malik, I., Richter, K., Korotkov, V. S., Sass, P., Rübsamen-Schaeff, H., Madl, T., Brötz-Oesterhelt, H., and Sieber, S. a (2015) AAA+ chaperones and acyldepsipeptides activate the ClpP protease via conformational control. *Nat. Commun.* **6**, 6320

27. Famulla, K., Sass, P., Malik, I., Akopian, T., Kandror, O., Alber, M., Hinzen, B., Ruebsamen-Schaeff, H., Kalscheuer, R., Goldberg, A. L., and Brötz-Oesterhelt, H. (2016) Acyldepsipeptide antibiotics kill mycobacteria by preventing the physiological functions of the ClpP1P2 protease. *Mol. Microbiol.* **101**, 194–209

28. Frees, D., Qazi, S. N. A., Hill, P. J., and Ingmer, H. (2003) Alternative roles of ClpX and ClpP in Staphylococcus aureus stress tolerance and virulence. *Mol. Microbiol.* **48**, 1565–1578

29. Böttcher, T., and Sieber, S. A. (2008) β-lactones as specific inhibitors of ClpP attenuate the production of extracellular virulence factors of Staphylococcus aureus. *J. Am. Chem. Soc.* **130**, 14400–14401

30. Sass, P., Josten, M., Famulla, K., Schiffer, G., Sahl, H.-G., Hamoen, L., and Brötz-Oesterhelt, H. (2011) Antibiotic acyldepsipeptides activate ClpP peptidase to degrade the cell division protein FtsZ. *Proc. Natl. Acad. Sci. U. S. A.* **108**, 17474–9

31. Conlon, B. P., Nakayasu, E. S., Fleck, L. E., LaFleur, M. D., Isabella, V. M., Coleman, K., Leonard, S. N., Smith, R. D., Adkins, J. N., and Lewis, K. (2013) Activated ClpP kills persisters and eradicates a chronic biofilm infection. *Nature*. **503**, 365–370

32. Sassetti, C. M., Boyd, D. H., and Rubin, E. J. (2003) Genes required for mycobacterial growth defined by high density mutagenesis. *Mol. Microbiol.* **48**, 77–84

33. Ollinger, J., O'malley, T., Kesicki, E. A., Odingo, J., and Parish, T. (2012) Validation of the essential ClpP protease in Mycobacterium tuberculosis as a novel drug target. *J. Bacteriol.* **194**, 663–668

34. Ingvarsson, H., Maté, M. J., Högbom, M., Portnoï, D., Benaroudj, N., Alzari, P. M., Ortiz-Lombardía, M., and Unge, T. (2007) Insights into the inter-ring plasticity of caseinolytic proteases from the X-ray structure of Mycobacterium tuberculosis ClpP1. *Acta Crystallogr. Sect. D Biol. Crystallogr.* **63**, 249–259

35. Benaroudj, N., Raynal, B., Miot, M., and Ortiz-Lombardia, M. (2011) Assembly and proteolytic processing of mycobacterial ClpP1 and ClpP2. *BMC Biochem.* **12**, 61

36. Akopian, T., Kandror, O., Raju, R. M., Unnikrishnan, M., Rubin, E. J., and Goldberg, A. L. (2012) The active ClpP protease from M. tuberculosis is a complex composed of a heptameric ClpP1 and a ClpP2 ring. *EMBO J.* **31**, 1529–1541

37. Raju, R. M., Unnikrishnan, M., Rubin, D. H. F., Krishnamoorthy, V., Kandror, O., Akopian, T. N., Goldberg, A. L., and Rubin, E. J. (2012) Mycobacterium tuberculosis ClpP1 and ClpP2 function together in protein degradation and are required for viability in vitro and during infection. *PLoS Pathog.* **8**, e1002511

38. Frees, D., and Ingmer, H. (1999) ClpP participates in the degradation of misfolded protein in Lactococcus lactis. *Mol. Microbiol.* **31**, 79–87

39. Frees, D., Andersen, J. H., Hemmingsen, L., Koskenniemi, K., Bæk, K. T., Muhammed, M. K., Gudeta, D. D., Nyman, T. A., Sukura, A., Varmanen, P., and Savijoki, K. (2012) New insights into staphylococcus aureus stress tolerance and virulence regulation from an analysis of the role of the ClpP protease in the strains Newman, COL, and SA564. *J. Proteome Res.* **11**, 95–108

40. Böttcher, T., and Sieber, S. A. (2009) β-lactones decrease the intracellular virulence of Listeria monocytogenes in macrophages. *ChemMedChem*. **4**, 1260–1263

41. Weinandy, F., Lorenz-Baath, K., Korotkov, V. S., Böttcher, T., Sethi, S., Chakraborty, T., and Sieber, S. A. (2014) A β-lactone-based antivirulence drug ameliorates Staphylococcus aureus skin infections in mice. *ChemMedChem*. **9**, 710–713

42. Dickey, S. W., Cheung, G. Y. C., and Otto, M. (2017) Different drugs for bad bugs: antivirulence strategies in the age of antibiotic resistance. *Nat. Rev. Drug Discov.* **16**, 457–471

43. Alexopoulos, J. A., Guarné, A., and Ortega, J. (2012) ClpP: A structurally dynamic protease regulated by AAA+ proteins. *J. Struct. Biol.* **179**, 202–210

44. Carney, D. W., Compton, C. L., Schmitz, K. R., Stevens, J. P., Sauer, R. T., and Sello, J. K. (2014) A simple fragment of cyclic acyldepsipeptides is necessary and sufficient for ClpP activation and antibacterial activity. *Chembiochem*. **15**, 2216–2220

45. Malik, I. T., and Brötz-Oesterhelt, H. (2017) Conformational control of the bacterial Clp protease by natural product antibiotics. *Nat. Prod. Rep.* 10.1039/c6np00125d

46. Effantin, G., Maurizi, M. R., and Steven, A. C. (2010) Binding of the ClpA unfoldase opens the axial gate of ClpP peptidase. *J. Biol. Chem.* **285**, 14834–40

47. Hegemann, J. D., Zimmermann, M., Xie, X., and Marahiel, M. A. (2015) Lasso Peptides: An Intriguing Class of Bacterial Natural Products. *Acc. Chem. Res.* **48**, 1909–1919

48. Sowole, M. A., Alexopoulos, J. A., Cheng, Y. Q., Ortega, J., and Konermann, L. (2013) Activation of ClpP protease by ADEP antibiotics: Insights from hydrogen exchange mass spectrometry. *J. Mol. Biol.* **425**, 4508–4519

49. Alexopoulos, J., Ahsan, B., Homchaudhuri, L., Husain, N., Cheng, Y. Q., and Ortega, J. (2013) Structural determinants stabilizing the axial channel of ClpP for substrate translocation. *Mol. Microbiol.* **90**, 167–180

50. Leung, E., Datti, A., Cossette, M., Goodreid, J., McCaw, S. E., Mah, M., Nakhamchik, A., Ogata, K., El Bakkouri, M., Cheng, Y. Q., Wodak, S. J., Eger, B. T., Pai, E. F., Liu, J., Gray-Owen, S., Batey, R. A., and Houry, W. A. (2011) Activators of Cylindrical Proteases as Antimicrobials: Identification and Development of Small Molecule Activators of ClpP Protease. *Chem. Biol.* **18**, 1167–1178

51. Schmitt, E. K., Riwanto, M., Sambandamurthy, V., Roggo, S., Miault, C., Zwingelstein, C., Krastel, P., Noble, C., Beer, D., Rao, S. P. S., Au, M., Niyomrattanakit, P., Lim, V., Zheng, J., Jeffery, D., Pethe, K., and Camacho, L. R. (2011) The natural product cyclomarin kills mycobacterium tuberculosis by targeting the ClpC1 subunit of the caseinolytic protease. *Angew. Chemie - Int. Ed.* **50**, 5889–5891

52. Lee, H., and Suh, J. W. (2016) Anti-tuberculosis lead molecules from natural products targeting Mycobacterium tuberculosis ClpC1. *J. Ind. Microbiol. Biotechnol.* **43**, 205–212

53. Gavrish, E., Sit, C. S., Cao, S., Kandror, O., Spoering, A., Peoples, A., Ling, L., Fetterman, A., Hughes, D., Bissell, A., Torrey, H., Akopian, T., Mueller, A., Epstein, S., Goldberg, A., Clardy, J., and Lewis, K. (2014) Lassomycin, a ribosomally synthesized cyclic peptide, kills mycobacterium tuberculosis by targeting the ATP-dependent protease ClpC1P1P2. *Chem. Biol.* **21**, 509–518

54. Vasudevan, D., Rao, S. P. S., and Noble, C. G. (2013) Structural basis of mycobacterial inhibition by Cyclomarin A. *J. Biol. Chem.* **288**, 30883–30891

55. Kang, S. G., Dimitrova, M. N., Ortega, J., Ginsburg, A., and Maurizi, M. R. (2005) Human mitochondrial ClpP is a stable heptamer that assembles into a tetradecamer in the presence of ClpX. *J. Biol. Chem.* **280**, 35424–35432

56. Geiger, S. R., Böttcher, T., Sieber, S. A., and Cramer, P. (2011) A conformational switch underlies ClpP protease function. *Angew. Chemie - Int. Ed.* **50**, 5749–5752

57. Ye, F., Zhang, J., Liu, H., Hilgenfeld, R., Zhang, R., Kong, X., Li, L., Lu, J., Zhang, X., Li, D., Jiang, H., Yang, C. G., and Luo, C. (2013) Helix unfolding/refolding characterizes the functional dynamics of staphylococcus aureus clp protease. *J. Biol. Chem.* **288**, 17643–17653

58. Böttcher, T., and Sieber, S. A. (2009) Structurally refined β-lactones as potent inhibitors of devastating bacterial virulence factors. *ChemBioChem*. **10**, 663–666

59. Tymiak, A. A., Culver, C. A., Malley, M. F., and Gougoutas, J. Z. (1985) Structure of obafluorin: an antibacterial β-lactone from Pseudomonas fluorescens. *J. Org. Chem.* **50**, 5491–5495

60. Aldridge, D. C., Giles, D., and Turner, W. B. (1971) Antibiotic 1233A: a fungal β-lactone. *J. Chem. Soc. C*. **0**, 3888–3891

61. Böttcher, T., and Sieber, S. A. (2008) B-Lactones As Privileged Structures for the Active-Site Labeling of Versatile Bacterial Enzyme Classes. *Angew. Chemie - Int. Ed.* **47**, 4600–4603

62. Gersch, M., Gut, F., Korotkov, V. S., Lehmann, J., Böttcher, T., Rusch, M., Hedberg, C., Waldmann, H., Klebe, G., and Sieber, S. A. (2013) The mechanism of caseinolytic protease (ClpP) inhibition. *Angew. Chemie - Int. Ed.* **52**, 3009–3014

63. Gersch, M., List, A., Groll, M., and Sieber, S. A. (2012) Insights into structural network responsible for oligomerization and activity of bacterial virulence regulator caseinolytic protease P (ClpP) protein. *J. Biol. Chem.* **287**, 9484–9494

64. Martin, A., Baker, T. A., and Sauer, R. T. (2007) Distinct Static and Dynamic Interactions Control ATPase-Peptidase Communication in a AAA+ Protease. *Mol. Cell*. **27**, 41–52

65. Bewley, M. C., Graziano, V., Griffin, K., and Flanagan, J. M. (2009) Turned on for degradation: ATPase-independent degradation by ClpP. *J. Struct. Biol.* **165**, 118–125

66. Ni, T., Ye, F., Liu, X., Zhang, J., Liu, H., Li, J., Zhang, Y., Sun, Y., Wang, M., Luo, C., Jiang, H., Lan, L., Gan, J., Zhang, A., Zhou, H., and Yang, C. G. (2016) Characterization of Gain-of-Function Mutant Provides New Insights into ClpP Structure. *ACS Chem. Biol.* **11**, 1964–1972

List of publications and personal contributions

1.) Malte Gersch, Kirsten Famulla, Maria Dahmen, Christoph Göbl, **Imran Malik**, Klaus Richter, Vadim s. Korotkov, Peter Sass, Helga Rübsamen-Schaeff, Tobias Madl, Heike Brötz-Oesterhelt & Stephan A. Sieber. AAA+ chaperones and acyldepsipeptides activate the ClpP protease via conformational control. *Nat. Commun.* 6:6320 (2015).

Production and purification of wild-type BsClpP and establishment of chromatography methodology for obtaining pure oligomeric fractions (e. g. monomeric and tetradecameric fractions). Generation of BsClpP active site mutants D172N and D172A *via* site-directed mutagenesis and establishment of native tag-free purification protocols *via* anion-exchange chromatography. Biochemical characterization of obtained proteins with the help of *in vitro* suc-LY-amc and FITC-casein degradation assays in the absence or the presence of ADEP2 were performed as control experiments (see Supplementary Figure 13 for chapter 2). The respective experiments were designed and conducted by me under the supervision of H. B.-O. The respective experimental procedures were provided in writing.

2.) Kirsten Famulla, Peter Sass, **Imran Malik**, Tatos Akopian, Olga Kandror, Marina Alber, Berthold Hinzen, Helga Ruebsamen-Schaeff, Rainer Kalscheuer, Alfred L. Goldberg, and Heike Brötz-Oesterhelt. Acyldepsipeptide antibiotics kill mycobacteria by preventing the physiological functions of the ClpP1P2 protease. *Molecular Microbiology* (2016) 101(2), 194–209.

Conceptualization as well as establishment of an *in vitro* competition assay system to determine the binding site of Z-LL on BsClpP under the guidance of H. B.-O. Respective Methods section was provided by me.

3.) **I. T. Malik** and H. Brötz-Oesterhelt. Conformational control of the bacterial Clp protease by natural product antibiotics. *Natural Product Reports* (2017) 34(7), 815-831.

The review article was written by me under the supervision of Heike Brötz-Oesterhelt.

4.) **Imran T. Malik**, Mohamed A. Marahiel, Julian D. Hegemann, Heike Brötz-Oesterhelt, paper in submission. Lasso peptides modified to mimic ClpX IGF-loops activate ClpP and reveal a novel site relevant for ClpX/ClpP interaction.

J. D. H. generated, purified and kindly provided the MccJ25 loop mutants along with the corresponding methods section. Planning and execution of the

remaining experiments as well as writing of the original draft were performed by me under the guidance of Heike Brötz-Oesterhelt. Corrections and editing were performed by Heike Brötz-Oesterhelt.

Appendix

Supporting information for Chapter 1

Table S1. Primer used in this study.

primer	sequence	restriction site
Construction of *M. bovis* BCG Pasteur *clpP1-tet off:*		
clpP1-F1-fwd	5`-TTTTTTTTCCATAAATTGGAGCCCGGTTCAATGAGTTGC-3`	*Van*91I
clpP1-F1-rev	5`-TTTTTTTTCCATTTCTTGGTCAGGGGCACCTGCTTTCC-3`	*Van*91I
clpP1-F2-fwd	5`-TTTTTTTGCATCTTTTGCCAAACCGTATTCCAGGG-3`	*Bst*API
clpP1-F2-rev	5`-TTTTTTTTGCATAGATTGCATGAGCCAAGTGACTGACATGC-3`	*Bst*API
c-*clpP1*-fwd	5'-ACGAAGCGACAACGTGAC-3'	
c-*clpP1*-rev	5'-GGGAATTCACTGTGCTTCTC-3'	
seq-*clpP1*-fwd	5'-CACGACTTCGAGGTGTTC-3'	
seq-*clpP2*-rev	5'-GGGAATTCACTGTGCTTCTC-3'	
rev-tetR-fwd	5´-TTTTTGAATTCATGAGCACGATCCGCGGTACCATC-3´	*Eco*R1
rev-tetR-rev	5´-TTTTTAAGCTTAGGAGCCGCTCTCGCACTTCAG-3´	*Hin*dIII
Cloning of MTB *ftsZ:*		
MTB *ftsZ*-fwd	5'-TTTCCATGGCCCCCCCGCACAACTACC-3'	*Nco*I
MTB *ftsZ*-rev	5'-AAAAAGCTTGCGGCGCATGAAGGGCGG-3'	*Hin*dIII
qRT-PCR of MTB *clpP* expression:		
q*clpP1*-fwd	5'- TGAGCCAAGTGACTGACAT-3'	
q*clpP1*-rev	5'- GATGTAGAGGCTGATGTCCT-3'	

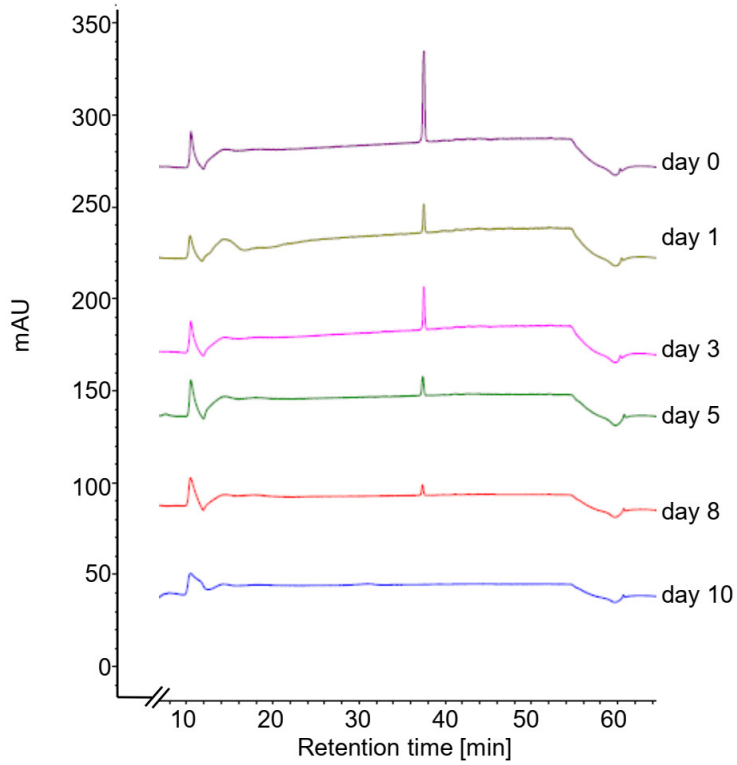

Figure S1. Chemical stability of ADEP2 in culture broth is limited. HPLC chromatograms at different times of incubation of ADEP2 in minimal medium at 37 °C.

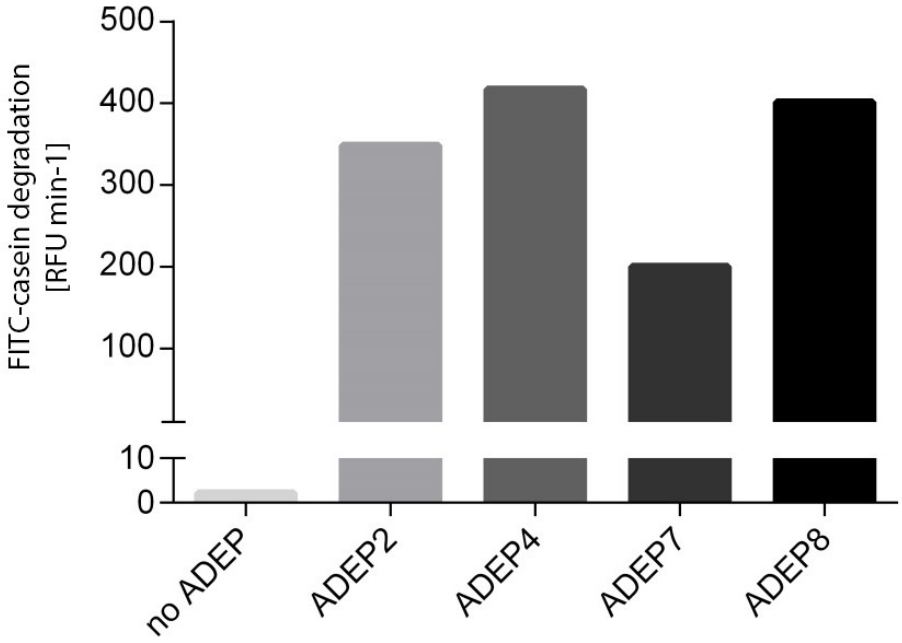

Figure S2. Degradation of FITC-casein by BS ClpP. Reaction rate [increase in RUF min^{-1}] calculated from the initial linear period of enzyme activity (10 min). ADEPs activate BS ClpP much more strongly than MT ClpP1P2 under the same assay conditions.

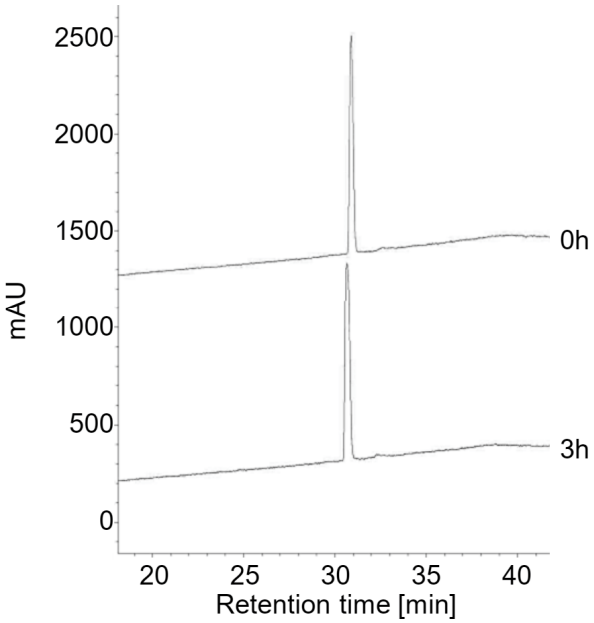

	retention time [min]	area [mAu*s]
0 h	30.66	1.79E+04
3 h	30.67	1.52E+04

Figure S 3. The HPLC chromatogram shows that Z-LL is not degraded by BS ClpP after 3 hours of incubation at 37 °C.

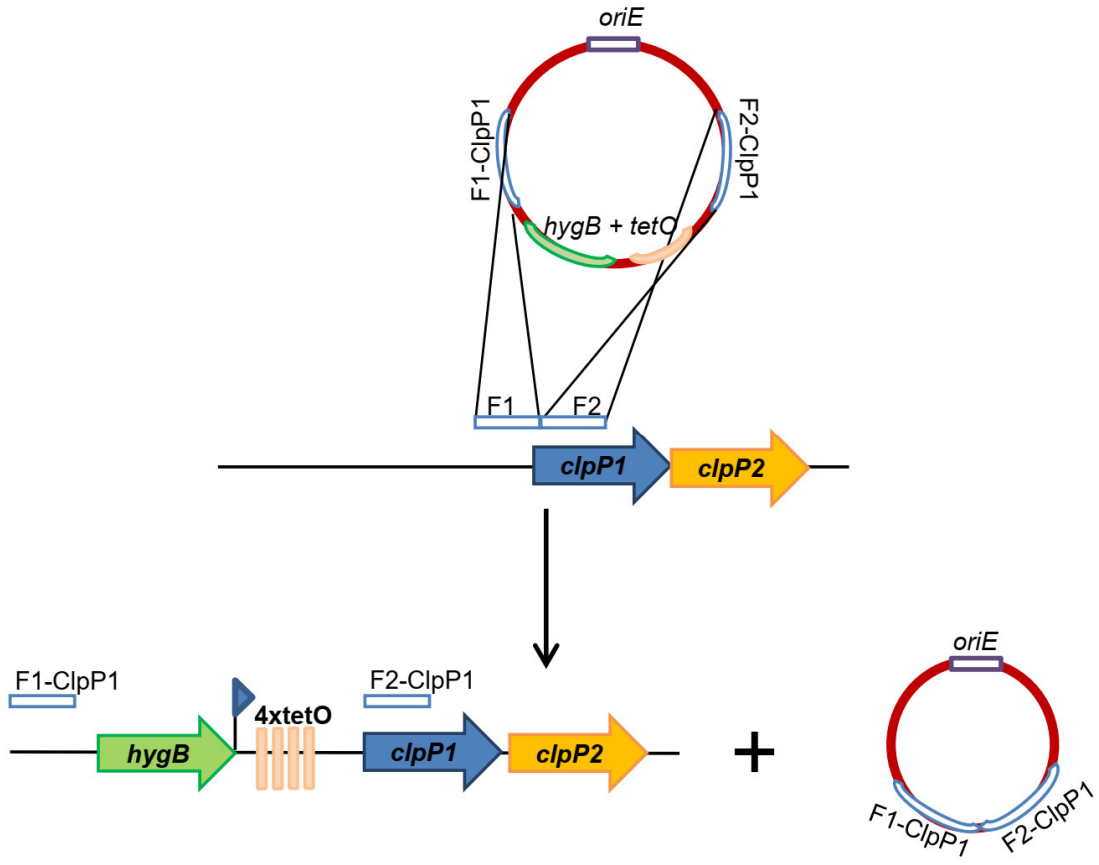

Figure S4. Construction of *M. bovis* BCG *clpP1-tetoff*. The *hyg*-P*myc1*-4x*tetO* cassette was inserted upstream of the *clpP1P2* operon via homologous recombination. Then, the plasmid which expresses the TetR repressor was introduced to obtain *M. bovis* BCG *clpP1-tetoff*.

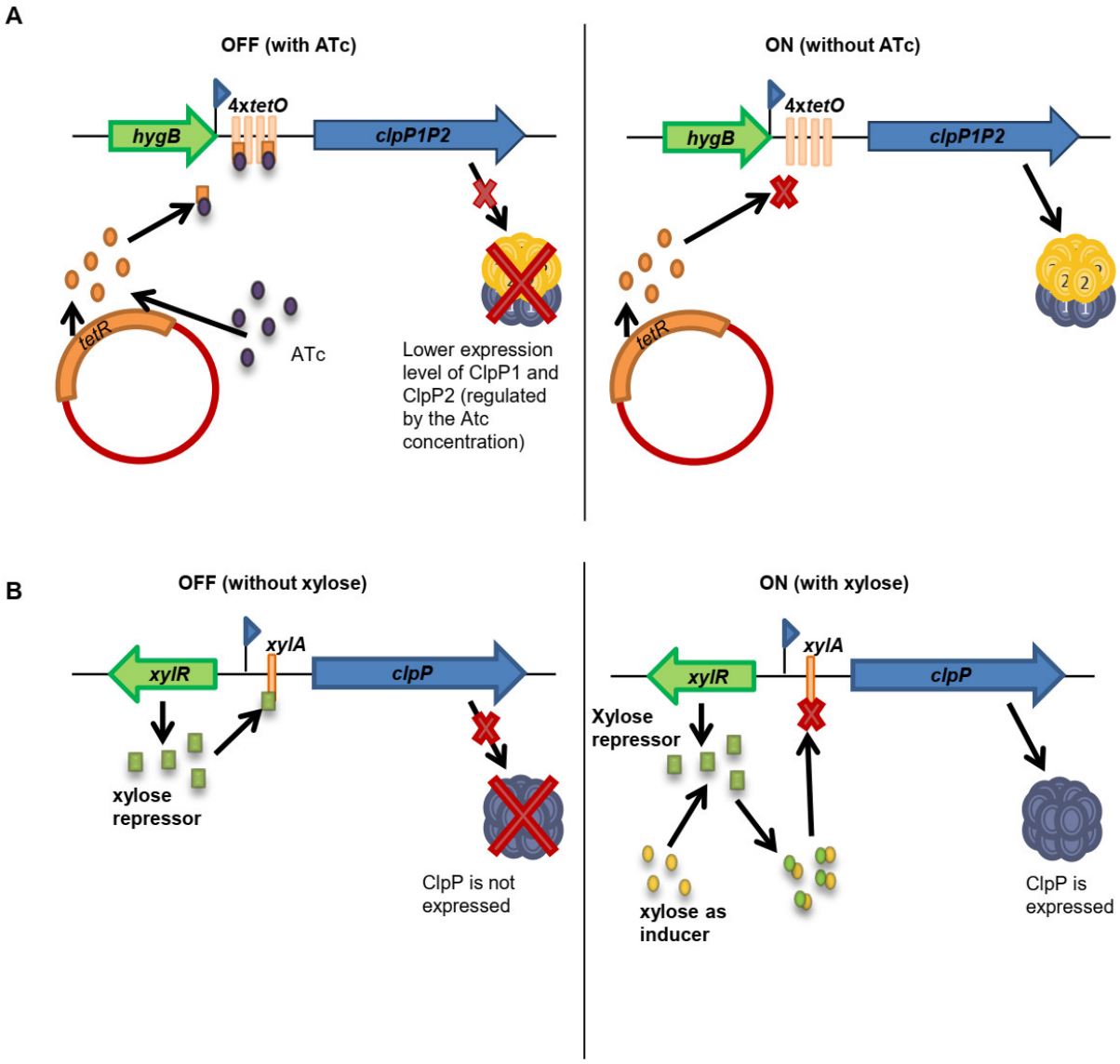

Figure S5. Schematic representation of the inducible mutants used in this study.
A. Operating mode of the Tet-Off system in strain *M. bovis* BCG *clpP1-tetoff* in the absence and presence of ATc. In the absence of ATc, the TetR repressor cannot bind to the *tetO* sites upstream the *clpP1P2* operon, *clpP1* and *clpP2* are expressed. In the presence of ATc, TetR undergoes conformational change that now allows binding to the *tetO* sites. Thus, the expression level of *clpP1P2* can be regulated via the ATc concentration.
B. Operating mode of the Xyl-On system in *B. subtilis* 168-pX2-*clpP* in the absence and presence of xylose. In the absence of xylose, the repressor XylR can bind to the *xylA* operator palindrome upstream of *clpP*, thereby silencing *clpP* expression. Xylose functions as an inducer in this system. The presence of xylose leads to a conformational change in XylR, which is now incapable to bind to *xylA* operator, thereby allowing *clpP* expression.

Supplementary Figures and Methods for Chapter 2

Supplementary Figures

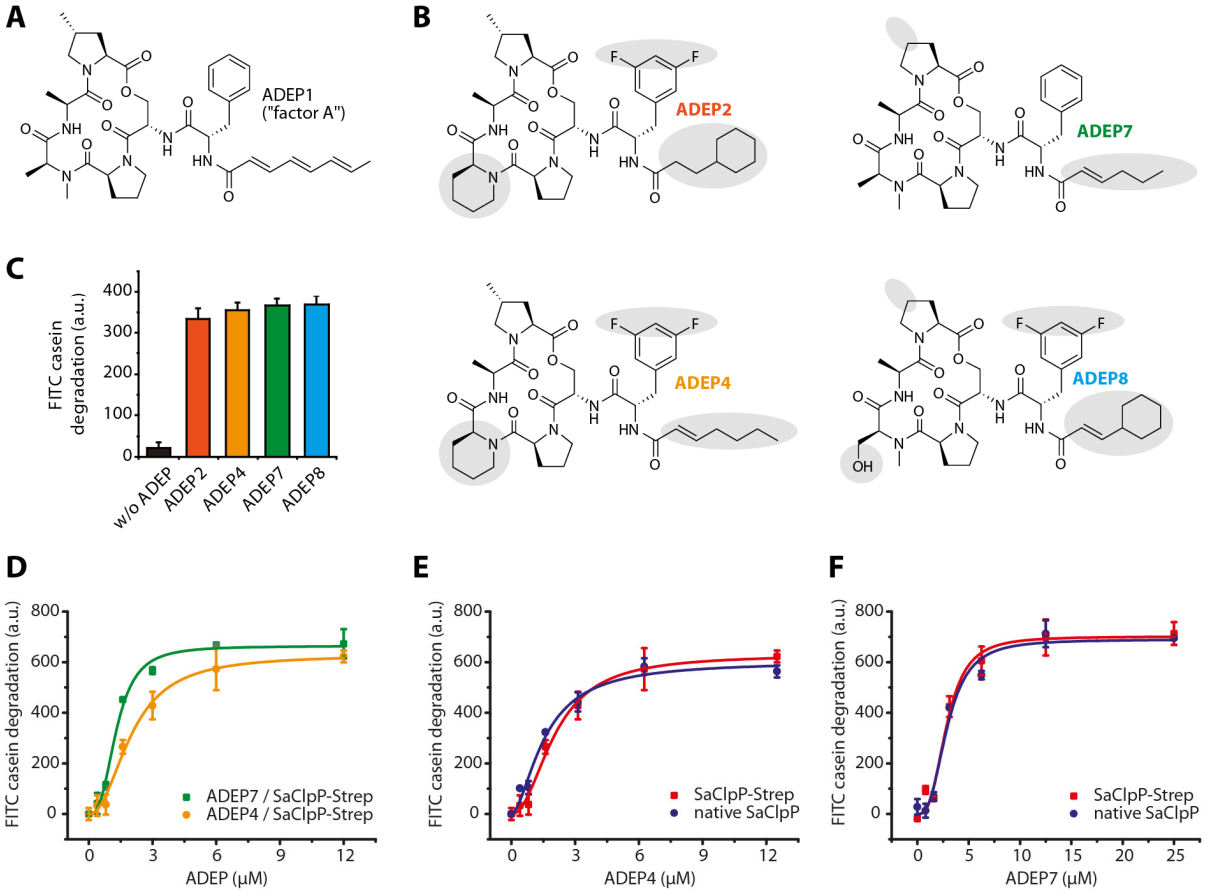

Supplementary Figure 1. Comparison of different ADEP derivatives for SaClpP activation. **A.** Structure of the natural product ADEP1. **B.** Structures of ADEPs used in this study. **C.** Comparison of ADEPs (12 μM) in the stimulation of proteolytic activity of SaClpP (1 μM). **D.** Concentration-dependent stimulation of SaClpP by ADEP4 and ADEP7. **E.** Comparison of C-terminally Strep-tagged SaClpP and tagfree SaClpP for concentration-dependent stimulation by ADEP4. **F.** Comparison of C-terminally Strep-tagged SaClpP and tagfree SaClpP for concentration-dependent stimulation by ADEP7. Mean ± s.d. is shown in all experiments.

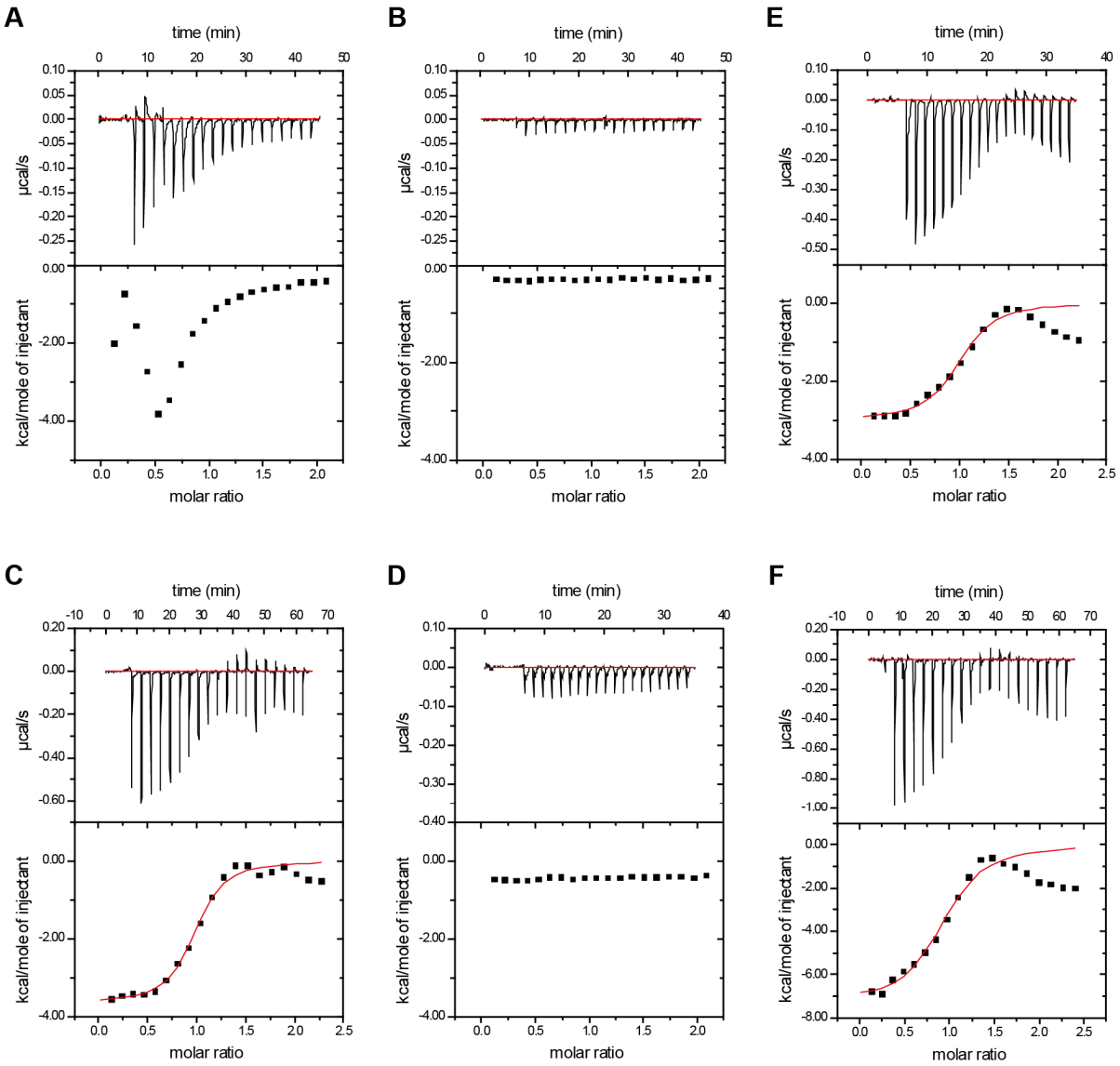

Supplementary Figure 2. Replicate and control isothermal titration experiments. **A.** Titration of ADEP7 (500 µM) into a solution of SaClpP (50 µM). Replicate of ITC experiment shown in Figure 1D. **B.** Titration of ADEP7 (500 µM) into buffer. **C.** Titration of SaClpP (1250 µM) into a solution of ADEP7 (125 µM). Replicate of ITC experiment shown in Figure 1E. **D.** Titration of SaClpP (1000 µM) into buffer. **E.** Titration of SaClpP-S98A (1050 µM) into a solution of ADEP7 (100 µM). **F.** Titration of SaClpP-D172N (1091 µM) into a solution of ADEP7 (93 µM). All ITC experiments were carried out as described in the methods section. See Supplementary Table 1 for a compilation of all obtained parameters.

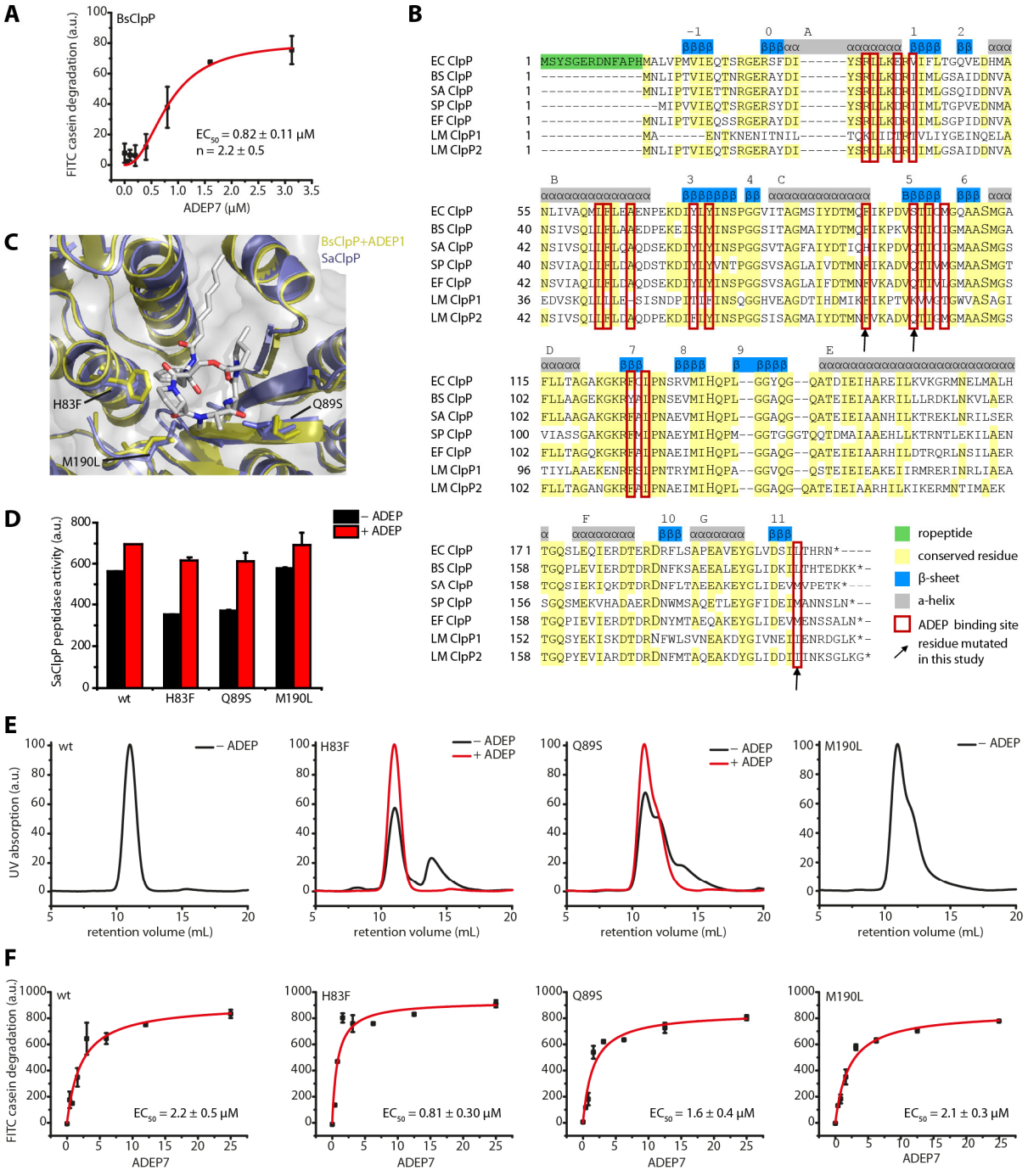

Supplementary Figure 3. Characterization of SaClpP ADEP binding site mutants. **A.** Proteolytic activation of BsClpP by ADEP7. **B.** Alignment of ClpP sequences from different bacterial organisms. EC: *Escherichia coli* (Uniprot-ID: P0A6G7); BS; *Bacillus subtilis* (Uniprot-ID: P80244); SA: *Staphylococcus aureus* (Uniprot-ID: D6UC74); SP: *Streptococcus pneumoniae* (Uniprot-ID: P63788); EF: *Enterococcus faecalis* (Uniprot-ID: Q837R0); LM ClpP1: *Listeria monocytogenes* ClpP1 (Uniprot-ID: Q720U2); LM ClpP2: *Listeria monocytogenes* ClpP2 (Uniprot-ID: Q71WV9). **C.** Close-up view on the BsClpP binding site of ADEP1 (PDB ID: 3KTI) with residues different in SaClpP (PDB ID: 3V5E) indicated. **D.** SaClpP peptidase activity of wild type and ADEP binding site mutant proteins. **E.** Analytical size exclusion chromatograms of SaClpP with / without ADEP. **F.** Proteolytic activation of SaClpP wild type and mutant proteins. Mean ± s.d. is given in all experiments.

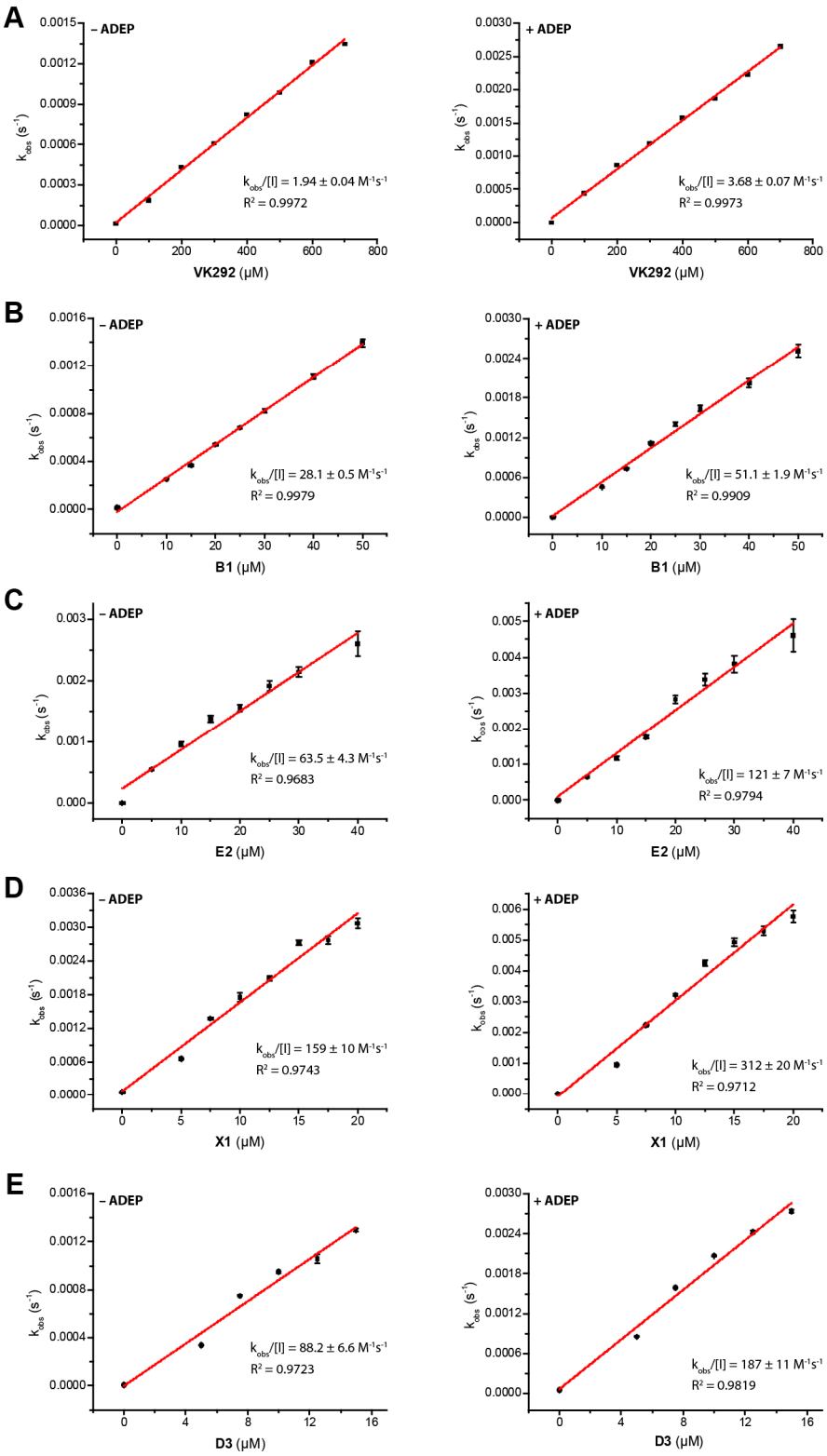

Supplementary Figure 4. Catalytic efficiencies of the reactions of SaClpP with different β-lactones in the absence or presence of ADEP7. Reaction of SaClpP with the fluorogenic substrate Suc-LY-AMC was followed. Raw data fits to an exponential equation are shown in each upper panel. The obtained exponential coefficients plotted against the β-lactone concentration are shown in each lower panel. **A.** VK292, **B.** B1, **C.** E2, **D.** X1, **E.** D3, Mean ± s.d. is given for all linear plots. **F.** $k_{obs}/[I]$ values for different lactones plotted without scaling (data used for Figure 2A, error bars denote fitting errors).

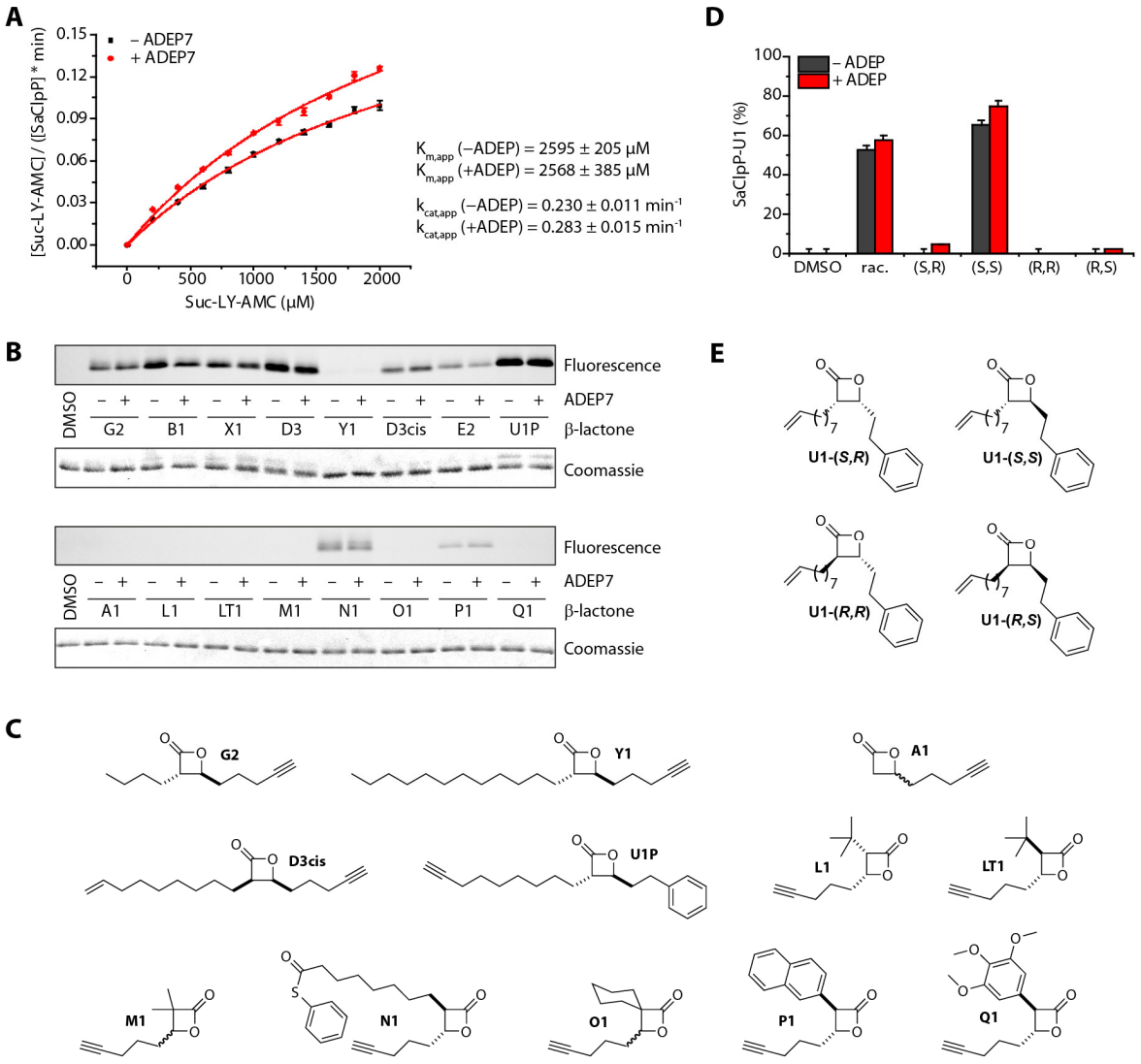

Supplementary Figure 5. Analysis of ADEP-induced, functional changes in the SaClpP binding site. **A.** Turnover of the fluorogenic substrate Suc-LY-AMC in the presence or absence of ADEP7 by SaClpP (0.5 µM). The data were fit to a Michaelis-Menten equation and K_M and k_{cat} values were obtained. These values are labeled 'apparent' because the highest substrate concentration employed is lower than the apparent K_M. Quenching effects precluded the use of higher substrate concentrations. ADEP7 led to an increase of $k_{cat,app}$ by approximately 20% while $K_{M,app}$ was left unchanged, thus pointing away from ADEP7-induced structural changes in the substrate binding pocket. **B.** *In-vitro* activity-based protein labeling experiments with SaClpP and different β-lactone probes. SaClpP was incubated with β-lactone probes or DMSO, a fluorescent tag was then appended via click chemistry and samples separated via SDS-PAGE. **C.** Structures of β-lactone probes used for in-vitro labeling experiments (see Figure 2B for additional structures). **D.** Degree of covalent modification of SaClpP (1 µM) by different lactone U1 stereoisomers (100 µM) after incubation at 32°C for 2 h in the presence or absence of ADEP7 (mean ± s.d.). 'rac' denotes a racemic mixture of *trans*-configured U1 lactones (i.e. (*S*,*S*) and (*R*,*R*)). **E.** Structures of enantiopure U1 lactones used for the experiment shown in D. Mean ± s.d. is given in all panels.

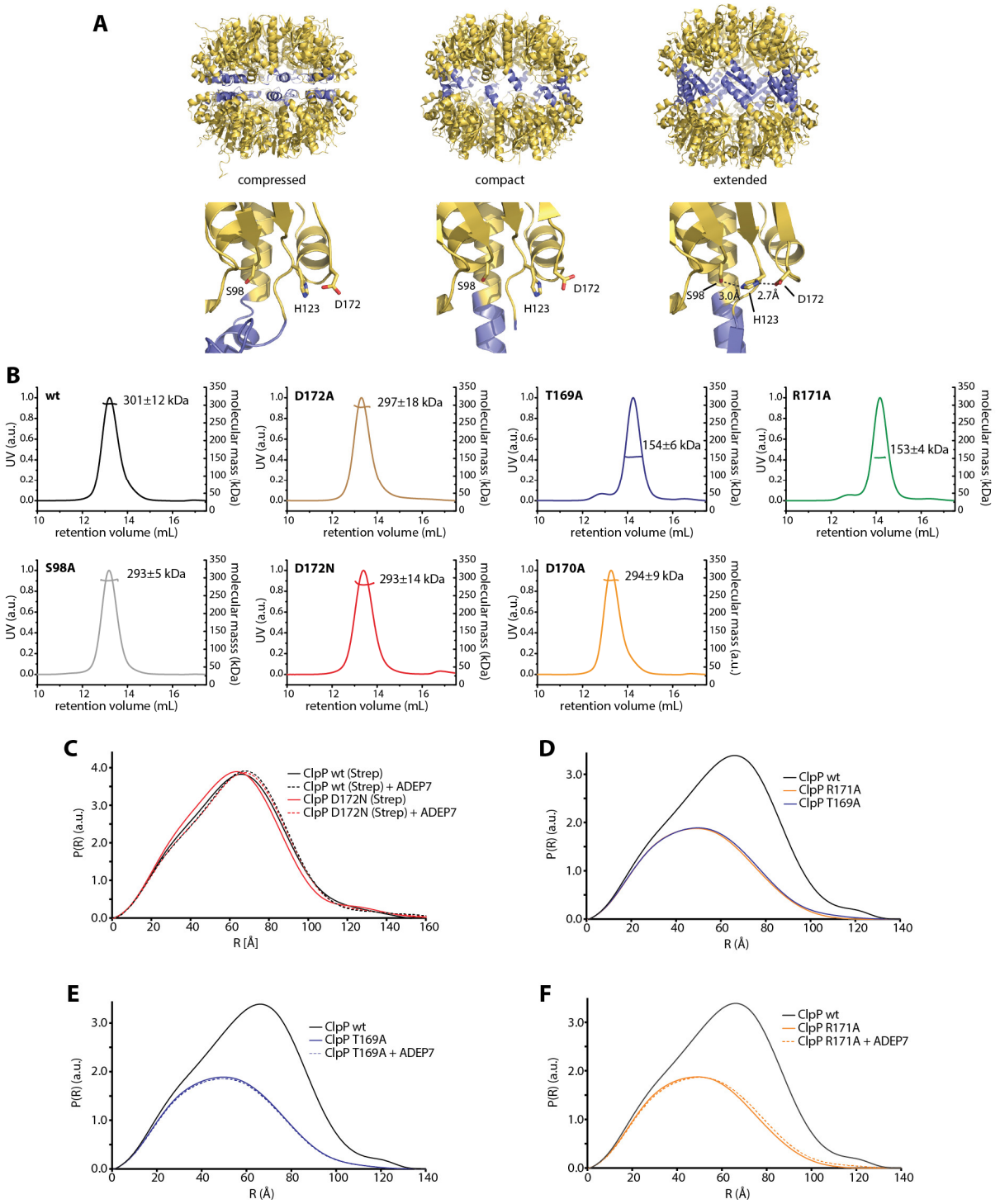

Supplementary Figure 6. Comparison of SaClpP conformations, SEC-MALS analysis and additional SAXS data. **A.** Comparison of SaClpP conformations based on X-ray structures (PDB IDs: compressed, 3QWD; compact, 4EMM; extended, 3V5E). Upper panel: Cartoon representation of tetradecameric assemblies, the handle region is colored in blue. Lower panel: SaClpP monomers with residues of the catalytic triad depicted as sticks. **B.** SEC-MALS analysis of SaClpP proteins corresponding to Figure 3B. **C.-F.** Small angle X-ray scattering data. **C.** C-terminally Strep-tagged SaClpP with/without ADEP7. **D.** Tetradecameric wild type SaClpP and heptameric mutants R171A and T169A. **E.**, **F.** ADEP7 does not cause a reassembly of the heptameric mutants T169A and R171A. (The ClpP wt curve is taken from Supp. Figure 6B and shown for comparison in Supp. Figures 6C-E; the ClpP T169A and R171A curves from Supp. Figure 6C is shown in Supp. Figure 6D and 6E for comparison).

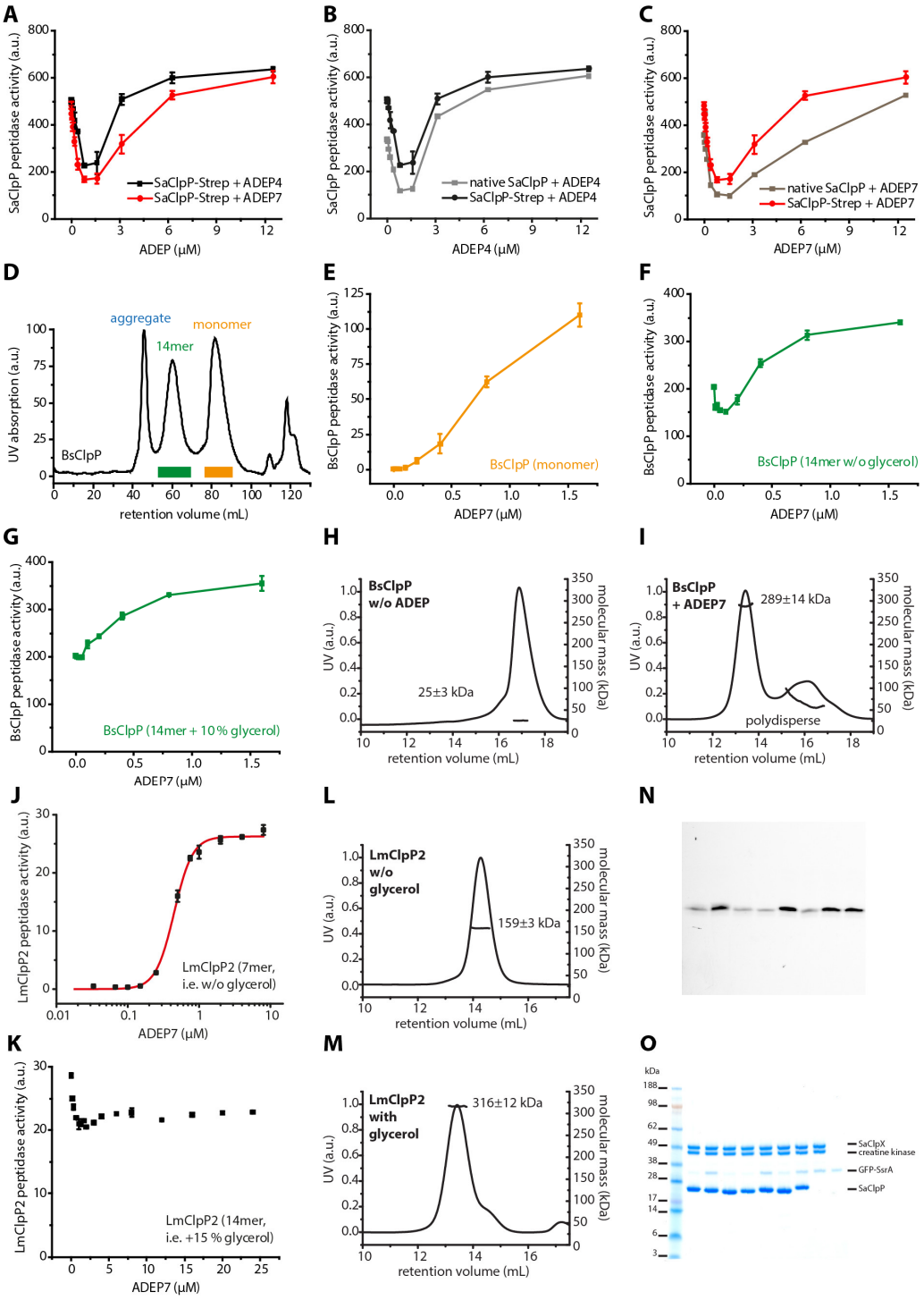

Supplementary Figure 7. Low ADEP concentrations partially inhibit tetradecameric ClpP. **A.** Both ADEP4 and ADEP7 partially inhibit SaClpP (1 μM) peptidase activity at low concentrations. **B.**, **C.** The partial inhibition is also observed with tagfree SaClpP (curves from A. repeated for easy comparison). **D.** Preparative size exclusion chromatogram of BsClpP on a Superdex 200 pg column. Oligomerization states were assigned based on calibration runs and indicated fractions were used in subsequent experiments. **E.** Dimeric BsClpP is peptidase-inactive and can be stimulated by ADEP7. **F.**, **G.** Pre-assembled tetradecameric BsClpP also shows partial inhibition in the presence of low concentrations of ADEP7, while the effect is not visible in the presence of glycerol. **H.**, **I.** SEC-MALS analysis of monomeric BsClpP in the absence and presence of ADEP. **J.**, **K.** Heptameric LmClpP2 (i.e. in a buffer without glycerol) can be stimulated by ADEP7 similarly to dimeric BsClpP in a cooperative manner (EC_{50} = 0.44 ± 0.01 μM; n = 3.4 ± 0.3), while preorganized, tetradecameric LmClpP2 (i.e. in the presence of glycerol) shows partial inhibition at low amounts of ADEP7. **L.**, **M.** SEC-MALS analysis of LmClpP2 in the absence and presence of glycerol, corroborating previous results.[1] **N.**, **O.** Uncropped images of gels shown in Figure 5B. Mean ± s.d. is given in panels A-C, E-G, J-K.

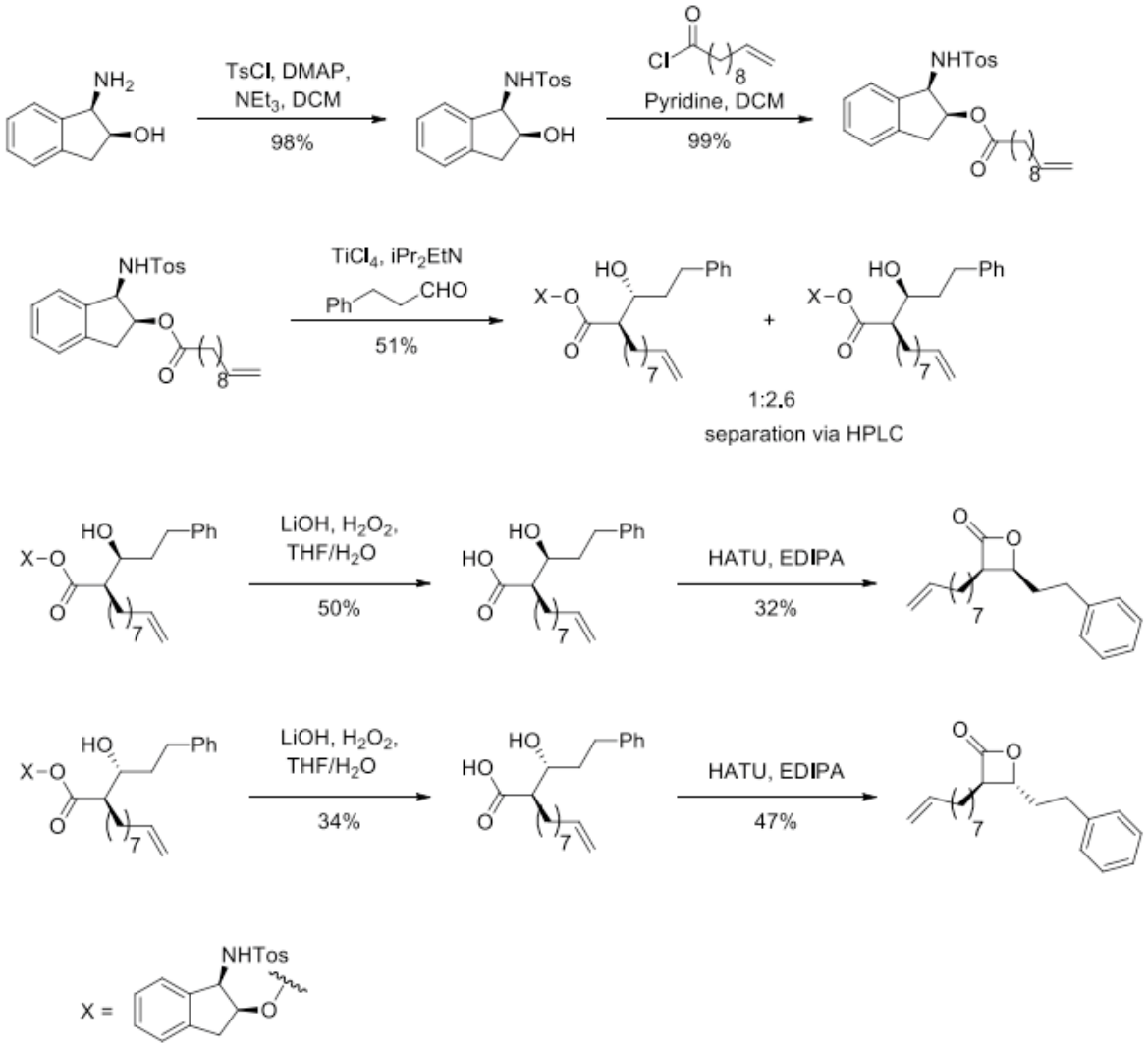

Supplementary Figure 8. Reaction scheme for the synthesis of enantiomerically pure lactones.

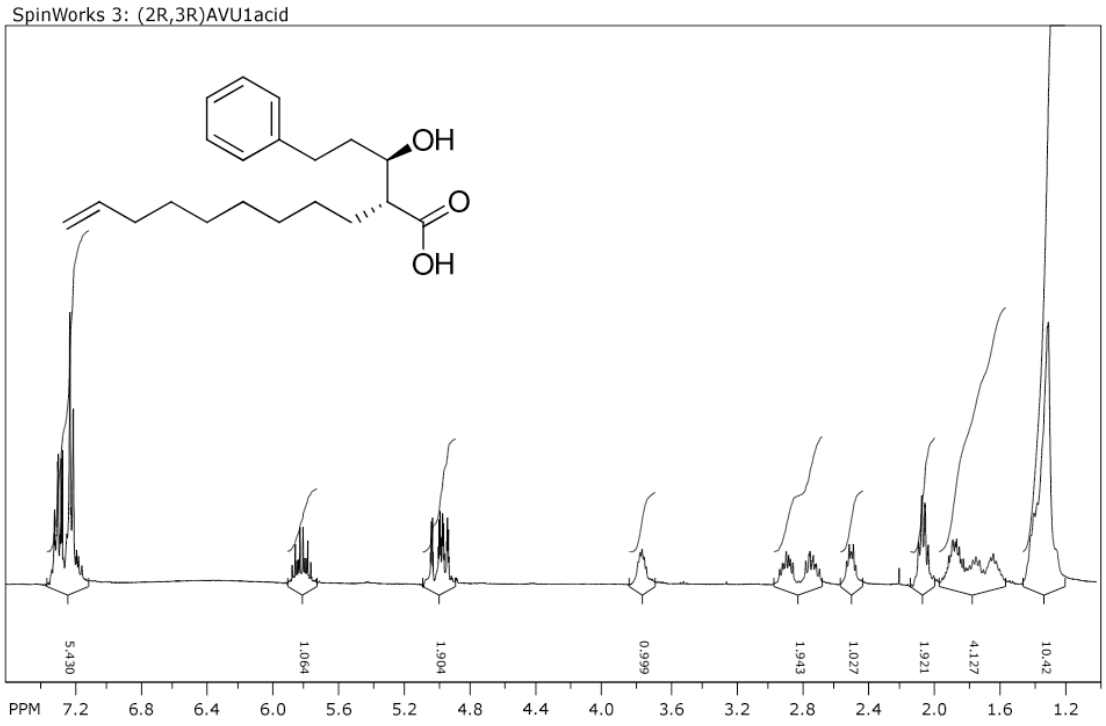

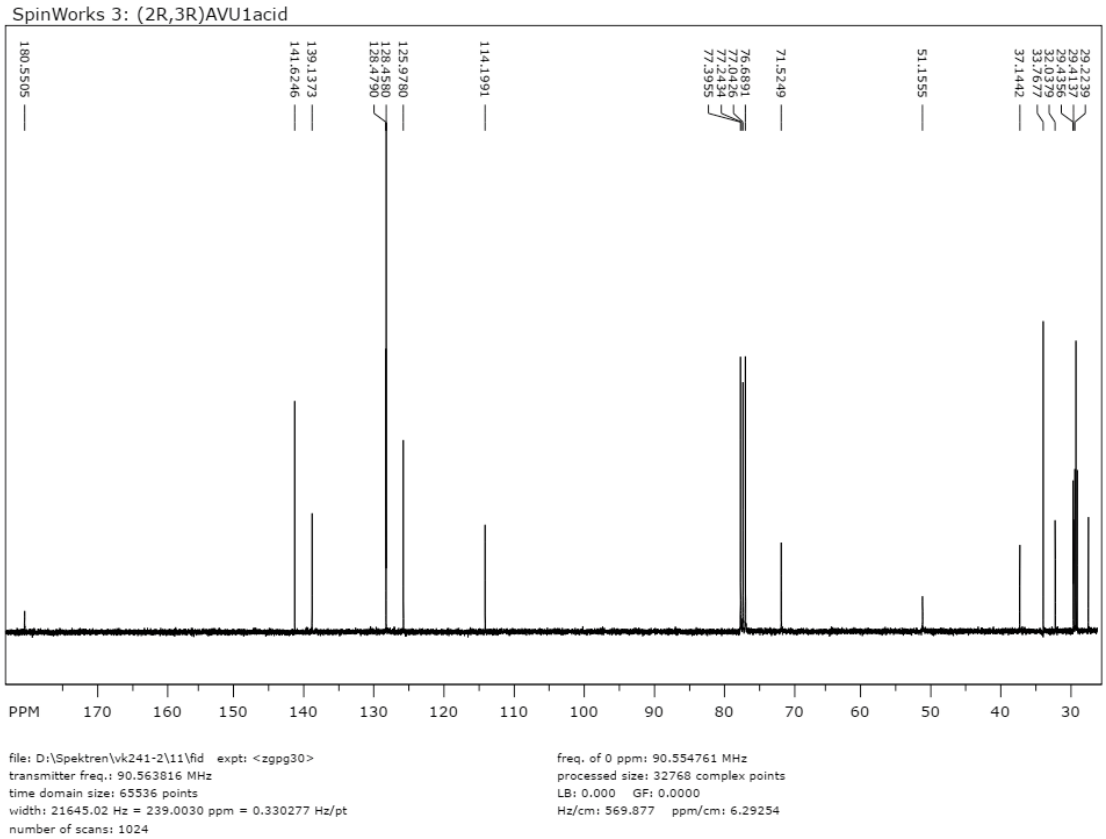

Supplementary Figure 9. ^{1}H and ^{13}C NMR spectra of (2*R*,3*R*)-3-hydroxy-2-(non-8-enyl)-5-phenylpentanoic acid.

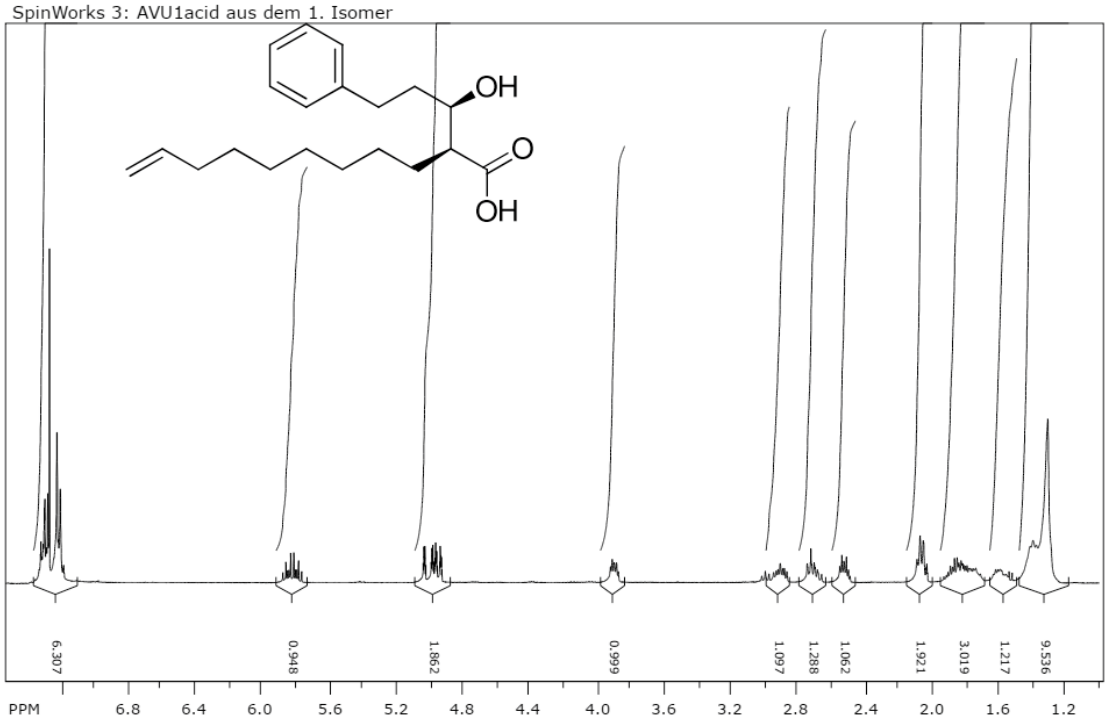

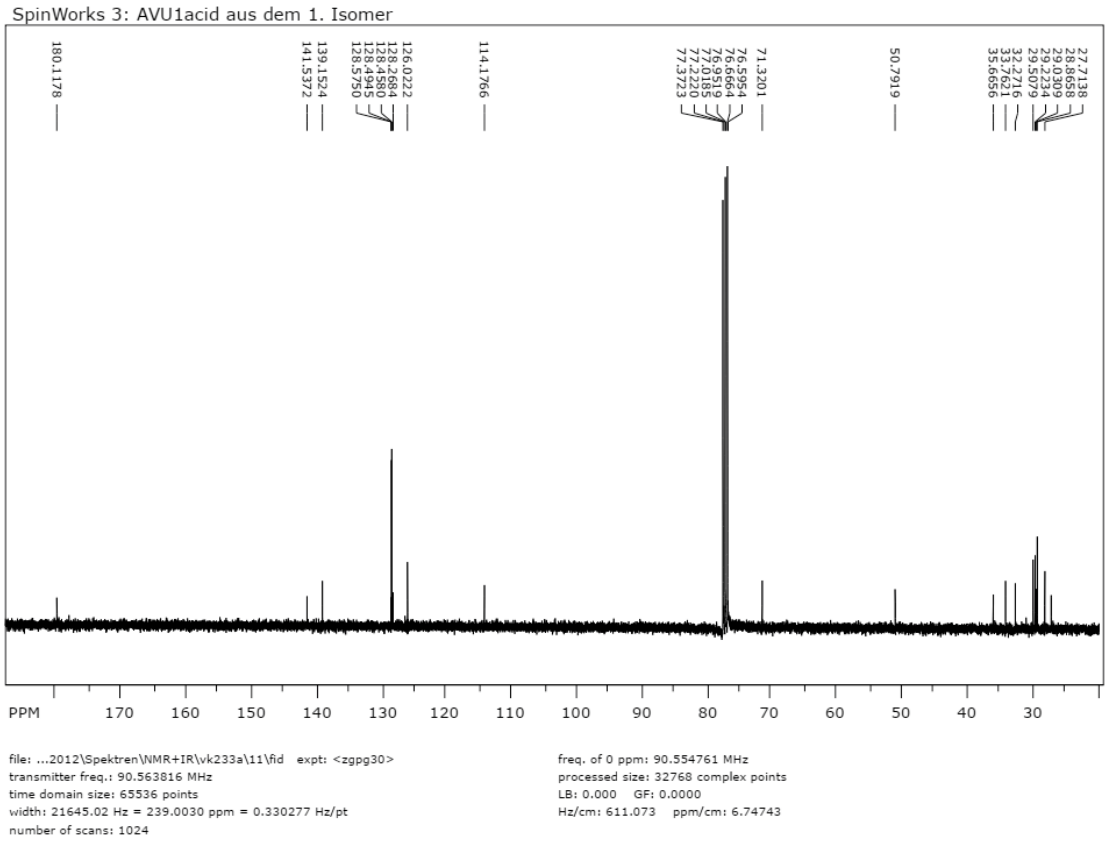

Supplementary Figure 10. ^{1}H and ^{13}C NMR spectra of (2*S*,3*R*)-3-hydroxy-2-(non-8-enyl)-5-phenylpentanoic acid.

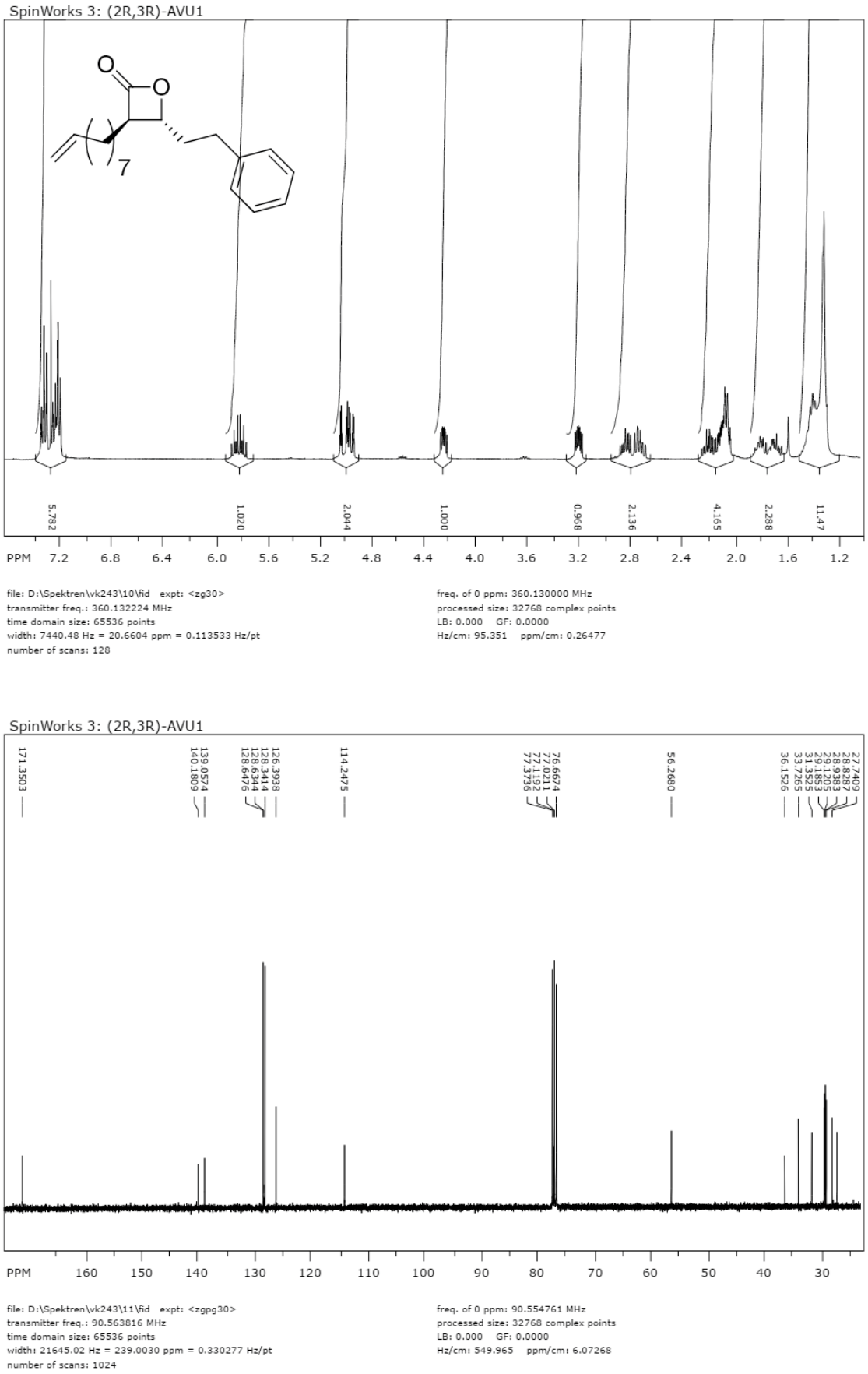

Supplementary Figure 11. ^{1}H and ^{13}C NMR spectra of (3*R*,4*R*)-3-(8-Nonenyl)-4-(2-phenylethyl)-oxetan-2-one.

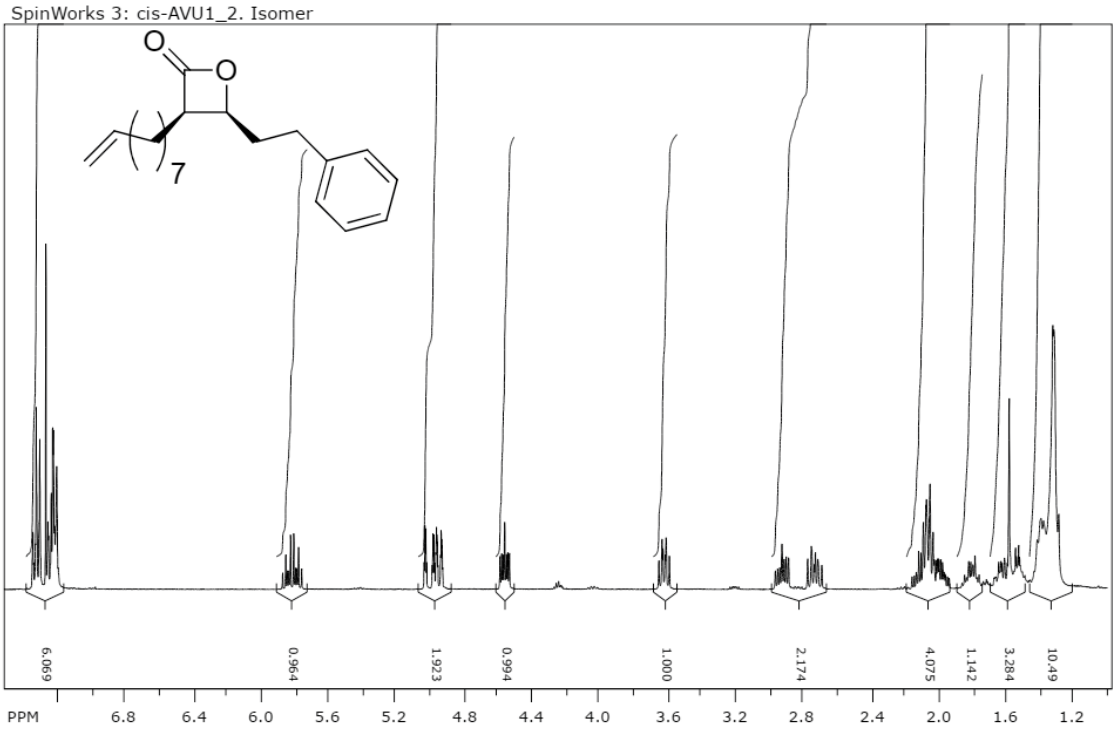

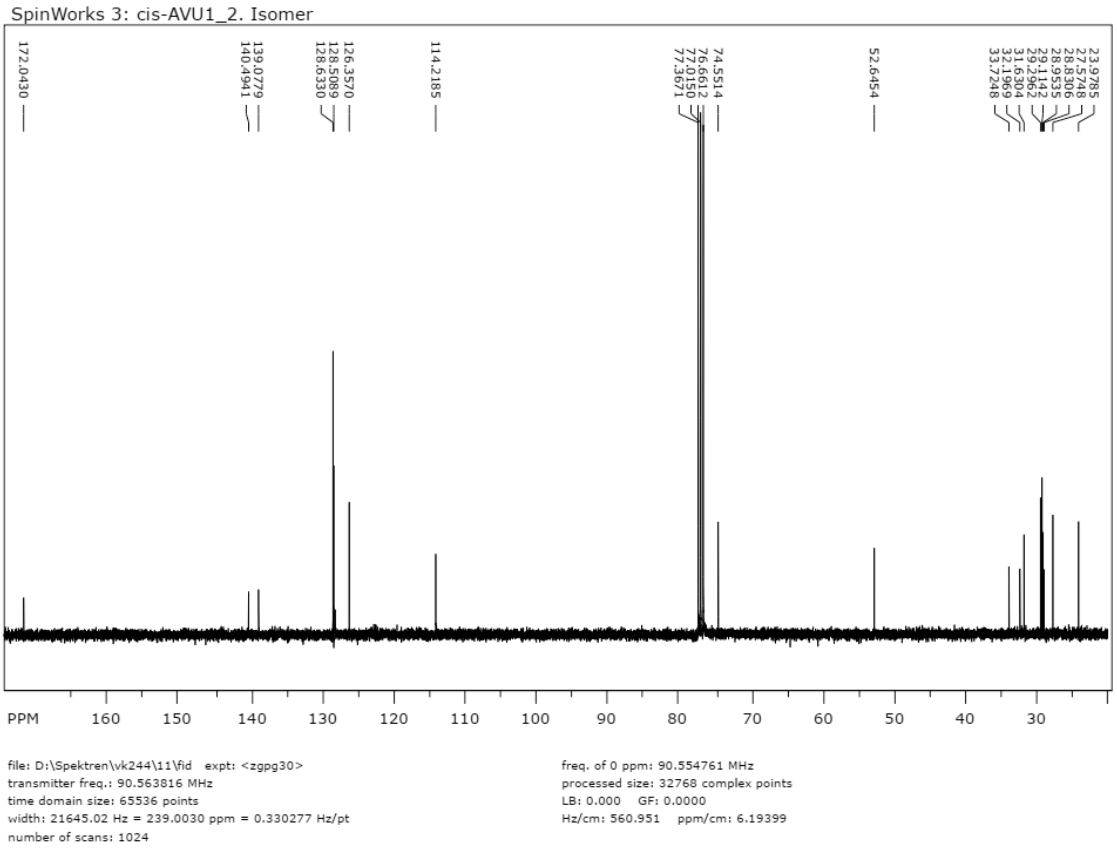

Supplementary Figure 12. ^{1}H and ^{13}C NMR spectra of (3*R*,4*S*)-3-(8-Nonenyl)-4-(2-phenethyl)-oxetan-2-one.

Conformational control of BsClpP by ADEPs

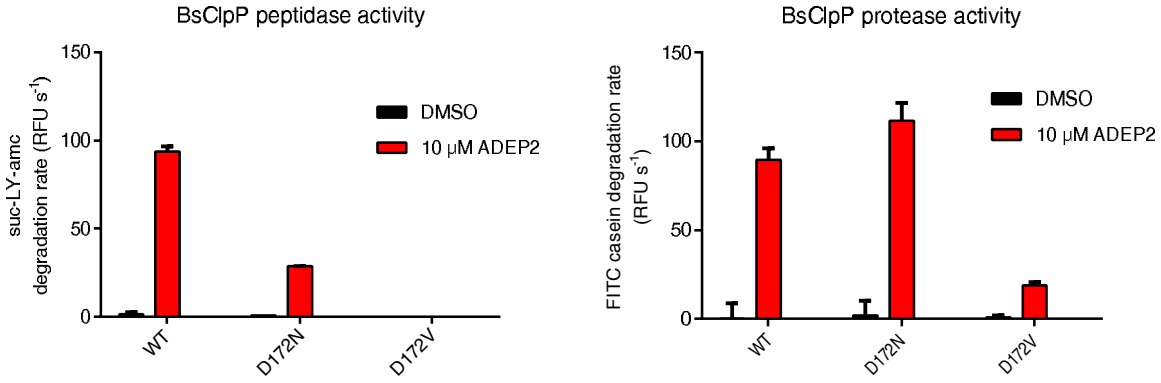

Supplementary Figure 13 (unpublished). The BsClpP active site mutant D172N displayed reduced peptide degradation capabilities and was able to degrade FITC-casein on wild-type level in the presence of ADEP2. This finding is in accordance with the data obtained for SaClpP with the exception that BsClpP does not exhibit peptide hydrolysis on its own but requires functional tetradecamer assembly by the addition of ADEP2. The D172N mutant was employed in SaClpP to demonstrate the conformational control ADEPs exert on ClpP by binding the H-pocket, since the mutant displayed an overall more compacted conformation in SAXS analysis resulting in lower intrinsic peptidase activity which could be reverted by addition of ADEP. ADEPs rescued peptide hydrolysis capabilities of SaClpP D172N to a degree also observed here for BsClpP. However, since BsClpP does not assemble to a functional tetradecamer under our *in vitro* conditions, an intrinsic hydrolysis rate of the BsClpP D172N mutant could not be investigated. Still, the activation profile achieved with the help of ADEP2 closely matches that of SaClpP and strongly suggests that ADEPs also control BsClpP conformation.

Supplementary Tables

Supplementary Table 1. Compilation of parameters obtained from ITC experiments with SaClpP proteins and ADEP7. See the supporting methods for details (data for two replicate experiments are shown for wild type SaClpP). The stoichiometry factor refers to the ration of monomeric SaClpP and ADEP7. A value of 1 is equivalent to 14 ADEP molecules binding per $SaClpP_{14}$.

Figure	SaClpP	sites (*n*)	K_d in µM	ΔH in cal/mol	ΔS in cal/mol/K
1E	wt	1.01 ± 0.02	2.1 ± 0.5	−3369 ± 100	13.8
S2C	wt	1.03 ± 0.01	2.2 ± 0.4	−3319 ± 59	15.0
S2E	S98A	0.99 ± 0.02	3.1 ± 0.6	−2999 ± 68	15.3
S2F	D172N	1.07 ± 0.04	6.1 ± 1.8	−6828 ± 265	1.32

Supplementary Table 2. Predicted (black) and measured (red/blue) m/z ratios of b and y ions for the peptide shown in Figure 2D showing covalent modification of serine 98 of SaClpP with β-lactone D3.

#1	b^{+}	b^{2+}	b^{3+}	b^{4+}	Seq.	y^{+}	y^{2+}	y^{3+}	y^{4+}	#2
1	116.03423	58.52075	39.34959	29.76401	D					51
2	229.11830	115.06279	77.04428	58.03503	I	5436.83385	2718.92056	1812.94947	1359.96392	50
3	392.18162	196.59445	131.39872	98.80086	Y	5323.74978	2662.37853	1775.25478	1331.69290	49
4	505.26569	253.13648	169.09341	127.07188	L	5160.68646	2580.84687	1720.90034	1290.92707	48
5	668.32901	334.66814	223.44785	167.83771	Y	5047.60239	2524.30483	1683.20565	1262.65606	47
6	781.41308	391.21018	261.14254	196.10873	I	4884.53907	2442.77317	1628.85121	1221.89023	46
7	895.45601	448.23164	299.15685	224.61946	N	4771.45500	2386.23114	1591.15652	1193.61921	45
8	982.48804	491.74766	328.16753	246.37747	S	4657.41207	2329.20967	1553.14221	1165.10848	44
9	1079.54081	540.27404	360.51845	270.64066	P	4570.38004	2285.69366	1524.13153	1143.35047	43
10	1136.56228	568.78478	379.52561	284.89603	G	4473.32727	2237.16727	1491.78061	1119.08728	42
11	1193.58375	597.29551	398.53277	299.15139	G	4416.30580	2208.65654	1472.77345	1104.83191	41
12	1280.61578	640.81153	427.54344	320.90940	S	4359.28433	2180.14580	1453.76629	1090.57654	40
13	1379.68420	690.34574	460.56625	345.67651	V	4272.25230	2136.62979	1424.75562	1068.81853	39
14	1480.73188	740.86958	494.24881	370.93843	T	4173.18388	2087.09558	1391.73281	1044.05143	38
15	1551.76900	776.38814	517.92785	388.69771	A	4072.13620	2036.57174	1358.05025	1018.78951	37
16	1608.79047	804.89887	536.93501	402.95307	G	4001.09908	2001.05318	1334.37121	1001.03023	36
17	1755.85889	878.43308	585.95781	439.72018	F	3944.07761	1972.54244	1315.36405	986.77486	35
18	1826.89601	913.95164	609.63685	457.47946	A	3797.00919	1899.00823	1266.34125	950.00776	34
19	1939.98008	970.49368	647.33154	485.75048	I	3725.97207	1863.48967	1242.66221	932.24848	33
20	2103.04340	1052.02534	701.68598	526.51631	Y	3612.88800	1806.94764	1204.96752	903.97746	32
21	2218.07035	1109.53881	740.02830	555.27304	D	3449.82468	1725.41598	1150.61308	863.21163	31
22	2319.11803	1160.06265	773.71086	580.53496	T	3334.79773	1667.90250	1112.27076	834.45489	30
23	2432.20210	1216.60469	811.40555	608.80598	I	3233.75005	1617.37866	1078.58820	809.19297	29
24	2560.26068	1280.63398	854.09174	640.82063	Q	3120.66598	1560.83663	1040.89351	780.92195	28
25	2697.31959	1349.16343	899.77805	675.08535	H	2992.60740	1496.80734	998.20732	748.90731	27
26	2810.40366	1405.70547	937.47274	703.35637	I	2855.54849	1428.27788	952.52101	714.64258	26
27	2938.49863	1469.75295	980.17106	735.38011	K	2742.46442	1371.73585	914.82632	686.37156	25
28	3035.55140	1518.27934	1012.52198	759.64331	P	2614.36945	1307.68836	872.12800	654.34782	24
29	3150.57835	1575.79281	1050.86430	788.40004	D	2517.31668	1259.16198	839.77708	630.08463	23
30	3249.64677	1625.32702	1083.88711	813.16715	V	2402.28973	1201.64850	801.43476	601.32789	22
31	3377.70535	1689.35631	1126.57330	845.18179	Q	2303.22131	1152.11429	768.41195	576.56079	21
32	3478.75303	1739.88015	1160.25586	870.44371	T	2175.16273	1088.08500	725.72576	544.54614	20
33	3591.83710	1796.42219	1197.95055	898.71473	I	2074.11505	1037.56116	692.04320	519.28422	19
34	3694.84629	1847.92678	1232.28695	924.46703	C	1961.03098	981.01913	654.34851	491.01320	18
35	3807.93036	1904.46882	1269.98164	952.73805	I	1858.02179	929.51453	620.01211	465.26091	17
36	3864.95183	1932.97955	1288.98879	966.99341	G	1744.93772	872.97250	582.31742	436.98989	16
37	3995.99233	1998.49980	1332.66896	999.75354	M	1687.91625	844.46176	563.31027	422.73452	15
38	4067.02945	2034.01836	1356.34800	1017.51282	A	1556.87575	778.94151	519.63010	389.97440	14
39	4138.06657	2069.53692	1380.02704	1035.27210	A	1485.83863	743.42295	495.95106	372.21512	13
40	4487.29188	2244.14958	1496.43548	1122.57843	**S-D3**	1414.80151	707.90439	472.27202	354.45584	12
41	4618.33238	2309.66983	1540.11564	1155.33855	M	1065.57620	533.29174	355.86358	267.14951	11
42	4675.35385	2338.18056	1559.12280	1169.59392	G	934.53570	467.77149	312.18342	234.38938	10
43	4762.38588	2381.69658	1588.13348	1191.35193	S	877.51423	439.26075	293.17626	220.13402	9
44	4909.45430	2455.23079	1637.15628	1228.11903	F	790.48220	395.74474	264.16558	198.37601	8
45	5022.53837	2511.77282	1674.85097	1256.39005	L	643.41378	322.21053	215.14278	161.60890	7
46	5135.62244	2568.31486	1712.54566	1284.66107	L	530.32971	265.66849	177.44809	133.33789	6
47	5206.65956	2603.83342	1736.22470	1302.42035	A	417.24564	209.12646	139.75340	105.06687	5
48	5277.69668	2639.35198	1759.90374	1320.17963	A	346.20852	173.60790	116.07436	87.30759	4
49	5334.71815	2667.86271	1778.91090	1334.43499	G	275.17140	138.08934	92.39532	69.54831	3
50	5405.75527	2703.38127	1802.58994	1352.19427	A	218.14993	109.57860	73.38816	55.29294	2
51					K	147.11281	74.06004	49.70912	37.53366	1

Supplementary Table 3. Masses of SaClpP proteins measured by intact protein mass spectrometry.

SaClpP protein	M (expected) in Da	M (found) in Da
Wild type	22554	22553
S98A	22538	22537
D172A	22510	22509
D172N	22553	22552
T169A	22524	22523
D170A	22510	22509
R171A	22469	22468

Supplementary Table 4. List of primers used in this study.

Name	Sequence (5'-3')
SaClpP-H83F-for	gatacaattcattaaacctgatgttc
SaClpP-H83F-rev	gaacatcaggtttaatgaattgaattgtatc
SaClpP-Q89S-for	cattaaacctgatgtttcaacaatttgtatcg
SaClpP-Q89S-rev	ccataccgatacaaattgttgtaacatcagg
SaClpP-M190L-for	cttaattgatgaaggtgctggtacctgaaac
SaClpP-M190L-rev	gtttcaggtaccagcacttcatcaattaagc
GFP-ssrA-for	ggggacaagtttgtacaaaaaagcaggctacgtgagcaagggcgaggag
GFP-ssrA-rev	ggggaccactttgtacaagaaagctgggtgttaagctgctaaagcgtagttttcgtcgtttgctgcgctgcccag ctcgtccttcttgtacag
SaClpX-for	ggggacaagtttgtacaaaaaagcaggctttgagaatctttattttcagggctttaaattcaatgaagatgaag
SaClpX-rev	ggggaccactttgtacaagaaagctgggtgttaagctgatgttttactattattaat
SaClpP-H123A-for	gcgttaccaaatgcagaagtaatgattgcccaaccattaggtg
SaClpP-H123A-rev	cacctaatggttgggcaatcattacttctgcatttggtaacgc
SaClpP-H123N-for	gcgttaccaaatgcagaagtaatgattaaccaaccattaggt
SaClpP-H123N-rev	acctaatggttggttaatcattacttctgcatttggtaacgc
SaClpP-D172A-for	aatacaaaaagacacagatcgtgctaacttcttaactgcagaagaag
SaClpP-D172A-rev	cttcttctgcagttaagaagttagcacgatctgtgtctttttgtatt
SaClpP-D172N-for	aaaatacaaaaagacacagatcgtaataacttcttaactgcagaagaag
SaClpP-D172N-rev	cttcttctgcagttaagaagttattacgatctgtgtctttttgtatttt

Supplementary Methods

General remarks

All reactions were carried out under argon in oven-dried glassware unless noted otherwise. All chemicals were of reagent grade or better and used without further purification. Chemicals and solvents were purchased from Sigma Aldrich unless noted otherwise. Solvents for chromatography and workup purposes were generally of reagent grade. In all reactions, temperatures were measured externally. ^{1}H NMR and ^{13}C spectra of small molecules were recorded on Bruker instruments (360 MHz or 500 MHz) and referenced to the residual proton signal of $CDCl_3$ (7.26 ppm). Carbon samples were referenced against the residual ^{13}C signal of $CDCl_3$ (77.16 ppm). HR-MS-ESI spectra were recorded on a Thermo Scientific LTQ FT. HPLC purification was accomplished with a Waters 2545 quaternary gradient module, a XBridge™ prep C18 10 µm column (50x250 mm) and a Waters 2998 PDA detector. Enantiomeric purity of chiral compounds was determined by chiral HPLC (column Daicel Chiracel, OD-H, 250x4.6) and by polarimetry (Krüss P3002RS).

Synthetic procedures

See Supplementary Fig. 8 for a reaction scheme. Tosylation and acylation of 1-aminoindan-2-oles was carried out as described by A.K. Ghosh *et al*. *J. Am. Chem. Soc.* **1996**, *118*, 2527-2528[2] and A.K. Ghosh *et al*. *Org. Lett.* **2000**, *2*, 2405-2407.[3] Chiral auxiliary-mediated aldol reactions according to A.K. Ghosh *et al*. *J. Org. Chem.* **1998**, *63*, 6146-6152[4] gave mixtures of the respective *syn*- and *anti*-configured aldol products that were separated by HPLC. Saponification yielded enantiomerically pure 3-hydroxycarboxylic acids that were cyclized as described previously in Gersch *et al*. *Angew. Chem. Int. Ed.* **2013**, *52*, 3009-3014.[5]

Stereochemical assignment

The *cis*-*trans*-configuration of the obtained isomeric β-lactones was determined by comparing their ^{1}H-spectra with the known spectra of *cis*- and *trans*-3-methyl-4-(2-

phenylethyl)-oxetan-2-ones.[6] (I. Shiina *et al*., *J. Org. Chem*. **2012**, *77*, 4885–4901). In *cis*-lactones, the signals of C-4 and C-3 protons of the ring are found at 4.5–4.6 and 3.5–3.8 ppm, respectively, whereas in *trans*-lactones the corresponding signals can be observed at 4.1–4.3 and 3.2–3.3 ppm. Since the stereo-configuration is retained during the synthesis, *syn*-configuration of aldol products corresponds to *cis*-configuration of the β-lactones and *anti*-configuration of aldol products corresponds to *trans*-lactones.

The exact configuration (*RR* or *SS*) of the anti-products was established in close analogy to the products formed in similar reaction (A.K. Ghosh *et al*. *J. Org. Chem.* **1998**, *63*, 6146-6152.).[4] The exact configuration of *syn*-products was determined by comparing optical rotatory power values of the corresponding 3-hydroxy-2-(non-8-enyl)-5-phenylpentanoic acid with the (2*S*,3*R*)-3-hydroxy-2-(non-8-enyl)-5-phenylpentanoic acid samples obtained from the product the aldol reaction (D.A Evans *et al*. *J. Am. Chem. Soc.* **1990**, *112*, 5290-5313).[7]

For detailed chromatography settings and spectral data of the intermediates and products of the reaction scheme depicted in Supplemental Figure 8, refer to the complete supplementary material online.

Supplementary References

1. Zeiler, E. et al. Vibralactone as a Tool to Study the Activity and Structure of the ClpP1P2 Complex from Listeria monocytogenes. *Angew Chem Int Ed* **50**, 11001-4 (2011).
2. Ghosh, A.K. & Onishi, M. Synthesis of Enantiomerically Pure Anti-Aldols: A Highly Stereoselective Ester-Derived Titanium Enolate Aldol Reaction. *J. Am. Chem. Soc.* **118**, 2527-2528 (1996).
3. Ghosh, A.K. & Fidanze, S. Asymmetric Synthesis of (−)-Tetrahydrolipstatin: An anti-Aldol-Based Strategy. *Org Lett* **2**, 2405-2407 (2000).
4. Ghosh, A.K. & Fidanze, S. Transition-State Mimetics for HIV Protease Inhibitors: Stereocontrolled Synthesis of Hydroxyethylene and Hydroxyethylamine Isosteres by Ester-Derived Titanium Enolate Syn and Anti-Aldol Reactions. *J Org Chem* **63**, 6146-6152 (1998).
5. Gersch, M. et al. The mechanism of caseinolytic protease (ClpP) inhibition. *Angew Chem Int Ed* **52**, 3009-14 (2013).
6. Shiina, I. et al. MNBA-mediated beta-lactone formation: mechanistic studies and application for the asymmetric total synthesis of tetrahydrolipstatin. *J Org Chem* **77**, 4885-901 (2012).
7. Evans, D.A., Dow, R.L., Shih, T.L., Takacs, J.M. & Zahler, R. Total synthesis of the polyether antibiotic ionomycin. *J Am Chem Soc* **112**, 5290–5313 (1990).

Supporting information for Chapter 3

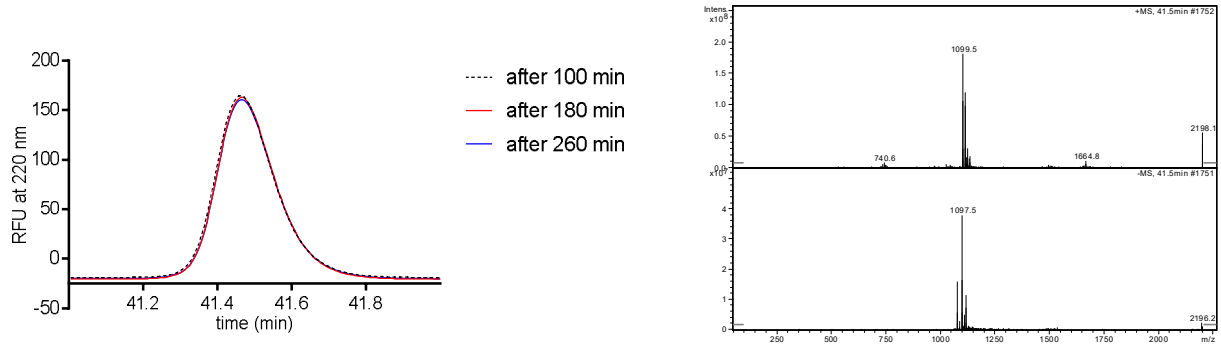

Figure S1. LC-MS analysis of SaClpP with 12IGF. SaClpP (1µM) and 12IGF (46 µM) were incubated under *in vitro* assay conditions for up to 260 min and analyzed via HPLC. No reduction in 12IGF amounts could be observed. Identity of 12IGF (2196 kDa) was confirmed by mass spectrometry at a retention volume of 41.5 ml.

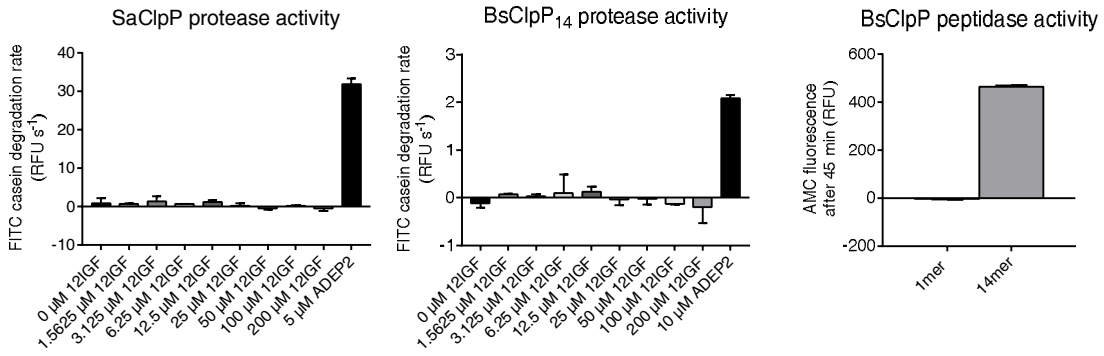

Figure S2. FITC-casein degradation by SaClpP and tetradecameric BsClpP (tetradecamer conditions applied as described before (22)) at different 12IGF concentrations and 5 µM or 10 µM ADEP2 as positive controls, respectively. No activation of casein degradation by 12IGF was detected. *Right panel*, the tetradecameric state of BsClpP was confirmed by stand-alone peptide hydrolysis (i. e. without addition of ADEP2 or 12IGF) with a monomeric preparation as a negative control.

Table S1. SLIM primers for mutagenesis of *mcjA* in the pTUC202 plasmid. SLIM overhangs are underlined and mutated bases are highlighted in bold.

name	sequence
mcjA_SLIM_FP	TTC TAT GGC TGA TAT TCT GAA AGA AGA ACT CTG
mcjA_SLIM_RP	CTC AGG CAC ATG TCC TGC ACC ACC
mcjA_SLIM_11IGL_Tail_FP	TAT TTT **ATT** GGG **CTG** GGT ACA CCT ATA TCT TTC TAT GGC TGA TAT TCT GAA AGA AGA ACT CTG
mcjA_SLIM_11IGL_Tail_RP	AGA TAT AGG TGT ACC **CAG** CCC **AAT** AAA ATA CTC AGG CAC ATG TCC TGC ACC ACC
mcjA_SLIM_11IGF_Tail_FP	TAT TTT **ATT** GGG **TTT** GGT ACA CCT ATA TCT TTC TAT GGC TGA TAT TCT GAA AGA AGA ACT CTG
mcjA_SLIM_11IGF_Tail_RP	AGA TAT AGG TGT ACC **AAA** CCC **AAT** AAA ATA CTC AGG CAC ATG TCC TGC ACC ACC
mcjA_SLIM_11VGF_Tail_FP	TAT TTT GTG GGG **TTT** GGT ACA CCT ATA TCT TTC TAT GGC TGA TAT TCT GAA AGA AGA ACT CTG
mcjA_SLIM_11VGF_Tail_RP	AGA TAT AGG TGT ACC **AAA** CCC CAC AAA ATA CTC AGG CAC ATG TCC TGC ACC ACC
mcjA_SLIM_12IGL_Tail_FP	TAT TTT GTG **ATT GGC CTG** ACA CCT ATA TCT TTC TAT GGC TGA TAT TCT GAA AGA AGA ACT CTG
mcjA_SLIM_12IGL_Tail_RP	AGA TAT AGG TGT **CAG GCC AAT** CAC AAA ATA CTC AGG CAC ATG TCC TGC ACC ACC
mcjA_SLIM_12IGF_Tail_FP	TAT TTT GTG **ATT GGC TTT** ACA CCT ATA TCT TTC TAT GGC TGA TAT TCT GAA AGA AGA ACT CTG
mcjA_SLIM_12IGF_Tail_RP	AGA TAT AGG TGT **AAA GCC AAT** CAC AAA ATA CTC AGG CAC ATG TCC TGC ACC ACC
mcjA_SLIM_12VGF_Tail_FP	TAT TTT GTG **GTG GGC TTT** ACA CCT ATA TCT TTC TAT GGC TGA TAT TCT GAA AGA AGA ACT CTG
mcjA_SLIM_12VGF_Tail_RP	AGA TAT AGG TGT **AAA GCC CAC** CAC AAA ATA CTC AGG CAC ATG TCC TGC ACC ACC
mcjA_SLIM_13IGL_Tail_FP	TAT TTT GTG GGG ATT GGT **CTG** CCT ATA TCT TTC TAT GGC TGA TAT TCT GAA AGA AGA ACT CTG
mcjA_SLIM_13IGL_Tail_RP	AGA TAT AGG **CAG** ACC AAT CCC CAC AAA ATA CTC AGG CAC ATG TCC TGC ACC ACC
mcjA_SLIM_13IGF_Tail_FP	TAT TTT GTG GGG ATT GGT **TTT** CCT ATA TCT TTC TAT GGC TGA TAT TCT GAA AGA AGA ACT CTG
mcjA_SLIM_13IGF_Tail_RP	AGA TAT AGG **AAA** ACC AAT CCC CAC AAA ATA CTC AGG CAC ATG TCC TGC ACC ACC
mcjA_SLIM_13VGF_Tail_FP	TAT TTT GTG GGG **GTG** GGT **TTT** CCT ATA TCT TTC TAT GGC TGA TAT TCT GAA AGA AGA ACT CTG
mcjA_SLIM_13VGF_Tail_RP	AGA TAT AGG **AAA** ACC **CAC** CCC CAC AAA ATA CTC AGG CAC ATG TCC TGC ACC ACC

Table S2. List of primers used for site-directed mutagenesis of SaClpP. Mutated bases are highlighted in bold.

name	sequence
pET301-Q82A for	GCG ATT TAT GAT ACA ATT **GCG** CAC ATT AAA CCT G
pET301-Q82A rev	CAG GTT TAA TGT G**CG C**AA TTG TAT CAT AAA TCG C
pET301-M190T for	GGC TTA ATT GAT GAA GTG **ACG** GTA CCT GAA AC
pET301-M190T rev	GTT TCA GGT AC**C GT**C ACT TCA TCA ATT AAG CC
pET301-Y78A-Q82A for	GCT GGT TTT GCG ATT **GCT** GAT ACA ATT **GCG** CAC ATT AAA CC
pET301-Y78A-Q82A rev	GGT TTA ATG TG**C GC**A ATT GTA TC**A GC**A ATC GCA AAA CCA GC
pET-Y78-single for	CAG CTG GTT TTG CGA TT**G CT**G ATA CAA TTC AAC ACA TTA AAC C
pET-Y78-single rev	GGT TTA ATG TGT TGA ATT GTA TC**A GC**A ATC GCA AAA CCA GCT G